UNSTEADY FLOW CONDITIONS AT DAM BOTTOM OUTLET WORKS DUE TO AIR ENTRAINMENT DURING GATE CLOSURE: BERG RIVER DAM MODEL

by

Adèle Vos

Thesis presented at the University of Stellenbosch
in partial fulfilment of the requirements for the
degree of

Master of Science in Civil Engineering

Department of Civil Engineering
University of Stellenbosch
Private Bag X1, 7602 Matieland, South Africa

Study Leader: Prof. G.R. Basson

November 2011

DECLARATION

Herewith I declare that I know the meaning of plagiarism and that all the text, calculations, results, drawings and graphs in this thesis are primarily my own work. All other work has been cited as appropriate in accordance with the prescribed referencing method.

Name: .....

Student Number: .....

Signed: .....

Date: .....

SINOPSIS

Onbestendige Vloeitoestande weens Lugmeesleuring tydens Sluissluiting by Dambodemuitlaatwerke: Bergrivierdammodel

'n Toetssluiting van die noodsluis van die Bergrivierdam is op 12 Junie 2008 deur die TCTA (Trans-Caledon Tunnel Authority) uitgevoer. Die lugskag stroomaf van die noodsluis is ontwerp om lug in te voer om die verwagte negatiewe drukke tydens die noodsluissluiting te beperk. Die noodsluis moet sluit indien die radiaalsluis aan die einde van die uitlaatpyp sou faal. In teenstelling met die teoretiese ontwerp, het die gemete lugsnelhede in die lugskag in die veld aangedui dat groot volumes lug voortdurend uit die lugskag vrygelaat word wanneer die noodsluis ongeveer 30% toe is (dit wil sê 70% oop). Dit is in teenstelling met die ontwerp, want die lugskag is ontwerp vir die insuig van lug.

Hierdie tesis het ten doel om die redes vir die vrylating van groot volumes lug uit die lugskag vas te stel met behulp van 'n 1:14.066 fisiese skaalmodel van die uitlaatwerke en lugskag van die Bergrivierdam soos getoets tydens die inwydingstoetssluiting in 2008. Die toetse op die model het getoon dat die lugsnelheid in die lugskag onafhankik van die sluistoemaak tyd is, maar verhoog met die toename in die watervlak. Die Bergrivier dam probleem was bepaal as die van lug terugslag.

Die model is gewysig ten einde te bepaal of die spesifieke samestelling van die uitlaatwerke die oorsaak van die vrystelling van lug uit die lugskag is. Die analises en verandering aan die uitleg toon aan dat die skuins afwaartse dak van die uitlaattonnel om die radiaalsluiskamer te huisves die rede was vir die vrylating van die lug uit die lugskag. 'n Addisionele lugskag was gebou in die dak van die uitlaattonnel reg bo die sametrekking, maar was oneffektief om die terug vloei van lug te verminder. Die gevolgtrekking is dat daar geen rasionele strukturele verandering aangebring kan word aan die Bergrivier dam om die vrystelling van lug uit die lugskag te verhoed of te verminder nie.

'n Aanbeveling vir toekomstige ontwerpe is dus dat die uitlaattonnel nie beperkend by die uitlaat-end moet wees nie.

SYNOPSIS

Unsteady Flow Conditions at Dam Bottom Outlet Works due to Air Entrainment during Gate Closure: Berg River Dam Model

A trial closure of the emergency gate of the Berg River Dam was undertaken by the Trans-Caledon Tunnel Authority (TCTA) on 12 June 2008. The air vent downstream of the emergency gate was designed to introduce air to mitigate the negative pressures that were expected in the conduit during emergency gate operations. The emergency gate has to close when the radial gate at the downstream end of the outlet conduit fails. Contrary to the theoretical design, the measured air vent velocities in the field indicated that, while the emergency gate was closing, very large volumes of air were apparently continuously being released from the air vent, commencing when the gate was about 30% closed (i.e. 70% open). This is in contrast to what the design intended, namely that air should have been drawn into the vent.

This thesis is concerned with the testing of a 1:14.066 physical model representing the outlet works and air vent of the Berg River Dam as a means to determine the reasons for the release of large volumes of air from the air vent during the trial closure in 2008. It also seeks solutions to mitigate the excessive airflow from the air vent. It was concluded that the air velocity in the air vent was independent of the rate of closure of the emergency gate, but to increase with increasing water head. The problem at the Berg River Dam was determined to be one of air blowback.

Modifications were made to the configuration of the model in order to determine whether the configuration of the outlet works caused air to be released from the air vent. It was determined that the downward sloping roof at the outlet of the conduit, used to accommodate the radial gate chamber, was the cause of the air blowback phenomenon. An additional air vent was fitted directly onto the conduit at the constriction was found to be ineffective in reducing the air blowback. It was concluded that there are no rational structural change that can prevent or inhibit a recurrence of the blowback phenomenon in the Berg River Dam outlet conduit.

The recommendation follows that the outlet conduit should not be constricted by any structural or mechanism further downstream in the conduit.

LIST OF ABBREVIATES

A	Area (m^2)
B	Gate width (m)
BWP	Berg Water Project
CFD	Computation fluid dynamics
D	Conduit diameter or height (m)
DWA	Department of Water Affairs
F_r	Froude number
Fr_c	Froude number at vena contracta
g	Gravitational constant (m/s^2)
G	Percentage of gate opening
h	Full size of gate opening
Hz	Hertz
km	Kilometre
L	Tunnel length
m	Metre
m^2	Metre square
mA	Milli-ampere
masl	Meters above sea level
mm	Millimetre
p	Prototype
Q_a	Air flow (m^3/s)
Q_w	Water flow (m^3/s)
R_e	Reynolds number
s	Seconds
T	Top width of flow passage (m)
TCTA	Trans-Caledon Tunnel Authority
V	Mean flow velocity (m/s)
V	Volt
v	Kinematic viscosity of water
W_e	Webber number
y	Flow depth (m)

y_e	Effective flow depth (m)
z	Elevation (m)
α	Alpha
β	Air demand ratio
Ω	Ohm
γ_w	Water specific weight
ΔP	Sub-atmospheric pressure after gate
ρ_w	Water density

ACKNOWLEDGEMENTS

I would like to express my sincere gratitude to the following people who have contributed to making this work succeed:

- My father, Johann Vos, who always encouraged me, and my mother, Amanda Vos, for all the moral support.
- My study leader, Prof. Gerrit Basson, for his great leadership and granting me this opportunity.
- The Water Research Commission and the TCTA, for giving me the opportunity to perform this research.
- Christiaan Visser, thank you for all the help at the Stellenbosch Hydraulic Laboratory.

TABLE OF CONTENTS

LIST OF FIGURES

LIST OF TABLES

1. INTRODUCTION

1.1 Berg Water Project

Water is of critical importance to protect and maintain healthy ecosystems. It supports South Africa's mines, power generation and industries, and it is used for recreational purposes. Water is the key to development and a good quality of life.

The Berg Water Project (BWP) is the result of a 14-year strategic integrated planning process carried out by the Department of Water Affairs (DWA) to identify suitable measures to address the increasing water demand in the Greater Cape Town region. The BWP includes the Berg River Dam (previously known as the Skuifraam Dam) and supplement scheme, which pumps a portion of the winter high flows from downstream tributaries back into the Berg River Dam to augment the water from the Berg River as an additional water supply to the Greater Cape Town region and to supply environmental requirements. The Berg River Dam is situated in the La Motte plantation, about 6 km west of Franschhoek, and the supplement scheme is located approximately 10 km downstream of the dam (TCTA, 2008).

1.2 Berg River Dam

The Berg River Dam on the Berg River forms a major part of the Berg Water Project. The dam is operational alongside the Theewaterskloof Dam, situated in the Breede River catchment. The Riviersonderend inter-basin transfer tunnel, constructed through the Franschhoek Mountain range, links the two dams to provide water to the Greater Cape Town area (**Figure 1.1**) (TCTA, 2008).

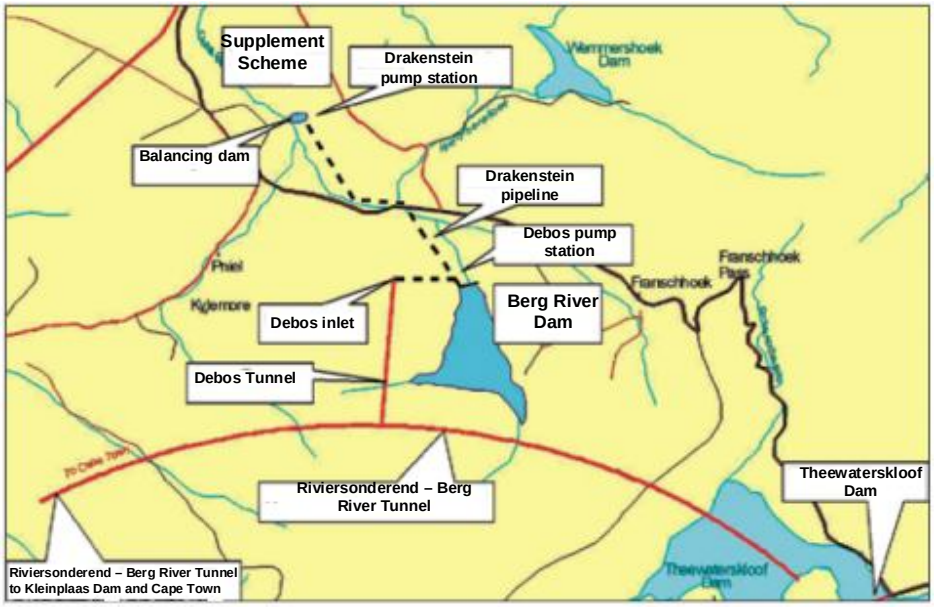

Figure 1.1: Scheme layout

The Berg River Dam is a concrete-faced rockfill embankment, approximately 65 m high and 990 m wide, with a base width of 220 m, as shown in **Figure 1.2** (TCTA, 2008). It has a gross storage capacity of 130 million m^3. Refer to ***Annexure A*** for the as-built drawings of the Berg River Dam outlet works.

Figure 1.2: Berg River Dam

The Berg River Dam is the first of its kind in South Africa, comprising structures that permit the release of both low and high flows, the latter up to 200 m^3/s. The ecological reserve water release, downstream of the dam, had been determined beforehand for the BWP, which ensures that the aquatic ecosystems downstream of the dam are protected. This reserve prescribes low and high flow releases, as well as the quality of the water to be released (TCTA, 2006).

The Berg River Dam was designed to inter alia cater for the ecological reserve, and this is made possible by the intake tower (**Figure 1.3**). The intake tower is divided into a north and south section. The north section is a dry well equipped with multi-level inlets, pipes and valves, which enable the facilities for extracting water from the dam into the supply system to the Greater Cape Town region, as well as making provision for low flow environmental releases (less than 12 m^3/s). The southern section of the intake tower is an open vertical wet well with multi-level gates designed to draw water from the dam for high flows, which imitate the occurrence of natural flood events (up to 200 m^3/s). The wet well is connected to the concrete bottom outlet underneath the dam embankment. This system, for releasing high floods, is a requirement of the Ecological Reserve and is unique to the Berg River Dam. Surplus water spills over the 40 m side spillway with modified Roberts splitters and flows down the concrete chute to the ski-jump (TCTA, 2006). **Figure 1.3** shows a cross-sectional view of the intake tower of the Berg River Dam.

The outflow for the environmental flood release is controlled by a radial gate at the end of the outlet conduit. If this gate should fail, the dam would empty, giving rise to hazardous conditions as a result of downstream river bank erosion. An emergency gate therefore is required that can close under its own weight when the radial gate fails. The design speed of this closure is 12 minutes (Van Vuuren, 2003).

The Berg River Dam and its appurtenant structures were the first large water resource infrastructure project in South Africa to be subjected to the National Water Act of 1998 (Act 36) and the World Commission on Dams (WCD) Report of 2000 (Abban et al., 2008). It is anticipated that a prerequisite for future dam-related projects in South Africa will be that they have to make provision for ecological or environmental flow releases to maintain the integrity of the rivers and to ensure a

healthy ecosystem. Therefore it is fundamental that lessons learned from the BWP are shared with the engineering industry.

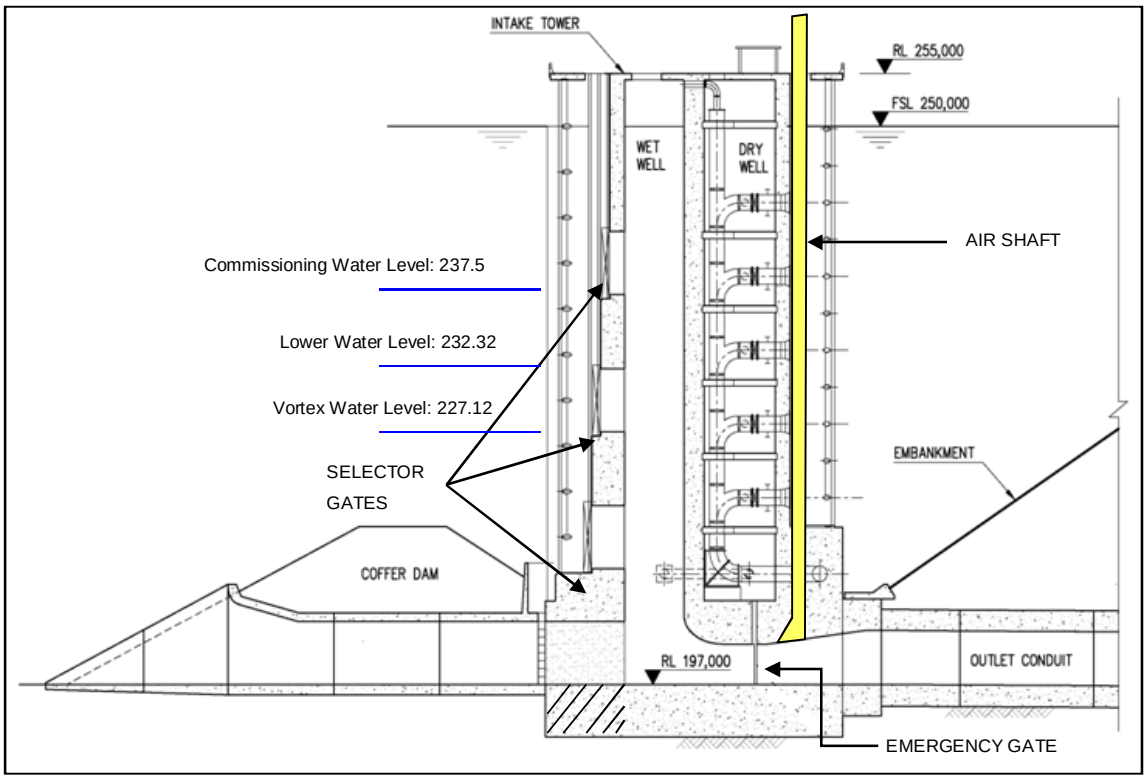

(a)

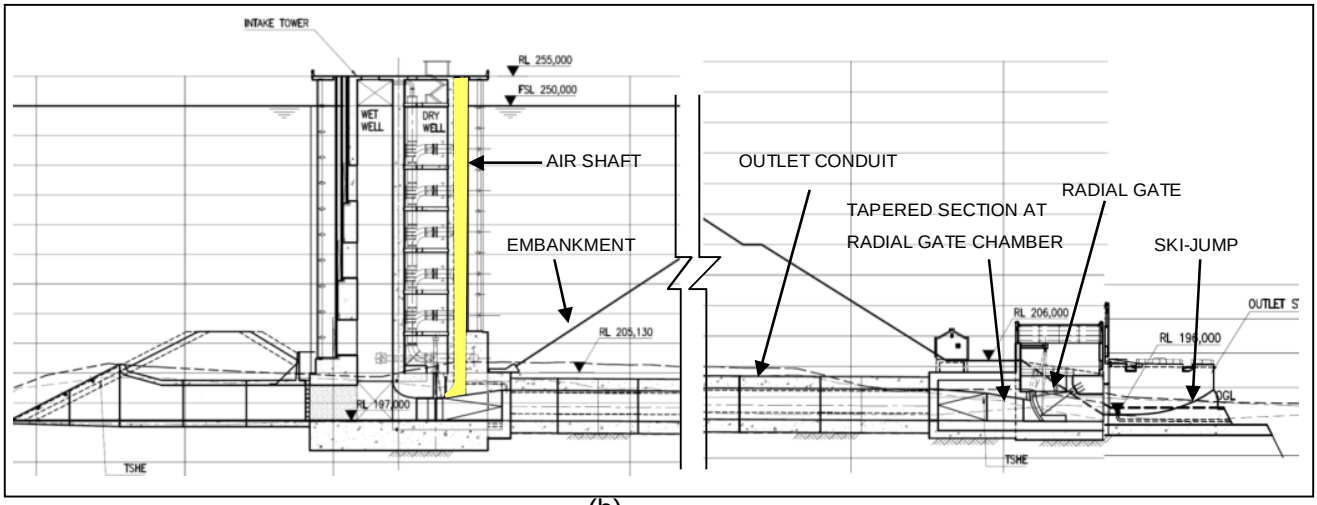

(b)

Figure 1.3: Cross-section of the as constructed Berg River Dam intake tower (a) and outlet structure (b)

1.3 Background to the Project

The commissioning of the closing procedure of the emergency gate (**Figure 1.4**) of the Berg River Dam was undertaken by the TCTA on 12 June 2008. An air vent, downstream of the emergency gate was designed to introduce air downstream of the gate to counteract the negative pressures that were expected in the conduit during emergency gate operations. Contrary to the theoretical design, manual field observations during commissioning indicated that, while the emergency gate was closing, very large volumes of air were released in a surging manner from the 1.8 m^2 air vent, commencing when the gate was about 30% closed (i.e. 70% open), (refer to ***Annexure B*** for a report on the record of the manual observations during the commissioning test on the Berg River Dam in June 2008).

The 1.8 m^2 Mentis grid cover on top of the was air vent was blown off and lifted to a height of about 3 to 4 m, tipping the observer off the vent top and against the upstream concrete wall, and then fell back to the ground, striking/injuring the observer's right foot.

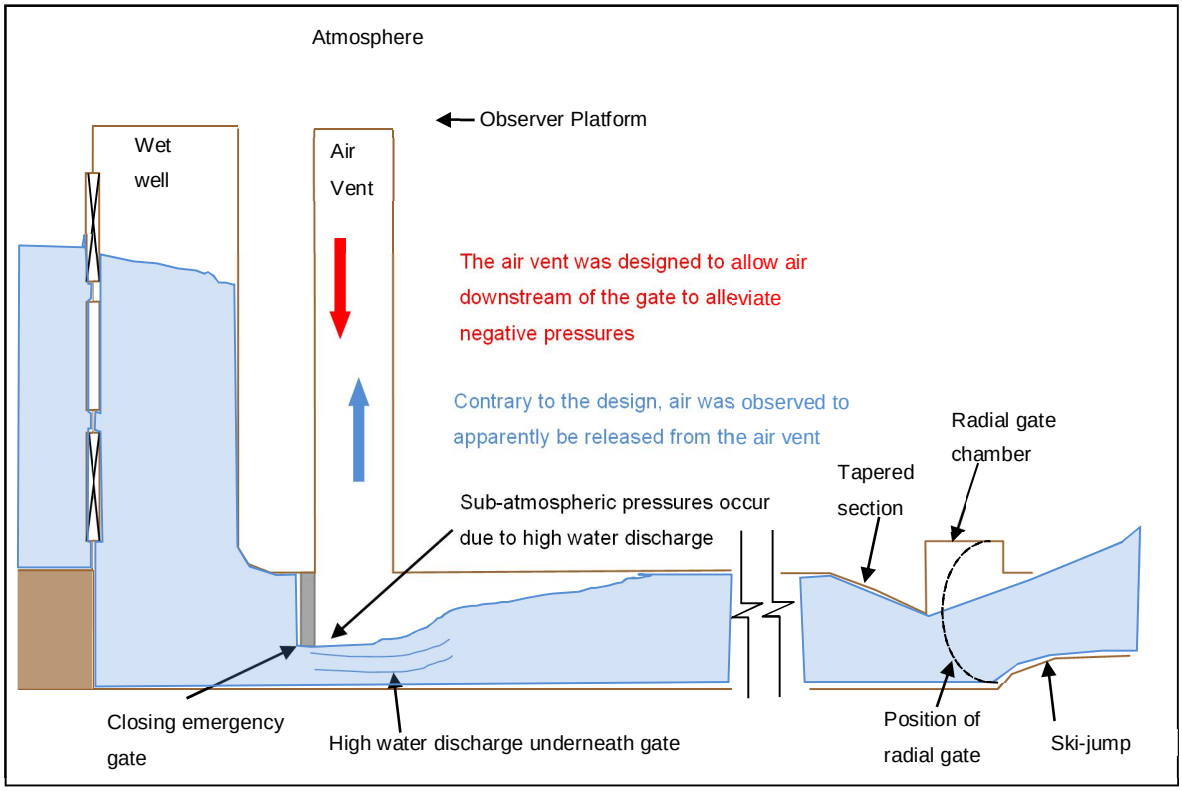

Figure 1.4: Commissioning test of 2008

In this thesis the full-scale structure under investigation is referred to as the prototype (p), and the smaller version of the prototype as the model (m). In 2003 a 1:18.966 scale model of the Berg River Dam was tested by Sinotech in Pretoria, and this test formed part of the detailed design process of the BWP. The study was specifically carried out to test the bottom outlet and concluded that air would be drawn down the vent and that no visible vortex formed at the intake in the reservoir. Emergency gate operations/closures were not simulated, since it was accepted that air would be drawn into the air vent to alleviate the negative pressures that form downstream of the gate (Van Vuuren, 2003).

Guidelines for the design and operation of bottom outlet works with emergency gate closure were investigated, analysed and developed by the University of Stellenbosch in 2009. This project was commissioned by the South African Water Research Commission (WRC), who appointed the University of Stellenbosch to undertake the work. The University initially investigated the air vent operation by means of a physical 1:40 scale model and a two-dimensional computation fluid dynamic (CFD) analysis. The physical model was originally used during the 2003 detailed design to mitigate the bottom outlet ski-jump operation. The study provided inconclusive results regarding air release from the air vent, as observed during the June 2008 commissioning test. The study concluded that the flow of air through the air vent and the potential for formation of vortices at the intake vent on the physical model would not be as proficient as they would be on the prototype and, hence, that the entrainment of air could not be analysed accurately on the 1:40 scale model, as the model was too small and this was also not the original purpose of the model. It also concluded that a three-dimensional CFD analysis would be required for reliable computer simulation of the problem.

For the purposes of this thesis, the University of Stellenbosch constructed a significantly larger (1:14.066 - undistorted scale) physical model of the outlet works and air vent of the Berg River Dam, to enable an investigation of air flow which would be less subjected to scale effects than the previously employed smaller scale models.

1.4 Objectives of the Model Study

The objectives of the model study were as follows:

1. Determine reasons for the release of very large air volumes and fluctuating positive and negative air flow from the air vent, as observed during the commissioning test closure of the emergency gate on 12 June 2008.
2. Provide a solution to mitigate the excessive airflow.

1.5 Thesis Outline

Chapter 2 presents a literature review covering model scale effects, the basic principles of bottom outlet conduits and air entrainment. The importance of air vents in bottom outlet works and the dimensioning of an air vent are also discussed.

The model setup for the Berg River Dam is discussed in *Chapter 3*. The measuring equipment used in the recording procedures is discussed. The methodology used to analyse the water and air flow conditions during gate closures of the Berg River Dam model is also discussed.

The results and evaluation obtained from the model study are discussed in detail in *Chapter 4*.

Chapter 5 provides a summary and conclusions of thesis.

The thesis concludes in *Chapter 6* with concluding remarks and recommendations.

2. LITERATURE STUDY

2.1 Bottom Outlet Conduits

2.1.1 Introduction

Bottom outlets are used primarily for the emergency drawdown of reservoirs. They are also used for sediment flushing or to regulate the water level in the reservoir. In recent years, bottom outlets connected to multi-level intake towers have been designed for drawing water from the reservoir, as required by the Ecological Reserve downstream of dams (Najafi & Zarrati, 2010).

A bottom outlet must be designed to cater for all the flow release scenarios for which it was planned. Generally, the system is designed with two control gates, the emergency gate, which is either open or closed, and the service gate, with a variable opening. **Figure 2.1** illustrates the hydraulic configuration of a typical bottom outlet (Vischer & Hager, 1998).

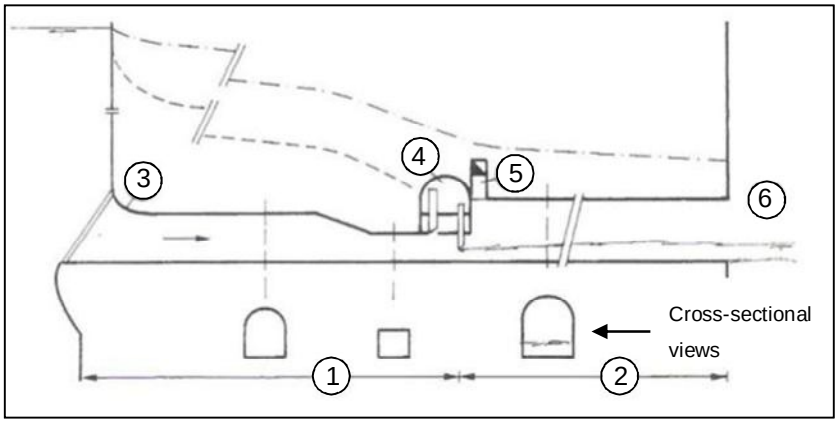

Figure 2.1: Hydraulic configuration of bottom outlet

(---) pressure head line
(-·-·) energy head line
(1): pressurised flow portion (submerged flow)
(2): free surface flow portion
(3): tunnel inlet
(4): gate chamber
(5): air supply
(6): tunnel outlet

The bottom part of **Figure 2.1** illustrates the cross-section of the outlet tunnel at specific sections.

It can be observed from **Figure 2.1** that pressurised flow occurs upstream from the gate (1), and free surface flow occurs downstream from the gate (2). The water is accelerated to the tunnel velocity at the tunnel inlet (3). The cross-section contracts to a rectangular section just upstream of the gate chamber (4), with the aim to create the necessary backpressure and to accommodate the gates. An air vent (5) discharging air behind the gate chamber to supply air to achieve free surface flow under atmospheric pressure and to inhibit sub-atmospheric pressures in the conduit. To avoid the submergence of the gate chamber, the transition from pressurised to free surface flow must occur exactly behind the gate (Vischer & Hager, 1998).

Air-water related failures of bottom outlets and inadequate aeration at gates causes hydraulic problems as cavitation, abrasion and aerated flow due to the high velocity (V) at the outlet. The velocity at the bottom outlet is almost as high as the velocity obtained from the Torcelli formula, $V = (2gH_0)^{1/2}$ [**Equation 2.1**], where H_0 is the head on the outlet (m) and g the gravitational acceleration (m/s^2). A bottom outlet must not be used permanently due to the hydraulic problems associated with cavitation, abrasion, vibrations, air entrainment, hydrodynamic forces, energy dissipation, vortex formation at intakes and erosion (Vischer & Hager, 1998).

Air blowback can also occur in bottom outlet works, which is when water and air are blown back into the intake tower in the reverse water flow direction, as in the case of the Berg River Dam. This phenomenon creates operational problems. Air blowback has also caused serious damage to the Bureau of Reclamation's Navajo Dam and at the Denver Water's Dillon Dam (FEMA, 2004). Please refer to **Section 2.3** for more blowback case studies. Air demand requirements should be considered at design stage in order to minimize the possibility of outlet works failure due to air blowback.

2.1.2 Flow under gates

The primary cause of air demand just downstream of the emergency gate is the flow conditions at the gate. The types of flow that occur at gates in high-headed conduits

may be either free surface flow or pressurised flow (submerged flow). For *pressurised flow* the space upstream of the gate is submerged and pressurised. For *free surface flow* the space downstream of the gate is filled with air. A *hydraulic jump* is the result of the transition from the one flow type to the other (pressurised flow to free surface flow, refer to **Figure 2.1**) (Naudacher, 1991). However, the hydraulic jump is unstable, because the flow downstream of the gate is not subcritical (Fr > 1). Pressurised flow increases the risk for cavitation and vibration damage and should be avoided, as discussed in **Section 2.1.1**. Thus, a bottom outlet should always be designed for free surface flow, as it reduces the potential structural damage (Vischer & Hager, 1998).

Figure 2.2 depicts the three different sources of air entrainment in the outflow in gated bottom outlet tunnels (Vischer & Hager, 1998).

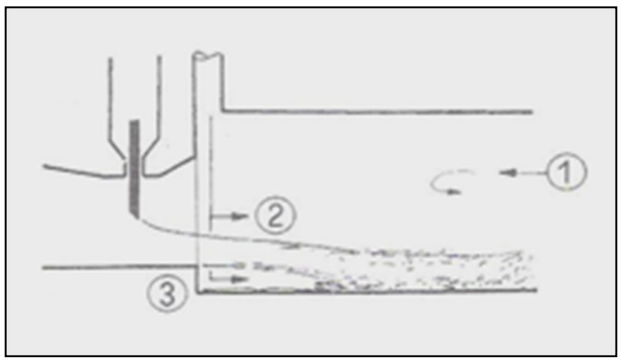

Figure 2.2: Origin of aeration

The aeration of flow may originate from three different sources, namely (1) the counter-current air from the tunnel, (2) the air vent for surface aeration and (3) the bottom aerator (Vischer & Hager, 1998).

The air discharge through the air vent depends on the rate of the air entrained by the high-velocity water discharge, and on the rate that air above the air-water mixture is being discharged at the exit of the conduit due to air-water shear forces. Both these factors vary as they are influenced by structural and hydraulic features of the conduit and the method used to operate the conduit. **Figure 2.3** (Falvey, 1980) gives a good explanation of the shear stress of the water on the air above it. The shear stress of

the water on the air above it causes air pressure to increase with distance downstream if the outflow of air at the end is restricted. It is this compressed air that could lead to intermittent explosive air blow-back. The longer the stroke/fetch distance is the higher the pressure at the restricted end would be (Falvey, 1980). **Figure 2.4** (Wong et al., 2008) shows the increase in pressure with distance in a partially filled pipe with restricted downstream end.

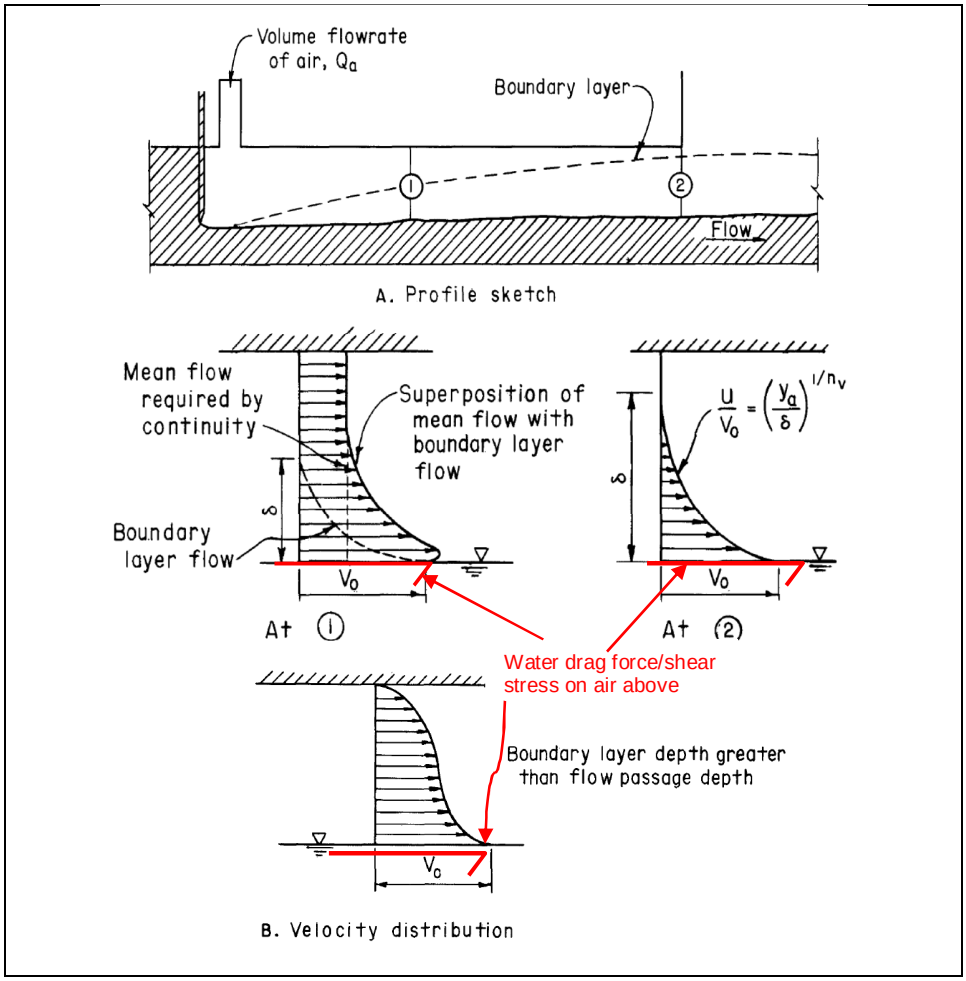

Figure 2.3: Airflow above water surface

Figure 2.4 (a) shows the air and water velocities inside a vertical drainage stack in a high rise building. Positive and negative pressures are reflected by the pressure profile of the drain pipe (**Figure 2.4 (b)**). The pressure inside the pipe varied with height. The velocity profile inside the pipe is depicted by **Figure 2.4 (c)**. The air pressure increased with distance along the direction of the water flow. The vertical

drain pipe (stack) flowed partial full with an air vent on top and a restricted air flow at its bottom due to the bend from vertical to horizontal. There was an increase in water velocity, but it became near constant (e.g. between 2.8 m and 4 m in **Figure 2.4 (c)**) while the air pressure over this distance still kept increasing (**Figure 2.4 (b)**). This demonstrates that air pressure can increase in a dam outlet conduit with an upstream air vent and a restricted air escape at the downstream end.

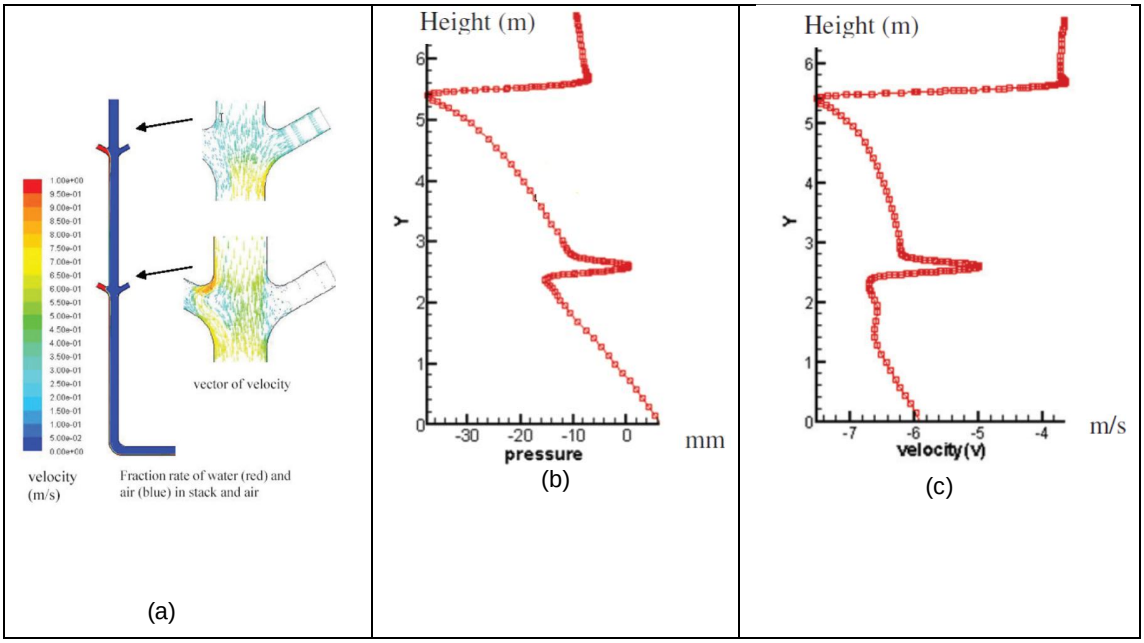

Figure 2.4: (a) Air and water velocities in vertical drainage stack, (b) pressure profile and (c) velocity profile

Studies conducted by Sharma classified two-phase flow regimes downstream of a gate in bottom outlets without bottom aerators, which is similar to the Berg River Dam outlet configuration. Six types of flow that cause air demand were identified and are illustrated in **Figure 2.5** below (Sharma, 1976):

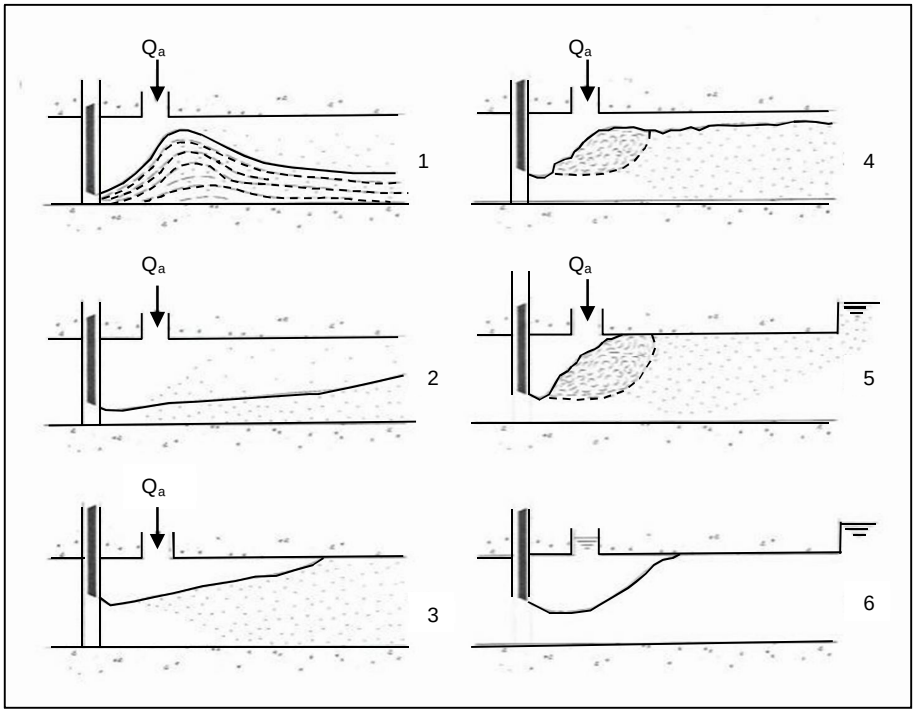

Figure 2.5: Classification of flow types in bottom outlets without bottom aerators

The classification of the flow types, as illustrated in **Figure 2.5**, is as follows (Sharma, 1976):

1. *Spray flow* for relatively small gate opening below 10%, with an extremely high air entrainment.
2. *Free flow* as typical for bottom outlets, and accompanied by features of supercritical flow, such as shockwaves and two-phase flow.
3. *Foamy flow* for a tunnel almost full with an air-water flow, but still not flowing under pressure.
4. *Hydraulic jump* followed by free surface tailwater flow due to tailwater submergence (transition from pressurised flow to free surface flow).
5. *Hydraulic jump with transition to pressurised tailwater flow* (pipe flow).
6. *Fully pressurised flow caused by deep tailwater submergence, no air demand.*

From the above mentioned it is clear that, when the discharge in the conduit is not influenced by tailwater conditions and a hydraulic jump does not form in the conduit, the jet from small gate openings forms spray flow, which fills the conduit and is dragged downstream of the conduit by the underlying flow velocity (USACE, 1980).

A hydraulic jump forms in the conduit at large gate openings, the jet will entrain air as mentioned previously, but the turbulence of the jump will entrain air that is discharged at the top of the conduit and will be pumped downstream into the conduit by the jump action. Both these air flow conditions in the conduit are responsible for pressure reduction behind the gate and at the air vent exit, which results in air being discharged through the air vent into the conduit to stabilise the hydraulic pressures behind the emergency gate (USACE, 1980).

Under free surface flow conditions, the pressure in the tunnel just downstream of the gate, $\Delta p/\gamma \leq 0$, is dependent on the air entrainment intensity in the emerging water jet and the ventilation efficiency through the air vent. If it is assumed that the velocity distribution in the emerging jet is uniform, then the discharge under a high-headed gate may be expressed by the following formula (Naudacher, 1991):

$$\boldsymbol{Q = C_c ab\sqrt{2g(H - H_e - C_c a - h_a)}} \qquad \textbf{Equation 2.2}$$

where

Q: discharge (m^3/s)
C_c: contraction coefficient
a: gate opening (m)
b: gate width (m)
H: head in reservoir (m)
H_e: energy loss from the entrance to the gate section (m)
h: head on contracted jet (m)

The symbols in **Equation 2.2** are explained in **Figure 2.6** below (Vischer & Hager, 1998).

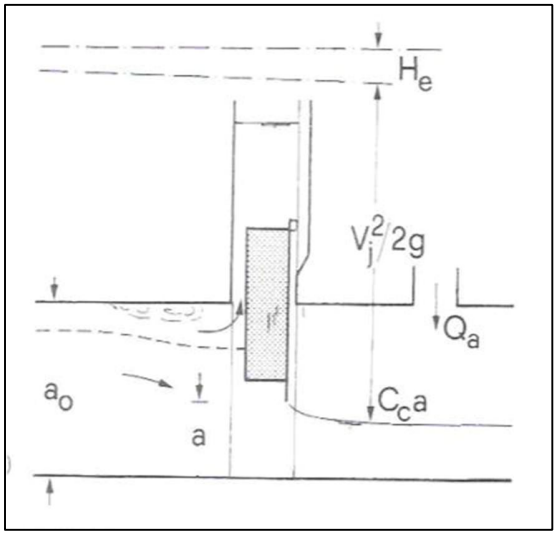

Figure 2.6: Definition sketch for free flow

It is clear from **Figure 2.6** that air must be sucked into the conduit through the air vent, which is in contrast to the measured air vent velocities during the commissioning test in 2008 (air blowback through air vent). Therefore, it is deemed necessary to investigate the reasons for the release of air through the air vent.

The discharge coefficient C_d of the flow underneath the gate can be obtained by the following formula:

$$C_d = \frac{Q}{\sqrt{2g\Delta H}} \qquad \textbf{Equation 2.3}$$

where ΔH is the difference in head according to the underflow discharge formula. The parameter C_d is dependent on various parameters, namely the relative gate opening, $\eta = C_c ab/A_0$ [**Equation 2.4**], with $A_0 = a_0 b_0$ as the approach section, the loss factor, the aspect ratio and the distribution of the approaching velocity. The literature recommended the use of the contraction coefficient C_C in the equations, rather than the lump parameter C_d. The contraction coefficient C_C is dependent on the Froude number ($Fj = Vj/(gC_Ca)^{1/2}$) [**Equation 2.5**] of the flow downstream of the gate, provided that the Froude number is less than four. Large Froude numbers are normally present in the high-headed gate prototype, thus neither the free surface nor

the viscosity effect on the flow need to be taken into account. The geometry of the gate has a significant effect on C_C (Vischer & Hager, 1998).

Another formula for discharge under a vertical sluice gate under free flow conditions was developed by Franke and Valentin by means of measuring the pressure at the floor directly below the gate lip and comparing this value to the geometry of the jet. This formula has been extended by Yong and Fellerman for submerged flow conditions. The general formula for discharge under a gate is as follows (Lewin, 2001):

$$Q = C_d \times G_o \times W\sqrt{2gH} \qquad \textbf{Equation 2.6}$$

where

Q: discharge (m^3/s)
C_d: coefficient of discharge (dimensionless)
G_o: gate opening (m) (represented by *b* in Figure 2.7)
W: gate width (m)
g: gravitational constant (m/s^2)
H: upstream water head (m)

The flow line characteristics of the approaching flow and the flow leaving the orifice are the primary parameters that influence the coefficient of discharge. In turn, these flow lines depend on the gate opening (G_o), and the upstream water head (H). **Figure 2.7** shows these variables, which affect the discharge characteristics (Lewin, 2001). Y_1 (m) is the upstream water depth and Y_3 (m) is the water depth downstream of the gate, with *b* the gate opening (m).

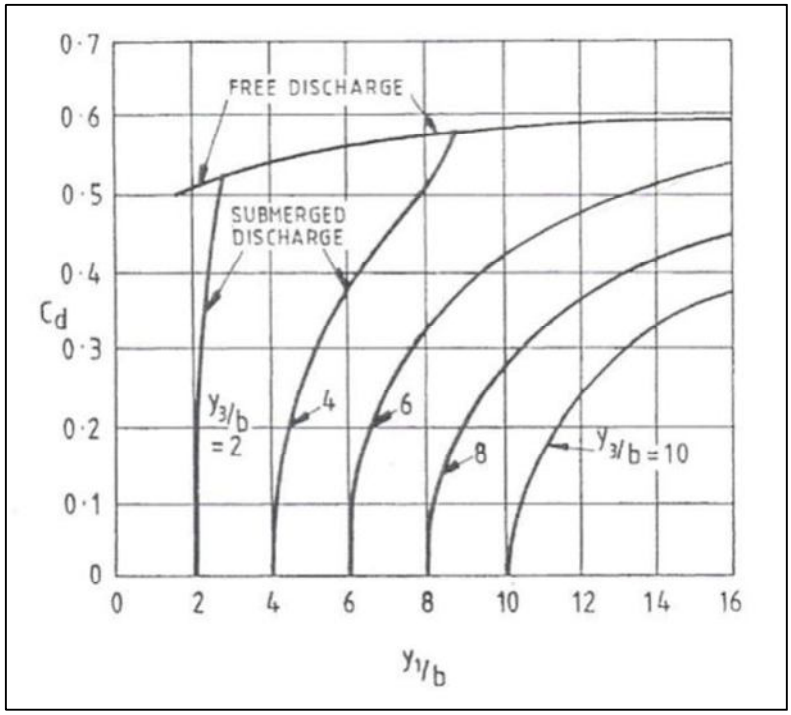

Figure 2.7: Coefficient of discharge for free and submerged flow under a vertical gate

The hydraulics of air-water flow in high-headed bottom outlets has been studied by numerous researchers. The problem of determining the air demand is not yet fully understood and is not amenable to rigorous mathematical formulas, due to the inherent limitations. As a result, only empirical equations have been collaborated to determine the air demand, and these are based on laboratory and field measurements. These equations compare the ratio of the volumetric airflow rate (Q_a) to that of the water (Q_w) (henceforth called *air demand ratio*, indicated by $\beta=Q_a/Q_w$) to the Froude number of the flow at the vena contracta if free flow conditions are experienced, or at the location of the jump in case a hydraulic jump occurs. The β-values obtained from these equations differ substantially from one another, so that it is impossible to select a β-value that will meet all the requirements. Consequently, hydraulic modelling is recommended for important case studies. According to Sharma (1976), the problem to determine the required quantity of air for the different flow types remains unsolved, as field measurements have indicated that the air demand ratio (β) in prototypes is larger than what was predicted by his model studies.

Unequal distribution of water flow through the gate chamber could be avoided by eliminating unnecessary curvature of the outlet conduit near a gate.

2.1.3 Air Entrainment

High flow velocities occur downstream of a partially opened gate of a high-head outlet conduit, resulting in *sub-atmospheric* pressures along the bottom surface of the gate. These pressures can theoretically be as low as the vapour pressure of water, which causes structural damage due to destructive cavitation and vibration, and are therefore undesirable from an operating and structural point of view (Sharma, 1976). Cavitation occurs when flow velocities reach or exceed 13 to 15 m/s (Lewin, 2001). If the pressure behind the gate reduces to vapour pressure, water column separation and re-joining may occur, which leads to water hammer problems (Aydin, 2002). Cavitation is the consecutive formation and collapse of air pockets causing low-pressure areas in high-velocity flow. **Figure 2.8** shows the pressures that were measured on a model of a dam with a submergible gate where the flow underneath the gate had venture-like characteristics (USACE, 1980). It can be seen that the piezometer head of the issuing jet from the partially closed gate approached vapour pressure causing cavitation.

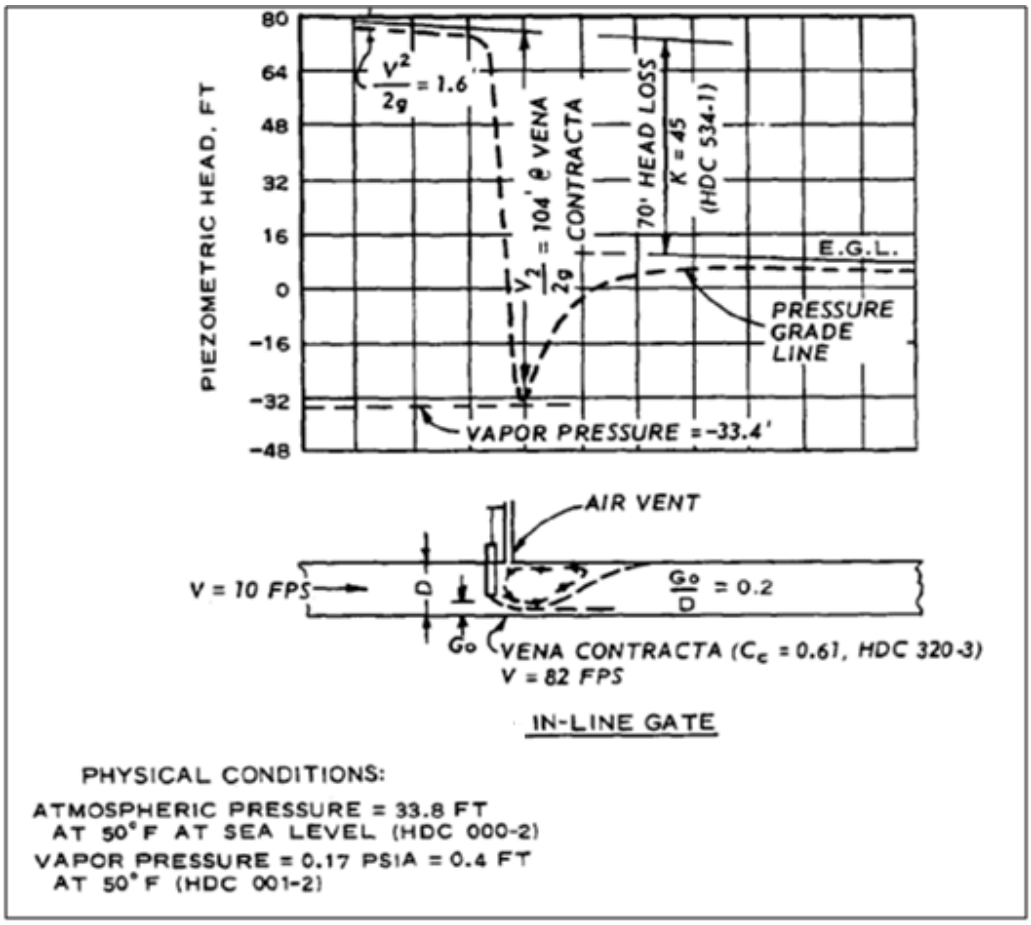

Figure 2.8: Example of cavitation hydraulics

For a case such as shown in **Figure 2.9** (i.e. relative low upstream bend submerged on a bottom outlet gate) air is entrained in the form of bubbles in the air/water transition area and in the air flowing above the transition region because of the drag force of the fast-flowing mixture. The air bubbles will accumulate upstream of the gate and will form air pockets. These air pockets will partially be drawn under the gate due to the high water flow velocity. When the pressurised air is released downstream of the gate, atmospheric pressure is reached almost instantaneously, with an explosive force. A high quantity of air is entrained at small gate openings as the emerging jet is accompanied with spray flow (refer to **Figure 2.5** and **Figure 2.9**).

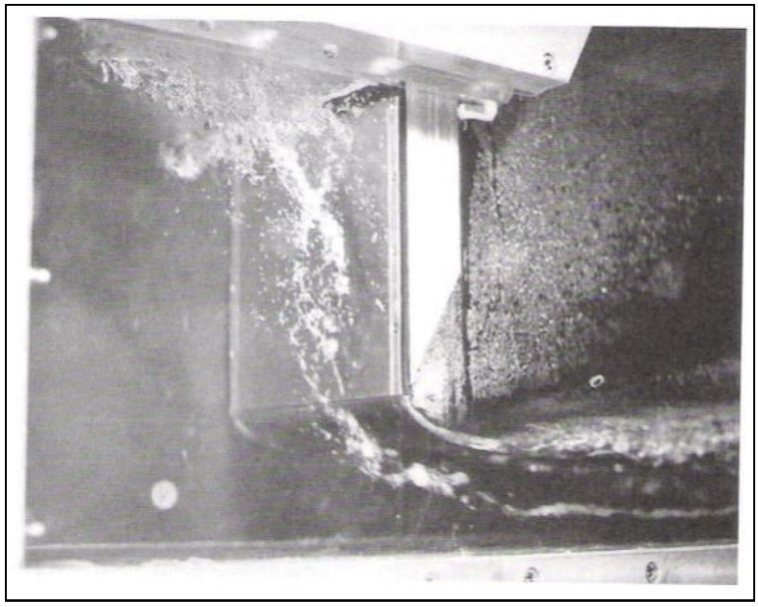

Figure 2.9: Water entrainment upstream of gate end. Spray flow downstream of gate (Lewin, 2001)

An air vent discharging air behind the emergency gate chamber (with relative high upstream head) to supply air to achieve free surface flow under atmospheric pressure is needed to inhibit sub-atmospheric pressures in the conduit (also refer to **Figure 2.8**). Therefore, it is imperative that sufficient quantities of air be supplied to minimise structural damage. The volume of air required depends on air entrainment and the varying flow capacity, whereas the decrease in pressure behind the gate is a function of the length, shape and diameter of the air vent. It is possible to design the air vent in such a way to ensure that the pressure downstream of the gate is within desirable limits by accurately determining the entraining and carrying capacity of the flow (Sharma, 1976).

Figure 2.10 depicts the different flow types which cause air entrainment and the approximate amounts.

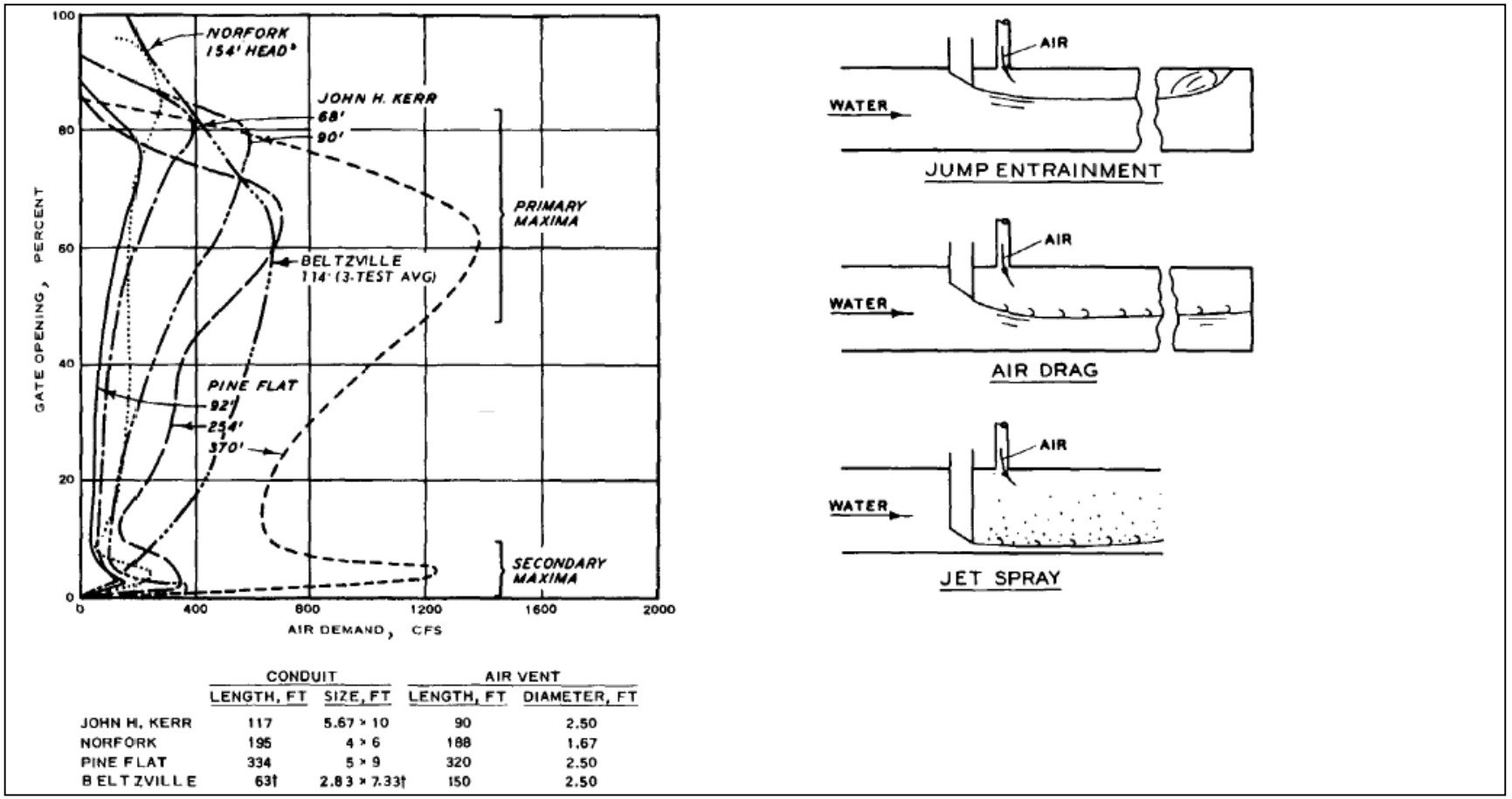

	CONDUIT		AIR VENT	
	LENGTH, FT	SIZE, FT	LENGTH, FT	DIAMETER, FT
JOHN H. KERR	117	5.67 × 10	90	2.50
NORFORK	195	4 × 6	188	1.67
PINE FLAT	334	5 × 9	320	2.50
BELTZVILLE	63†	2.83 × 7.33†	150	2.50

Figure 2.10: Air Demand: Primary and Secondary Maxima

No provision was made for air vents in the earlier high-head gate designs, which resulted in severe damage to the gates and conduits. The Pathfinder Dam in the USA was constructed in 1909 with four slide gates, each 1.1 m by 1.96 m. Hammering and echoing sounds were heard when the dam was in operation. As the flow through the gates increased, the intensity of the sounds increased. At maximum discharged, the dam started to shake. After the conduit was closed, large masses of concrete and rock were found below the damaged gate and the 19 mm steel lining was torn. An air vent was cut through the roof immediately downstream of the gates and the conduit was repaired. This solution proved to be successful once the dam was put into service again. High-head gate designs have been provided with air vents since this incident in order to allow large volumes of air into the water passage downstream of the gate to keep pressures near atmospheric pressure (Erbisti, 2004).

Studies have shown that high-head gates should not be operated at small gate openings (less than 100 mm), as cavitation damage is time dependent. Following this guideline will also minimise erosion damage downstream in the conduit of the gate (Lewin, 2001).

Najafi and Zarrati (2010) used a 3D numerical model to simulate flow conditions in a tunnel of a high headed outlet with ten gate openings from 10% to 100%. The aeration ratio (β) obtained from the 3D numerical model was compared with empirical equations and a physical model as shown in **Figure 2.11** (Najafi & Zarrati, 2010). It can be seen that the results of the numerical model had a better agreement with the physical measurement when compaired with the results obtained from the empirical equations.

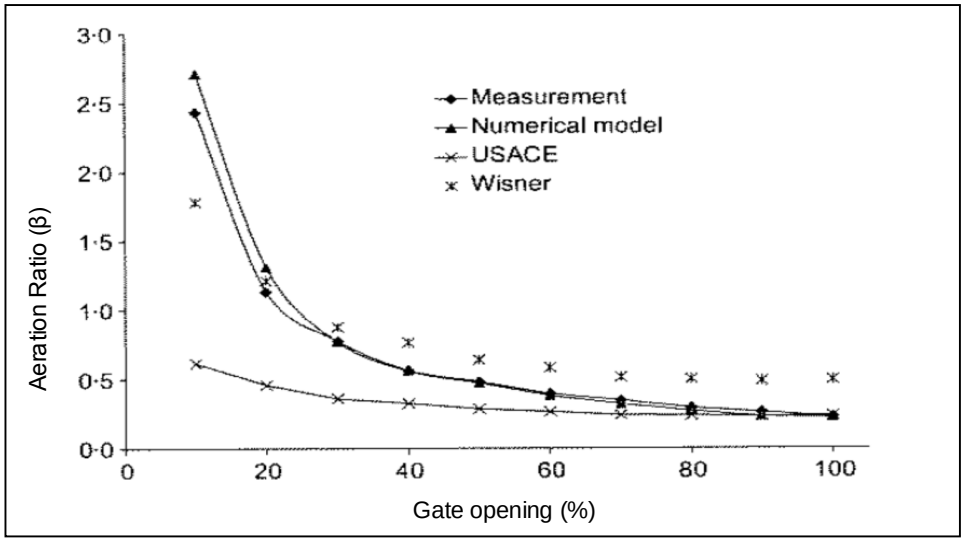

Figure 2.11: Comparison of measured aeration versus gate opening with 3D numerical model and two empirical equations

2.1.4 Functions and Features of Air Vents

Air vents are essential in high-head gates that are located upstream from the conduit exit. For each service gate an air vent is required. The primary functions of air vents are as follows (Erbisti, 2004):

a) Sub-atmospheric pressure is reduced or eliminated in the conduit during emergency or partial gate operations.

b) It makes it possible to drain the conduit.

c) It allows air to escape when the conduit is being filled.

It is vital that the inlet of an air vent be constructed above the maximum reservoir water level on the downstream face of the dam to avoid interference with the air flow. Generally, air vents are circular in shape, but sometimes square or rectangular cross-sections are used to simplify the moulding process. The vent must be as straight as possible, with the minimum number of bends and sharp corners, and there may not be an abrupt change in the cross-section to prevent losses and unnecessary noise (Erbisti, 2004).

Usually, air vents are constructed in the conduit ceiling immediately downstream of the gate, as the air requirements in this region are the most critical and reach a

maximum value when the gate is operated at some partial opening under the highest reservoir head (refer to **Figure 2.8**). For optimal effectiveness the outlet of the vent should not be located further than **2 m** from the emergency gate (Erbisti, 2004).

The velocity of the air being drawn into the conduit may not exceed 40 to 50 m/s in order to avoid discomfort for the maintenance staff and to prevent the vacuum behind the gate from increasing (Borodina, 1969). Air may not be drawn in from either structural cavities or from nearby areas where staff work (Erbisti, 2004).

2.1.5 Air Demand (β)

Various studies have been conducted by numerous researchers to develop formulas for calculating the ratio of air flow to water flow (β), but in most cases air demand is not subject to a rigid analysis. Therefore, for design purposes the quantitative empirical estimations of the air required have been based on suitable experimental and prototype data (USACE, 1980).

A study by Kalinske and Robertson (1943) concluded that the entrainment of air is a function of the Froude number upstream of the hydraulic jump, and expressed the air demand ratio (β) in terms of the air discharge and water discharge. It is defined as follows (Kalinske & Robertson, 1943):

$$\boldsymbol{\beta = \frac{Q_a}{Q_w} = 0.0066(Fr - 1)^{1.4}} \qquad \textbf{Equation 2.7}$$

where

β: air demand ratio (dimensionless)
Q_a: flow rate of air (m^3/s)
Q_w: water discharge (m^3/s)
Fr: Froude number

Figure 2.12 shows the suggested air demand design curve according to Kalinske and Robertson (1943). The relation curves of air demand against the gate opening for the different dams are irregular. This indicates that air demand is not a rigid analysis.

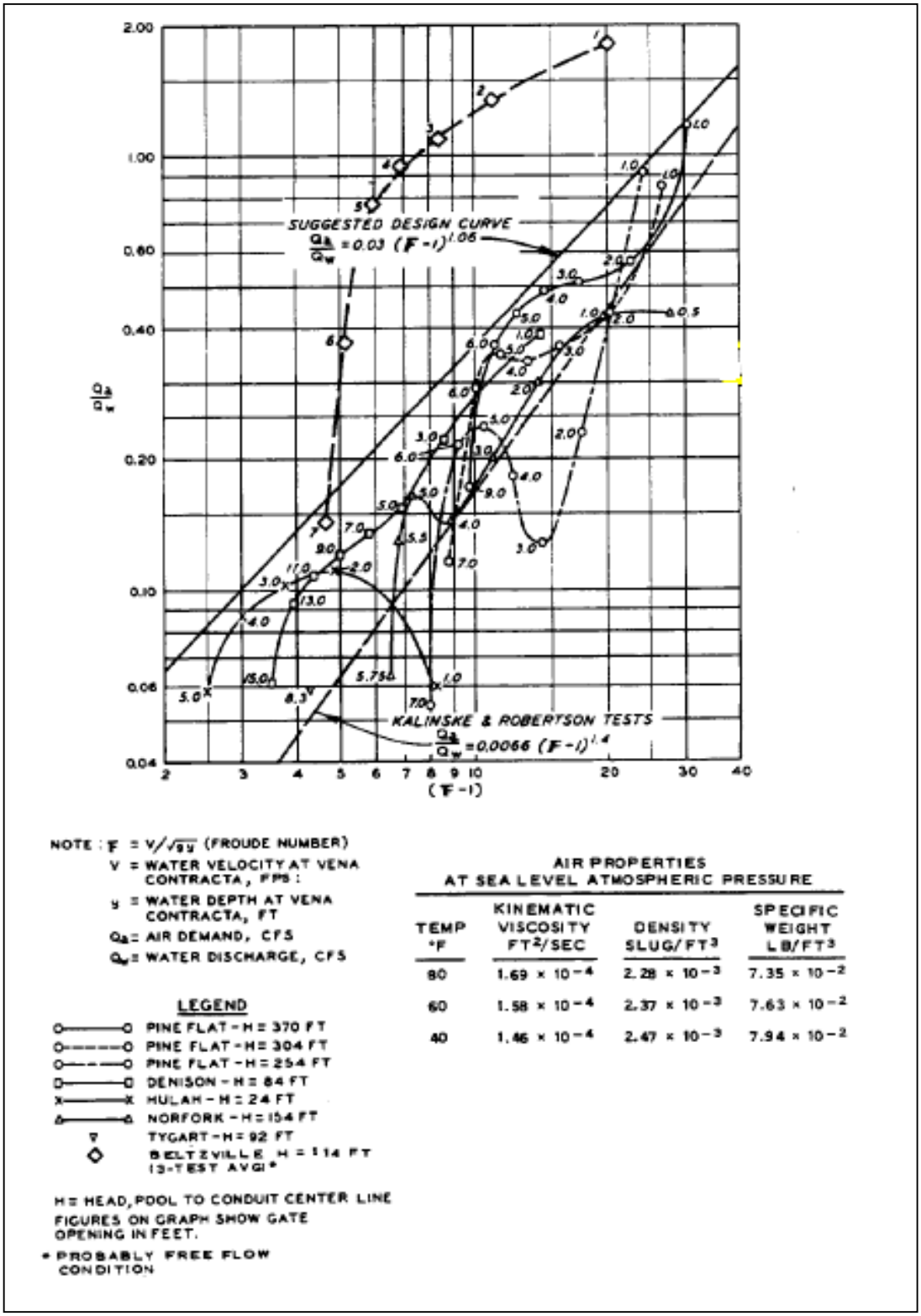

Figure 2.12: Air Demand

The air demand ratio (β) is dependent on various parameters, for instance the geometry of the conduit and gate, the water flow velocity and the depth at the vena contracta and the water head. Another recommend formula for calculating the air demand ratio is as follows (Erbisti, 2004):

$$\beta = K(F_c)^n \qquad \textbf{Equation 2.8}$$

where

K and n: empirical coefficients

F_c: Froude number at vena contracta

$$= F_c = \frac{V_c}{\sqrt{gh_c}} = \frac{\sqrt{2gH}}{\sqrt{gh_c}} = \sqrt{\frac{2H}{h_c}} \qquad \textit{Equation 2.9}$$

g: gravitational acceleration (m/s^2)

V_c: velocity of water at vena contracta (m/s)

h_c: depth of water at vena contracta (m) (refer to **Figure 2.13**)

H: effective head at vena contracta (m) (refer to **Figure 2.13**)

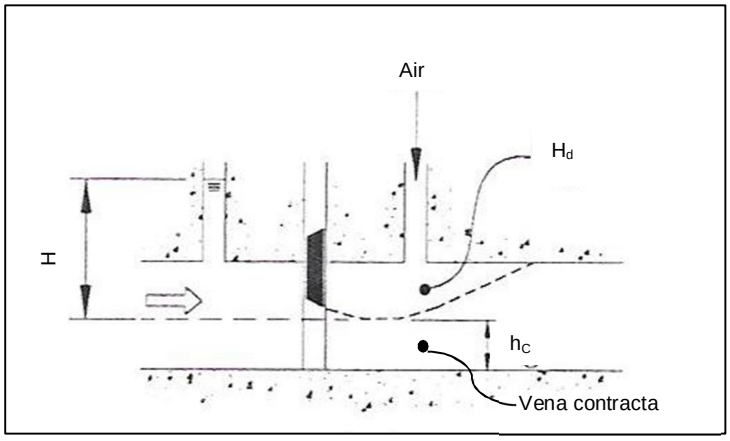

Figure 2.13: Schematic layout of parameters influencing air entrainment

The recommended formula for air entrainment in conduits *without* a hydraulic jump is as follows (USACE, 1980):

$$\beta = 0.03(F_r - 1)^{1.06} \qquad \textbf{Equation 2.10}$$

The results regarding air demand obtained from other studies are described below.

a) Rabben and Rouvè (1985)

Air demand was defined by introducing a fictitious conduit cross-section of $A_a{}^* = A_a(1 + \sum \xi_i)^{-1/2}$ [**Equation 2.11**], where $\sum \xi_i$ represents the sum of all head losses from the atmosphere to the gate chamber. For spray flow (refer to **Figure 2.5** (1)) when the gate opening is less than 6% and $F_c \geq 20$ (Froude number at vena contracta), the air ratio obtained is as follows (Rabben & Rouvè, 1985):

$$\boldsymbol{\beta = \left(A_a{}^* / A_d \right) F_c} \qquad \textbf{Equation 2.12}$$

where

A_d: tailwater area section (m^2)

F_c: Froude number at the vena contracta

$$= \boldsymbol{F_c = q / \left[g (C_c a)^3 \right]^{1/2}} \qquad \textbf{Equation 2.13}$$

Where the water discharge is defined as $Q_w = qb_g$, with b_g being the gate width (m), q is the specific discharge per unit width (m^2/s), g is the gravitational acceleration (m/s^2) and *a* is the gate opening (m).

Under free surface flow conditions (**Figure 2.5** (2) and (3)) with a gate opening greater than 12% and $F_c \geq 40$, an expression for the air ratio, according to Rabben and Rouvè, is as follows (1985):

$$\boldsymbol{\beta = 0.94 \left(A_a{}^* / A_d \right)^{0.90} F_c{}^{0.62}} \qquad \textbf{Equation 2.14}$$

Under tunnel flow conditions where a hydraulic jump occurs (**Figure 2.5** (4) and (5)), the tailwater depth or the corresponding pressure head for pipe flow must be determined by means of a backwater curve for similar

conditions to free flow. The air demand can be determined by the following formula (Rabben & Rouvè, 1985):

$$\beta = 0.019\left({A_a}^* / A_d\right) F_c \qquad \textbf{Equation 2.15}$$

The above three approaches were established for short tunnels. Less air will be entrained in longer conduits due to de-aeration processes (Vischer & Hager, 1998).

b) *Campbell and Guyton* (Erbisti, 2004)

For gated conduits, the air demand ratio according to the study conducted by Campbell and Guyton is defined as follows (Erbisti, 2004):

$$\beta = 0.04(F_c - 1)^{0.85} \qquad \textbf{Equation 2.16}$$

The Froude number in the above formula refers to the flow immediately downstream of the gate at the vena contracta. This formula assumes that the maximum air demand occurs when the conduit is flowing half full.

c) *Levin* (Erbisti, 2004)

According to Levin (Erbisti, 2004), the air demand ratio is defined as follows:

$$\beta = K(F_c - 1) \qquad \textbf{Equation 2.17}$$

The coefficient K is taken according to **Table 2.1** below (Erbisti, 2004).

Table 2.1: K-coefficient

Conditions	K
Vertical lift on gate in circular tunnel	0.025 to 0.04
Same as above, with progressive transition from circular to rectangular section, followed by a very progressive transition (invert angle with horizontal lower than 10°) to circular section	0.04 to 0.06
Same as above, with fast transition from circular to rectangular section, and from rectangular to circular section	0.08 to 0.12

d) Sharma (1976)

The first four flow types as classified in **Figure 2.5** correspond to free surface flow. Under these scenarios, prototype observations have shown that air demand is dependent on the Froude number at the vena contracta, the ratio of the conduit length downstream of the gate (L_g) and the diameter or height of the conduit (D_g). **Figure 2.14** shows a series of curves that is based on experimental data of free-flowing conduits in the form of (1+β) versus $\left(\frac{A_C}{A_T}\right)$for different Froude numbers. A_C is the area of flow at the vena contracta (m^2) and A_T is the cross-sectional area of the conduit (m^2). The values obtained from this graph are only approximations and are not accurate, as the curves were based on specific values of L_g/D_g (Sharma, 1976).

The following formula represents the upper curve on the graph (Erbisti, 2004):

$$1 + \beta = \frac{1}{A_C/A_T} \qquad \textbf{Equation 2.18}$$

This formula relates to the maximum possible air flow through the tunnel where the Froude number at the vena contracta is large enough to create foamy flow and the flow depth at the vena contracta is comparable to the vertical dimension of the conduit. These two conditions are hardly ever satisfied in practice.

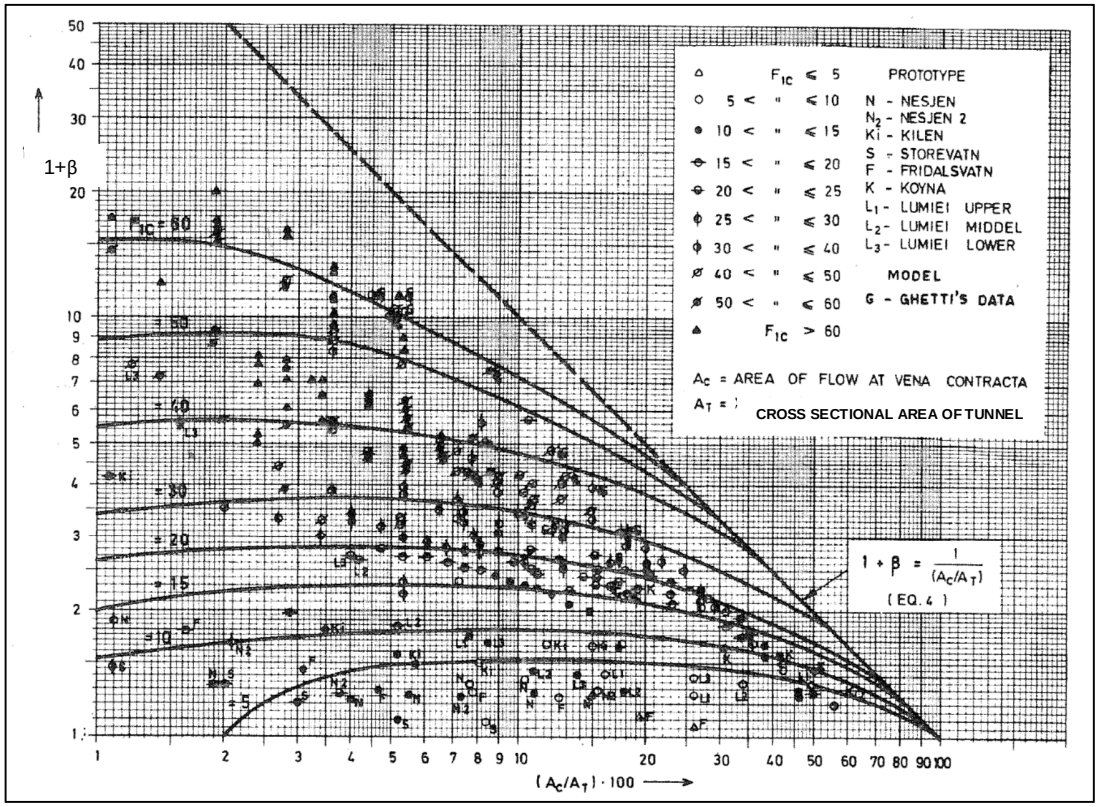

Figure 2.14: (1+β) versus (A_C/A_T) for different Froude numbers (Erbisti, 2004)

Figure 2.5 (5) shows the scenario in which a hydraulic jump occurs in a bottom outlet and is followed by pipe flow with the conduit exit submerged and a low L_g/D_g ratio, or during the emergency closure of the gates. For these scenarios, Sharma suggested a slight modification in the formula of Kalinske and Robertson, with replacement of the Froude number at the jump location by the Froude number at the vena contracta. The results obtained from the formula were found to give comparable results for model and prototype observations. The modified formula is as follows (Sharma, 1976):

$$\beta = 0.0066(F_c - 1)^{1.4} \qquad \textbf{Equation 2.19}$$

The comparison between the various calculation formulas for determining the air demand ratio for bottom outlets with the lower end drowned (type 5

flow) is illustrated in **Figure 2.15**. The coefficient K in Levin's curve was assumed to be equal to 0.04.

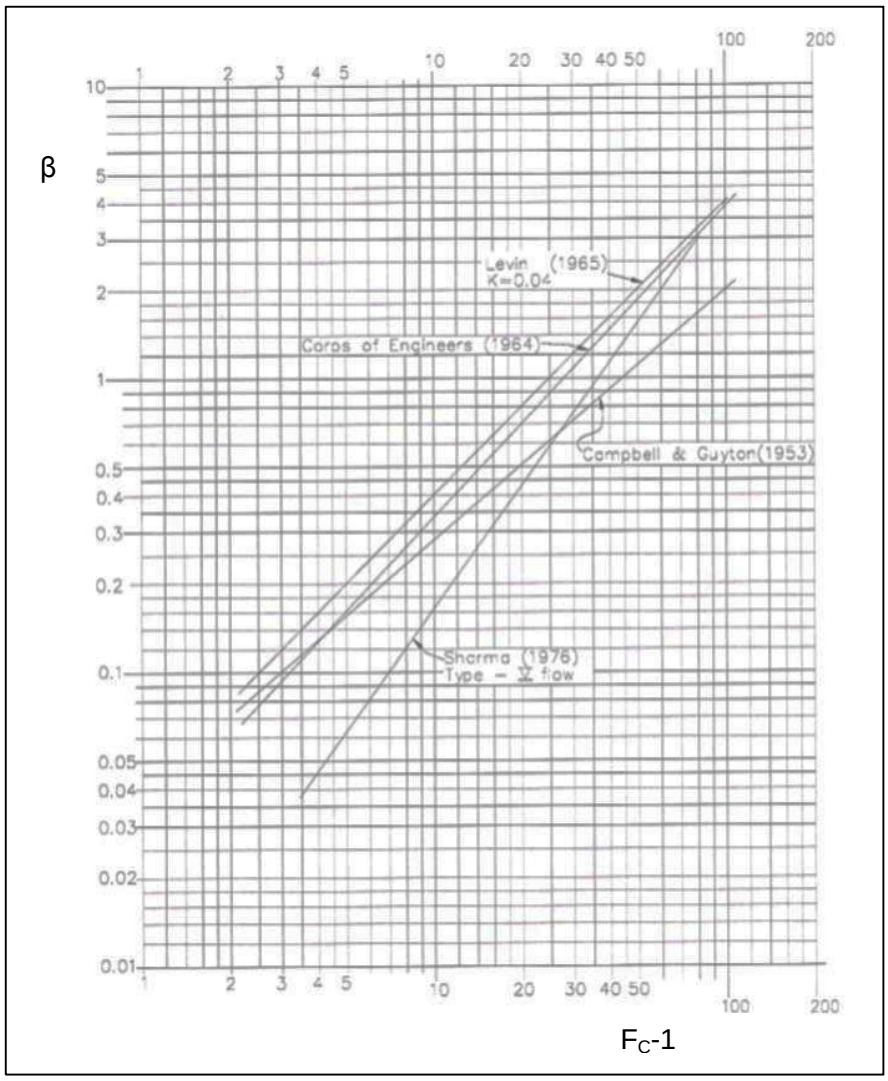

Figure 2.15: Comparison between the various calculation formulas

The maximum air demand under free surface flow conditions is generally not when the gates are fully open. Normally, two maximum air demand ratios exist, one for very small gate openings (4% to 8%), which result in spray flow, and the second when the gate opening is between 40% and 70% (Lewin, 2001), as depicted in **Figure 2.16**.

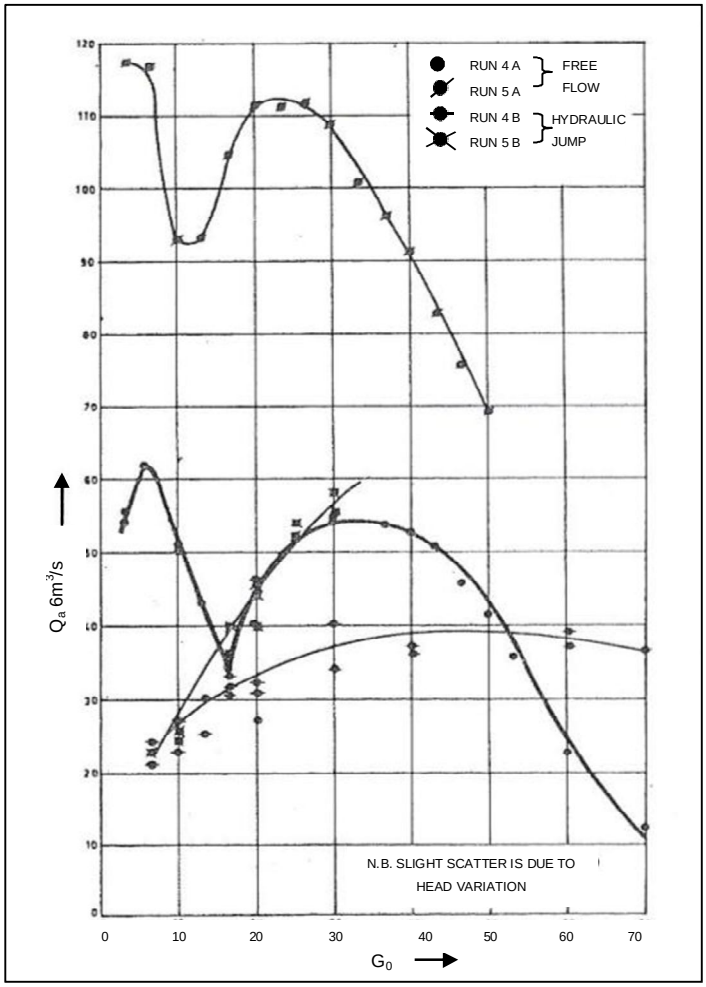

Figure 2.16: Air demand versus gate opening G_0 (Sharma, 1976)

According to Sharma (1976), the maximum air demand can be assumed to occur at a gate opening of 80%. The gate contraction coefficient can be expected to be 0.8 for a 45° gate lip and 0.6 for a sharp-edged gate lip. The maximum air velocity must be limited to 45 m/s to prevent excessive pressure loss due to flow resistance in the conduit (USACE, 1980).

The empirical formulas for calculating the air demand are not very accurate, as discussed above. Therefore, physical modelling of gated tunnels is required for the purpose of determining the aeration ratio (β), the gate rating curve, the pressures and the cavitation index along the conduit, and the flow conditions downstream of the gate.

2.1.6 Air Vent Dimensioning

The maximum airflow rate must first be estimated in order to design an air vent. The permissible velocity, in addition to the air demand, determines the required size of the air vent. Undesirable noises and excessive reduction in pressure in the conduit are caused by extremely high airflow velocities. Field studies of prototypes have concluded that the airflow velocity should not exceed 45 m/s, which will result in a nominal head loss in the vent or pressure drop in the conduit. To minimise cavitation tendencies, the total pressure drop across the air vent should be limited to 1.5 m water head. Dimensioning the air vent and calculating the pressure drop along the air vent makes it possible to estimate the reduced pressure that is acting downstream of the gate, which is an important parameter to analyse the imposed loads on the structural components (USACE, 1980).

The airflow in the air vent can be calculated by the following formula (Erbisti, 2004):

$$Q_a = 28 m_a A \sqrt{2 g H_d} \qquad \textbf{Equation 2.20}$$

where

Q_a: airflow in air vent (m^3/s)

m_a: flow coefficient of air vent (dimensionless) (refer to **Equation 2.24** below for calculation method)

A: cross-sectional area of air vent (m^2)

g: gravitational acceleration (m/s^2)

H_d: air pressure below atmosphere downstream of the gate (m water) (refer to **Figure 2.13**)

The water discharge is determined by the following formula (Erbisti, 2004):

$$Q_w = B_c h_c \sqrt{2 g H} \qquad \textbf{Equation 2.21}$$

where

(Refer to **Figure 2.13**)

Q_w: Water discharge (m^3/s)

B_c: width of water at vena contracta (m)

h_c: depth of water at vena contracta (m)

g: gravitational acceleration (m/s^2)

H: effective head at vena contracta (m)

The volumetric airflow is related to the water flow as follows, as discussed in **Section 2.1.5:**

$$Q_a = \beta Q_w \qquad \textbf{Equation 2.22}$$

Thus, the cross-sectional area of the air vent can be determined as follows:

$$28 m_a A \sqrt{2gH_d} = \beta B_c h_c \sqrt{2gH}$$

$$\therefore A = \frac{\beta B_c h_c}{28 m_a} \sqrt{\frac{H}{H_d}} \qquad \textbf{Equation 2.23}$$

The flow coefficient of the air vent is calculated with the following formula (Erbisti, 2004):

$$m_a = \frac{1}{\sqrt{\sum C_0 + \lambda \frac{L}{d}}} \qquad \textbf{Equation 2.24}$$

where

m_a: flow coefficient of air vent (dimensionless)

ΣC_0: sum of loss coefficients of obstacles such as entrances, exits, elbows, curves and screens

λ: friction loss coefficient (dimensionless)

L: length of air vent (m)

d: diameter of air vent (m)

The Moody chart can be used to determine the friction loss coefficient (λ) in the air vent as a function of the Reynolds number and relative roughness (ε/d).

The flow coefficient (m_a) of the air in the vent is determined by trial and error, by starting with the air vent geometry and estimating a value for the diameter, after which head losses and the cross-section area can be determined. The diameter also must be verified; if it differs from the initially assumed value attributed to it, another value for the diameter must be assumed and the above calculation must be repeated (Erbisti, 2004).

The air velocity in the air vent is dependent on the depression downstream of the gate. If the flow coefficient (m_a) is less than 0.5, the airflow velocity can be determined by the following formula (Erbisti, 2004):

$$V_a = 28 m_a \sqrt{2 g H_d} \qquad \textbf{Equation 2.25}$$

where

V_a: airflow velocity (m/s)

m_a: flow coefficient (dimensionless)

g: gravitational acceleration (m/s^2)

H_d: depression downstream of gate (m) – refer to **Figure 4.12**

The depression (H_d) downstream of the gate should not exceed certain limits, as described above (H_d < 1.5 m), to reduce the probability of cavitation.

The cross-section of rectangular air vents is calculated as if the section was circular. The following ASHREA formula gives the equivalent sections for circular and rectangular vents that have the same length, flow and head losses (Erbisti, 2004):

$$D_e = 1.3 \sqrt[8]{\frac{(ab)^5}{(a+b)^2}} = 1.3 \frac{(ab)^{0.625}}{(a+b)^{0.25}} \qquad \textbf{Equation 2.26}$$

where

D_e: diameter of the equivalent circular section (m)

a: rectangular dimensions (m)

b: rectangular dimensions (m)

For the particular case of a square cross-section, the equivalence is given by:

$$D_e = 1.093\ a \qquad \textbf{Equation 2.27}$$

where *a* is the length of the square side (m).

An empirical equation was developed by Sarkaira and Hom to calculate the diameter of an air vent for closed conduits without surge tanks. The formula is as follows (Sarkaria & Hom, 1959):

$$\boldsymbol{d = 0.291\left(\frac{P^2 L}{H_n{}^2}\right)^{0.273}} \qquad \textbf{Equation 2.28}$$

where

d: diameter of the air vent (m)

P: rated output of the turbine (MW)

L: length of the air vent (m)

H_n: rated head of the turbine (m)

Erbisti (2004) recommended that the diameter of the air vent as calculated by the above formula be considered as the minimum.

2.2 Vortices

Vortices usually occur at free-surface flows into a closed conduit with low heads with high discharges, however, they had been observed at intakes with high water heads as much as 18 m to 30.5 m. Free surface vortices can be defined as turbulent flow caused by residual angular momentum in the water flow at close conduit intakes. Refer to **Figure 2.17** which shows a vortex at Horspranget Hydropower intake in Sweden on 15 August 1949 (Rindels & Gulliver, 1983).

Figure 2.17: Free surface vortex

A vortex gives unpredicted flow patterns at an intake which decreases the efficiency. Free surface vortices can cause cavitation, resonance vibration and structural damage. The flow capacity of an intake tower will be reduce if the surface vortex has an air core. The formation of free vortices at the intake must be avoided, as larger volumes of air will then be entrained (Lewin, 2001).

The vortex intensity at an intake is a function of the submergence of the intake (S), the water discharge (Q_W) and the intake and channel geometry. Gordon has developed curves which depicts different regions of vortex formations and is recommended for determining the minimum submergence depth to avoid vortex formation as seen in **Figure 2.18**. According to Gordon the submergence of the intake is directly related to the penstock velocity (V) and conduit diameter (D) (Rindels & Gulliver, 1983):

$$S = CVD^{1/2} \qquad \textbf{Equation 2.29}$$

One limitation to Gordon's relationship is that only four tests included in the data experienced vortex problems (refer to **Figure 2.18**). The second disadvantage is that Gordon's relationship cannot be considered universal for all intake types, since the data is not dimensionless (Rindels & Gulliver, 1983).

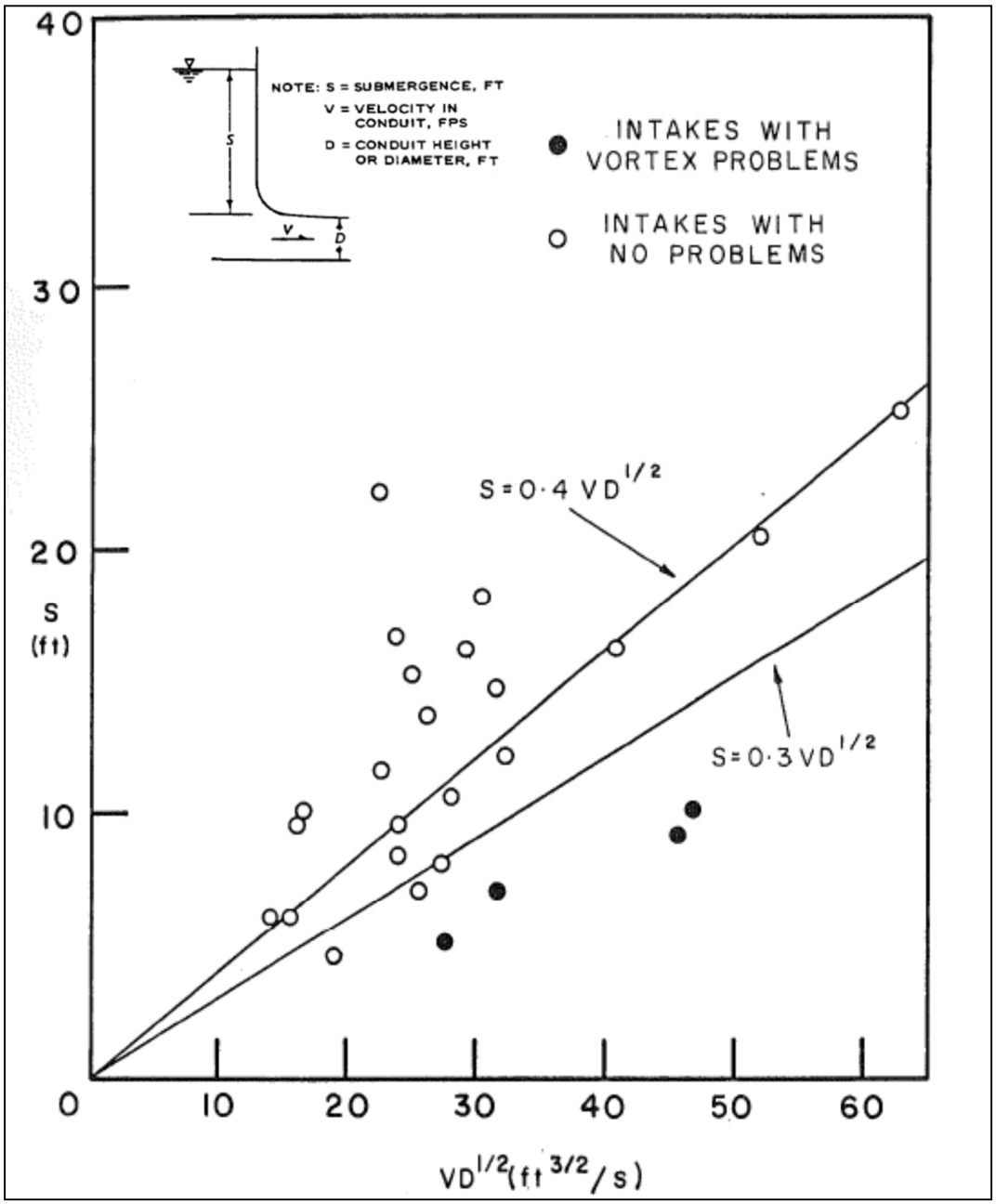

Figure 2.18: Vortex Formation Chart (Rindels & Gulliver, 1983)

2.3 Air Blowback Phenomenon

Prototype cases in which air blowback (large air pockets moving against flow) occurred was investigated by Sailer (Falvey, 1980). **Figure 2.19** (Falvey, 1980) delineate the air reverse flow region. The five prototype structures that experienced air blowbacks are indicated by a cross (+). Two of these blowback cases lay within the blowback zone at design discharge i.e. valve openings at 100% open. The other three cases had to pass through the blowback zone when the flow is reduced from the design discharge, which means that these three cases would experience blowback at valve openings smaller than 100%, since with smaller valve openings these three "+"-plot locations would move to the left on the graph until they cross the line marked "Limit for air pocket movement" (Falvey, 1980).

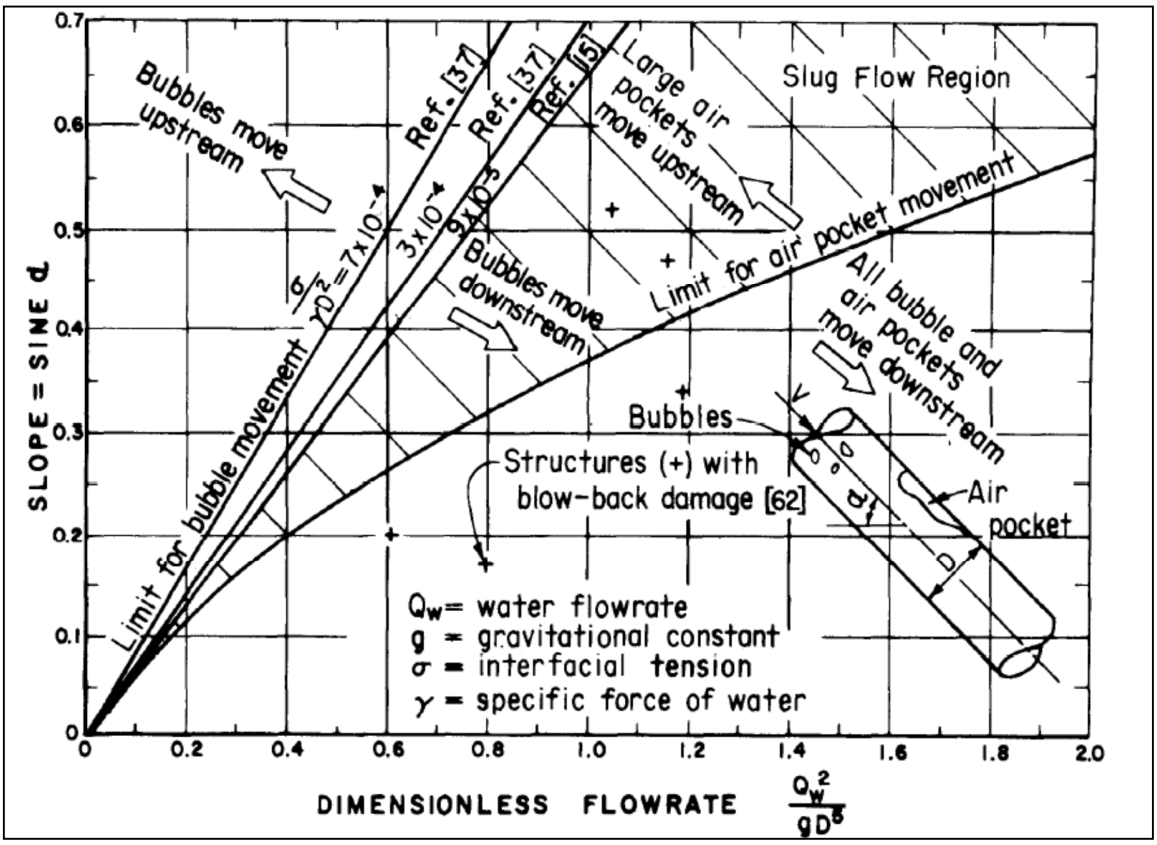

Figure 2.19: Bubble motion in closed conduits flowing full

The literature review pointed out that explosive blowback incidents occurred on numerous internationally high-headed conduit schemes. For example, the blowback

of air occurred twice on the Gautape Dam Stage 1 intake tower in Colombia (Villegas, 1994).

Webby (2003) described the air blowback incidents which occurred on the Rangipo Power Station in New Zealand. The evidence available of the blowback phenomenons on the power station showed that the head loss between the head-pond and the intake shaft increased when the intake screens were blocked. As a result, free-surface flow occurred in the outlet conduit which entrained large quantities of air. Air entrained by the water accumulated as a large air pocket along the outlet conduit soffit. When the discharge was reduced the air was explosively blown back into the intake shaft. A vertical air shaft/vent (300 mm diameter) was drilled into the conduit soffit downstream of the drop-shaft bend to mitigate the air blowback problem.

Lowe (1944) described the air blowback phenomenon which occurred on the Owyhee Dam in Oregon, USA. The long-section of the dam showed that the horizontal conduit ends in a stilling basin. Wave action was experienced in the stilling basin which sealed the exit of the outlet conduit for short periods. The intake air was compressed when the conduit outlet was chocked by the waves. This resulted in the compressed air being released both downstream and upstream - the latter called the blowback of the compressed air. There are similarities between this case study and the Berg River Dam in the basic mechanism that causes air blowback (Berg River Dam has a constriction for the radial gate chamber at the outlet).

Figure 2.20 shows the suggested design curve for tunnel/conduit exits which had been based on model and prototype data (USACE, 1980). Please note that the elevation of the hydraulic grade line (pressure gradient line or water surface) at the exit is lower than the soffit/crown of the conduit, thus the flow inside the conduit is unrestricted, since flow depth (y_p) is less than the conduit diameter (D). To prevent blowback it is recommended that flow in high headed outlet, flowing partially full, is never constricted by any structure or mechanism further downstream in the conduit.

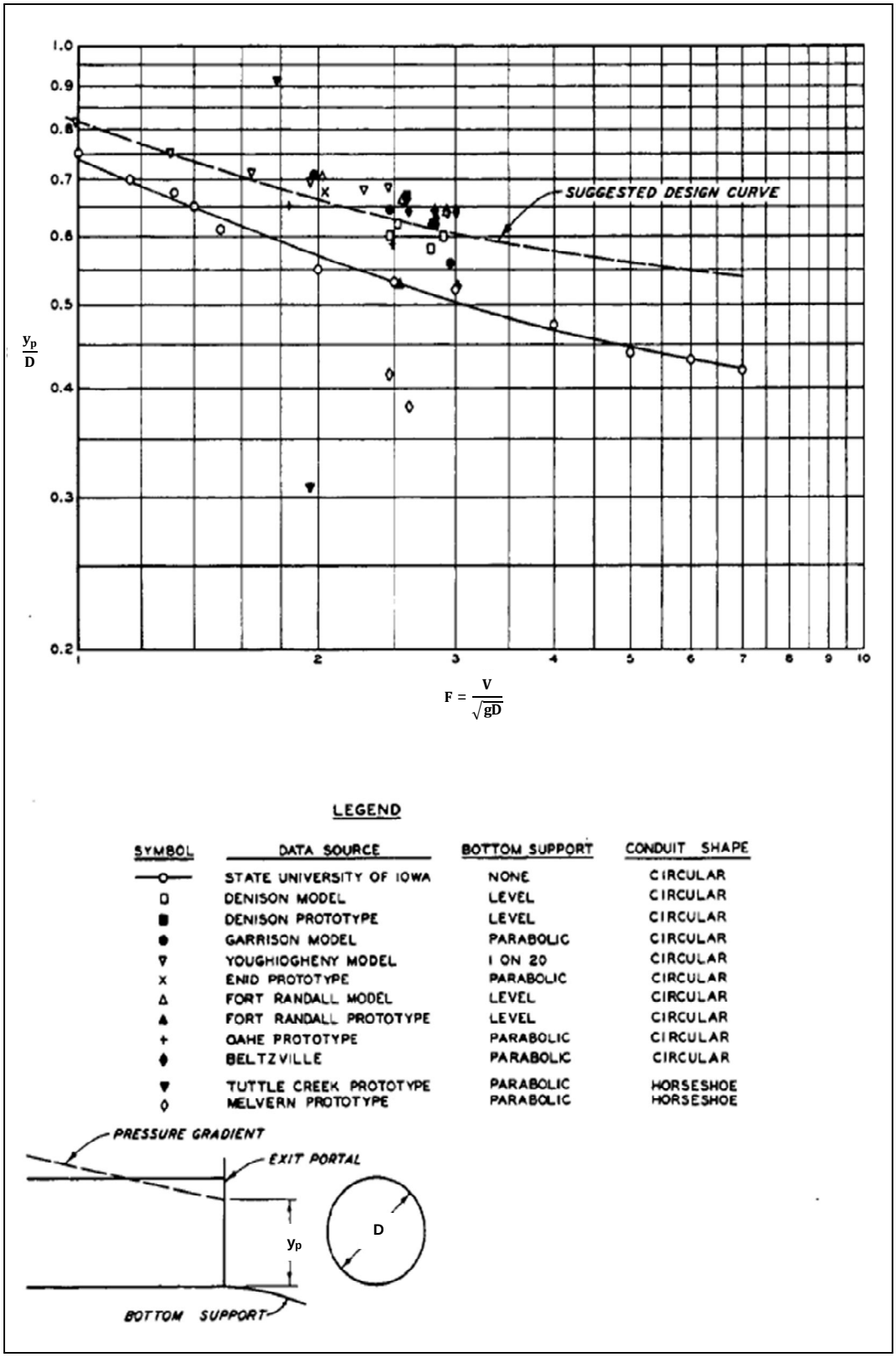

Figure 2.20: Exist Portal Pressures

3. MODEL OF THE BERG RIVER DAM

3.1 General Description of the Model

A hydraulic model of the Berg River Dam was constructed to simulate the closure of the emergency gate under similar water levels and intake gate configuration as at the time of the commissioning test in 2008 (refer to **Figure 3.1**) (report on 2008 commissioning test is attached in ***Addendum B***).

The model was constructed inside the hydraulics laboratory of Stellenbosch University in Stellenbosch, South Africa. The laboratory protected the model from the weather and provided a sufficient water supply from the sump pumps and a constant head tank to imitate the release of the high flows. It also provided other important services necessary for the construction and operation of the model of the Berg River Dam.

The extent of the model was chosen in order to ensure that no artificial conditions would impose on the model by ensuring that the boundaries were far enough from the critical sections in order not to have an impact on the results. The physical model included a distance of 7.6 m (101.51 m converted to prototype value) upstream of the emergency gate and 15.3 m (214.58 m converted to prototype value) downstream of the emergency gate. The total length of the model was 22.5 m (316.09 m converted to prototype value). The main components are demonstrated by means of **Figure 3.1**.

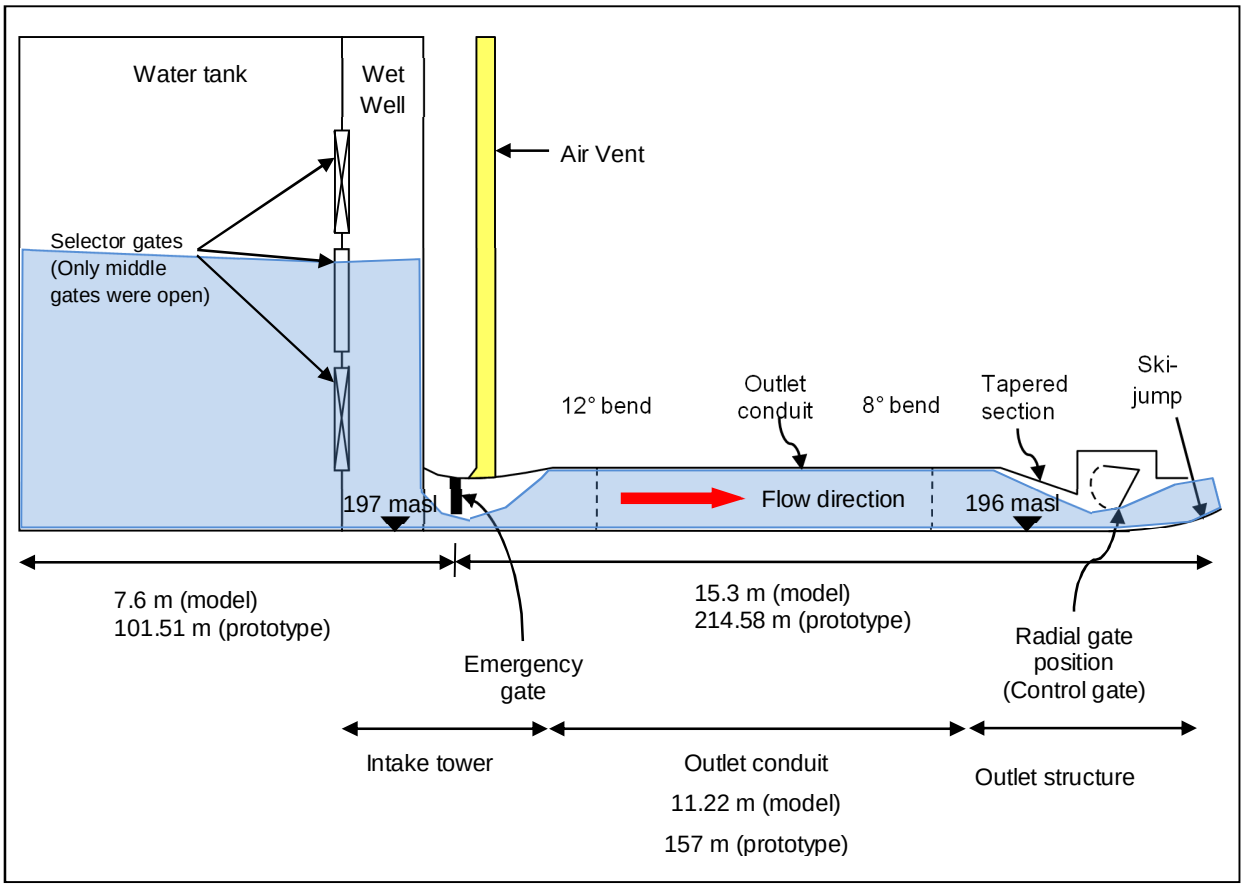

Figure 3.1: Cross-section of Berg River Dam model

The model consisted of the following main components:

- Water supply
- Water tank
- Wet well
- Outlet conduit
- Emergency gate
- Air vent
- Radial gate chamber
- Ski-jump

It should be noted that the parameters recorded in the model study and presented in this thesis have been transformed to reflect the values as would

have been observed in the prototype, unless stated otherwise. Elevations of both the prototype and the model were reduced to meters above sea level (masl).

The photographs (refer to ***Annexure C1***) provide details of the layout of the model and highlight the important components. Refer to ***Annexure C2*** for photographs of the important components of the prototype.

The wet well, which houses the selector gates, was modelled upstream of the emergency gate. Downstream of the emergency gate chamber, which had a rectangular cross-section of 3.8 m x 3.2 m, the outlet conduit, with a diameter of 5.5 m, a 1.8 m^2 air vent, a radial gate chamber and the ski-jump were modelled as shown in **Figure 3.2**. It must be noted that the horizontal angle deflection (12° and 8° bends) of the outlet conduit was also modelled, as it was accepted that it could have some influence on air entrainment. Transparent Perspex was used to model the wet well, air vent, outlet conduit, emergency gate, radial gate chamber and ski-jump to clearly observe the flow behaviour, as well as satisfy the requirements for a smooth surface.

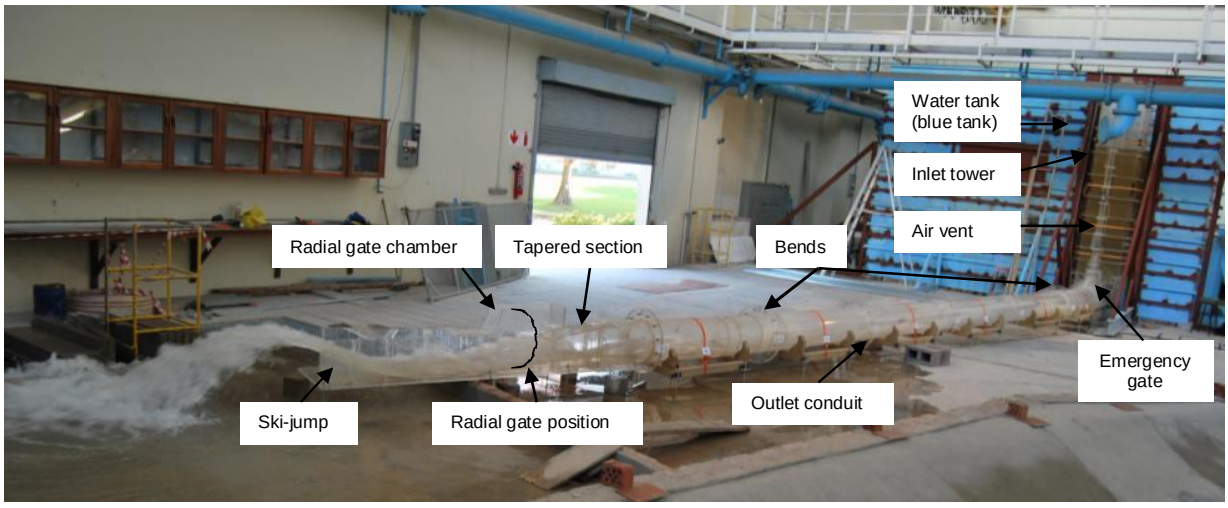

Figure 3.2: Configuration of the model

3.2 Model Scale

The model of the Berg River Dam was designed at a 1:14.066 natural scale. The odd scale of the model was determined by the inside diameter of the available Perspex

pipe that was used to model the outlet conduit. Therefore, the scale of the model could not be a round number.

A free surface gradient was present in the outlet conduit when the largest volume of air was released from the air vent when the emergency gate was about 40% to 30% open. Gravitational and inertial forces were thus the dominant forces that influence the motion of the fluid in the system, therefore the ***Froude's Law*** is the criterion (Webber, 1971).

In this model study the gravity and inertia forces are dominant as discussed above. The accurate modelling of the two phases, air and water flow, require that viscosity and surface tension also be simulated. This implies that the Froude, Reynolds and Weber similarity laws have to be fulfilled simultaneously. If the Froude law is used, the scale should be sufficiently large to minimise the scale effects due to not fulfilling the Reynolds and Weber laws. According to Speerli (1999) a Froude scale model of a bottom outlet should be larger than 1:20. Therefore a scale of 1:14.066 was selected for the Berg River model. Refer to ***Annexure D*** for an exposition of the various scalar laws.

The large scale of the model also made it possible to readily observe the detailed behaviour of the flow.

There is geometric similarity between the model and the prototype, and the flows initiated by the model act in accordance with Froude's Law. The ratio of gravitational and inertial forces acting on the fluid particles is the same in the model and in the prototype resulting in the Froude numbers (F_r) of the model and the prototype to be equal:

$$F_{r_{Prototype}} = F_{r_{Model}} \qquad \textbf{Equation 3.1}$$

The Froude number (Fr) is defined as:

$$F_r = \frac{V}{\sqrt{gL}} \qquad \textbf{Equation 3.2}$$

where

V: flow velocity (m/s)

g: gravitational constant (9.81 m/s^2)

L: characteristic dimension (depth/length)

Using suffix 'm' to denote model and 'p' to denote prototype dimensions, the following scale relationships are true for the model of the Berg Rive Dam for a scale of 1:x, assuming equality of the Froude number and geometric similarity between the model and the prototype:

Linear ratio: $\frac{L_p}{L_m} = x =$ 14.066

Area ratio: $\frac{{L_p}^2}{{L_m}^2} = x^2 =$ 197.852

Volume ratio: $\frac{{L_p}^3}{{L_m}^3} = x^3 =$ 2782.991

Velocity ratio: $\frac{V_p}{V_m} = x^{1/2} =$ 3.750

Discharge ratio: (Velocity ratio) x (Area ratio)

$$\frac{V_p}{V_m} \times \frac{L_p}{L_m} = x^{5/2} = \quad 742.0387$$

Time ratio: $\frac{(Length\ ratio)}{(Velocity\ ratio)} = x^{1/2} = 3.750$

Froude number ratio: ${x_p}^{0.5}/{x_m}^{0.5} = 1$

3.3 Typical Model/Prototype Values

The model and prototype values for the main structures are tabulated in **Table 3.1**.

Table 3.1: Typical Model/Prototype Values

Characteristic	Prototype value	Model value
Conduit invert level of wet well	197 masl	14.01 m
Conduit invert level at radial gate	196 masl	13.93 m
Bottom outlet conduit length	157.8 m	11.22 m
Bottom outlet conduit diameter	5.5 m	0.39 m
Air vent cross section area	1.8 m^2	0.01 m^2

3.4 Measuring Equipment and Techniques

The scientific value of hydraulic models is dependent on the availability of instruments for the accurate measurement of the water level, bed level, pressure, current velocity and direction, temperature and sediment transport (Webber, 1971).

3.4.1 Pressure Measurements

Eight S-10 type pressure transducers were used to measure the static pressures and pressure fluctuations in the water tank, water shaft and outlet conduit.

The positions of the pressure transducers are shown in **Figure 3.3**. One pressure transducer was placed in the water tank and one in the wet well. Six pressure transducers were placed along the floor of the outlet conduit.

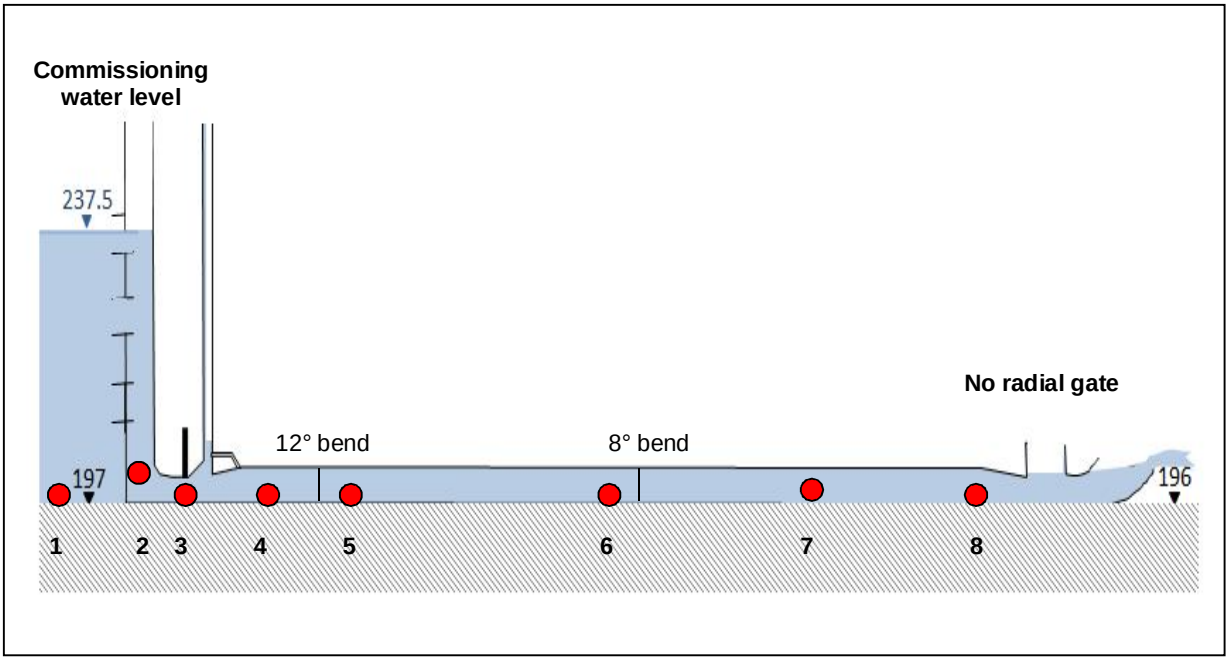

Figure 3.3: Positions of pressure transducers (sectional elevation view)

Two types of S10 pressure transducers were used, namely a 20 mA and 4 mA (selection of transducer type based on maximum range). **Table 3.2** summarises the pressure range of each pressure transmitter type and at which position it had been installed in the model with reference to **Figure 3.3**.

Table 3.2: Pressure Transducers

Pressure transmitters	Maximum measure range	Minimum measure range	Location
20 mA	+ 5 m	- 1 m	1, 2, 3, 4, 5 and 6
4 mA	+ 1 m	- 1 m	7 and 8

The pressure transducers measured the pressure in milli-Ampere (mA). This was converted to Volt (V) by a 120 Ω resistor (R), since V = I x R. In turn, the pressure

measured in Volt was converted to metres (m water), according to **Equation 3.3** and **Equation 3.4** for the 20 mA and 4 mA pressure transmitters respectively:

$$Y_{[m]} = \frac{(+5_{[m]})-(-1_{[m]})}{(20_{[mA]})-(4_{[mA]})} \times \left(\frac{x_{[Volt]}}{120_{\Omega}} \times 1000\right)^{-2.5} \qquad \textbf{Equation 3.3}$$

$$Y_{[m]} = \frac{(+1_{[m]})-(-1_{[m]})}{(20_{[mA]})-(4_{[mA]})} \times \left(\frac{x_{[Volt]}}{120_{\Omega}} \times 1000\right)^{-1.5} \qquad \textbf{Equation 3.4}$$

The frequency of both sets of pressure transducers was 20 Hz, with an accuracy of ±0.5% over the total pressure range, thus 30 mm for the 20 mA pressure transducer and 10 mm for the 4 mA pressure transducer (model values).

3.4.2 Air Velocity Measurements and Direction Indicator

The air velocity in the air vent was measured by means of a Lutron hot-wire anemometer, from which the air discharge was calculated. The probe of the anemometer had a wire, which is heated. The anemometer measured the cooling rate of the wire when air was blowing over it, and this was converted to air velocity (m/s). Refer to ***Annexure D1*** for a photograph of the anemometer used in the study.

The combination of the hot wire and the standard thermistor of the anemometer deliver rapid and precise measurements, even at low air velocities. The measurement range of the anemometer is between 0.2 m/s and 20 m/s, which are measured at a resolution of 0.1 m/s. It has a ±5% accuracy over the total measurement range (0.2 m/s to 20 m/s), thus ±0.01 m/s at 0.2 m/s and ±1 m/s at 20 m/s. The apparatus had a frequency of 0.8 Hz.

A wind direction indicator that was constructed by Stellenbosch University was installed in the top section of the air vent in order not to impose on the air velocity within the air vent. This apparatus had a mechanical flap that would be in the zero position (horizontal) if no wind was blowing in the air vent and would be directed in the direction of the wind if air was being sucked into or released from the air vent. Air

sucked into the conduit was indicated by a positive sign (+), and air released from the air vent by a negative sign (-).

The wind direction indicator was not accurate for air velocities less than 0.5 m/s (model).

3.4.3 Water Discharge Measurements

The water flow discharge (Q_W) was measured with an electromagnetic flow meter (SAFMAG).

Applying **Equation 2.7**, as defined by Kalinske and Robertson (1943), the air demand ratio (β) was calculated by substituting the air velocities (Q_a) and discharge (Q_W) values as measured from the Berg River Dam model.

3.5 EXPERIMENTAL PROCEDURE

3.5.1 Role of Student

The author performed all the tests on the Berg River Dam model herself with the help of three other people (one person controlling the electric motor of the emergency gate and two persons controlling the water inlet valves). The author took the lead of all the tests performed on the model under the guidance of the study leader, Professor G.R. Basson. The author also collected and processed all the measured data herself in order to determine the reasons causing air to be released from the air vent of the Berg River Dam.

3.5.2 Experimental Boundaries

The emergency gate of the model was never fully closed (smallest gate opening: 20% open), as it was feared that the gate made of Perspex may be damaged under the pressure load of the water in the tank.

Only the two middle selector gates (refer to **Figure 3.1**) of the wet well were fully open for the duration of all the tests performed on the model, similar to the conditions in the field during the commissioning test in 2008.

The required water flow was supplied through a pipe that was linked to a constant pressure tank and a pump. The supply system fed the water into the model by pouring the water into the stabilisation tank. The flow approaching the inlet shaft was smoothed by installing a perforated plate and net (acting as baffles) in the stabilisation tank. The required water flow was obtained by keeping the water level in the tank constant at the water level under evaluation. An electric motor was used to close the emergency gate in order to obtain the required gate closure rate.

3.5.3 Stationary Emergency Gate Closing Simulations

Tests were conducted on the model (according to the as-built drawings – refer to **Figure 3.1**), initially with stationary emergency gate openings in order to examine the water and air flow requirements for each gate opening under steady flow conditions. The stationary gate openings used were from a 100% open to 20%, incremental changes being 10%.

The water level in the tank was kept constant at a level that corresponded with the water level measured during the commissioning test in 2008 (237.5 masl).

At each gate opening, as discussed above, the air velocity and direction in the air vent, the pressures in the conduit and the water discharge were measured. The gate was lowered slowly between each gate opening interval, after which there was a pause of approximately two minutes in order for the flow conditions to stabilise (no ripples or waves on the water surface in the water tank and the hydraulic jump pushed out of the conduit).

3.5.4 Transient Gate Closing Simulations

A total of 29 tests were conducted on the model with its configuration according to the **as-built drawings** (refer to **Figure 3.1**). The air flow in the air vent, water discharge and pressures in the conduit were measured. These tests were run at four (4) different gate closure times (continues gate closure) as depicted in **Table 3.3**.

Table 3.3: Gate Closure times

Gate Closure time number	Gate Closure Time (Model) 100% to 20% gate opening	Gate Closure Time (Prototype) 100% to 20% gate opening	Gate Closure Time (Prototype) 100% to 0% gate opening (if gate would have been fully closed)	Comment
1	4 min 16 sec	16 min	20 min	A 20 min emergency gate closing rate used during the **commissioning test of 2008** (Basson, 2011).
2	2 min 30 sec	9 min 23 sec	12 min	Designed emergency gate closure rate (12 min) according to the **Berg River Dam design report** (Van Vuuren, 2003).
3	1 min 17 sec	4 min 48 sec	6 min	Time was chosen to investigate the flow conditions for a **shorter** gate closure rate.
4	6 min 24 sec	24 min	30 min	Time was chosen to investigate the flow conditions for a **longer** gate closure rate.

The initial gate closure rates of 12 minutes and 20 minutes were selected on the basis of the design manual for operating the emergency closing gate (Van Vuuren, 2003) and the emergency gate closure rate used in the Commissioning Test of 2008 (Basson, 2011) respectively, as listed in **Table 3.3**. Further rates were selected as the experimental work progressed, namely six minutes and 30 minutes. However, it was found that the air velocity in the air vent was independent of the emergency gate closure rate, but increased with increasing water head (higher head = higher air velocity). Given this, the initial stationary gate simulations were not redone to include the six minute and 30 minute closure rates.

The transient gate closing simulations were also conducted at three (3) different water levels for each of the four abovementioned gate closure rates. The water levels are summarised in **Table 3.4**.

Table 3.4: Water Levels

WATER LEVEL NAME	PROTOTYPE (masl) [Datum = bottom of outlet conduit at air vent = 197 masl]	MODEL (masl) [Datum = bottom of outlet conduit at air vent = 14.01 masl]
Full supply water level	250.0	17.8
Commissioning test water level	237.5	16.9
Lower water level	232.32	16.5

The *commissioning test water level* corresponds to the water level that was measured in the field during the commissioning test of the Berg River Dam in June 2008. The level where vortices started to form in the water tank (vortex water level) was determined to be 227.12 masl. This is 0.12 m (prototype) above the soffit of the vertical selector gates. The *lower water level* mentioned in **Table 3.4** was taken halfway between the commission test water level and the vortex water level.

The water level in the tank was kept constant at the level under evaluation. A tolerance of 50 mm upwards and 50 mm downwards (0.7 m in prototype) of the water level in the water tank was deemed acceptable. The reason for this assumption was that the water level in the water tank of the model was controlled by hand (the inlet valves were slightly closed when a rise in water level was observed and vice versa when the water level went down). **Figure 3.4** shows the inlet pipe and manually operated valve for the model.

Figure 3.4: Model inlet pipe and valves

4. RESULTS AND FINDINGS

4.1 General

Since the main aim of the thesis is to determine the cause of air flow reversal (air blowback) in the air vent of the Berg River Dam's bottom outlet, tests were performed and presented in the following sequence:

- Tests on the as-built outlet conduit to investigate:
  - Possible vortex air entrainment upstream of the emergency gate which could cause reverse flow in the air vent.
  - Other causes of reverse flow in the air vent.
- Tests on modifications to the as-built outlet to solve/mitigate the air flow reversal phenomena.

The logic way of performing model tests on the as-built outlet of the model would be to calibrate/verify the model with the prototype recordings. The only air flow recordings available for the purpose at the time of the thesis were the observations made during the outlet commissioning exercise. The recordings of the outlet commissioning test would first be presented and its suitability for calibration discussed.

4.2 Calibration of Berg River Dam model

Figure 4.1 shows the measured air velocity in the air vent for the commissioning test of 2008 in the field. The last air velocity measured (45 m/s guessed) in the field occurred at a gate opening of 22.2%, just before the Mentis grid cover blew off the top of the air vent, injuring the observer (refer to ***Annexure C*** for a report on the commissioning test of 2008).

It must be pointed out that the field measurements were done intermittently (not continuously) with a hand-held anemometer which recorded only velocity and not direction. The observer commented at about 40% gate opening the air flow was surging at 10 cycles per minute. Since the air direction was not recorded continuously it could be at this stage that intermittent in and outflow occurred in the air vent. The field recordings were therefore not ideal and more rigorous recordings

(instrumentation recording on a continuous basis both velocity and direction) in future is required.

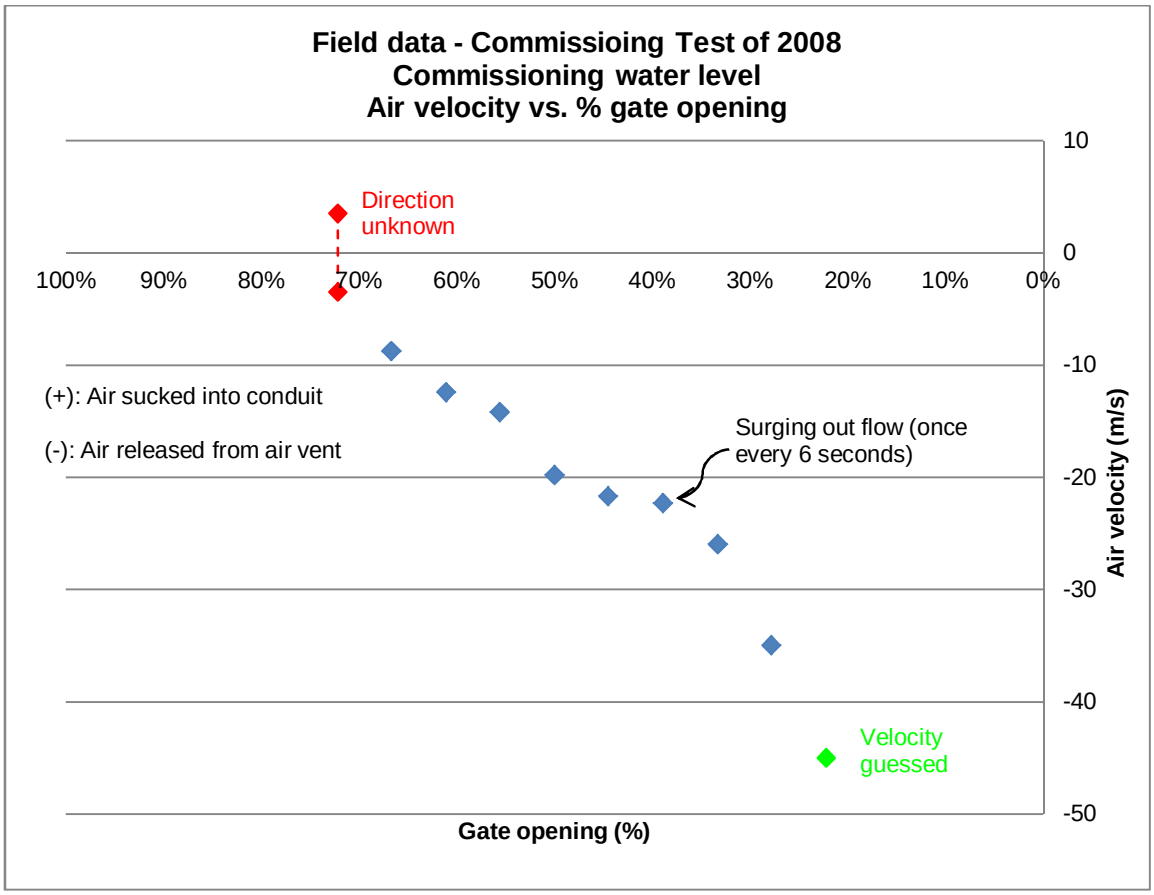

Figure 4.1: Air flow recordings of commissioning test of 2008

The deficiencies of the air flow observations of the commissioning test of 2008 are as follows:

i. Hand-held anemometer only measured the velocity and not the air direction.
ii. Velocities were recorded once every minute and not continuously.
iii. Although outflow was observed at a frequency of about six seconds, it is not certain if downward flow occurred between outflow surges. A cyclic in-out flow can only be recorded on continuous basis with both velocity and direction sensors. The human experience of outflow (**Figure 4.2 (a)**) from a conduit is more pronounced than the inflow (**Figure 4.2 (b)**) which is more subtle.

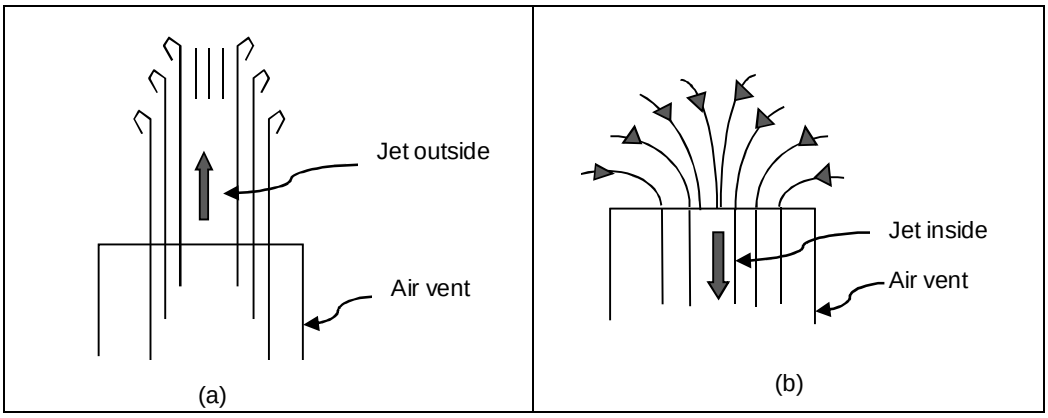

Figure 4.2: Schematic sketch of outflow (a) and inflow (b) into air vent

From the listed deficiencies it is not impossible that the manual velocities recorded could mainly be the outflow velocities – it would be the human tendency to measure when one sense/feels the out-flowing jet. The suitability of the commissioning air flow recordings for calibration purposes is therefore doubtful. Due to time constrains of this thesis, proper field recordings of air velocity and direction could not be performed during the thesis investigation period.

4.3 Tests performed on as-built outlet conduit model

4.3.1 Radial gate partially closed

At the outset of the thesis it was believed that the radial gate was *not* fully opened during the prototype commissioning test in 2008. Later, however, it came to light that the radial gate was in the fully open position during the commissioning test.

Most of the tests performed on the 1:14.066 model of the Berg River Dam were done with the radial gate *fully* open. This was done to determine the reasons for the release of air from the air vent which occurred during the 2008 Commissioning Test, and also because it was how the prototype was designed (Basson, 2011).

A test was performed on the **as-built** outlet conduit on the initial assumption that the radial gate was not in the fully open position. This test was performed at commissioning water level (237.5 masl) with the radial gate closed by 197 mm

(prototype) in order to restrict the water discharge to 204 m^3/s (measured by electromagnetic flow meter) as depicted in (**Figure 4.3**).

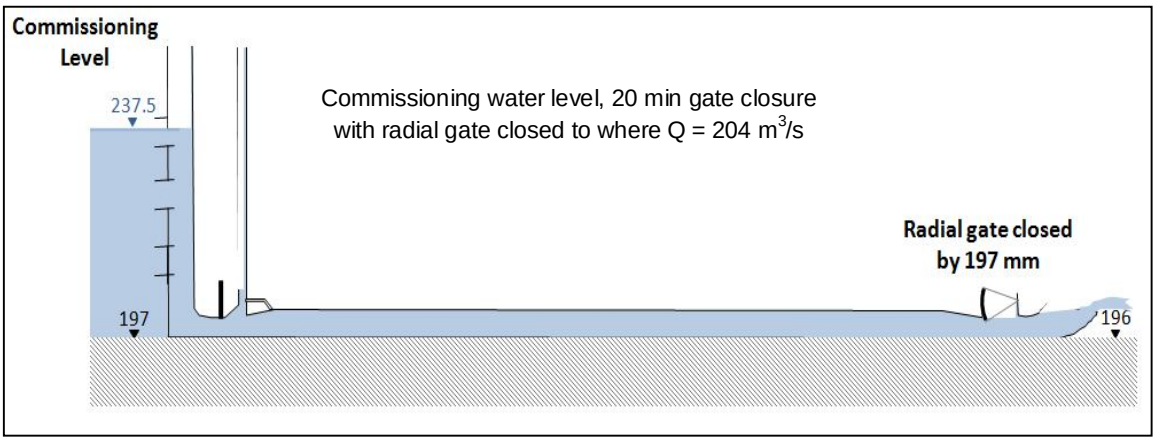

Figure 4.3: Partial closed radial gate test

It was observed that the flow patterns were very similar to the tests performed with the radial gate 100% open which is discussed under **Section 4.3.3.2.2**. The pressures were slightly higher and the air outflow occurred slightly later during the emergency gate closure when the results are compared to the tests with the radial gate 100% open. The sensitivity analysis showed that the partially closed gate (0.197 m or 5.8% closed) had a minimal effect on the flow. Therefore, the tests done on the model with the radial gate 100% open (as discussed under **Section 4.3.3.2.2**) were not repeated with the radial gate closed by 197 mm (prototype).

Please refer to ***Annexure F*** for the comparison between the tests performed with the radial gate partially closed and with the radial gate 100% open on the as-built outlet conduit at commissioning water level.

4.3.2 Possible Vortex Air Entrainment Upstream of Emergency Gate

4.3.2.1 Manual stirring

Test on the **as-built** outlet conduit at the commissioning water level (237.5 masl - prototype) where performed to determine if air entrainment upstream of the emergency gate due to vortex formation in the wet well, by means of *manual*

stirring, could cause reverse flow in the air vent. **Figure 4.4** shows the model configuration used.

The abovementioned tests were done with the radial gate closed to where the discharge through the conduit was restricted to 204 m^3/s (radial gate closed by 197 mm – prototype).

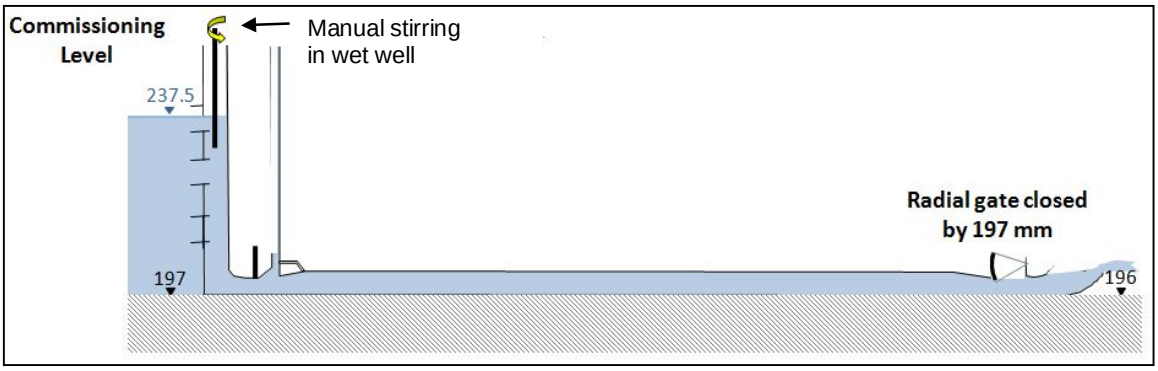

Figure 4.4: Stirring in Wet Well in Attempt to Create Vortices

It was concluded from the results obtained air entraining vortices did not occur in the wet well for any test at the commissioning level (237.5 masl).

4.3.2.2 Without manual stirring

The critical reservoir level at which air is entrained via a vortex, without manual stirring, was determined to be 227.12 masl (prototype). Tests were done on the **as-built** outlet conduit with the radial gate closed by 197 mm (prototype). Refer to **Figure 4.5** for model layout.

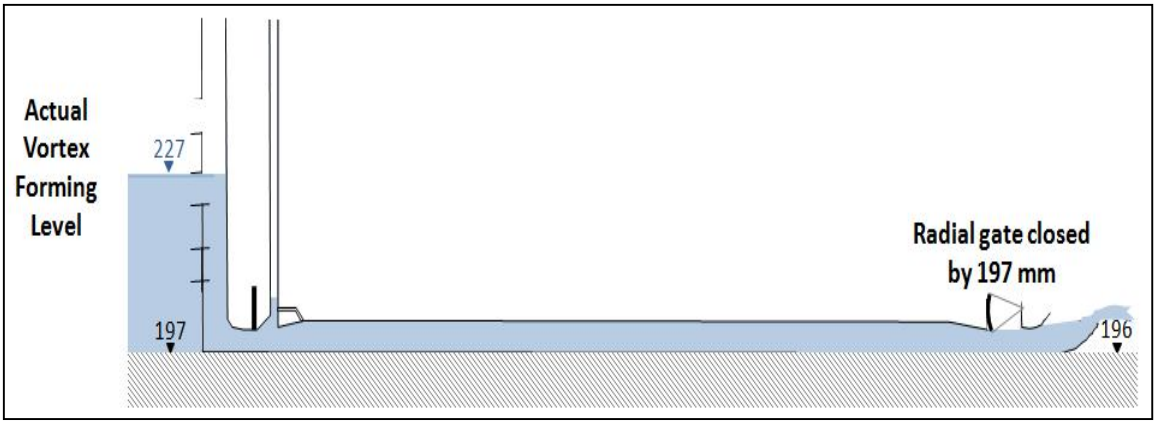

Figure 4.5: Actual Vortex forming water level

The emergency gate was closed while the water level in the wet well was kept at 227.12 masl. The air flow and direction in the air vent and the instantaneous pressure along the outlet conduit were measured for a 20 minute gate closure. The measured air velocity and direction and pressures for the different tests were converted to prototype values and are shown in **Figure 4.10 (a)** and **(b)** respectively.

During gate closure at the vortex formation water level (227 masl), no outflow of air was recorded through the air vent, except during the initial stage (**Figure 4.6**). The air that was sucked in through the vortices travelled down the outlet conduit throughout the duration of the test. However, air velocities of similar magnitude were recorded to those tests performed at commissioning water level with the radial gate partially closed (**Section 4.3.1**). The same trends with pressures, however lower, were recorded.

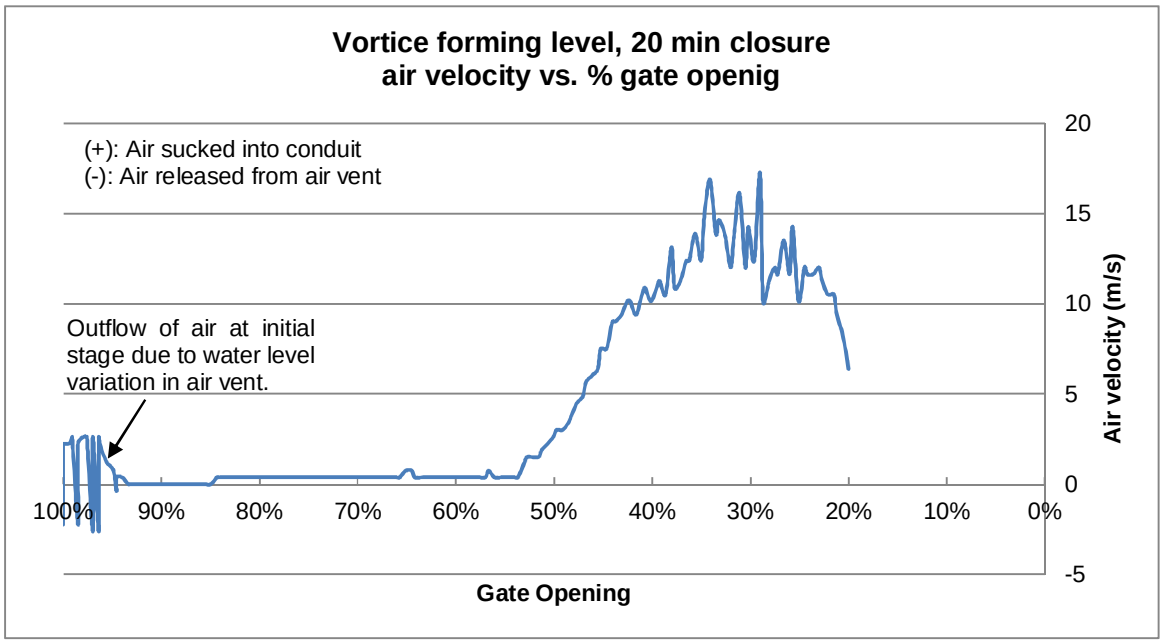

(a)

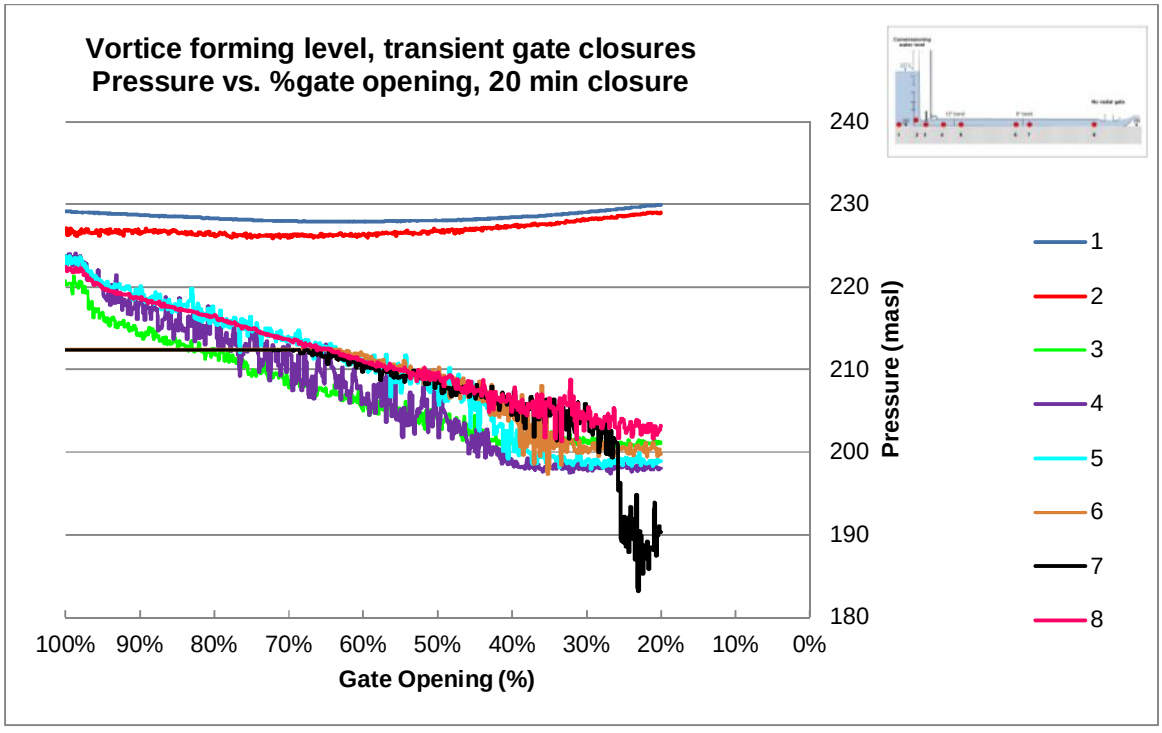

(b)

Figure 4.6: (a) Air velocity and (b) Pressures for transient gate closure rates (vortex water level of 227 masl and as-built, partially closed radial gate)

Gordon (USACE, 1980) has developed a design guideline to help prevent the formation of undesirable vortices, where the intensity of the vortex such that it would draw air and surface debris into the structure as seen in **Figure 4.7**. The critical reservoir level at which air is entrained via a vortex without stirring (227.0 masl) on the Berg River Dam model is compared with the literature in **Figure 4.7**. The results indicated that the intensity of the vortices set up around the intake tower of the Berg River Dam falls inside the “non-vortex” region.

Given the above results of the tests on vortex formation it appears that the formation of vortices is not the reason for the release of air through the air vent.

Observed prototype vortex data at Enid and Denison Dams had been included on **Figure 4.7**.

Please refer to ***Annexure G*** for the results obtained on the as-built outlet conduit at the vortex formation water level with the radial gate partially closed.

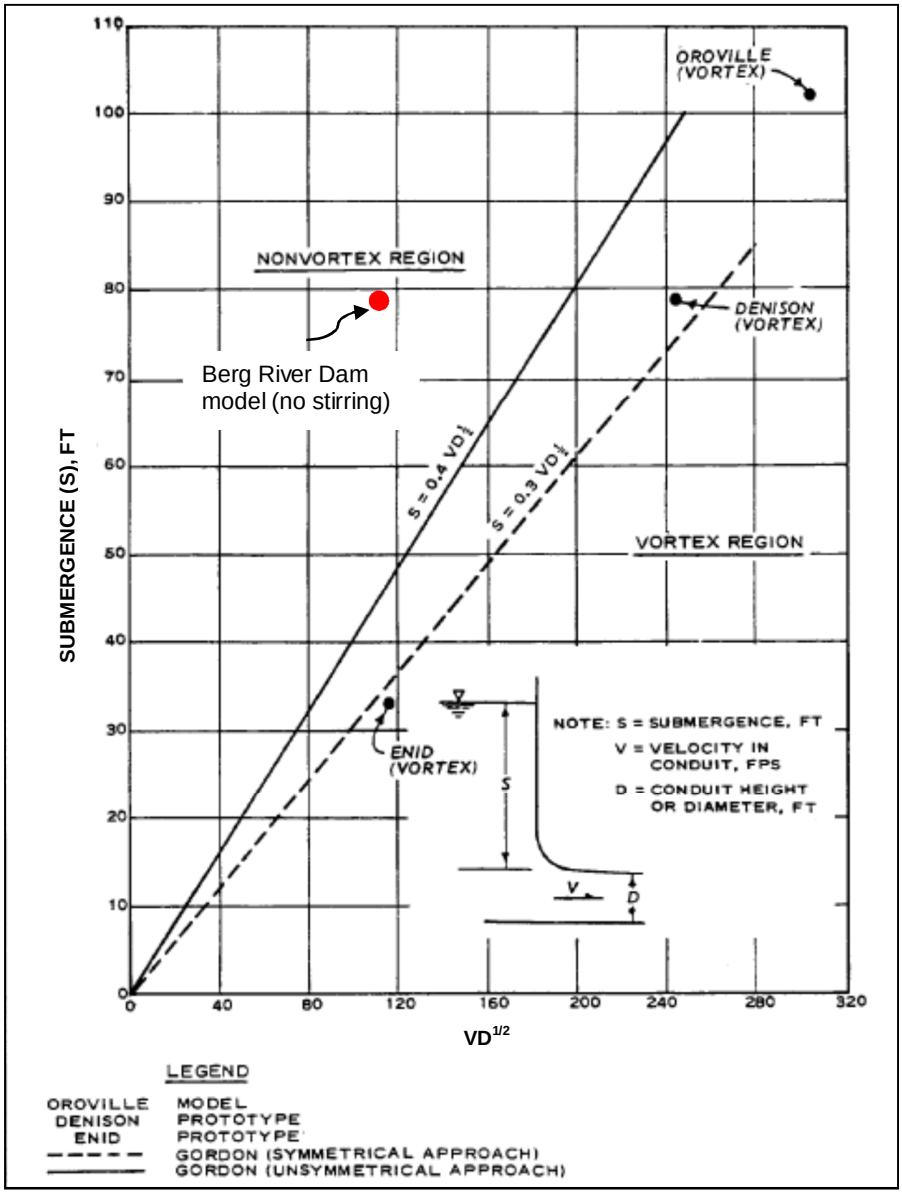

Figure 4.7: Vortex formation chart

4.3.3 Tests to search for other causes of reverse air flow in air vent

4.3.3.1 Stationary Emergency Gate Opening Simulations

The physical model of the Berg River Dam was utilised to simulate the flow conditions in the conduit with stationary emergency gate openings (100% gate opening down to 20% gate opening, at 10% intervals). Stationary gate openings refer to fixed gate openings and not to the continuous closure of the emergency

gate. The required water flow was achieved by keeping the water level in the tank constant, at the water level as for the commissioning test (237.5 masl). The gate was lowered slowly between each gate opening interval, after which there was a stabilisation period of approximately two minutes (no measurements were taken), in order for the flow conditions to stabilise (no ripples or waves on the water surface in the water tank).

It is important to note that the radial gate was not model for these tests, since the radial gate was fully open during the commissioning test of the Berg River Dam of 2008.

Figure 4.8 (a) depicts the average air velocity in the air vent (prototype values) versus gate opening.

No air was released from the air vent for the stationary gate openings, which can be seen in **Figure 4.8 (a).** The phenomenon where air was released from the air vent occurred when the gate was closing (for gate openings between 35% to 25%), but was not displayed by the measured results from the model. The reason for this was that measurements were taken only after the break of two minutes in order to simulate steady flow conditions, and the release of air through the air vent was not reflected by the results. Thus, the phenomenon where air is released from the air vent (air blow back) cannot be investigated by stationary gate opening simulations. The phenomenon where air is released from the air vent only occurred for the transient closing gate simulations, which are discussed in the sections to follow.

The aeration ratio (β) (air discharge/water discharge) was calculated for each gate opening by substituting the measured water discharge and air velocity at each gate opening in **Equation 2.7**. In **Figure 4.8 (b**) the aeration ratio (β) is plotted against the specific gate opening (prototype values).

Two maximum air demand ratios occurred, namely at a 20% gate opening and a 50% gate opening, as seen in **Figure 4.8 (b)**. This corresponds with the literature as shown in **Figure 2.16**.

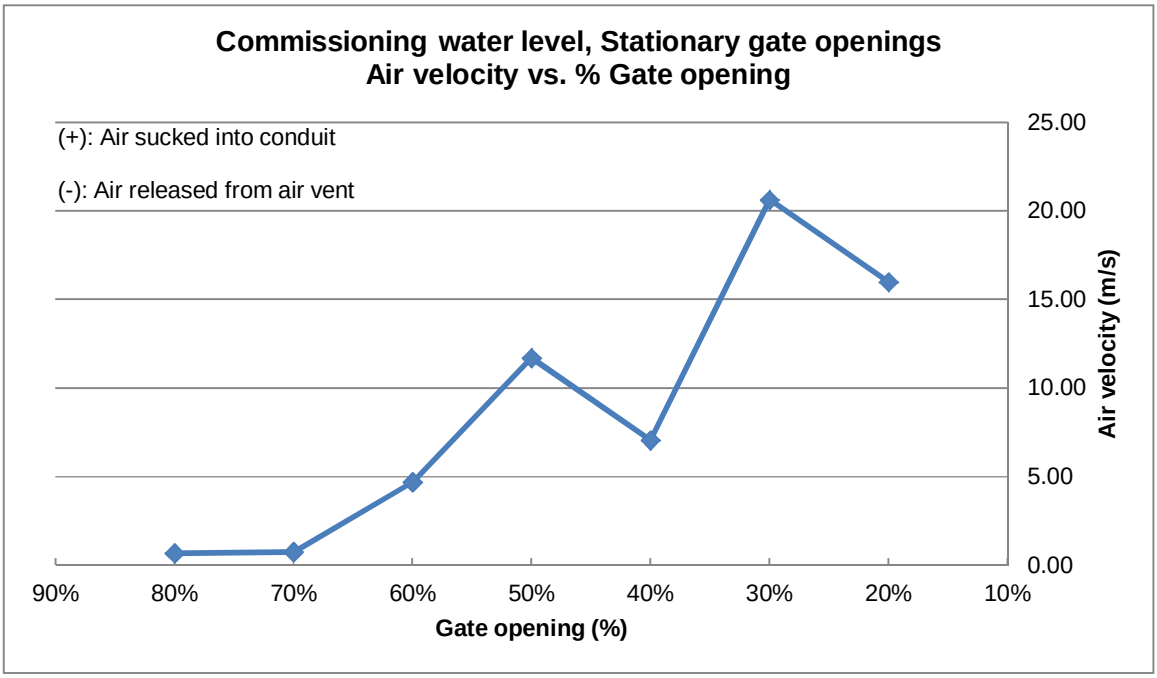

(a)

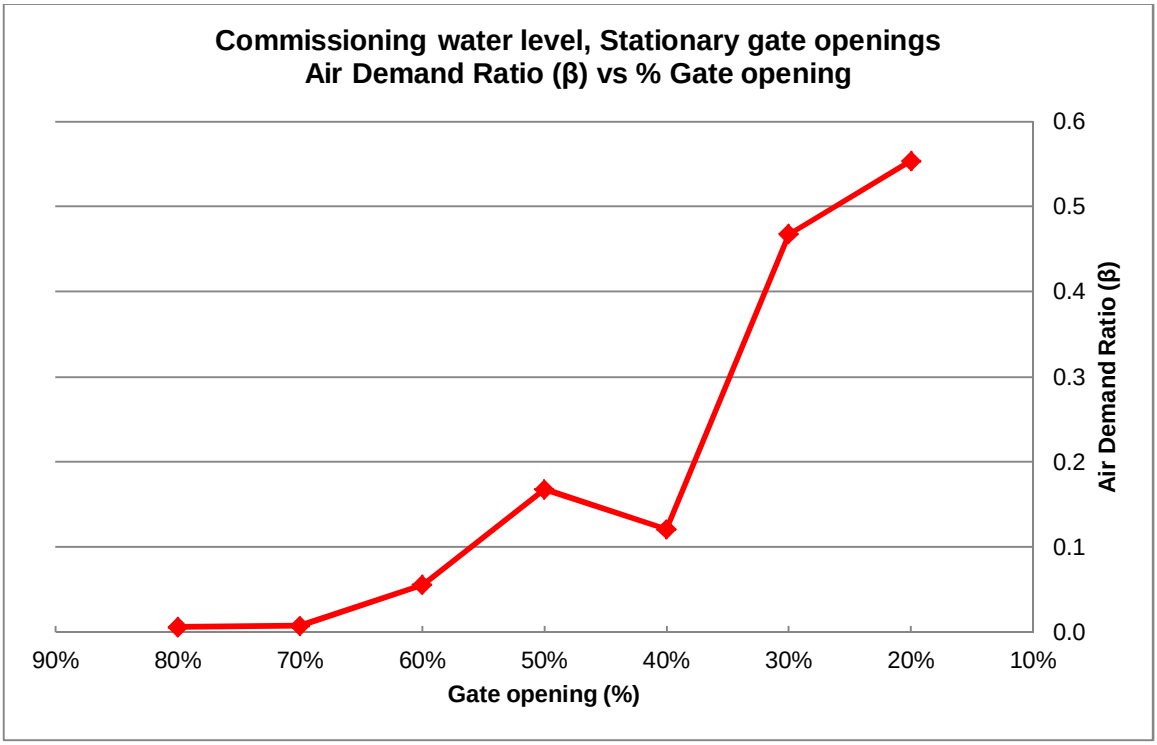

(b)

Figure 4.8: (a) Air velocity and (b) air demand vs. gate opening (commissioning water level, stationary gate)

Figure 4.9 (a) shows the average water pressures measured for each fixed gate opening (100% to 20% in 10% closure intervals and two minute model stabilisation period between readings) at each pressure transducer locations. The commissioning water level was under evaluation. These tests were conducted on the model with its configuration according to the as-built drawings.

No negative pressures were recorded.

The pressures in the water tank (reservoir) and water shaft (wet well) were relatively constant for all the different gate openings (position 1 and 2). This means that the water level in the tank was kept relatively constant at the required water level for the duration of the test.

Figure 4.9 (b) depicts the pressures for each gate opening along the distance of the conduit for the stationary gate opening simulations. It is evident from **Figure 4.9 (b)** that the pressures decrease drastically for emergency gate openings of 50% and smaller. The pressures along the conduit for gate openings of 60% and greater are of similar magnitude.

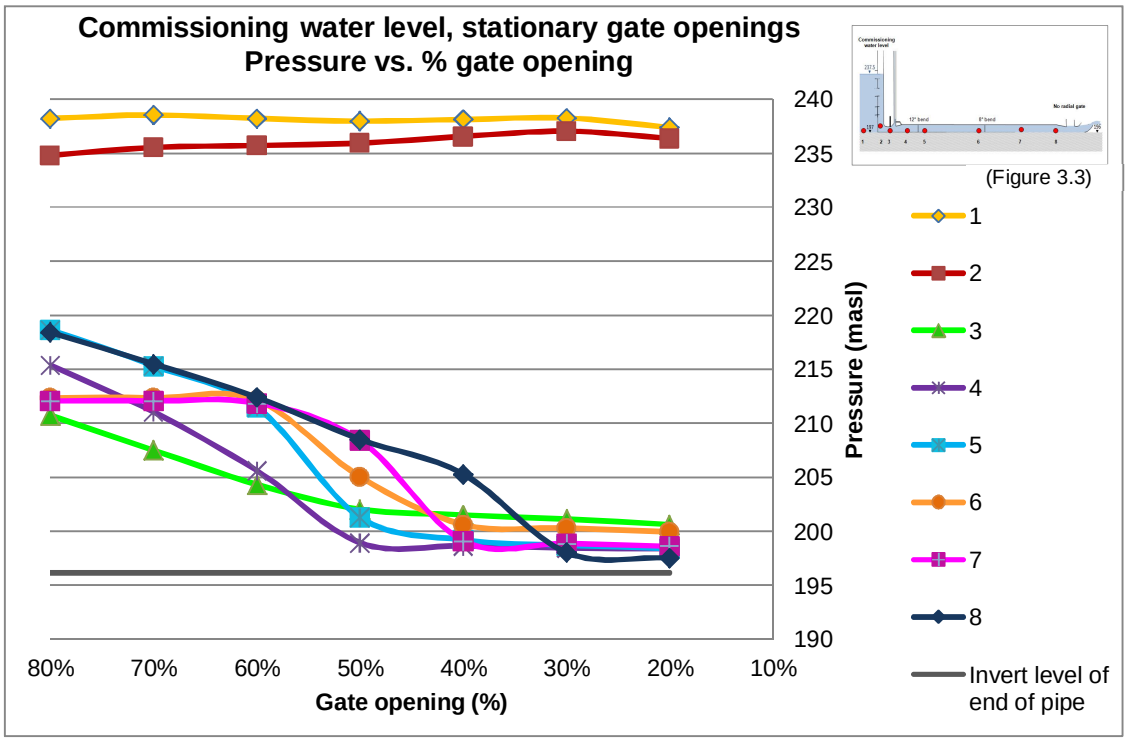

(a)

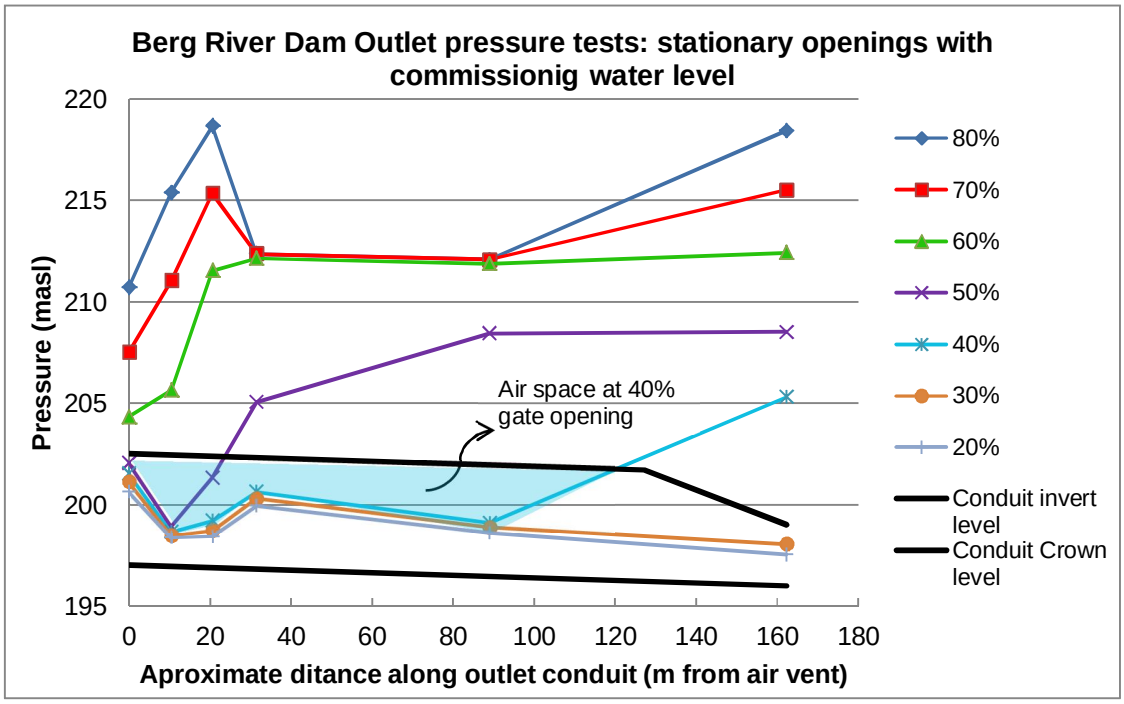

(b)

Figure 4.9: (a) Pressure vs. gate opening and (b) Pressure along conduit per gate opening (commissioning water level, stationary gate)

4.3.3.2 Transient Gate Closure Simulations

4.3.3.2.1 Full Supply Water Level (FSL 250.0 masl)

The air flow and direction in the air vent and the instantaneous pressure along the outlet conduit were measured for the tests conducted on the model with its configuration according to the **as-built drawings**. The tests were run at three (3) different gate closure rates, namely six minutes, 12 minutes and 20 minutes. All the tests were subjected to the full supply water level (FSL = 250 masl - prototype). The measured air velocity and direction and pressures for the different tests were converted to prototype values and are shown in **Figure 4.10 (a)** and **(b)** respectively.

4.3.3.2.1.1 Discussion: Air Velocity and direction (FSL 250.0 masl)

The air flow direction indicator installed in the air vent indicated air being sucked into the air vent with a positive sign (+) and air released from the air vent with a negative sign (-). The air velocity and the corresponding sign (positive or negative) indicating the air direction was plotted against the percentage gate opening in **Figure 4.10 (a)**.

For gate openings between 100% and 65%, the air vent acted as a surge tower (**Figure 4.12**) and the water oscillated in the air vent. Air was released from (negative airflow) and sucked into (positive airflow) the air vent according to the oscillating water in the vent, which can be seen in **Figure 4.10 (a)** for gate openings between 100% and 65%.

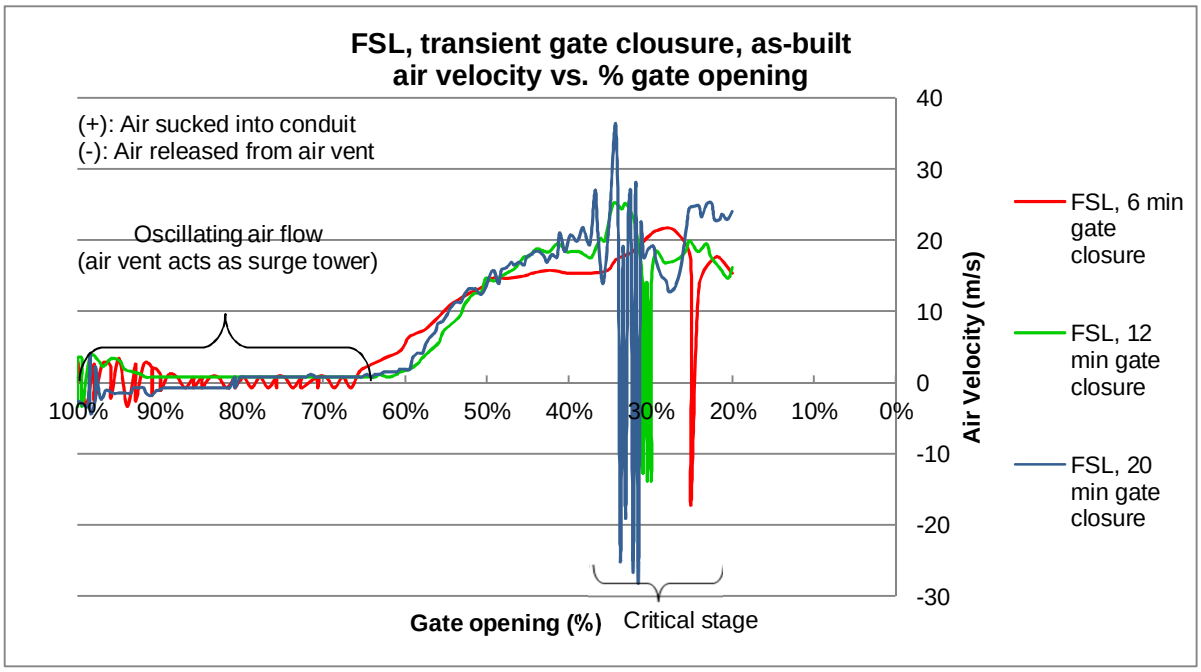

(a)

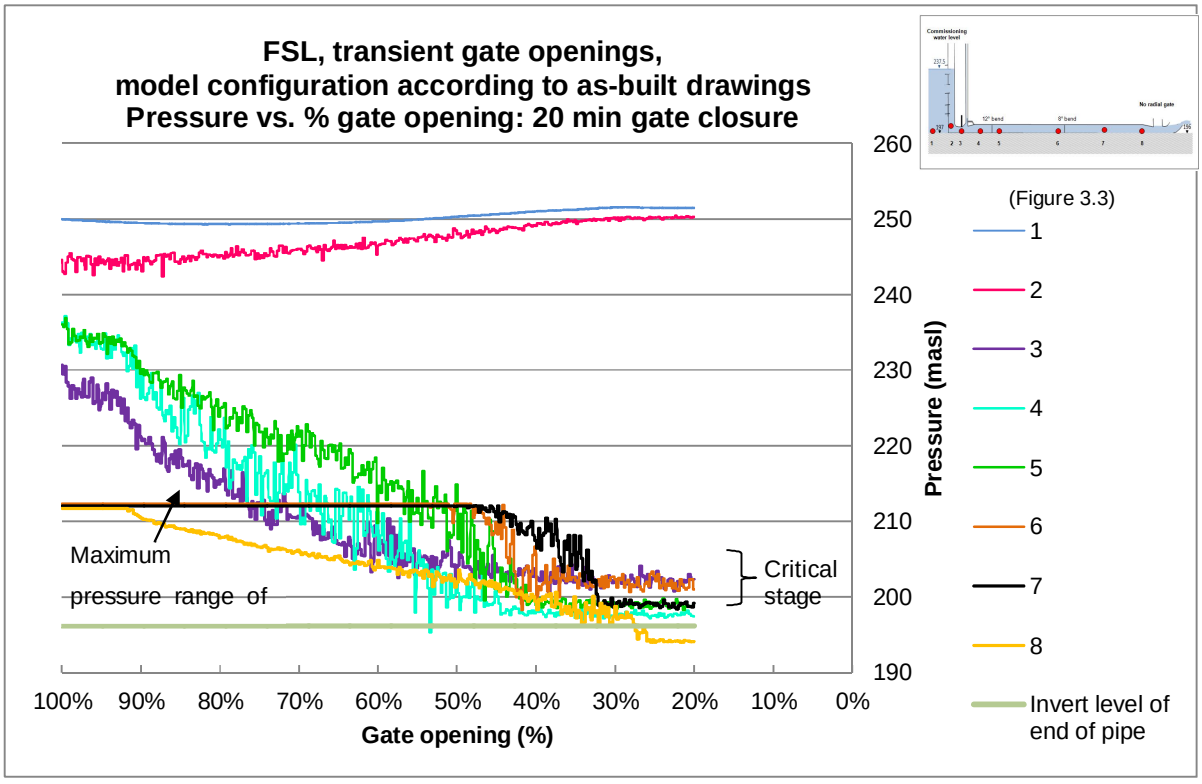

(b)

Figure 4.10: (a) Air velocity and (b) Pressures for transient gate closure (FSL and as-built)

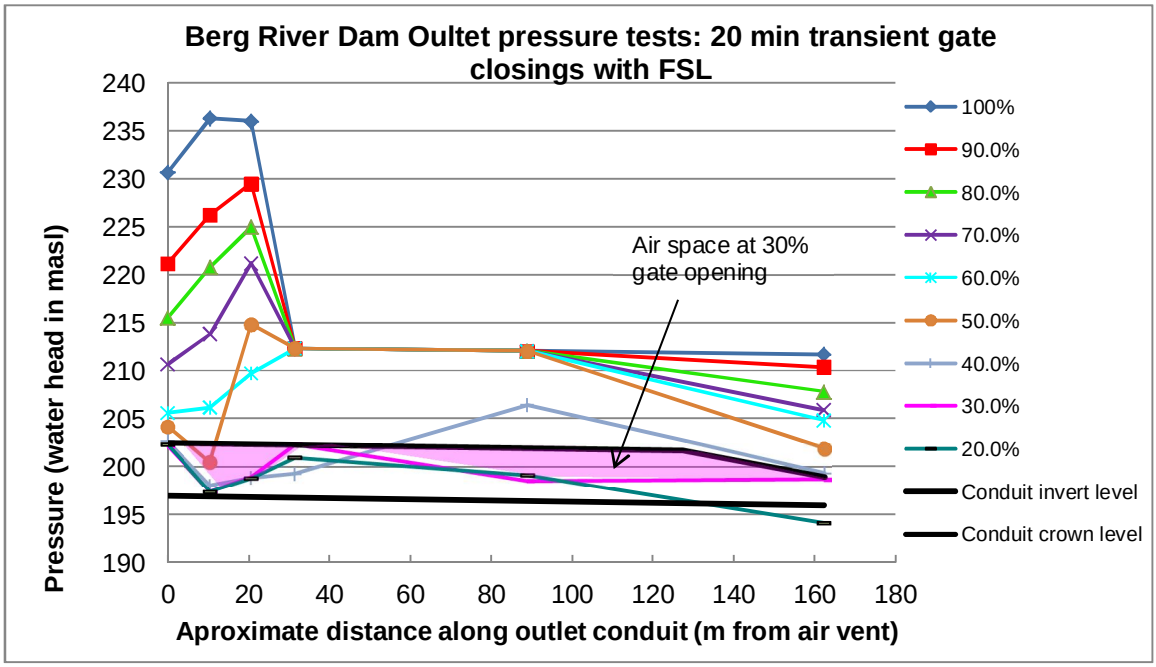

Figure 4.11: Pressure along conduit per gate opening for FSL

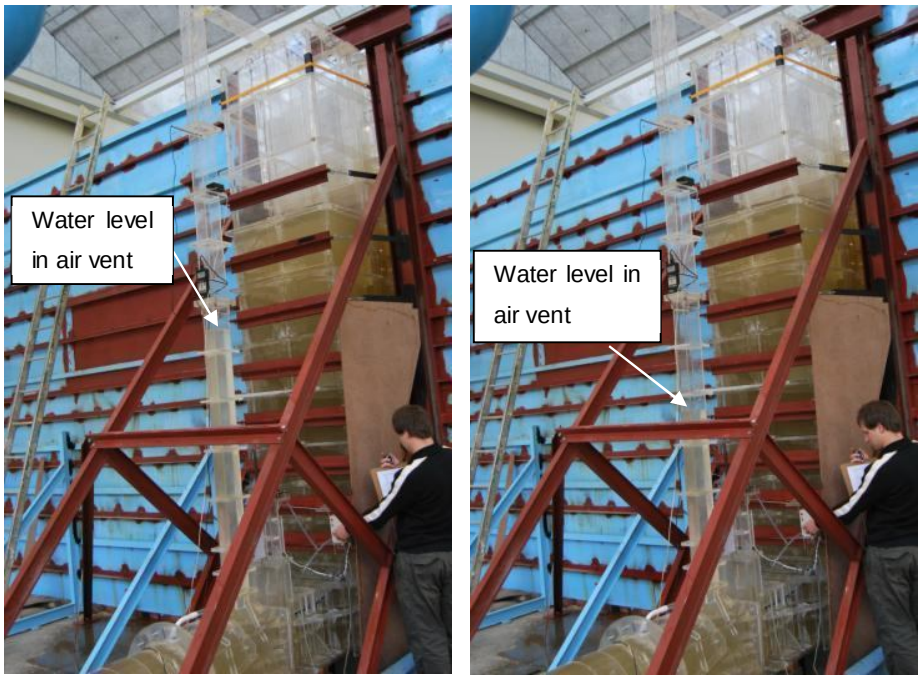

Figure 4.12: Air vent acting as surge tower for 100% to 65% gate opening

It was observed during the gate openings of approximately 35% to 25% critical stage that the air release fluctuated from being sucked in through the air vent to being released. The air flow direction was changing rapidly (approximately four times per every 4 seconds (prototype) which is equivalent to a frequency of 1.0 Hz). It appears that the duration of these fluctuation periods was shorter for the shorter gate closure periods. A probable explanation is that the unstable hydraulic jump has not reached the radial gate at the ski-jump.

Figure 4.10 (a) shows that the movement of air through the air vent is not sensitive to the gate closure rate, because air was still released for gate openings between 35% and 25% (critical stage), irrespective of the specific gate closure rate under evaluation.

The maximum air velocities released from and sucked into the air vent for the three different gate closure rates, with the corresponding gate openings shown in **Figure 4.10 (a)**, is summarised in **Table 4.1**.

Table 4.1: Maximum/Minimum Air flow in Air Vent (FSL, Transient gate, As-built)

Gate closure rate (prototype values)	Gate opening (%)	Maximum air velocity released from air vent (m/s) (prototype values)	Gate opening (%)	Maximum air velocity sucked into conduit (m/s) (prototype values)
6 min	25%	-17.3	29%	21.4
12 min	30%	-13.9	35%	25.1
20 min	31%	-28.1	34%	36.4

It can be seen from **Table 4.1** that, when examining the percentage gate opening versus the maximum air velocity (released or sucked in), the transient conditions are variable. This might be the result of the formation of the unstable hydraulic jump not fully developed from the emergency gate to the radial gate chamber for the faster gate closure rates. The maximum observed air velocities through the air vent were less than the maximum allowable velocity of 45 m/s recommended in the literature.

Refer to ***Annexure H1*** for the air velocity graphs of the various gate opening periods for the FSL.

4.3.3.2.1.2 Discussion: Pressure (FSL)

In **Figure 4.10 (b)** it can be seen that the pressure sensors located upstream of the second bend (pressure transducer number 6) and upstream of the radial gate chamber (pressure transducer number 7) reached their maximum pressure limit for gate openings of 50% and greater, and therefore displayed as a constant (horizontal) line. A steep drop in pressure occurred for gate openings between 33% to 30% at these locations (numbers 6 and 7).

The pressures in the water tank (reservoir – pressure transducer number 1) and water shaft (wet well – pressure transducer number 2) were relatively constant for the duration of the simulation. This means that the water level in the tank was kept relatively constant at the water level under evaluation for the duration of the test.
Negative pressures formed at the radial gate camber (end of the conduit – pressure transmitter number 8 – pressure at 195 masl and elevation at 196 masl) for gate openings of 27% and smaller.

Figure 4.11 depicts the pressures for each gate opening along the distance of the conduit for the 20 min gate closure rate. It is evident from **Figure 4.11** that the pressures decrease drastically for emergency gate openings of 40% and smaller. Lower pressures results in higher flow velocities as the hydraulic gradient is fixed. The pressures along the conduit for gate openings of 50% and greater are of similar magnitude.

Refer to ***Annexure H1*** for the pressure against gate opening graphs of the various gate opening periods subjected to the FSL.

4.3.3.2.1.3 Conclusion (FSL, as-built)

It was observed that the air release fluctuated from being sucked in through the air vent to being released, and that a steep drop in pressure occurred at pressure transducers 6 and 7 (section upstream of the radial gate chamber) during the gate openings of approximately 33% to 30% critical stage when **Figure 4.10 (a)** and **(b)** are compared with each other for the 20 minute gate closure rate. Thus, the drop in

pressure upstream from the radial gate chamber occurred at the same time as when air blow-back occurred in the air vent. The same conclusion was made for the other gate closure rates.

The air velocity in the air shaft was found to be independent of the rate of closure of the emergency gate, but to increase with increasing water head for the range of tests carried out.

4.3.3.2.2 Commissioning Water Level (237.5 masl)

Figure 4.13 (a) shows the air velocity against the gate opening for the tests conducted on the **as-built** outlet conduit. The pressures were measured in the model for the range of tests, but only the pressures for the 20 minute gate closure rate is shown in **Figure 4.13 (b).** The water level under evaluation was the *commissioning test water level (237.5 masl)*. These tests were run at three (3) different gate closure rates, namely 20 minutes, 12 minutes and 30 minutes. The results were converted to prototype values.

4.3.3.2.2.1 Discussion: Air Velocity and direction (Commissioning Water Level, as-built)

For gate openings between 100% and 65%, the air vent acted as a surge tower and the water oscillated in the air vent. Air was released from (negative airflow) and sucked into (positive airflow) the air vent according to the oscillating water in the vent, which can be seen in **Figure 4.13 (a)**.

It is evident from **Figure 4.13 (a)** that the transient conditions are variable, because the maximum air released from and sucked into the air vent occurred at larger gate openings for slower gate closure rates. The reason for this is that the formation of the unstable hydraulic jump from the emergency gate to the radial gate chamber had not developed fully for the faster gate closure rates.

It was also observed from **Figure 4.13 (a)** that, during the critical testing sequence and a gate opening of approximately 37% to 32%, the air release fluctuated between being sucked in through the air vent and being released. The air flow direction was changing rapidly (five times per every 4 seconds (prototype), which is equivalent to a frequency of 1.25 Hz). It appears that the duration of these

fluctuation periods was shorter for the shorter gate closure periods. The explanation is that the formation of the unstable hydraulic jump had not yet exited the outlet pipe (reached the radial gate at the ski-jump), as discussed above.

The maximum air velocity release from the air vent and the maximum air velocity sucked into the conduit for the three different gate closure rates, with the corresponding gate openings shown in **Figure 4.13 (a)**, are summarised in **Table 4.2**.

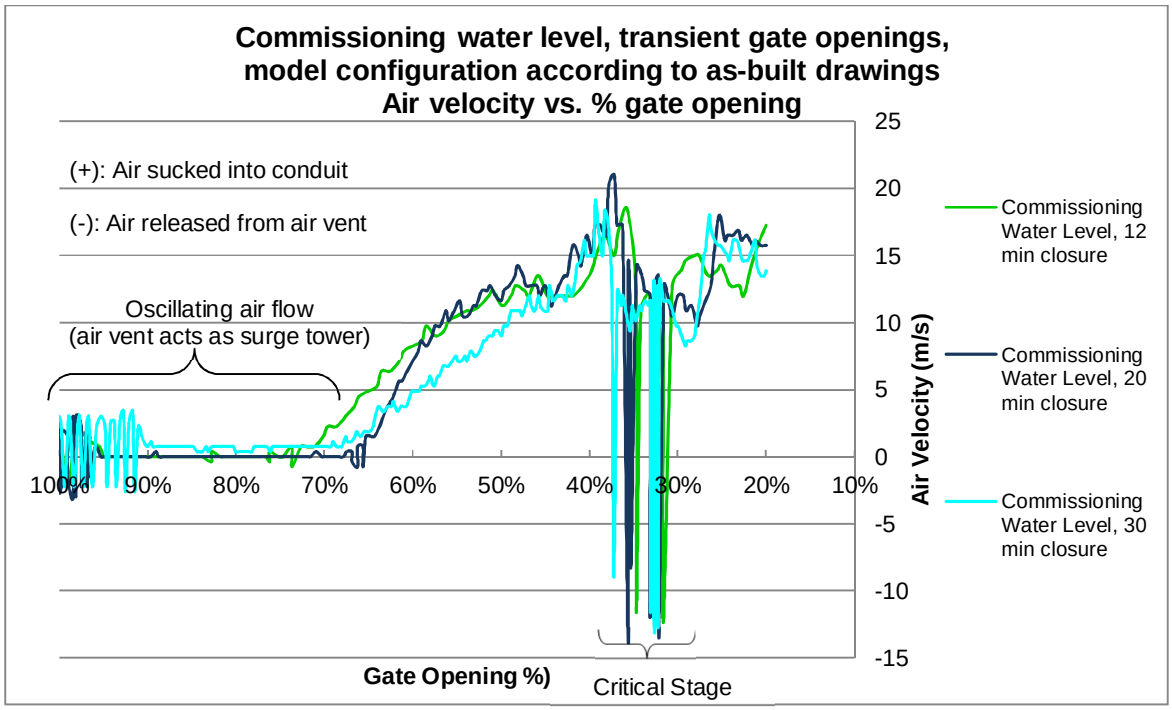

(a)

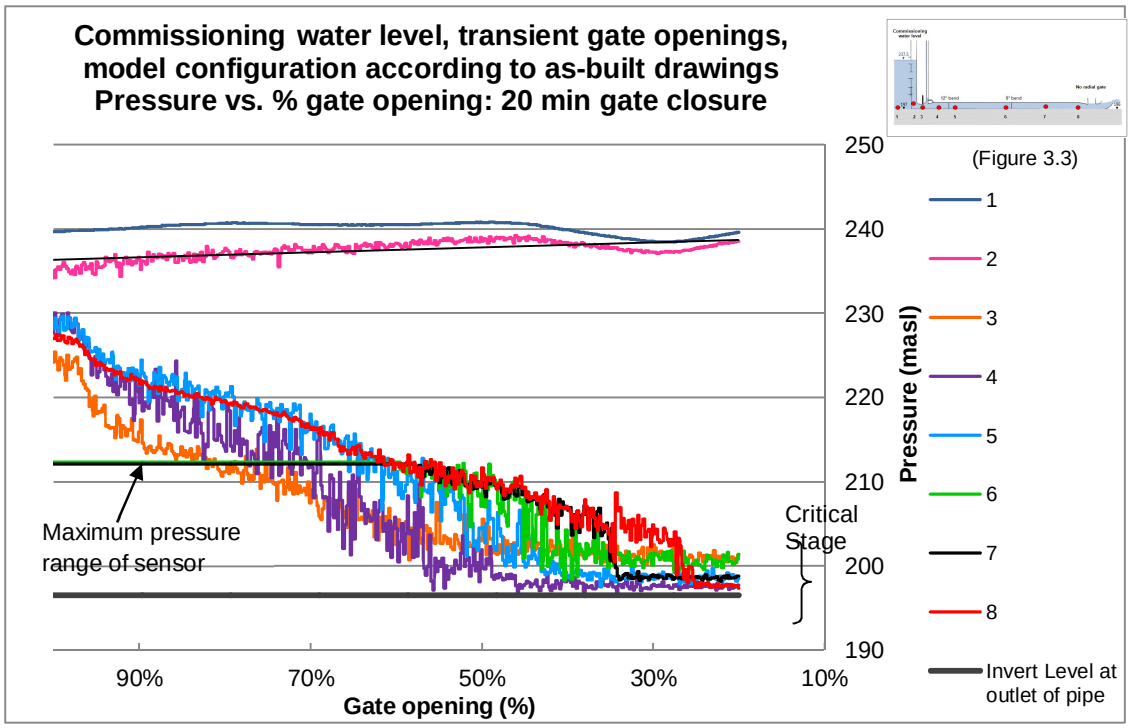

(b)

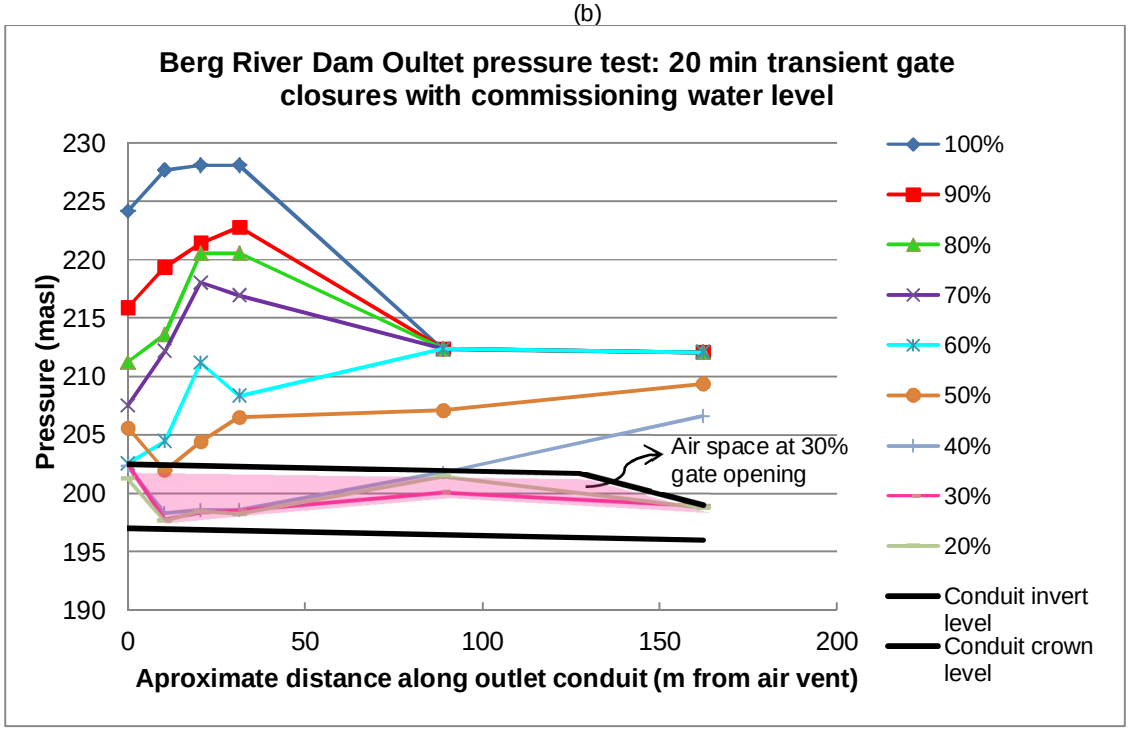

(c)

Figure 4.13: (a) Air velocity, (b) Pressures for transient gate closure and (c) Pressures along outlet conduit per gate opening (Commissioning Water Level and as-built)

Table 4.2: Maximum/Minimum Air flow into Air Vent (Commissioning Water Level, Transient gate, As-built)

Gate closure rate (prototype values)	Gate opening (%)	Maximum air velocity released from air vent (m/s) (prototype values)	Gate opening (%)	Maximum air velocity sucked into conduit (m/s) (prototype values)
12 min	32%	-12.4	36%	18.4
20 min	32%	-13.9	37 %	21.0
30 min	33%	-13.1	39%	19.1

It can be seen from **Table 4.2** that the maximum air velocity released from and sucked into the air vent occurred at relatively the same gate openings for all three emergency gate closure rates under evaluation. Thus, the movement of air through the air vent was not sensitive to the gate closure rate for the range of tests carried out. The maximum air velocities measured through the air vent were less than the maximum allowable velocity of 45 m/s recommended in the literature.

It was observed that the air velocity in the air vent was lower for the commissioning water level than for the FSL when comparing **Table 4.1** and **Table 4.2**. Thus, the air velocity through the air vent increased with increasing water head.

Refer to ***Annexure H2*** for the air velocity graphs of the various gate opening periods for the Commissioning Test water level.

4.3.3.2.2.2 Discussion: Pressure (Commissioning Water Level, as-built)

From **Figure 4.13 (b)** it can be seen that the pressures in the water tank (reservoir – pressure transducer number 1) and water shaft (pressure transducer number 2) were relatively constant for the duration of the simulation for the different gate closure rates. This means that the water level in the tank was kept relatively constant at the water level under evaluation for the duration of the test.

No negative pressures occurred for the 20 minute gate closure rate (**Figure 4.13 (b)**).

In **Figure 4.13 (b)** it can be seen that the pressure sensors located upstream of the second bend (pressure transducer number 6) (48.95 m downstream from wet well – prototype) and upstream of the radial gate chamber (pressure transducer number 7) (106.68 m downstream from wet well – prototype) reached their maximum pressure limit for gate openings of 50% and greater, and therefore displayed as a constant (horizontal) line. A steep drop in pressure occurred for gate openings between 37% to 35% at the section upstream of the radial gate chamber (pressure transmitter number 7).

Figure 4.13 (c) depicts the pressures for each gate opening along the distance of the conduit for the 20 min gate closure rate. It is evident from **Figure 4.13 (c)** that the pressures decrease drastically for emergency gate openings of 50% and smaller. The pressures along the conduit (100 m from emergency gate) for gate openings of 60% and greater are of similar magnitude.

Refer to ***Annexure H2*** for the pressure vs. gate opening graphs of the various gate opening periods subjected to the commissioning water level.

4.3.3.2.2.3 Conclusion (Commissioning Water Level, as-built)

It was observed that the air release fluctuated from being sucked in through the air vent to being released, and that a steep drop in pressure occurred at pressure transducer 7 (section upstream of the radial gate chamber) during the gate openings of approximately 37% to 35% critical stage when **Figure 4.13 (a)** and **(b)** are compared with each other for the 20 minute gate closure rate. Thus, the drop in pressure upstream from the radial gate chamber occurred at the same time as when air blow-back occurred in the air vent. The same conclusion was made for the other gate closure rates.

The movement of air through the air vent was not sensitive to the gate closure rate for the range of tests carried out, since air was still released from the air vent and the steep drop in pressure occurred, irrespective of the specific gate closure rate under evaluation.

These results correspond to the results obtained for the simulations with the FSL under evaluations, as discussed in **Section 4.3.3.2.1**.

4.3.3.2.3 Lower Water Level (232.32 masl)

The air flow and direction in the air vent were measured for the tests conducted on the **as-built** outlet conduit for various gate closure rates and are shown in **Figure 4.14 (a)**. The pressures were measured in the model for all the tests, but only the pressures for the 20 minute gate closure rate is shown in **Figure 4.14 (b)**. The water level under evaluation was the Lower Water Level (232.32 masl – prototype) which is exactly halfway between the Commissioning Test Water Level (237.5 masl) and the Vortex Water Level (227.12 masl) as discussed in **Section 3.5.4**.

4.3.3.2.3.1 Discussion: Air Velocity and direction (Lower Water Level, as-built)

For gate openings between 100% and 65%, the air vent acted as a surge tower and the water oscillated in the air vent. Air was released from (negative airflow) and sucked into (positive airflow) the air vent according to the oscillating water in the vent, which can be seen in **Figure 4.14 (a)**.

Figure 4.14 (a) shows that the movement of air through the air vent was independent to gate closure rate, as air was released from and sucked into the conduit at relatively the same gate openings for the different gate closure rates. However, it was observed that the air velocity in the air vent was lower for the lower water level than for the commissioning water level and FSL. Thus, the air velocity through the air vent is directly related to the water head.

From **Figure 4.14 (a)** it can also be seen when observing the percentage gate opening against maximum air velocity that the transient conditions are variable. The reason for this is that the formation of the unstable hydraulic jump had not developed fully for the faster gate closure rates. These results correspond to the results obtained for the simulations with the FSL and commissioning water level under evaluation, as discussed in **Sections 4.3.3.2.1.1** and **4.3.3.2.2.1** .

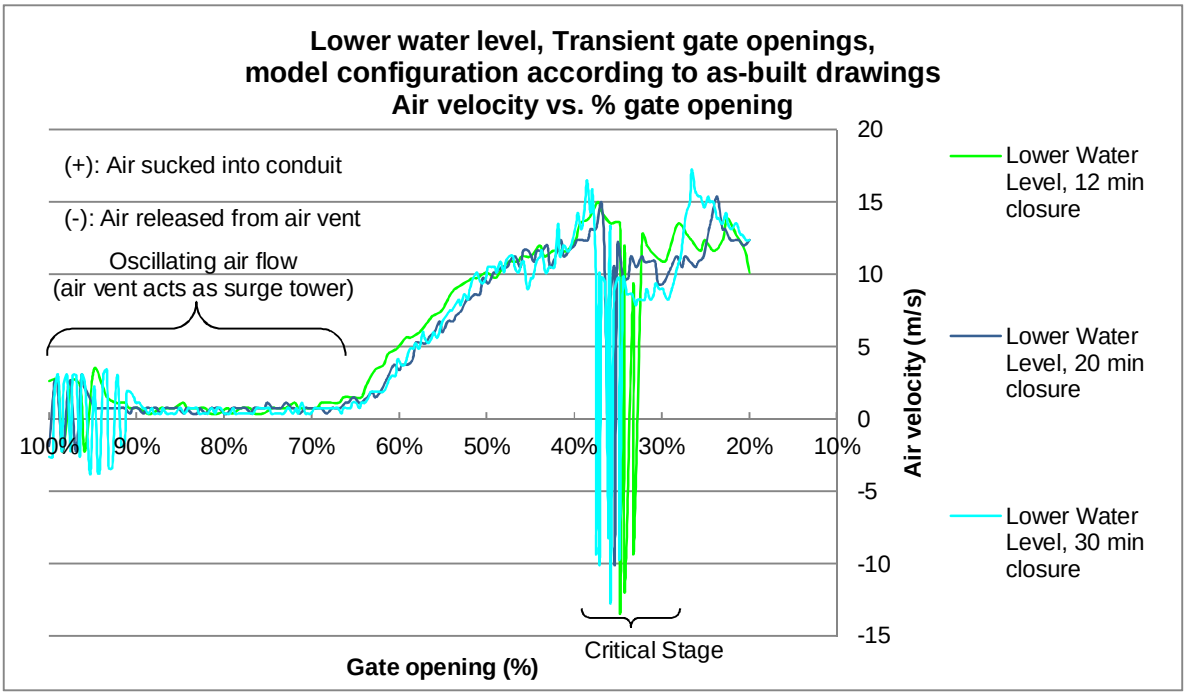

(a)

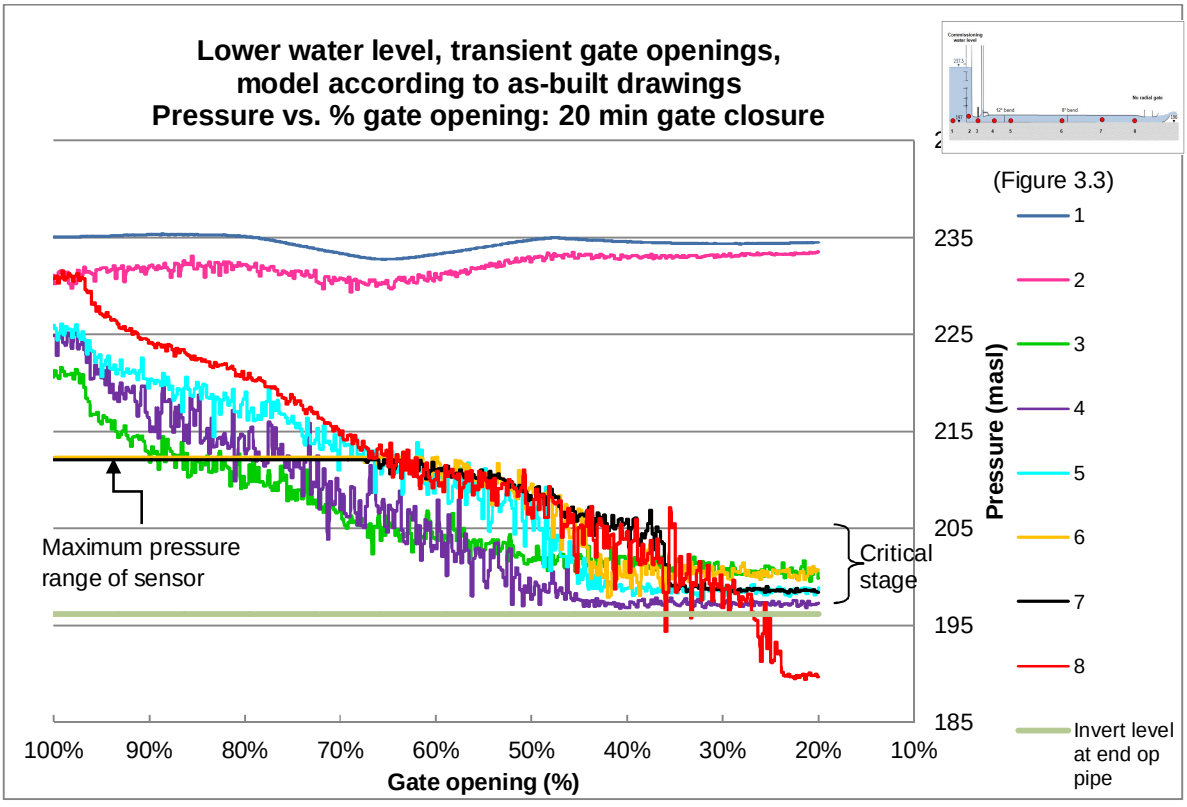

(b)

Figure 4.14: (a) Air velocity and (b) Pressures for transient gate closure (Lower Water Level and as-built)

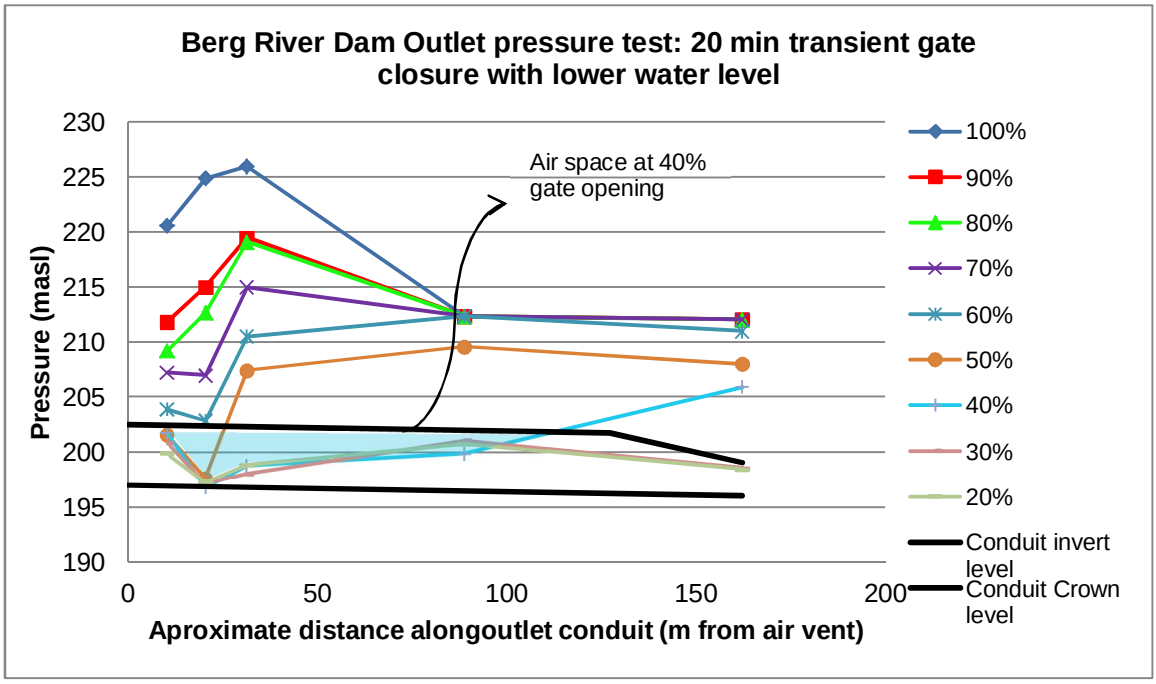

Figure 4.15: Pressure along conduit per gate opening for lower water level

It was also observed from **Figure 4.14 (a)** that, during the critical testing sequence and a gate opening of approximately 37% to 32%, the air release fluctuated from being sucked in through the air vent and being released. The air flow direction was changing rapidly (eight times per every 8 seconds (prototype) which is equivalent to a frequency of 1.1 Hz). It appears that the duration of these fluctuation periods was shorter for the shorter gate closure periods. The explanation for this is that the formation of the unstable hydraulic jump has not yet exited the outlet pipe (reached the radial gate at the ski-jump), as discussed above.

The maximum air released from and sucked into the air vent for the various gate opening rates as seen from **Figure 4.14 (a)** above are listed in **Table 4.3**.

Table 4.3: Maximum/Minimum Air flow into Air Vent (Lower Water Level, Transient gate, As-built)

Gate closure rate (prototype values)	Gate opening (%)	Maximum air velocity released from air vent (m/s) (prototype values)	Gate opening (%)	Maximum air velocity sucked into conduit (m/s) (prototype values)
12 min	35%	-13.5	37%	15.0
20 min	35%	-10.1	24%	15.4
30 min	36%	-12.8	27%	17.3

The maximum air velocity released from the air vent occurred at similar gate openings for the different gate closing rates and is not sensitive to the rate of closure, as air was still realised from the air vent for the different gate closure rates (**Table 4.3**).

These results correspond to the results obtained for the different water levels in the water reservoir.

Refer to ***Annexure H3*** for the air velocity graphs of the various gate opening periods for the lower water level.

4.3.3.2.3.2 Discussion: Pressure (Lower Water Level, as-built)

The instantaneous pressures measured for the 20 minute gate closure rate at the different locations in the model for the lower water level (232.32 masl) are shown in **Figure 4.14 (b)**.

It is evident from **Figure 4.14 (b)** that the pressures in the water tank (reservoir – pressure transducer number 1) and water shaft (wet well – pressure transducer number 2) were relatively constant for the duration of the simulation. This means that the water level in the tank was kept relatively constant at the water level under evaluation for the duration of the test.

In **Figure 4.14** (b) it can be seen that the pressure sensors located upstream of the second bend (pressure transducer number 6) (48.95 m downstream from wet well – prototype) and upstream of the radial gate chamber (pressure transducer number 7) (106.68 m downstream from wet well – prototype) reached their maximum pressure limit for gate openings of 65% and greater, and therefore displayed as a constant (horizontal) line. A steep drop in pressure occurred for gate openings between 37% to 35% at the section upstream of the radial gate chamber (pressure transducer number 7).

It can be seen from **Figure 4.14** (b) that negative pressures formed at the radial gate chamber (end of the conduit – pressure transducer number 8) for gate openings 36% and smaller.

Figure 4.15 depicts the pressures for each gate opening along the distance of the conduit for the 20 min gate closure rate. It is evident from **Figure 4.15** that the pressures decrease drastically for emergency gate openings of 40% and smaller. The pressures along the conduit (90 m from emergency gate) for gate openings of 50% and greater are of similar magnitude.

Refer to ***Annexure H3*** for the pressure vs. gate opening graphs of the various gate opening periods subjected to the lower water level.

4.3.3.2.3.3 Conclusion (Lower Water Level, as-built)

It was observed that the air release fluctuated from being sucked in through the air vent to being released, and that a steep drop in pressure occurred at pressure transducer number 7 (section upstream of the radial gate chamber) during the gate openings of approximately 37% to 35% critical stage when **Figure 4.13 (a)** and **(b)** are compared with each other for the 20 minute gate closure rate. Thus, the drop in pressure upstream from the radial gate chamber occurred at the same time as when air blow-back occurred in the air vent. The same conclusion was made for the other gate closure rates and different water levels.

It was found that the air velocity through the air vent is independent of the rate of closure of the emergency gate, but increase with increasing water head.

These results correspond to the results obtained for the simulations with the FSL and commissioning water level under evaluations, as discussed in **Section 4.3.3.2.1.3** and **Section 4.3.3.2.2.3** respectively.

4.3.4 Evaluation and discussions on as-built outlet

4.3.4.1 Impact of Water Level in Reservoir on air flow in vent

Figure 4.16 (a) and **Figure 4.16 (b)** illustrate the effect that the different water levels (commissioning water level, FSL and lower water level) had on the air velocity in the air vent for the 20 minute and 12 minute gate closure rates respectively, for the tests conducted on the model with its configuration according to the as-built drawings.

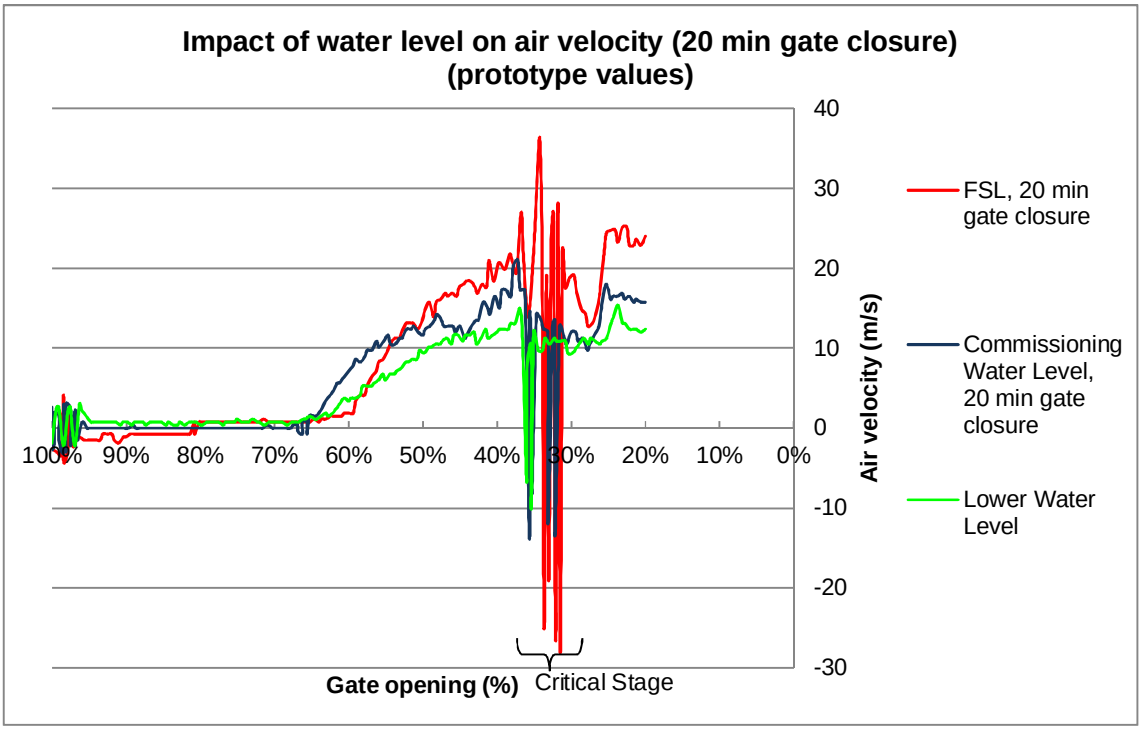

(a)

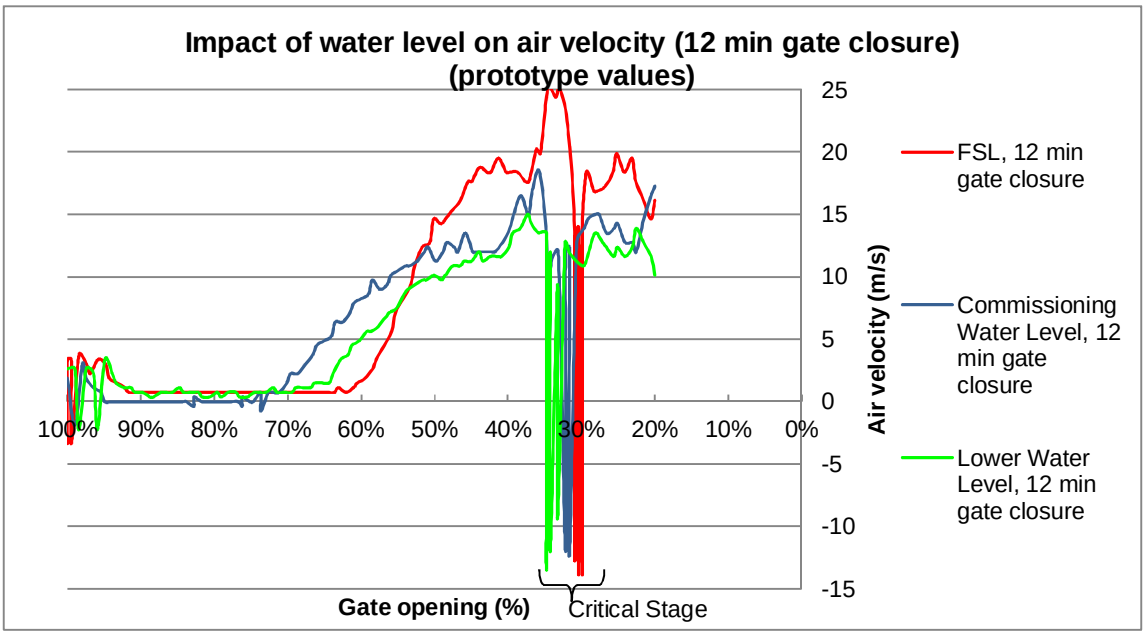

(b)

Figure 4.16: Effect of water level on air velocity (a) 20 min gate closure and (b) 12 min gate closure

From the above two figures it can be seen that the highest air velocity sucked into and released from the air vent was when the FSL was under evaluation. From **Figure 4.17** it can be seen that the higher the water level (H) the higher the water velocity (V_W), and the higher the water velocity the higher the air velocity (V_a) will be in the air vent. The water velocity (V_W) is therefore a function of the water level (H), and the air velocity (V_a) a function of the water velocity, which is depicted in **Equation 4.1** and **Equation 4.2** respectively.

$$Q_W = \underbrace{C_d A\sqrt{2gH}}_{\text{Water velocity } (V_W)} \qquad \textit{Equation 4.1}$$

$$V_a = f(V_W) \qquad \textit{Equation 4.2}$$

The air velocity (V_a) is directly dependant on the water velocity (V_W) [$V_a \propto V_W$] and the air discharge (Q_a) is directly dependant on the water discharge (Q_W) [$Q_a \propto Q_W$]. Thus, a higher the water level (H) would result in a higher water velocity (V_W) and therefore a higher air velocity (V_a).

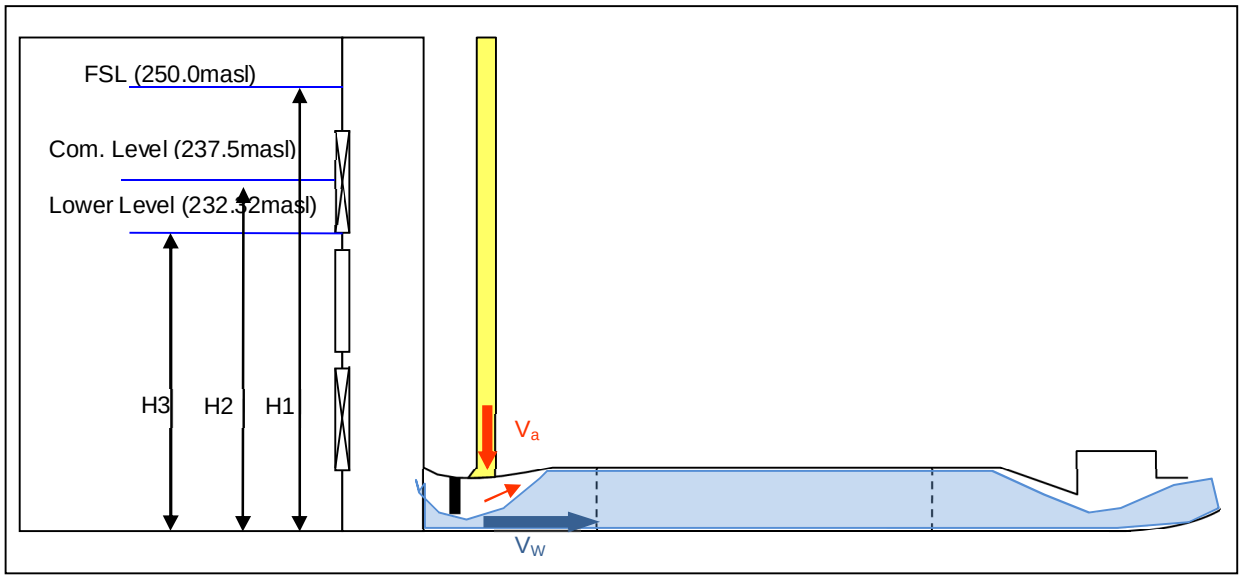

Figure 4.17: Air velocity dependant on water level

From **Figure 4.16 (a)** and **(b)** it can be seen that air was released for gate openings between 35% and 27%, irrespective of the specific water level under evaluation.

Figure 4.18 (a) and **(b)** illustrate the effect of the different water levels on the pressures in the outlet conduit section upstream of the radial gate chamber (pressure transducer number 7) for the 20 minute and 12 minute gate closure rates respectively for the tests conducted on the as-built outlet conduit. It is evident from these figures that a steep drop in pressure occurred for gate openings of between 43% and 30%, irrespective of the water level, which occurred approximately at the same time as when air blow-back occurred in the air vent (critical stage).

Figure 4.18 (a) and **(b)** illustrate that a higher pressure was exerted on the outlet conduit when the water level in the water tank was higher, which would explain the higher air velocities. These results were expected, as a higher head exerted a higher pressure on the trapped air above the water between the tapered section at the radial gate chamber (downstream) and the unstable upstream hydraulic jump. Thus, the air was released with a greater velocity for a higher head.

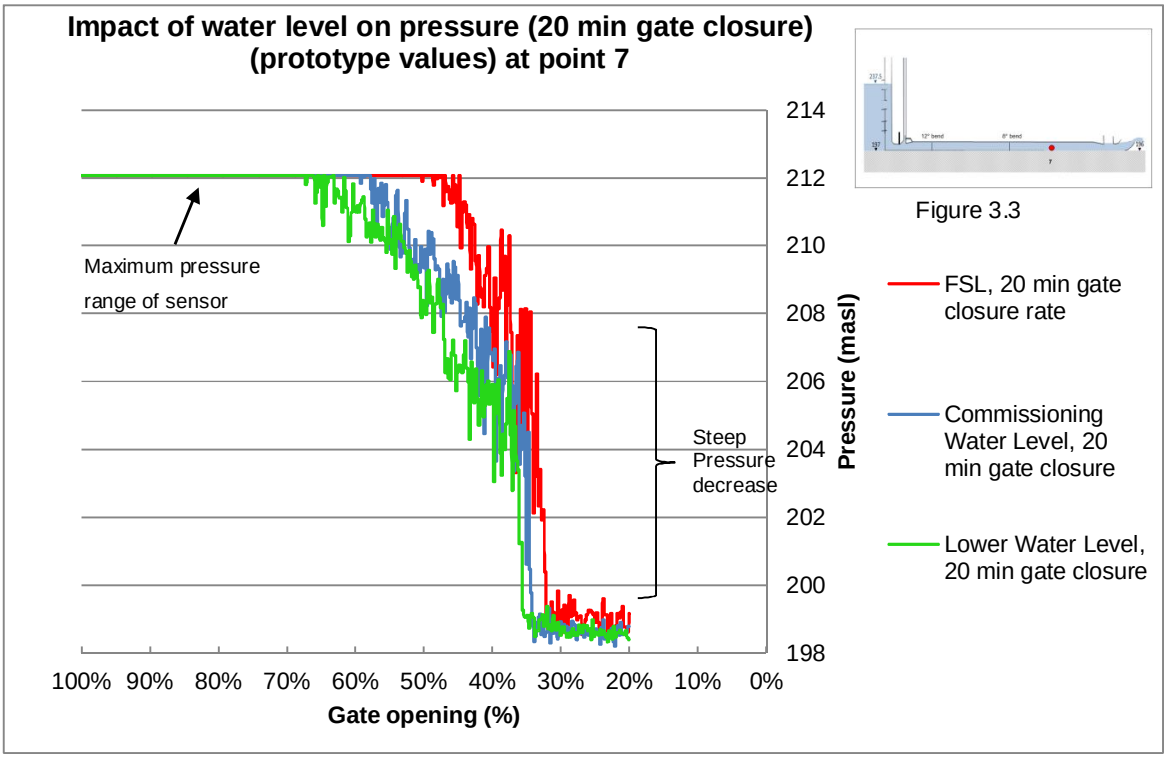

(a)

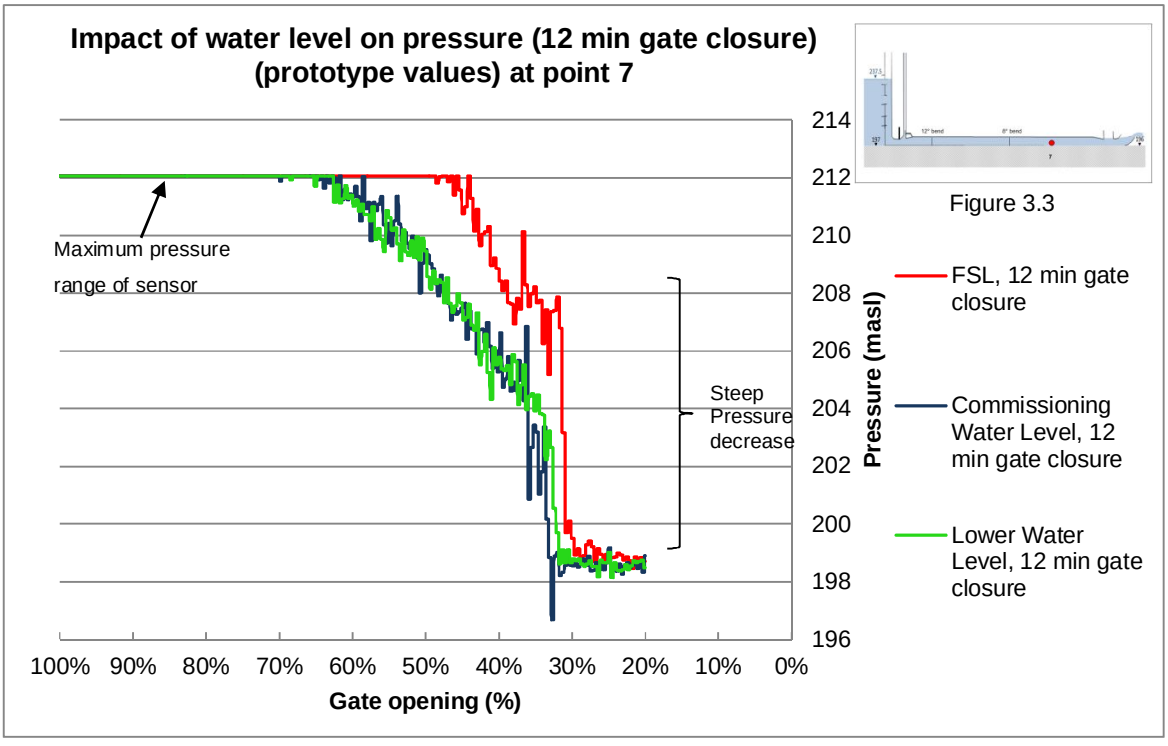

(b)

Figure 4.18: Effect of water level on pressure just upstream of radial gate chamber (a) 20 min gate closure and (b) 12 min gate closure

It therefore can be concluded that the air velocity depends on the water level in the water tank (dam of prototype), due to the pressure that the water level is exerting on the conduit. The air velocity (V_a) is also dependant on the water velocity (V_W), since a higher flow creates a higher hydraulic jump as shown in **Figure 4.19**. However, the release of air out of the air vent still occurred for all three different water levels. **Thus the water level in the water tank (dam of prototype) did not determine whether or not air was released from the air vent, but only had an impact on the air velocity in the air vent.**

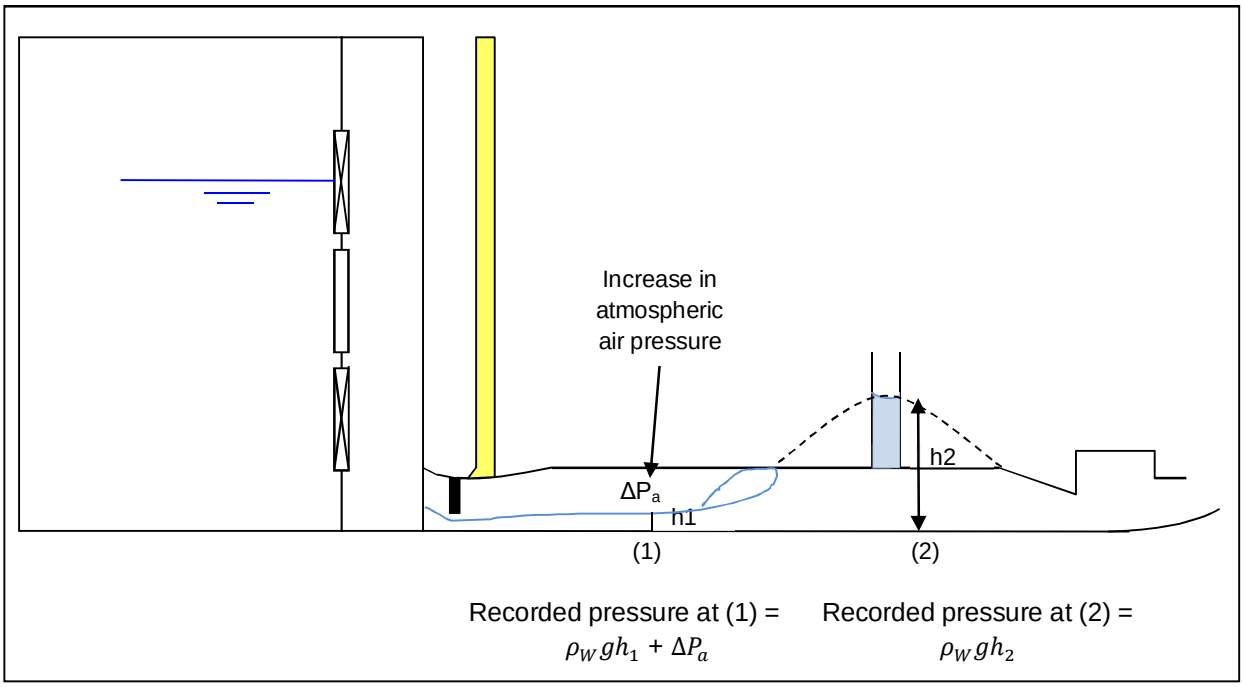

Figure 4.19: Pressure exerted on outlet conduit

It was observed that the maximum air velocity measured at the air vent for all the simulations was less than the maximum velocity of 45 m/s recommended in the literature. The measured air velocity was also less than the measured air velocity observed during the commissioning test of 2008 (field test). A possible reason for this is that the air is pressurised, which makes it difficult to model accurately, and air flow scale effects were not considered in the model for the air vent.

4.3.4.2 Impact of Gate Closure Rate

No air was released through the air vent for the stationary gate opening simulations, but it was observed that air was released from the air vent for the transient gate simulations. Thus, the phenomenon where air is released from the air vent could not be modelled by studying various fixed gate openings.

The effect of the different gates closure rates on the air velocity for the FSL, commissioning water level and lower water level is illustrated in **Figure 4.10 (a), Figure 4.13 (a)** and **Figure 4.14 (a)** respectively. These three figures indicate that air was released for gate openings between 35% and 25%. From the abovementioned figures it can be seen that air blow-back occurred for all the different water levels and gate closure rates, irrespective of the gate closure rate.

Figure 4.20, **Figure 4.21** and **Figure 4.22** illustrate the effect of the various gate closure rates on the pressures on the outlet conduit section upstream of the radial gate chamber (pressure transducer number 7) for the FSL, commissioning water level and lower water level respectively, for the tests conducted on the as-built conduit. A steep drop in pressure occurred for gate openings between 37% and 29%, irrespective of the gate closure rate. It can also be concluded from the above three figures that the pressure range for the different gate closure rates is very similar, except that the decrease in pressure for the six minute gate closure rate occurred more gradually than for the other gate closure rates.

The steep drop in pressure occurred approximately at the same time as when air blow-back occurred in the air vent (critical stage) when the above mentioned figures are compared with **Figure 4.12, Figure 4.13** and **Figure 4.14**.

It can be concluded that the air velocity in the air vent was independent of the rate of closure of the emergency gate.

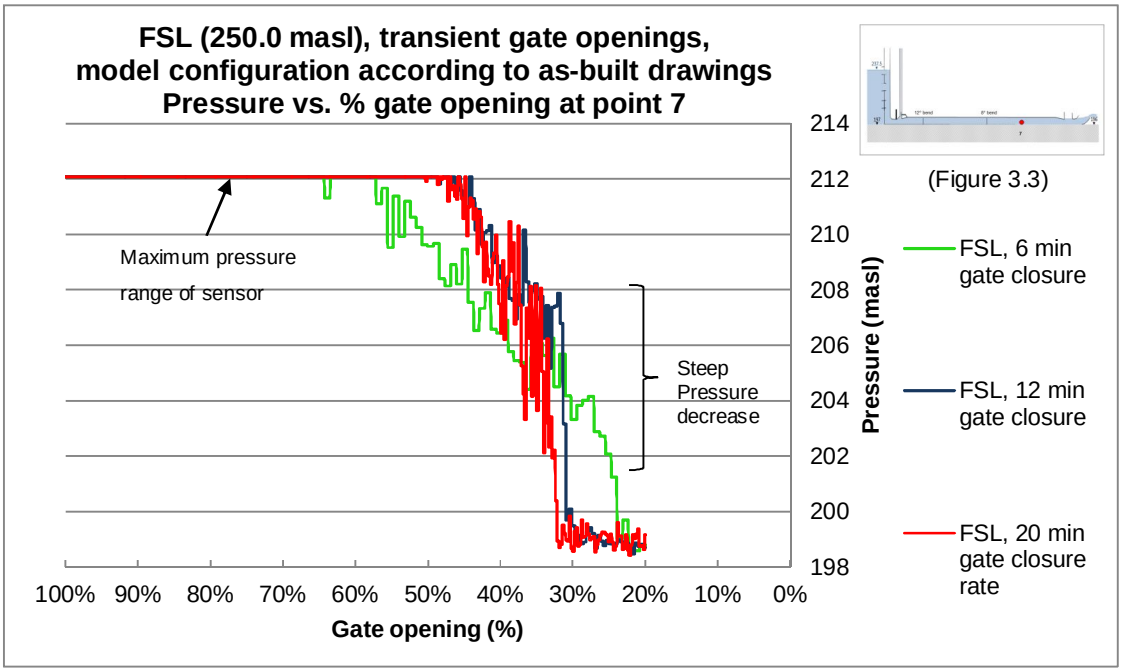

Figure 4.20: Effect of gate closure rate on pressure upstream of radial gate chamber (FSL)

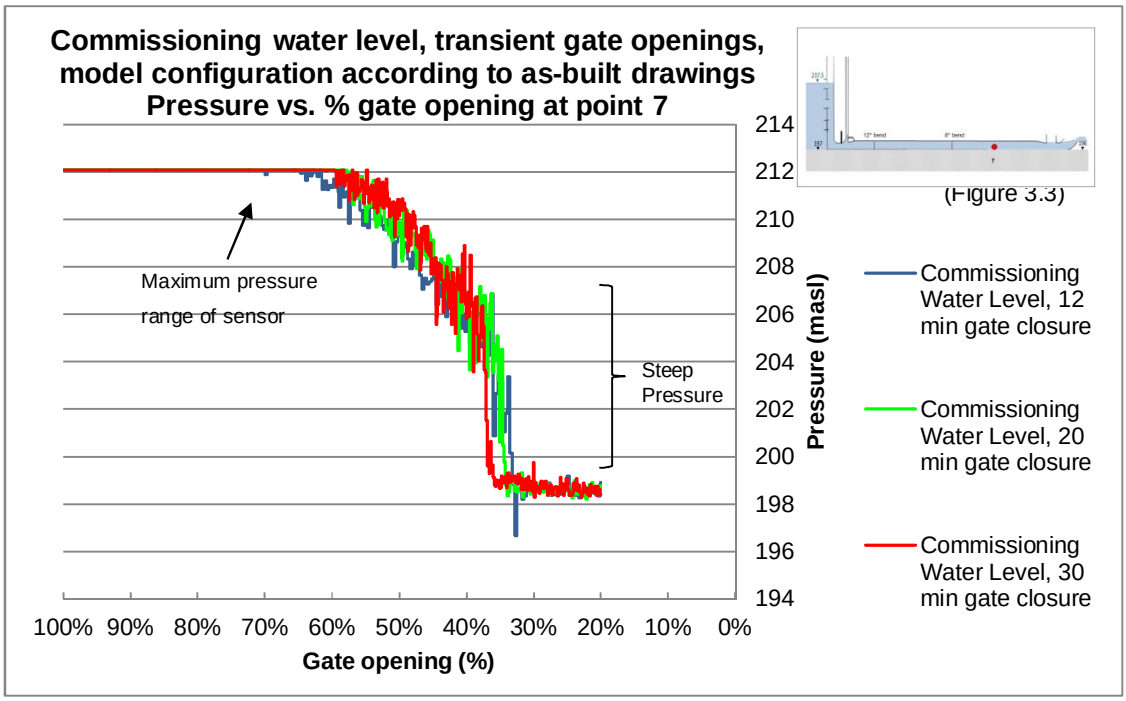

Figure 4.21: Effect of gate closure rate on pressure upstream of radial gate chamber (commissioning water level)

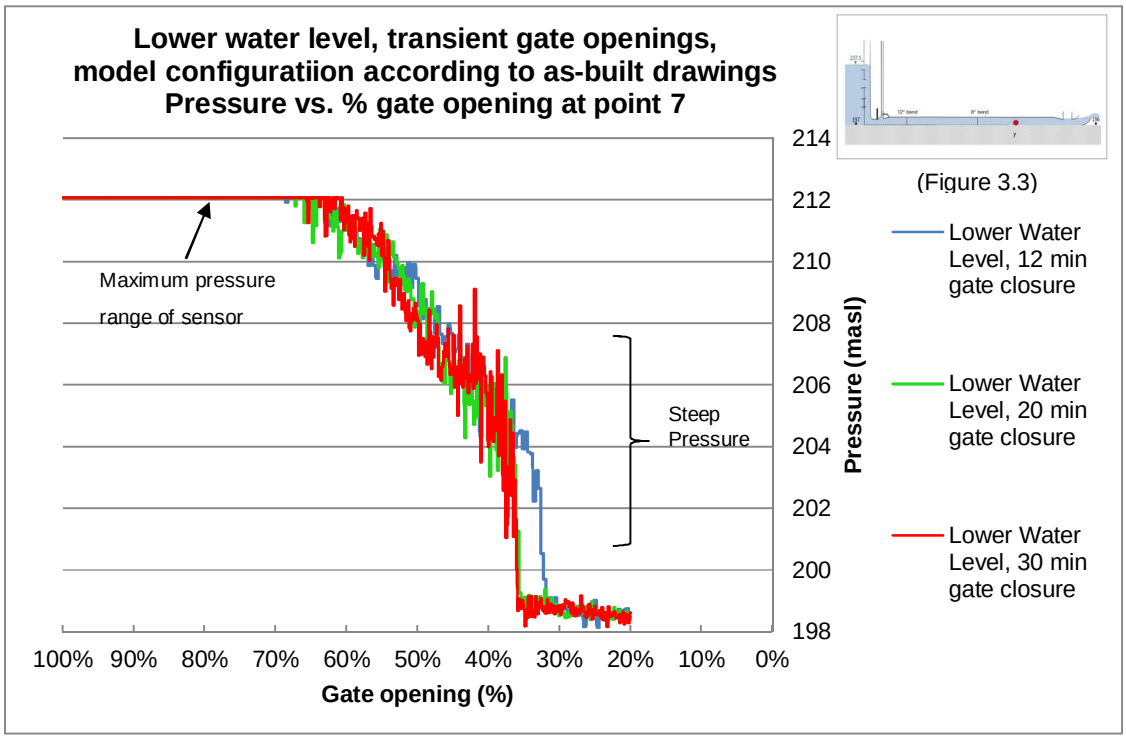

Figure 4.22: Effect of gate closure rate on pressure upstream of radial gate chamber (lower water level)

4.3.4.3 Possible reason for blow-back in Berg River Dam Air Vent

It was concluded in **Sections 4.3.4.1** and **4.3.4.2** that the release of air from the vent was not related to the *reservoir water level* or the *gate closure rate* (these aspects of the outlet structure was not the primary reason for blow back of air through the air vent).

From the tests performed on the as-built model of the Berg River Dam outlet works it was concluded that the air flow in the air vent was predominantly into the conduit (downwards) during emergency gate closures. However, rapid reverse air flow occurred between gate openings of 35% and 25%. The air flow problem of the Berg River Dam was therefore determined to be one of **air blowback** instead of continuous air inflow, as suggested by previous prototype tests.

Pulsating flow was observed for all simulations run on the model with its configuration according to the **as-built** drawings. Pulsating flow was as follows:

- An unstable hydraulic jump formed in the outlet conduit as a result of the transition from the pressurised flow to free surface flow. The hydraulic jump was unstable, because the flow downstream of the gate remained supercritical.
- Entrapment of air occurred between the unstable hydraulic jump and slanting roof of the radial gate section (**Figure 4.23 (a)**).
- The trapped air could not be released at the outlet of the conduit due to the slanting roof of the radial gate chamber (water seal formed) (**Figure 4.23 (a)**).
- The trapped air could not be released via the air vent, since the hydraulic jump formed the upstream water seal (**Figure 4.23 (a)**).
- The "trapped" air was pressurised (P_a) between the upstream and downstream water seals (**Figure 4.23 (a)**).
- Release of the trapped air out of the air vent became possible as the flow decreased due to gate closure, resulting in the unstable hydraulic jump braking contact with the roof of the outlet conduit. The water seal at the radial gate chamber was still in place (**Figure 4.23 (b)**). This resulted in the trapped air being intermittently released via the air vent.

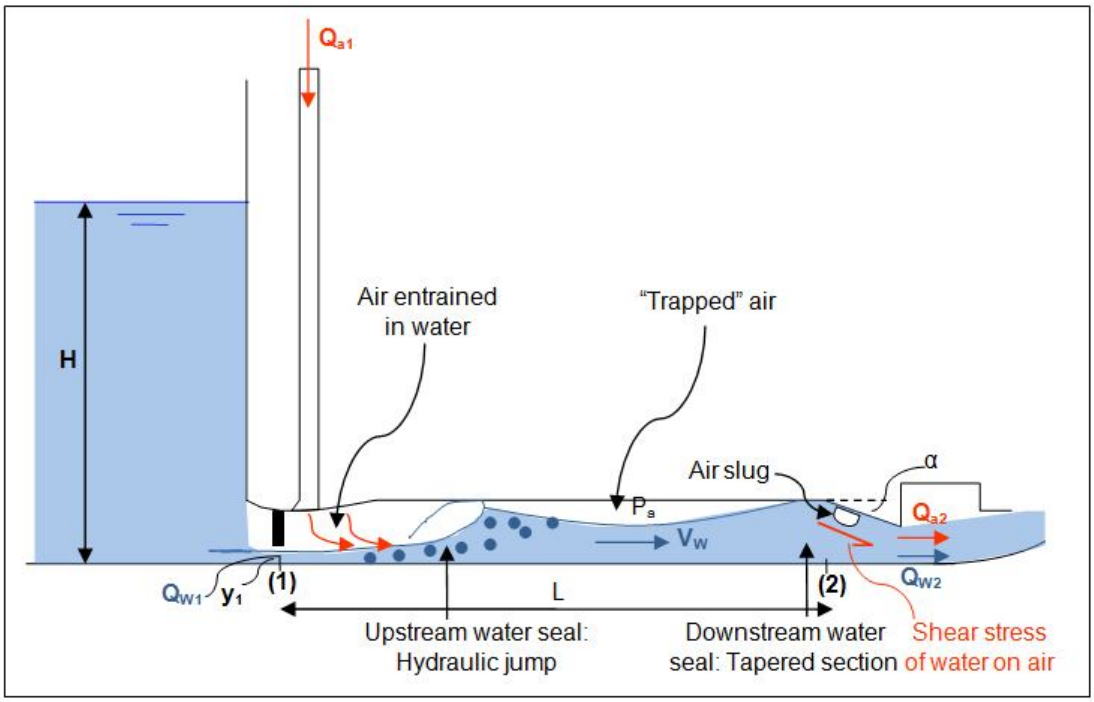

(a)

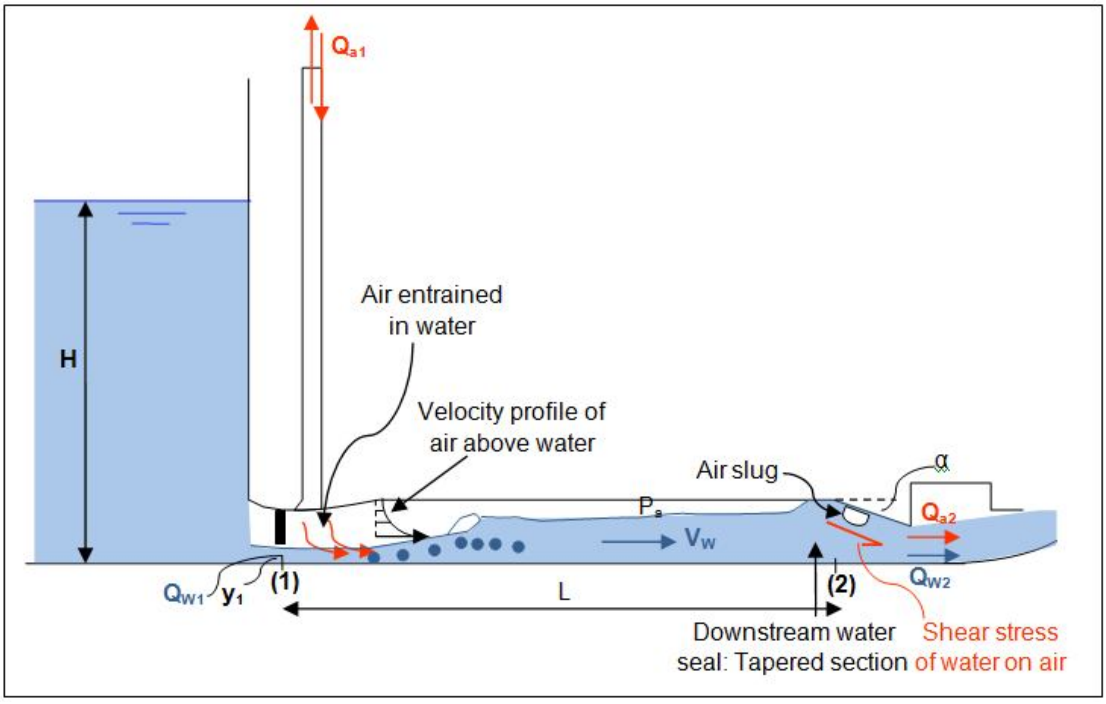

(b)

Figure 4.23: Reason for air blow-back – (a) "trapped" air; (b) air released via air vent

The total volume of air that enters the conduit is the sum of the air that is insufflated in the flow and the air above the water which is drawn downstream by viscous air-water shear forces. The following is true for partial full flow over length L in **Figure 4.23 (b)**:

$$Q_{a1} = [air\ entrained\ in\ water] + [air\ flow\ above\ water]$$

A significant air removal mechanism at section 2 in **Figure 4.23 (b)** is the escaping of air slugs. The capacity of air-slug removal at section 2 is a function of water discharge at section 2 (Q_{W2}) and the slope of the conduit roof (α) (refer to **Figure 4.24** (Falvey, 1980)). Based on the latter there will be a critical discharge, say Q^*_{W2}, below which air-slug removal at section 2 would stop.

This leads to $Q_{a2} < Q_{a1}$, and based on continuity in the control space between section 1 and section 2 air will accumulate and consequently pressure p_a will increase which could lead to explosive air blow-back through the air vent.

Q^*_{W2} can be estimated from **Figure 4.24** where:

Slope of the tapered section sin α = 0.1

D: diameter of outlet conduit just upstream of the slope = 5.5 m

$\frac{Q_{W2}^*}{gD^5}$ = 0.17 from **Figure 4.24**

The critical discharge, Q^*_{W2}, below which air-slug removal at section 2 would stop is 91.6 m^3/s (**Figure 4.25**). **Thus, blow back through the air vent would occur at discharge rates below 91.6m^3/s.**

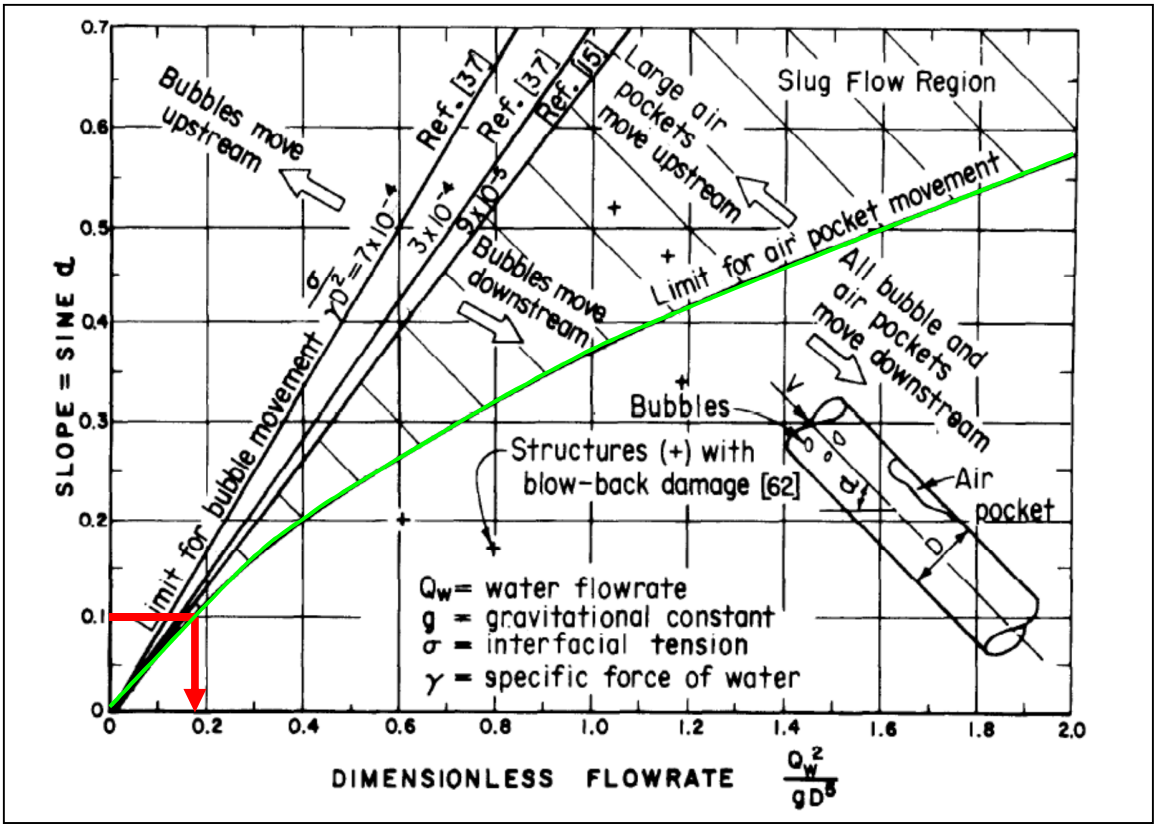

Figure 4.24: Bubble motion in closed full flowing conduits

If the reasoning that the tapered section at the radial gate chamber caused Q_{a1} to be larger than Q_{a2}, air will accumulate at the rate of $(Q_{a1} – Q_{a2})/\Delta t$. It is then logic that air reverse flow will occur earlier i.e. at larger gate openings for the slower valve closure cases. This is shown by all flow recordings in this thesis.

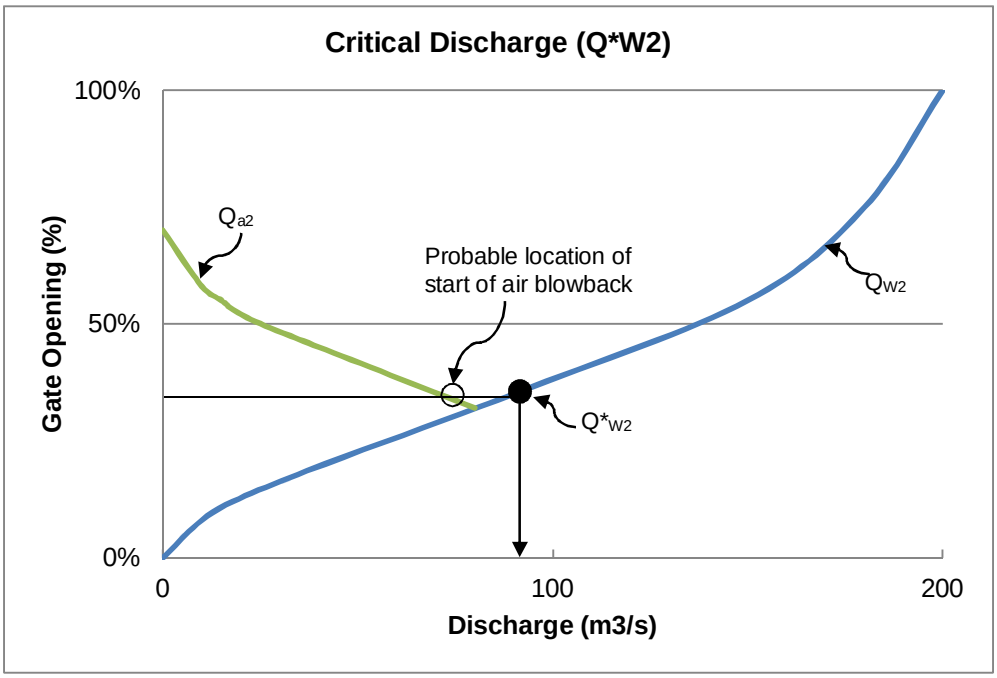

Figure 4.25: Critical Discharge

Based on the above, the most probable reason for the reverse air flow in the air vent is the tapered end of the conduit. The removal of the tapered section was tested to verify this and is treated in the next section. Although the bends in the conduit and the ski-jump channel downstream of the tapered section were not suspected to cause the air reverse flow, these were also removed and tested as modifications, the results of which are treated in the next section.

In an attempt to solve/mitigate the air reverse flow on the existing Berg River Dam outlet, an air vent upstream of the tapered end was also tested as part of the modification tests.

Please refer to ***Annexure I*** for photographs showing the flow pattern at each gate opening for the transient gate closure simulations.

4.4 Tests performed on Modified Model Configurations

4.4.1 Modified Model Configurations

Modifications were made to the model configuration in order to find solutions to mitigate the fluctuating air flow, and specifically the upward flow of air in the air vent. The modifications made to the model were as follows:

Modification 1: The ski-jump was removed at the end of the conduit, with the second bend and radial gate chamber still intact (**Figure 4.26**). The radial gate was not modelled.

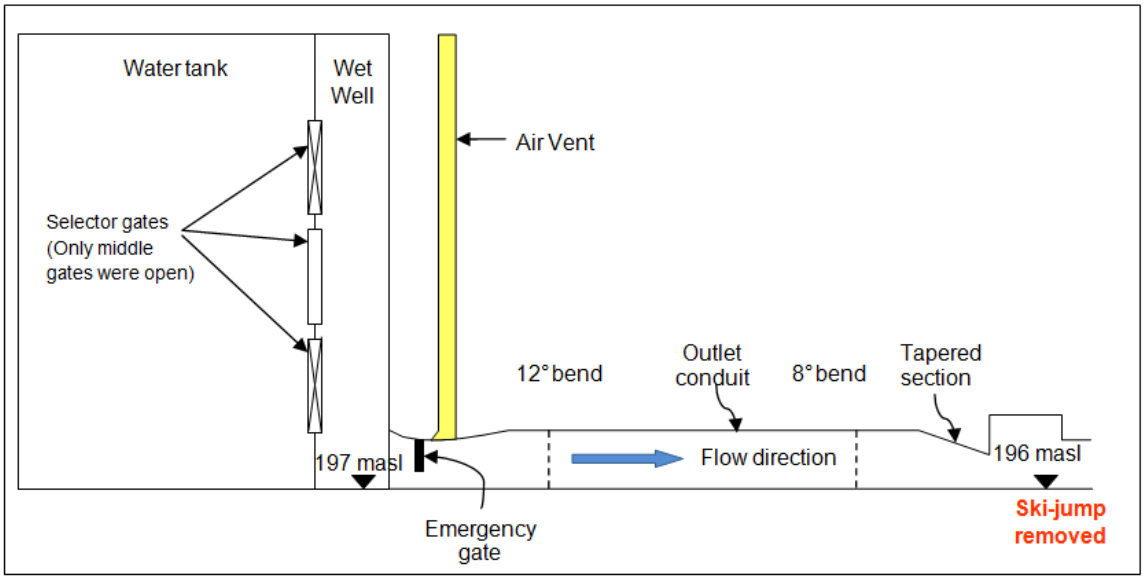

Figure 4.26: Modification 1 – ski-jump removed

Modification 2: The second bend (8°) and ski-jump were removed, but the radial gate chamber was still connected to the end of the outlet conduit (**Figure 4.27**).

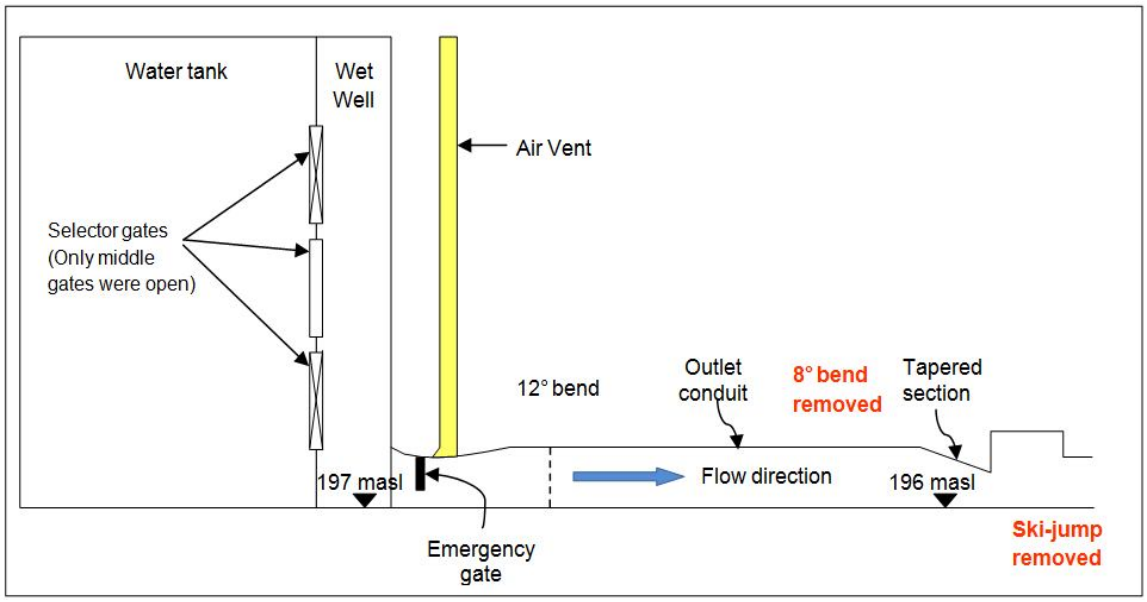

Figure 4.27: Modification 2 – ski-jump and second bend (8° bend) removed

Modification 3: Only the second bend (downstream) was removed, but the radial gate chamber and the ski-jump were still intact with the outlet conduit (**Figure 4.28**).

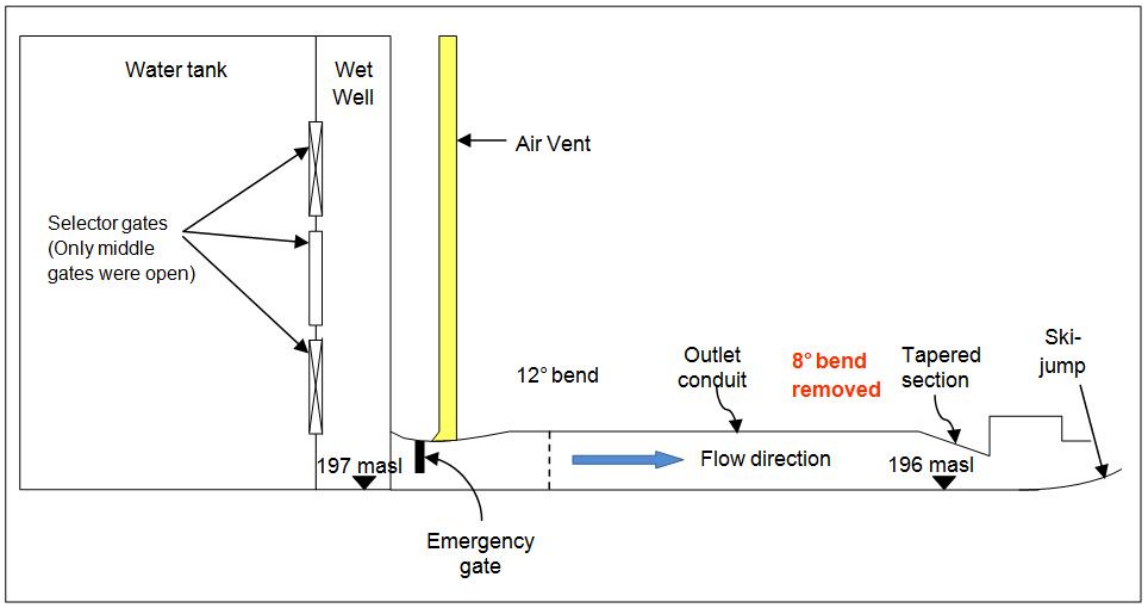

Figure 4.28: Modification 3 – second bend (8°) removed

Modification 4: The radial gate chamber and ski-jump were removed, but with the second bend still intact (**Figure 4.29**).

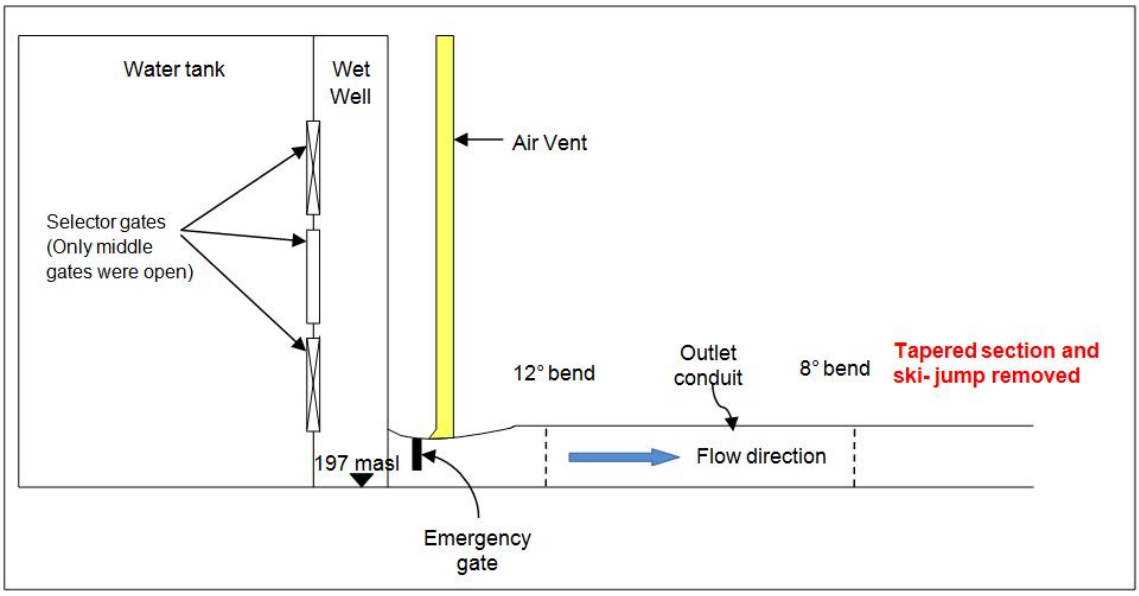

Figure 4.29: Modification 4 – ski-jump and radial gate chamber removed

Modification 5: Extra air outlet pipe before tapered section (450 mm, 2.4 m long – prototype) (**Figure 4.30**). The radial gate was closed by 197 mm (prototype) to restrict the discharge to 204 m^3/s. Please note that the tapered section formed part of the model configuration.

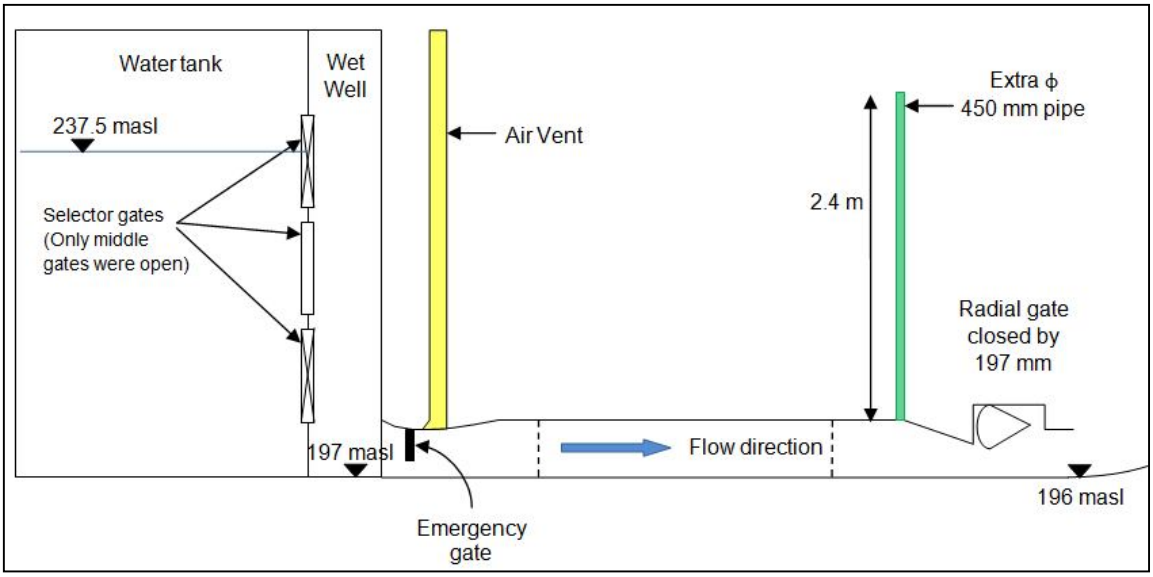

Figure 4.30: Modification 5 – Extra air outlet pipe

Tests were performed on the model for each of the five modified configurations as discussed above. The air flow in the air vent, the water discharge and the pressures in the conduit were measured.

The gate closure rates used for the various tests done on each modified configuration were the same as the four gate closure periods discussed in **Table** 3.3.

The water level during all the tests conducted on each of the modified configurations corresponded to the water level during the commissioning test of the Berg River Dam (237.5 masl), as it was concluded in **Sections 4.3.4.1** that the reservoir water level did not prevent air from being released from the air vent.

4.4.2 Results of Tests on Modified Model Configurations

4.4.2.1 Modification 1, 2 and 3

The results obtained from modification 1 (ski-jump removed), 2 (ski-jump and second bend removed) and 3 (second bend removed) were similar to the test

results for the unmodified model as discussed in **Section 4.3.3.2** (blowback of air still occurred).

Refer to ***Annexure I1***, ***2*** *and* ***3*** for the air velocity and pressure graphs of the various gate opening periods for modification 1, 2 and 3 respectively.

A comprehensive discussion of the results of modification 1, 2 and 3 are compiled in ***Annexure J***.

4.4.2.2 Modification 4 – Ski-jump and Radial Gate Chamber Removed

The model configuration was modified by removing the radial gate chamber and the ski-jump at the end of the conduit, but leaving the second bend (8°) intact (**Figure 4.29**). The air velocity and direction measured in the air vent and the calculated aeration ratio (β) for the various gate closure rates (six minutes, 12 minutes, 20 minutes and 30 minutes) subjected to the commissioning water level are shown in **Figure 4.31 (a)** and **(b)** respectively.

Figure 4.32 (a) shows the pressures measured along the outlet conduit for the 20 minute gate closure rate.

4.4.2.2.1 Discussion: Air Velocity and direction (Commissioning Water Level, modification 4)

At the commencement of the simulations, no air was released from the air vent, as the air vent did not act as a surge tower. No air was release from the air vent out of the system for the duration of all the tests performed on the model with its configuration corresponding to modification 4 (radial gate chamber and ski-jump removed - **Figure 4.29**). Free surface flow occurred downstream of the emergency gate for the duration of all the simulations run on the model with its configuration according to modification 4. **It can therefore be concluded that the constricted roof of the outlet conduit at the radial gate chamber prohibited the free flow of water, which prohibited free surface flow for large gate openings.**

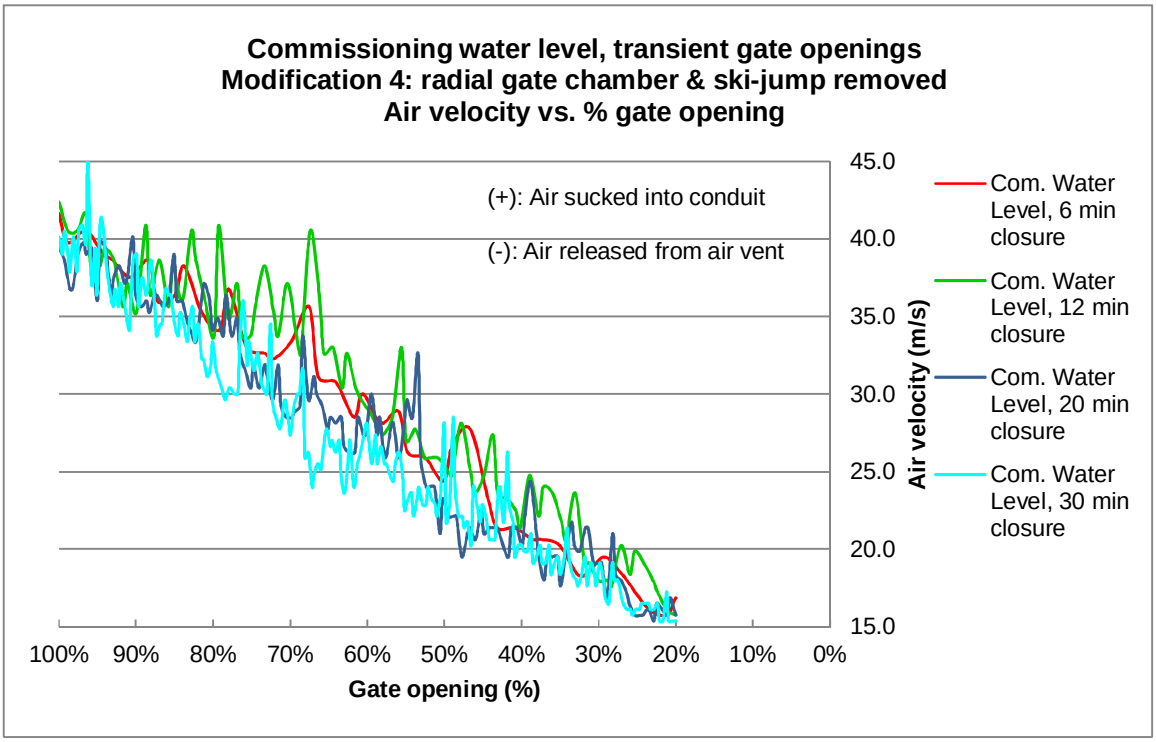

(a)

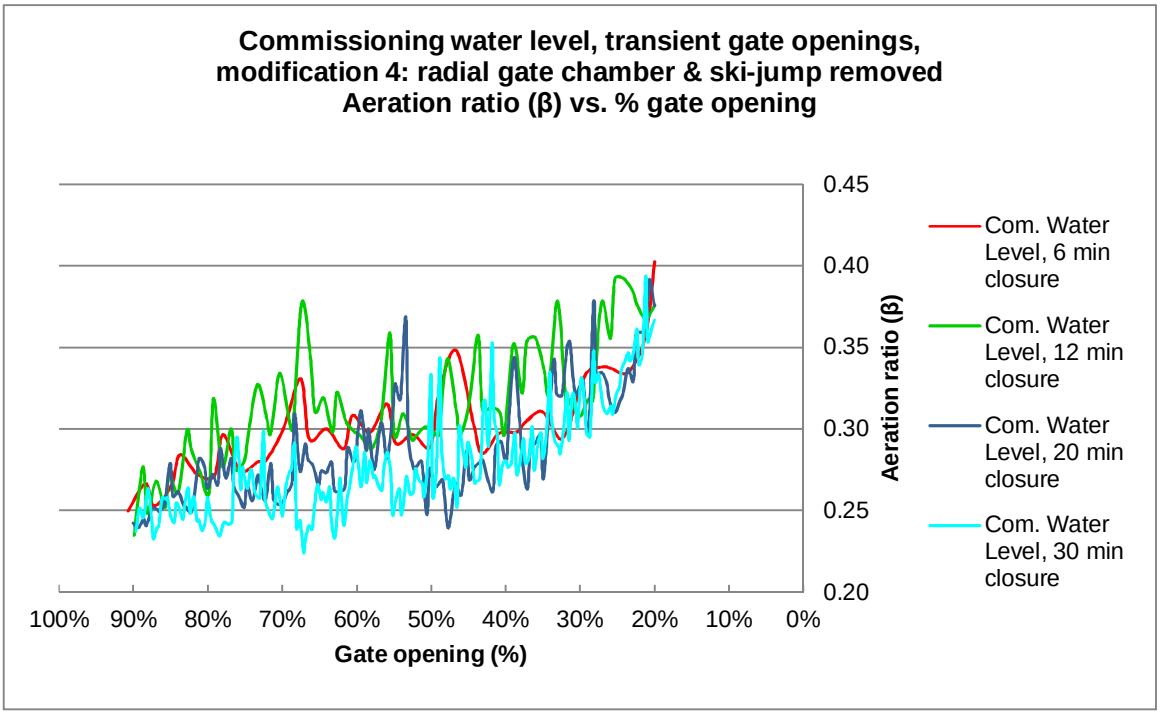

(b)

Figure 4.31: (a) Air velocity and (b) Aeration ratio (β) for different gate closure rates (Commissioning Water Level, transient gate closure, modification 4)

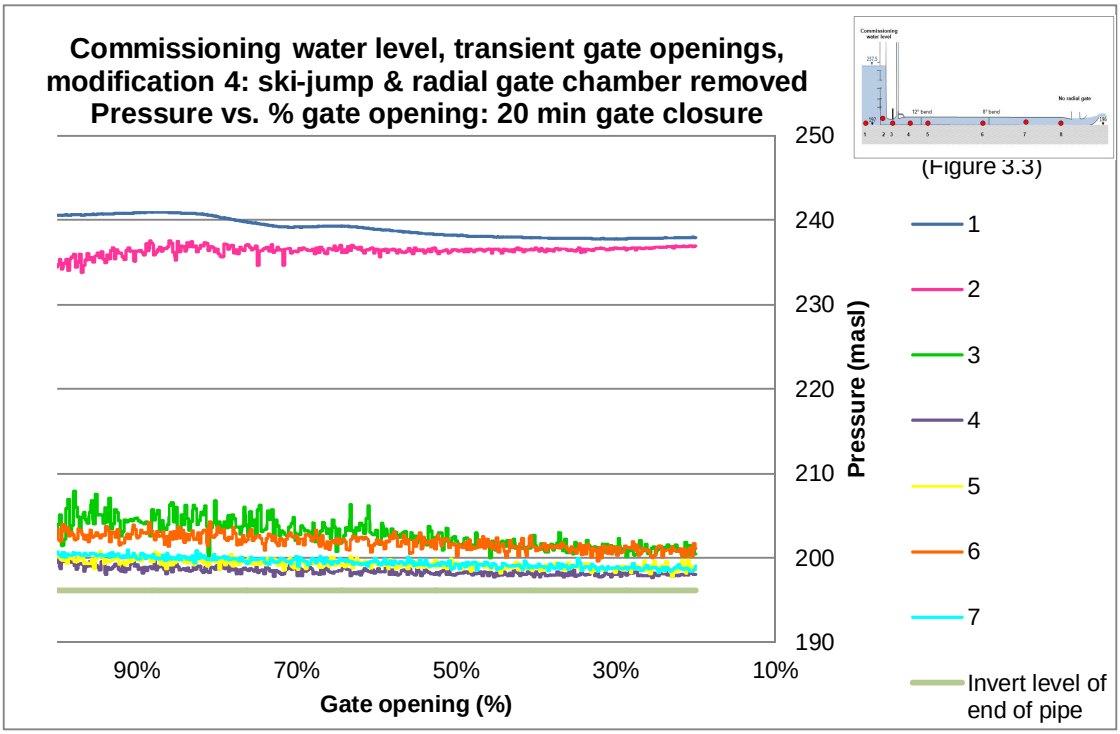

(a)

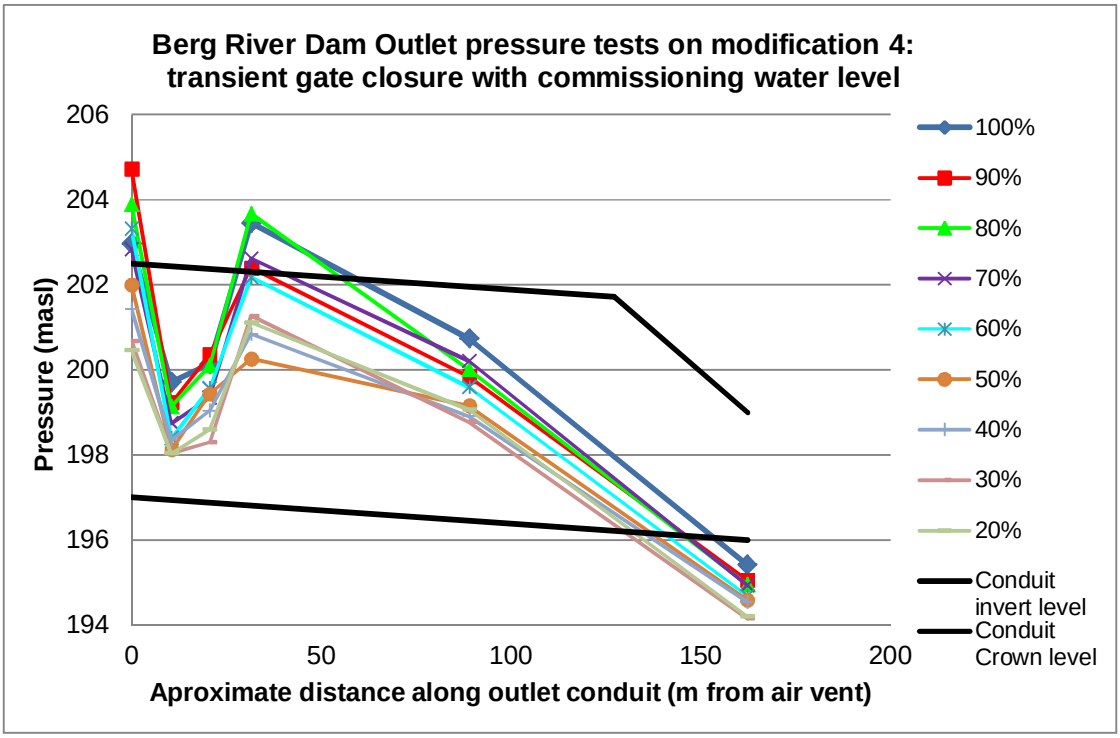

(b)

Figure 4.32: (a) Pressure for transient gate closure and (b) pressure along conduit per gate opening (Commissioning Water Level and modification 4)

The maximum and minimum air velocities recorded are summarised in **Table 4.4**.

Table 4.4: Maximum/Minimum Air entrained into Air Vent (Commissioning Water Level, Transient gate, Modification 4)

Gate closure rate (prototype values)	Gate opening (%)	Minimum air velocity sucked into conduit (m/s) (prototype values)	Gate opening (%)	Maximum air velocity sucked into conduit (m/s) (prototype values)
6 min	21%	15.75	100%	41.63
12 min	20%	15.75	100%	42.38
20 min	23%	15.38	100%	40.13
30 min	20%	15.38	96%	45.01

Table 4.4 also provides proof that no air was released through the air vent for the different gate closure rates for the simulations run on the model with the radial gate chamber and ski-jump removed (modification 4).

The aeration ratio (β) was calculated by means of **Equation 2.7**, since the empirical relations of β-values as a function of Froude number in the literature are for closed conduits that are not restricted at the outlet end, which is true only for modification 4. It can be seen from **Figure 4.31 (b)** that the aeration occurred at the commencement of the simulations. The aeration values for the different gate closure rates are very similar. The reason for this was that free surface flow occurred downstream of the emergency gate. Thus, no hydraulic jump formed (**Figure 4.33**) since the tapered section at the radial gate chamber had been removed.

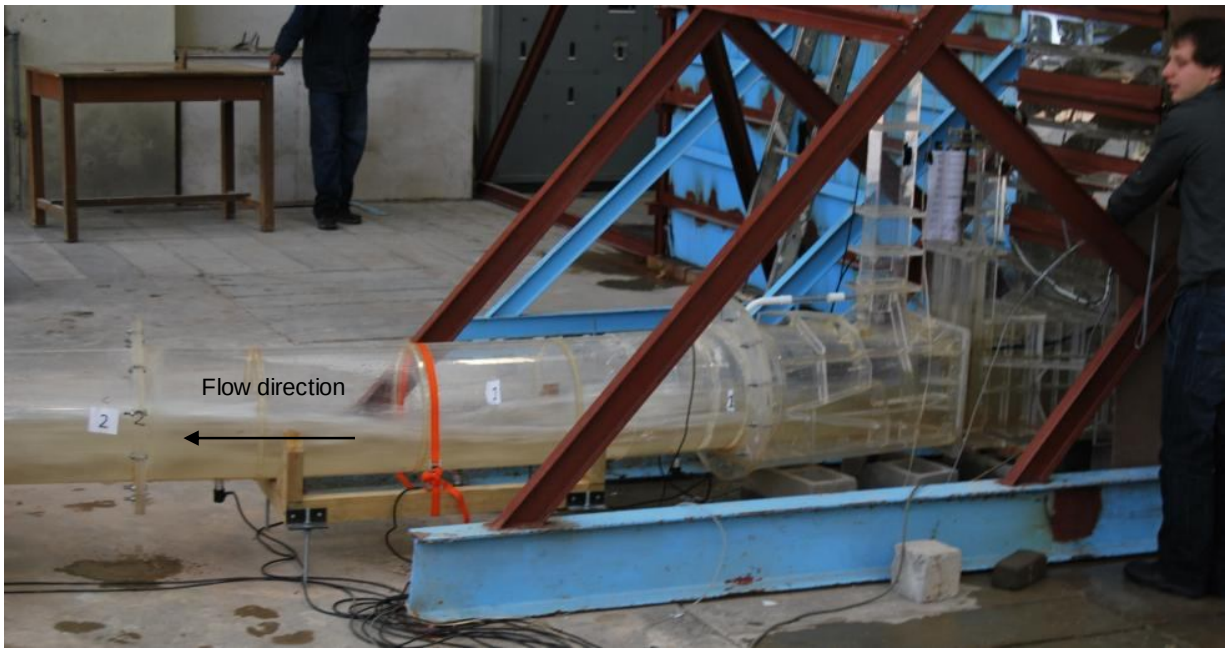

Figure 4.33: Free surface flow at emergency gate (modification 4)

Refer to ***Annexure I4*** for the air velocity graphs of the various gate opening periods for modification 4 (radial gate chamber and ski-jump removed) subjected to the commissioning water level.

4.4.2.2.2 Discussion: Pressure (Commissioning Water Level, modification 4)

From **Figure 4.32 (a)** it can be seen that the pressures in the water tank (reservoir - pressure transducer number 1) and water shaft (wet well - pressure transducer number 2) were relatively constant for the duration of the simulation. This means that the water level in the tank was kept relatively constant at the water level under evaluation for the duration of the test.

No sudden decrease in pressure occurred in the outlet conduit for the duration of the tests performed on the model with its configuration according to modification 4 (refer to **Figure 4.32 (a)**).

Figure 4.32 (b) depicts the pressures for each gate opening along the distance of the conduit for the stationary gate opening simulations. It is evident from **Figure 4.32 (b)** that the pressures per gate opening followed the same pattern and were less than the

pressures obtained for all the tests performed on the unmodified model and the other modified configurations (modifications 1, 2 and 3).

Refer to ***Annexure I4*** for the pressure vs. gate opening graphs of the various gate opening periods subjected to the commissioning water level for modification 4: ski-jump and radial gate chamber removed.

4.4.2.2.3 Conclusion (Commissioning Water Level, modification 4)

It is evident from the above that the removal of the tapered section and the radial gate prevented the formation of an unsteady hydraulic jump under transient gate closure conditions. In turn this mitigated the blow back of air through the air vent.

4.4.2.3 Modification 5 – Extra outlet pipe

It was concluded in **Section 4.4.2.2** that the tapered end of the conduit caused the air blowback through the air vent. In an attempt to solve/mitigate the air reverse flow on the existing Berg River Dam outlet, an air vent upstream of the tapered was tested. The as-built conduit was modified by adding an additional 450 mm diameter air outlet pipe (2.4 m long - prototype) before the tapered section (**Figure 4.30**). Refer to Photograph 11 in ***Annexure D2*** showing the additional air vent.

Figure 4.34 (a) shows the air velocity and direction measured in the air vent for various gate closure rates. **Figure 4.34 (b)** shows the pressures measured along the outlet conduit for a 20 minute gate closure rate. The commissioning water level was under evaluation. The radial gate was closed by 197 mm (prototype) in order to restrict the discharge to 204 m^3/s.

At the downstream end of the conduit the water oscillated in the extra air vent at the tapered section at the radial gate chamber for large emergency gate openings. As air was sucked into the outlet conduit, an air-water mixture pulsed out of the additional air vent pipe quite violently.

The results (air velocities and direction, and pressures) obtained from modification 5 (additional air outlet pipe) were similar to the test results for the unmodified model

as discussed in **Section 4.3.3.2** and modification 1, 2, and 3 in **Section 4.4.2.1** (refer to **Figure 4.34 (a)** and **(b)**). The extra 450 mm air outlet pipe had no visible effect on the recorded air velocities and pressures, and did not reduce the air blowback. Furthermore, the second air vent exacerbates the negative pressures at transducer 7 (negative pressures nearing 10 m which may result in cavitation and structural damage at the tapered section – refer to **Figure 4.34 (b)**).

It was concluded that a 450 mm (0.16 m^2) pipe just before the tapered section would not solve the reverse flow problem experienced at the Berg River Dam. Further tests could be done to determine whether a much larger pipe would mitigate the pulsation air flow at the main air vent.

Please refer to ***Annexure I5*** for the results obtained for modification 5 (additional 450 mm air vent at tapered section).

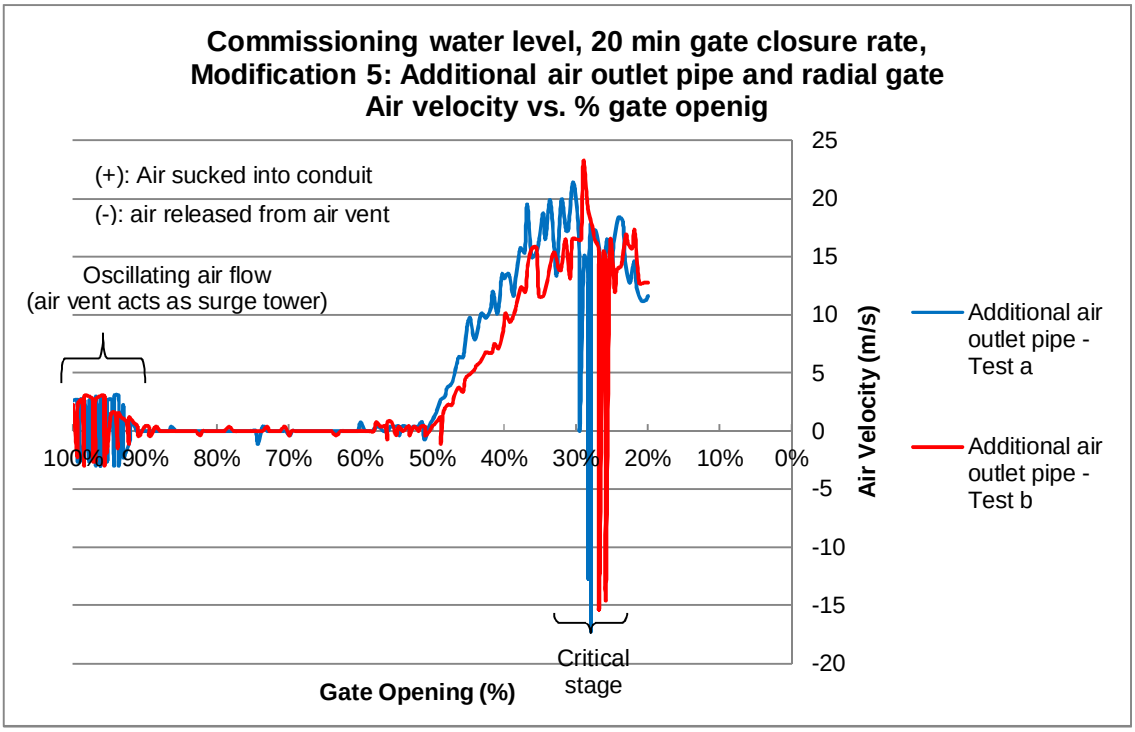

(a)

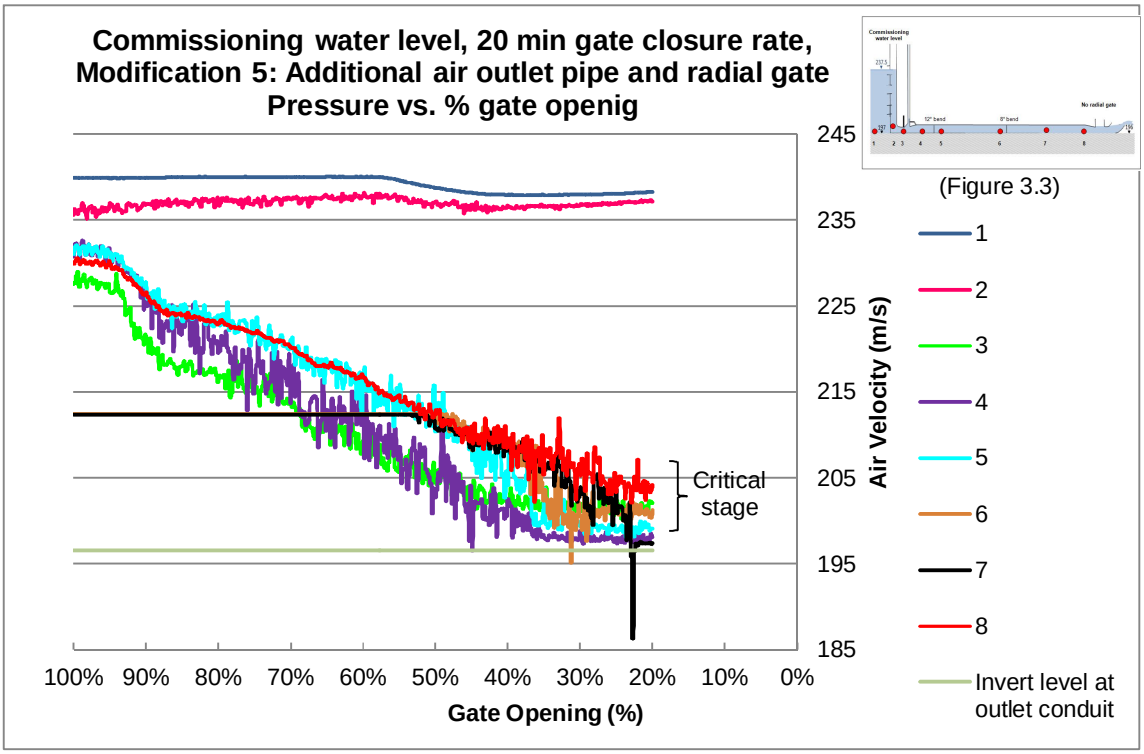

(b)

Figure 4.34: (a) Air velocity and (b) Instantaneous Pressures for different gate closure rates (Commissioning Water Level, transient gate closure, modification 5)

4.4.3 Evaluation and discussions on modified outlet

The model was modified to determine the reasons for the excessive airflow out of the air vent and find solutions to mitigate the airflow out of the air vent.

As described in **Section 4.4.2**, five modifications were made to the model. The impact of the modifications to the model on the air velocity and direction are illustrated in **Figure 4.35** for the 20 minute gate closure rate subjected to the commissioning water level (237.5 masl). Similar results were obtained for the other three gate closure rates (six minutes, 12 minutes and 30 minutes).

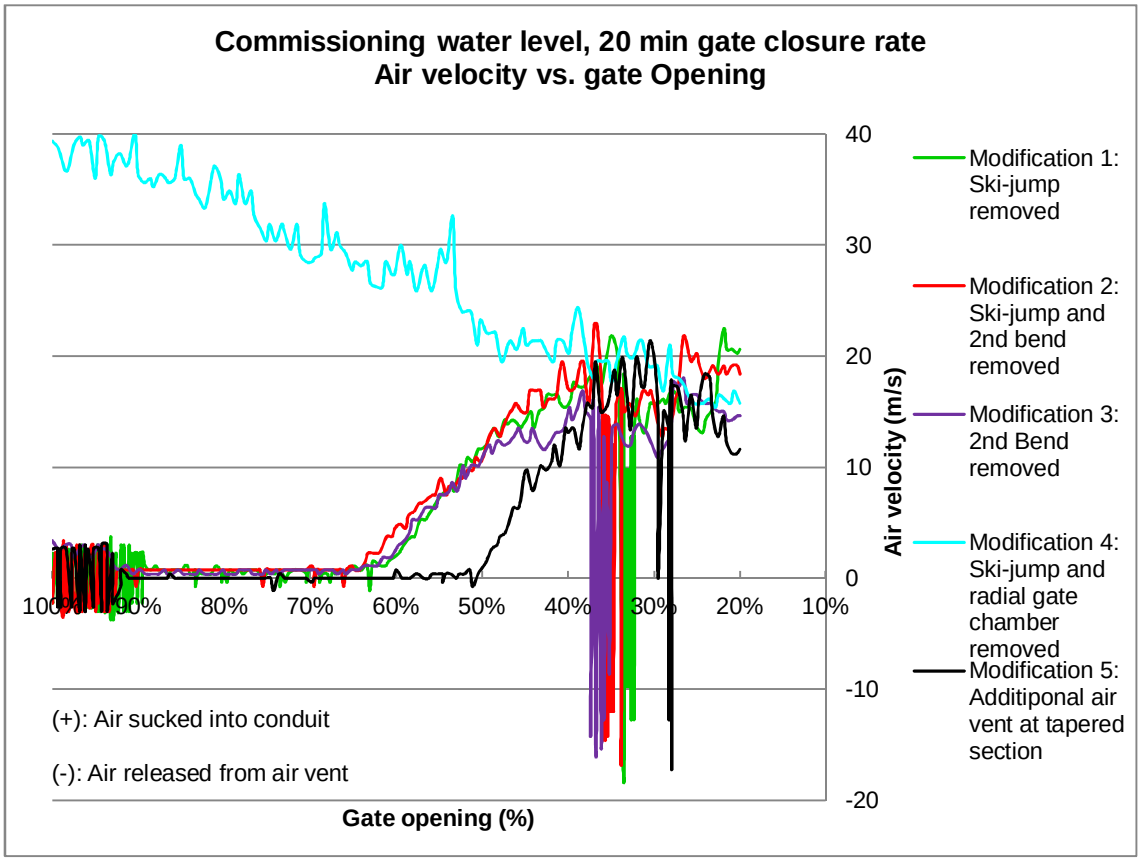

Figure 4.35: Impact of model configuration on air velocity and direction

It is evident from **Figure 4.35** that air was released from the air vent for gate openings between 35% and 28% for the four model configurations that *included* the radial gate chamber with the tapered section (modifications 1, 2, 3 and 5). In contrast, no air was released in the case of modification 4, in which the radial gate chamber (including the tapered section) and ski-jump were removed. The entrained air velocity in the air vent for the simulations run on modification 4 was much higher in comparison with the other four modifications for gate openings 40% and larger. The reason is because free surface flow occurred downstream of the emergency gate as no hydraulic jump formed for the simulations run on the model corresponding to modification 4. The air vent therefore did not act as a surge tower and aeration occurred from the 100% gate opening. For modifications 1, 2, 3 and 5 the measured air velocities after the unstable hydraulic jump has moved out of the conduit was similar to the air velocity for modification 4 for the same gate openings (40% and smaller), as seen in **Figure 4.35**.

Figure 4.36 illustrates the effect of the various model configurations on the pressures upstream of the radial gate chamber (pressure transducer number 7) for a 20 minute gate closure rate subjected to the commissioning water level.

From **Figure 4.36** it can be seen that a steep drop in pressure occurred upstream of the radial gate chamber (pressure transducer number 7) between gate openings between 40% and 23% for the four model configurations that included the radial gate chamber with the tapered section (modifications 1, 2, 3 and 5). During the simulations run on modifications 1, 2, 3 and 5 it was observed that the reverse air flow occurred when the sudden decrease in pressure occurred. It must be noted that **no** sudden decrease in pressure and reverse flow of air occurred for the simulations without the radial gate chamber (including the tapered section) and ski-jump (modification 4). **Thus, it can be concluded that the radial gate chamber with the tapered configuration caused air blowback experienced.**

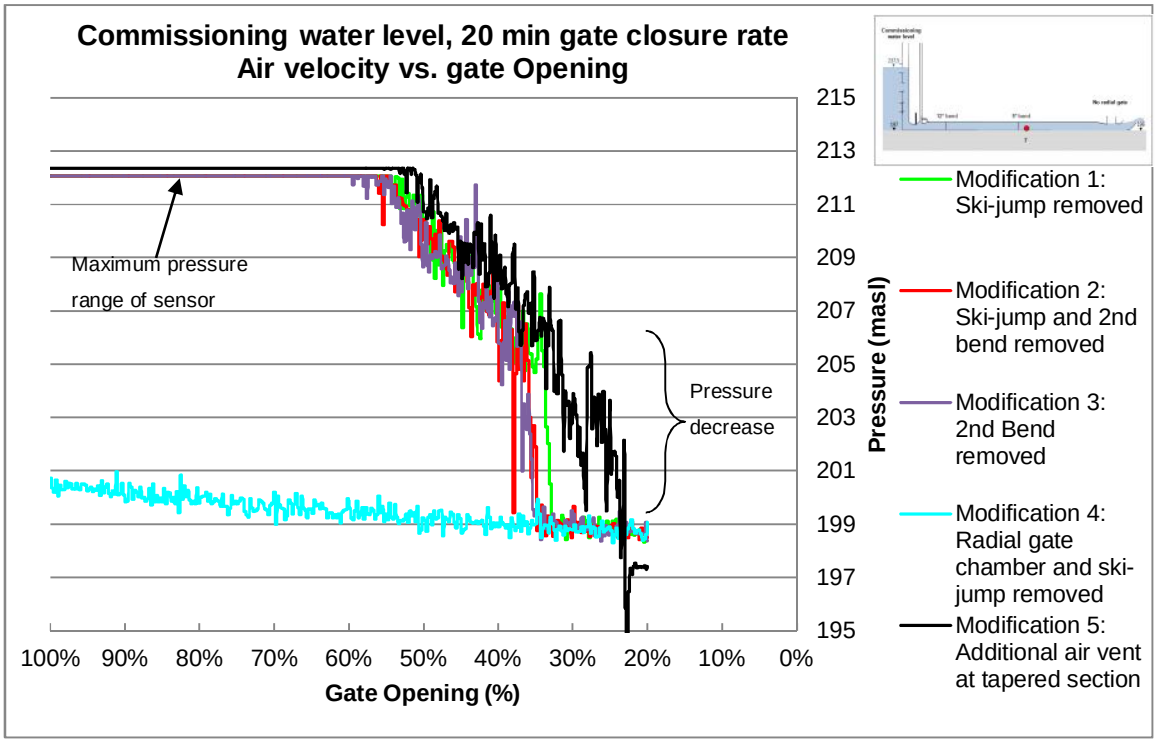

Figure 4.36: Impact of model configuration on pressure just upstream of radial gate chamber

An explanation for the air blowback phenomenon experienced on modifications 1, 2, 3 and 5 was postulated by evaluating the results obtained from the tests performed on the Berg River Dam model in conjunction with the relevant literature. Air entered the conduit through the air vent and was drawn downstream. At the downstream end of the conduit the air was restricted by the tapered section of the radial gate chamber (which has a downwards sloping ceiling forming a water seal), resulting in pressurisation of the air in the conduit. The entrained air was accumulated in an air pocket along the soffit of the outlet conduit, which can be seen in **Figure 4.37**. This pressure caused air to blow back in the air vent when the water surface broke contact with the conduit roof. This explains the sudden drop in pressure just upstream of the radial gate chamber when the pressurised trapped air (above the water) was blown out of the conduit via the air vent.

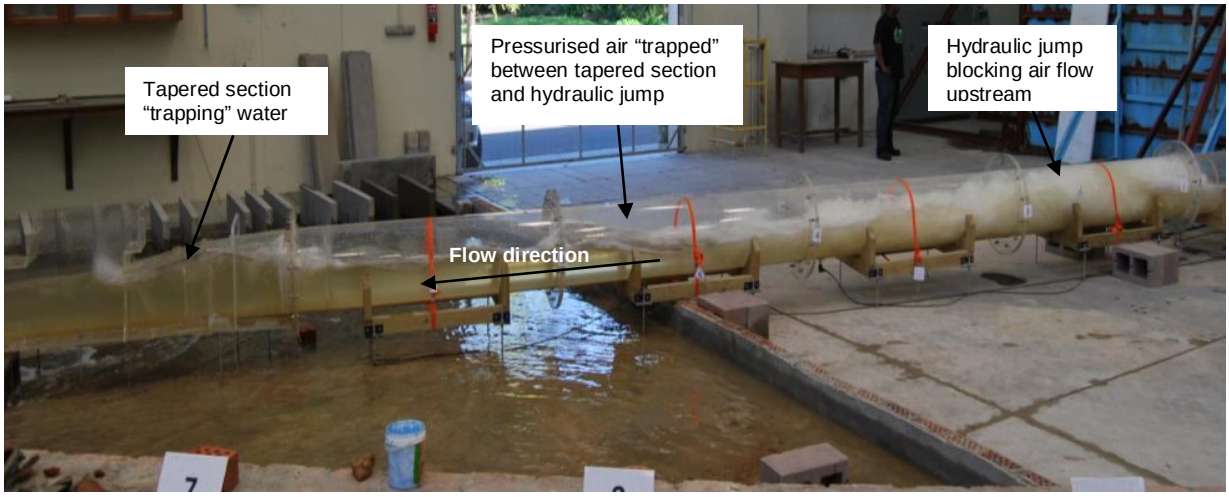

Figure 4.37: Illustration of air trapped between hydraulic jump and radial gate chamber

The tests performed on modification 4 where the radial gate constriction was removed confirmed that it had been the cause of the air blowback phenomenon experienced on the latter tests. Free surface flow occurred throughout the closure of the emergency gate as no water seal formed downstream. Thus normal circulation out of the air vent was possible and no air reversal in the air vent was experienced.

An additional 450 mm diameter air vent (prototype value) was fitted directly onto the conduit at the constriction (modification 5), but was found to be ineffective in reducing the air blowback.

The aeration ratio (β) obtained for the simulation run on the model with the radial gate chamber (including tapered section) and ski-jump removed (modification 4) can be compared with previous studies done on high pressure conduits and some of the available empirical equations shown in **Figure 4.38**. The results obtained from the physical model of the Berg River Dam (modification 4) had a better correlation with the equation of the US Army Corps of Engineers (Najafi & Zarrati, 2010).

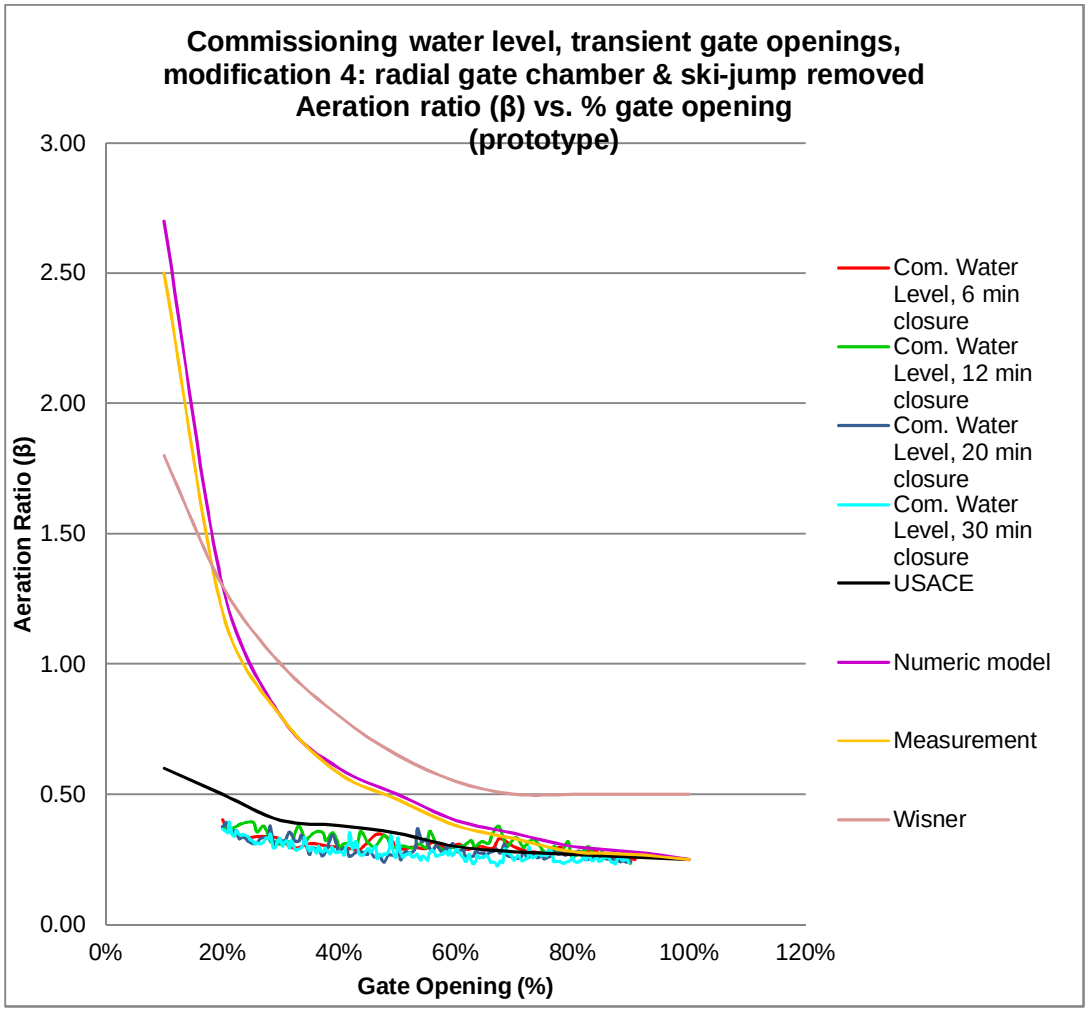

Figure 4.38: Comparison of measured aeration versus gate opening with 3D numerical model and two empirical equations

5. CONCLUSIONS

A trial closure of the emergency gate on the outlet conduit of the Berg River Dam was undertaken by the TCTA on 12 June 2008. An air vent is located downstream of the emergency gate with the purpose to introduce air downstream of the gate to counteract the negative pressures that were expected in the outlet conduit during emergency gate closures. Contrary to the expected introduction of air into the air vent, field measurements of air flow velocities indicated that, while the emergency gate was closing, very large volumes of air were apparently continuously released (up-flow) from the air vent.

A 1:14.066 physical model was used to investigate the observed flow patterns and characteristics of the Berg River Dam in order to meet the abovementioned objectives.

From the tests performed on the as-built model of the Berg River Dam outlet works it was concluded that the air flow in the air vent was predominantly into the conduit (downwards) during emergency gate closures. However, rapid reverse air flow occurred between gate openings of 35% and 25%. The air flow problem of the Berg River Dam was therefore determined to be one of air blowback instead of continuous air inflow, as suggested by previous prototype tests.

Section 4.3.4.3 explained the probable blowback phenomenon which occurred on the Berg River Dam. Air was essentially drawn into the conduit through the air vent and was dragged downstream either insufflated in the flow or above the water due to viscous air-water shear forces. At the downstream end of the conduit the outflow of air was restricted by the tapered section of the radial gate chamber (ceiling of conduit sloping downwards). The air in the conduit was pressurised due to the constriction. This pressure caused air blowback through the air vent when the upstream hydraulic jump broke contact with the roof of the conduit.

Tests performed with the tapered section at the radial gate chamber removed (modification 4) showed free-surface flow throughout the closure of the emergency gate and no reverse airflow occurred. It was therefore confirmed that the radial gate constriction was the cause of the air blowback phenomenon. Tests on the other modified model configurations (modification 1, 2 and 3) confirmed that the removal of the ski-jump and the second bend (8°) had little effect on the results. In an attempt to solve the air blowback on the existing

Berg River Dam outlet, an extra 450 mm diameter air vent was constructed directly upstream of the radial gate chamber constriction, but was found to be ineffective in reducing the blowback.

Air entrainment due to surface vortices did not occur in the wet well for tests performed at commissioning water level, even with manual stirring. The critical reservoir level at which air was entrained via a vortex was found to be 227.12 masl, 10.5 m below the commissioning water level.

The phenomenon where air is released from the air vent (air blow back) cannot be investigated by stationary gate opening simulations.

It was found that the air velocity in the air vent was independent of the gate closure rate, but increased with an increase in water head.

It was determined that the downwards sloping roof of the conduit, which accommodated the radial gate chamber, was the reason for the air blowback phenomenon. However, the downward sloping roof is required for the radial gate to perform satisfactorily under normal operation conditions.

Given the above conclusions, it does not appear to be any rational structural change to the Berg River Dam outlet works in order to prevent or hinder the recurrence of the blowback phenomenon.

6. RECOMMENDATIONS

6.1 Configuration

It was found that the cause of air blowback in the Berg River Dam model during emergency gate closures was the release of pressurised air which accumulated above the water at the tapered section of the radial gate chamber. The recommendation follows that the conduit should not be constricted in future designs, especially not at roof level. To prevent air blowback it is also recommended that the flow in high headed outlets flowing partially full should never be constricted by any structure or mechanism downstream of the conduit (e.g. wave action in stilling basin experienced at the Owyhee Dam).

A potential air blowback problem is presented if the radial gate at the end of the conduit should fail in a partially closed position. A possible solution would be a dual radial gate system in which each gate can operate at the full design discharge capacity (**Figure 6.1**). Under normal operation of the dam one gate could be used while the other gate remains closed. In the case of failure of a radial gate in a partially closed position, the other gate can be fully opened to allow unrestricted flow out of the conduit before the emergency gate is closed. Stoplog slots can also be constructed to allow normal operation should one of the gates be repaired.

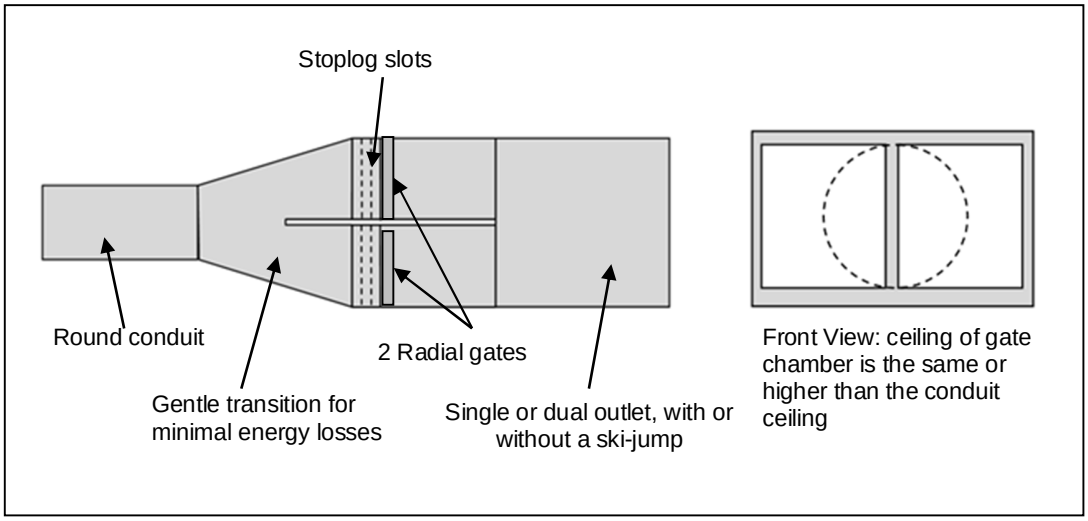

Figure 6.1: Possible radial gate configuration to prevent blowback

6.2 Berg River Dam Operation

During one of the model simulations the emergency gate was accidently opened too quickly. This increased the pressure on the radial gate chamber to such an extent that it caused the radial gate chamber to fail, as seen in **Figure 6.2**.

Figure 6.2: Failed radial gate chamber

Given this model failure, it is advised that the radial gate and emergency gate should never be operated simultaneously when the outlet conduit of the Berg River Dam has to be filled or drained.

6.3 Further Studies

It is recommended that further tests to be carried out on the Berg River Dam model used in this thesis for a partially open radial gate to determine whether a more severe restriction at the conduit outlet could result in a more serious problem. Further test could also be conducted to determine a possible alternative configuration of the extra air vent as suggested in **Figure 4.30**.

It is recommended that the results of the study of the Berg River Dam model should be compared with a three-dimensional CFD analysis of the closing gate simulations

(transient) in order to determine the capability of numerical modelling in simulating complex air-water flow and unstable hydraulic jumps in high-headed gated conduits.

For research purposes it would be valuable to perform another prototype emergency gate closure exercise (such as was done during commissioning in 2008) while recording the air flow velocity and direction on a continuous basis. An additional field test with recording of air velocity and direction in the air vent could provide meaningful validation data. However, such a test must be carefully considered and monitored by the engineers (BRC) and co-ordinated with the authorities (TCTA and DWA) with regard to the downstream effects and to avoid an unseasonal release.

7. GUIDELINES FOR THE DESIGN OF FUTURE BOTTOM OUTLETS

The following design guidelines should be adhere to in future designs to prevent air blowback:

- Bottom outlets should be designed to ensure free-surface flow conditions under all probable flow condition. The formation of hydraulic jumps should be avoided by maintaining supercritical flow (Fr > 1) in the outlet conduit (USACE, 1997).
- If the cross section of the outlet conduit has to change, air entrapment should be avoided by matching conduit crown heights rather than the invert levels (USACE, 1997).
- The upstream movement of air which can cause possible blowback problems should be avoided by keeping the slope of the outlet conduit as flat as possible (refer to **Figure 2.19**) (Falvey, 1980).
- The crest height of a ski-jump should not be so high that it could cause submergence of the conduit under low flow conditions.
- The flow in an outlet conduit should not be restricted for any foreseeable flow condition. If a radial gate fails in a partially closed position it could cause potentially dangerous air blowback during emergency gate closure. A possible conduit configuration to prevent blowbacks in this scenario is discussed in **Section 6.1**.
- Large scale hydraulic models (greater than 1:20) should be used in the design process for partially full flow outlet conduits to minimise scale effects and to readily observe the detailed flow behaviour. Emergency gate closure procedures should be included in the tests at design stage (Speerli, 1999).

8. REFERENCES

Abban, B., Shand, M., Kamish, W., Makhabane, M., Van Zyl, B., & Tente, T. (2008). *Decision Support Systme for the Berg River Dam and Supplement Scheme.* Stellenbosch: University of Stellenbosch.

Aydin, I. (2002). Air demand behind high head gates during emergency closure. *Journal Hydraulics Division, Vol 40, No.1*.

Basson, G. R. (2011, February 17). Commissioning Test of Berg River Dam in 2008. (A. Vos, Interviewer)

Borodina, L. (1969). Aeration behind low level gates. *Gidrotekhnicheskoe Stroitel'stvo, No. 9*, 32-37.

Erbisti, P. (2004). *Design of Hydraulic Gates.* Netherlands: Swets & Zeitlinger B. V.

Falvey, H. T. (1980). *Air-Water Flow in Hydraulic Structures: Engineering Monograph No. 41.* Denver: Water and Power Resources Service.

FEMA. (2004). *The National Dam Safety Program.* Denver, Colorado: Federal Emergency Management Agency.

Kalinske, A. A., & Robertson, J. M. (1943). Entrainment of Air in Flowing Water Closed Conduit Flow. *Transactions, ASCE, Vol. 108*, 1435-1447.

Levin, L. (1965). *Calcul Hydraulique des Conduits d'Aeration des Vidanges de Fond et Dispositifs Deversants, No. 2.* La Houille Blanche.

Lewin, J. (2001). *Hydraulic gates and valves in free surface flow and submerged outlets: Second Edition.* London: Jack Lewin and Thomas Telford Limited.

Lowe, F. C. (1944). *Hydraulic Model studies for the Glory-hole spillways at Owyhee Dam - Owyhee Project, Oregon-Idaho.* Denver: United States Department of the Interior Bureau of Reclamation.

Najafi, M., & Zarrati, A. (2010, July 27). Numerical simulatio of air-water flow in gated tunnels. *Water Management 163 Issue WM6*, pp. 289-295.

Naudacher, E. (1991). *Hydrodynamic Forces.* Rotterdam: A.A.Balkema.

Rabben, S. L., & Rouvè, G. (1985). Belüftung von Grundablässen. *Wasserwirtschaft 75(9)*, 393-399.

Rindels, A. J., & Gulliver, J. S. (1983). *An Experimental Study of Critical Submergence to avoid Free-Surface Vortices at Vertical Intakes.* Minneapolis, Minnesota: University of Minnesota.

Safavi, K., Zarrati, A., & Attari, J. (n.d.). Experimental study of air demand in high head gated tunnels. pp. 105-111.

Sarkaria, G., & Hom, O. (1959). Quick Design of Air Vents for Power Intakes. *Proceedings of ASCE, Journal of the Power Division*, PO6.

Shand, M. (2008). *Berg River Dam Emergency Gatre Commissioning Release of Air.* Cape Town.

Sharma, H. (1976). Air-Entrainment in High Head Gated Condiuts. *Journal of the Hydraulics Division*, 1629-1645.

Speerli, J. (1999). *Air Entrainment of Fee-surface Tunnel Flow.* Switzerland: Swiss Federal Institute of Technology.

TCTA. (2006). Modellin, Monitoring Nuts and Bolts of Dam Projects. *The Water Wheel*, 29-31.

TCTA. (2008). Berg River Dam: Designed with Rivers in Mind. *The Water Wheel*, 33-37.

US Army Corps of Engineers (USACE). (1980). *Hydraulic Design of Reservoir Outlet structues, EM 1110-2-1602.* Washington DC: Department of Army, Corps of Engineers.

US Army Corps of Engineers (USACE). (1997). *Engineering and Design - Tunnels and Shafts in Rock, Engineering Manual No 1110-2-2901.* U.S.A: Department of the Army, Corps of Engineers.

Van Vuuren, S. (2003). *Berg river Project Hydraulic Model Testing of the Outlet works Modele Scale 1:20.* South Africa: Sinotech CC.

Villegas, F. (1994). Preventing Accidents at Intake Towers. *Water Power and dam Construction*, 42-46.

Vischer, D., & Hager, W. (1998). *Dam Hydraulics.* West Sussex: John Wiley & Sons Ltd.

Webber, N. (1971). *Fluid Mechanics for Civil Engineers, S.I. Edition.* London: Champman and Hall Ltd.

Webby, M. G. (2003). *Investigatio of blowback Incidents on the Rangipo Power Station.* Wellington, New Zealand: Opus internatioal Consultants.

Wong, E. S., Chan, D. W., Jones, P., & Law, L. K. (2008). *Assessment of air Pressure inside a Drainage Stack.* Hong Kong: International MultiConference of Engineers and Computer Scientists.

APPENDICES

ANNEXURE A: As-Built Drawings of Berg River Dam Outlet Works

ANNEXURE B: Model Scale Effects

In various aspects of engineering, physical models can often prove to be more efficient than computer or numerical analysis to solve fluid hydraulic problems, due to the intricate characteristics of the physics and boundaries of the flow. Under these circumstances, laboratory-controlled models provide an advantage and give proven accurate results (Webber, 1971).

It is critical that the model must accurately represent the behaviour of the prototype, which requires that the layout of the prototype should be modelled correctly. It is essential that the phenomenon to be studied are understood clearly so that the results from the model are interpreted correctly. The laws of hydraulic similarity govern the relationship between the prototype and the performance of the model. Simultaneous compliance with all the laws is impossible, thus some discrepancies are inevitable when extrapolating the results from the model to the full scale, which is known as scale effects. The scale effects can be minimised by ensuring that the model is large enough, or by taking the necessary compensatory steps (Webber, 1971).

The expected performance of the prototype can be verified with hydraulic models. Models indicate the necessary modifications to the design, which saves a significant amount of construction cost and usually depicts the best design from and economical point of view (USACE, 1980).

The behaviour of the model under examination must relate to the behaviour of the prototype for accurate prototype conditions to be obtained. The two flow systems must be hydraulically similar in order to transfer the results from the model to the prototype. This entails that geometric similarity of boundaries be retained and that dynamic and kinematic similarity be established by assuring that the forces having an impact on the motion of the water particles in the model and prototype be of constant ratio to each other. Thus, the water particles in the model and prototype must flow in similar geometrical patterns in proportional times (USACE, 1980).

2.1. Geometric Similarity

Geometric similarity indicates similarity of shape and is obtained if the model is constructed in an undistorted manner according to the linear scale adopted. This is achieved if the ratio of any two dimensions of the model is the same as the corresponding ratio of the prototype. The scale ratio can be expressed as follows (USACE, 1980):

$$\frac{(L_1)_m}{(L_2)_m} = \frac{(L_1)_p}{(L_2)_p}$$

where

L_m: linear dimensions of the undistorted model (m)

L_p: linear dimensions of the prototype (m)

The area and volume ratios are the square and cube of the linear scale ratio respectively. Therefore, if the scale of the linear model is 1:x, then the scalar relationship for the area and volume can be represented as 1:x^2 and 1:x^3 respectively (USACE, 1980).

To obtain complete geometric similarity, the boundary roughness of the model and prototype should have a corresponding ratio. If k is defined as the sand grain diameter, the scalar roughness ratio k_m:k_p at corresponding positions on the surface of the model and prototype must be 1:x. The reproduction of the boundary roughness to this high level of conformity is not always possible, because of the irregular nature of the material finishes (Webber, 1971). In prototypes with boundaries with smooth surfaces (e.g. well-finished concrete or metal) it is impossible to achieve the additional degree of smoothness required for the surface of the model.

Bearing in mind the discrepancies in geometric similarity as described above, it should be remembered that it is most important that the hydraulic behaviour of the flow arising from the boundary conditions is of a similar ratio for the model and the prototype. Therefore, some geometric dissimilarity is unavoidable and tolerable (Webber, 1971).

2.2. Kinematic Similarity

Fulfilment of the requirements of kinematic similarity requires a consideration of the motion of the fluid. Kinematic similarity is satisfied if the velocities and acceleration at congruent points at congruent times in the both systems have the same ratio. The homologous direction of the motion in the two systems must also be the same. The ratio to comply with kinematic similarity is given by the following formula (Webber, 1971):

$$\frac{(v_1)_m}{(v_2)_m} = \frac{(v_1)_p}{(v_2)_p} \textbf{ and } \frac{(a_1)_m}{(a_2)_m} = \frac{(a_1)_p}{(a_2)_p}$$

where

v_m: velocity of fluid in model (m/s)

v_p: velocity of fluid in prototype (m/s)

a_m: acceleration of fluid in model (m/s^2)

a_p: acceleration of fluid in prototype (m/s^2)

It must be noted that geometric similarity of the surface boundaries is an important prerequisite to obtain similar flow patterns in order to achieve kinetic similarity.

2.3. Dynamic Similarity

The forces capable of influencing the motion of the fluid at homologous points in the model and prototype system must have the same ratio and act in the same direction to achieve dynamic similarity. The ratio to comply with dynamic similarity is given by the following formula (Webber, 1971):

$$\frac{(F_1)_m}{(F_2)_m} = \frac{(F_1)_p}{(F_2)_p}$$

where

F_m: forces acting on fluid in the model (kN)

F_p: forces acting on fluid in the prototype (kN)

The forces acting on the fluid in both systems are gravity, surface tension, elasticity and fluid viscosity. The regime of the flow can be defined by dimensionless numbers known

as Froude (gravity), Reynolds (viscosity), Webber (surface tension) and Euler (elasticity), which are specific combinations of the abovementioned forces. The regime of the flow is governed by the forces acting on the fluid particles, consequently geometric and kinematic similarity must also be obtained if dynamic similarity must exist throughout the two systems (Webber, 1971).

The connotations of the various similarity laws as discussed in above are as follows:

3.1. Euler's Law

The basic relationship between velocity (V) and pressure (p) is depicted by the Euler equation $\left(E = V/\sqrt{2\Delta p/\rho}\right)$. The Euler number is of particular significance in enclosed fluid system models where the turbulence of the fluid is fully developed, resulting in the viscous forces being irrelevant in relation to inertia forces acting on the fluid particles. Evidently, gravity and surface tension forces are completely absent. Thus, the applied pressure forces are the controlling factor and act as an independent variable. However, this is contrary to most fluid phenomena, in which the pressure force is a dependent variable, as it is consequential upon the motion of the fluid (Webber, 1971).

Euler's Law can be integrated into the corresponding model and prototype velocities as follows (Webber, 1971):

$$\frac{\boldsymbol{V_p}}{\boldsymbol{V_m}} = \frac{\boldsymbol{\Delta p_p}^{1/2}}{\boldsymbol{\Delta p_m}^{1/2}} \times \frac{\boldsymbol{\rho_m}^{1/2}}{\boldsymbol{\rho_p}^{1/2}}$$

where

V: velocity (m/s)

p: pressure (kN/m^2)

ρ: density (kg/litre)

It can be observed from the above equation that the relationship between the velocity and pressure is nonlinear and universally applicable whenever inertia forces are of great significance. The operating speed (or controlling pressure) will be within the researcher's judgment, provided that the model is large enough to ensure that all forces except pressure remains trivial (Webber, 1971).

3.2. Froude's Law

Gravity and inertia are the dominant forces that influence the motion of the fluid in systems where a free surface gradient is present, particularly those in open channels, spillways, weirs, rivers, etc. Dynamic similitude is achieved by designing the model according to Froude's Law. In other words, the Froude number in the model and prototype must be equal. The Froude number is defined as follows (USACE, 1980):

$$F_r = \frac{V}{\sqrt{gL}}$$

where

F_r: Froude number (dimensionless)

V: velocity (m/s)

g: acceleration of gravity (9.81 m/s^2)

L: characteristic linear dimension (m)

The corresponding velocities in the two systems must be of similar ratio to comply with Froude's Law (Webber, 1971)

$$\frac{V_p}{V_m} = \frac{(L_p)^{1/2}}{(L_m)^{1/2}} = x^{1/2}$$

Velocities that occur in models are less than those that occur in the prototype, which is beneficial, as improved measuring instruments are available in the laboratory, whereas pumping capacity is a limiting factor (Webber, 1971).

The discharge characteristics of models subjected to Froude's Law can generally be predicted within ± 5%, which is adequate for hydrometric purposes (Webber, 1971).

3.3. Reynolds Law

A real fluid has viscosity, therefore the potential influence of viscous shear drag on the fluid needs consideration. The Darcy-Weisbach coefficient as a function of the Reynolds number (Re) is used to reproduce the conduit surface irregularities affecting the motion of the fluid.

According to the Reynolds law ($Re = VL/v$), the corresponding velocities in the model and prototype must be related as follows (Webber, 1971):

$$\frac{V_p}{V_m} = \frac{v_p}{v_m}\frac{L_m}{L_p} = \frac{v_p}{v_m}\frac{1}{x}$$

where

V: velocity (m/s)

L: length of homologous sections in model and prototype (m)

v: kinematic viscosity (m^2/s) = 1.13 x 10^{-6} m^2/s

The equation above indicates that, if the same fluid at the same temperature is utilised in both systems, the prototype velocity must be x times greater than that of the model (Webber, 1971).

Viscous forces are generally a secondary influence on the fluid in the prototype because of the low viscosity of water. They are, however, important considering their influence on boundary frictions and their role as the origin of turbulence in fluids (Webber, 1971).

The model and prototype cannot be satisfied by both Froude's and Reynolds' laws at the same time. Variation in the Reynolds number is not of great importance, provided that both the prototype and the model have high Reynolds numbers (Re > 100 000) and have similar roughness-to-diameter ratios. Under these conditions, the head loss will be a function of the square of the velocity in both systems. If the Reynolds number of the model approaches the transition zone where the flow changes from turbulent to laminar flow, laminar flow might occur in the model, whereas turbulent flow will occur in the prototype. This can be avoided by choosing a minimum Reynolds number where the model must be operated. Models of pipelines often operate in this "transition zone" category, where the energy grade line dictates the motion of the fluid and not the pipeline slope (Lewin, 2001).

Under full-scale conditions, the Reynolds number of the prototype will be greater that in the model, but the overall friction factor will be less. Consequently, for fluids other than water, the model conduit must be shortened from the length required to comply with

geometric similarity in order to artificially reproduce the loss that will occur through the conduit (USACE, 1980).

The derived scalar relationships according to Froude's and Reynolds' laws are summarised in the below.

Table B1: Scalar Relationships for Models (Reynolds & Froude laws)

Hydraulic Similarity	Quantity	Dimensions	Reynolds law	Froude law	
			Natural scale 1:x	Natural scale 1:x	Distorted scales 1:x horiz.; 1:y vert
Geometric	Length	L	x	x	x (horiz.) y (vert.)
	Area	L^2	x^2	x^2	x^2 (plan) xy (sect.)
	Volume	L^3	x^3	x^3	x^2y
Kinematic	Time	T	x^2/v_r	$x^{1/2}$	$x/y^{1/2}$
	Velocity	L/T	v_r/x	$x^{1/2}$	$x/y^{1/2}$ (horiz.) $y^{3/2}/x$ (vert.)
	Acceleration	l/T^2	v_r^2/x^3	1	y/x (horiz.) y^2/x^2 (vert.)
	Discharge	L^3/T	$v_r x$	$x^{5/2}$	$xy^{3/2}$
Dynamics	Pressure	M/LT^2	$\rho_r v_r^2/x^2$	$\rho_r x$	$\rho_r y$ (sect.)
	Force	M/LT^2	$\rho_r v_r^2$	$\rho_r x^3$	$\rho_r xy^2$ (sect.)
	Energy	M^2/LT^2	$\rho_r v_r^2 x$	$\rho_r x^4$	$\rho_r xy^3$ (sect.)
	Power	M^2/LT^3	$\rho_r v_r^3/x$	$\rho_r x^{7/2}$	$\rho_r y^{7/2}$ (sect.)

3.4. Weber's Law

Surface tension is only of importance when an air-water boundary exists and the linear dimensions of the model are small. However, it is of great importance to study the influence of surface tension on the fluid in models, with very low weir heads, air entrainment, spray or splash (Webber, 1971).

The corresponding velocities in the prototype and model must relate as follows to comply with Webber's Law $\left(W = V/\sqrt{\sigma/L\rho}\right)$:

$$\frac{V_p}{V_m} = \frac{{\sigma_p}^{1/2}}{{\sigma_m}^{1/2}} \frac{{\rho_m}^{1/2}}{{\rho_p}^{1/2}} \frac{{L_m}^{1/2}}{{L_p}^{1/2}} = \frac{{\sigma_p}^{1/2}}{{\sigma_m}^{1/2}} \frac{{\rho_m}^{1/2}}{{\rho_p}^{1/2}} \frac{1}{x^{1/2}}$$

where

V: velocity (m/s)

L: length of homologous sections in model and prototype (m)

σ: stress (kN/m^2)

ρ: density (kg/litre)

The above equation indicates that the velocity in the prototype will be $x^{1/2}$ times greater than the velocity in the model.

Generally, surface tension has very little or no influence on the behaviour of fluid in the prototype. By ensuring that the model is large enough, the surface tension will still be insignificant at model scale, therefore it will be practical to abstain from complying with this law (Webber, 1971).

Sub-atmospheric pressures are another scalar discrepancy that requires attention. The model and prototype are both operated under atmospheric conditions, ensuring that pressures relative to atmospheric pressures are modelled to scale. On the contrary, absolute pressures are not reproduced to scale. The vaporisation of water is initiated when the pressure falls within a metre of absolute zero pressure. However, dissolved air is released from solution before this stage is reached. This phenomenon will occur at an earlier stage in the prototype than in the model, as pressures are lowered at the reduced scale. Judgement on the part of the modeller with regard to the interpretation of the results from the model is required to prevent incorrect predictions about the discontinuity of the flow and cavitation. Pressures of up to 5 m below atmospheric pressure are acceptable because a tolerable margin of dissimilarity of surface roughness, vorticity and/or turbulence may exist, which can create a temporary lowering of pressures in the prototype. Operating the model in a vacuum container is one solution to overcome the pressure relationship problem, but this is not always feasible, as attendant experimental complications are unavoidable (Webber, 1971).

ANNEXURE C: Commissioning Test on Berg River Dam - June 2008

BERG RIVER DAM EMERGENCY GATE COMMISSIONING
RELEASE OF AIR

Dr Mike Shand
30 June 2008

1. Introduction

Andy Griffiths of Goba and I discussed the possible reasons for the release of very large volumes of air from the air intake shaft during the trial closure of the emergency gate on 12 June 2008. We concluded that the only way that the volume of air released could arise is through the formation of and entrainment of air by a vortex in the intake shaft. Our reasons are set out below.

2. Design of Air Shaft

The air shaft was designed to allow air to be introduced immediately downstream of the emergency gate on account of the negative pressures that were expected to occur during its partial closure. The final design was based on the 1 in 20 scale hydraulic model tests, which had shown no evidence of vortex formation and had indicated that air would be drawn down the air shaft.

Immediately after the trial release, Prof. Gerrit Basson utilized the 1 in 40 scale hydraulic model that was also used for the original design and is still operational at the University of Stellenbosch, to re-simulate partial closure of the emergency gate but with the water level in the dam at full supply level. This modeling also showed no evidence of vortex formation and indicated that large volumes of air would be drawn down the air shaft.

3. Mechanism for Release of Air from Airshaft

Contrary to the design, James Metcalf's air shaft velocity measurements shown in Table 1 indicate that, while the emergency gate was closing, very large volumes of air were continuously

released from the 1,8 m^2 air shaft commencing when the gate was about 30% closed (i.e. 70% open). The time of commencement of the release of air seems to have coincided with the observations of the following:

- The time that the cavitation noise in the access shaft to the emergency gate ceased, which indicates the presence of air, and
- The time that the release of air from the flow commenced in the radial gate house.

James Metcalf's observations indicate that the velocities of air released through the 1,8 m^2 air shaft increased from 8,75 m/s (32 km/h) at 13h06 to about 45 m/s (160 km/h) at 13h14, corresponding to air releases increasing from 16 m^3/s to 80 m^3/s as indicated in Table 2. There are only two potential sources of air:

- The entrainment of air from the downstream end of the conduit at the radial gate: however this would not be possible because of the high velocity of the water flow in the conduit which causes air to be dragged downstream rather than upstream, and because the observations during the trial indicate that for much of the time the conduit was flowing full with considerable volumes of air entrained in the flow. Reports by observers in the housing of the radial gate also indicate that considerable volumes of air were released from the flow as it exited at the radial gate. However the removal of air was also reported and this may have been caused by the suction effect of intermittent fully aerated flow occupying the total area of the opening downstream of the radial gate.
- The only other potential source of air is via a vortex forming in the vertical shaft upstream of the emergency gate, and is the only explanation that is consistent with the velocity observations of the air releases from the air vent and from observations that the flow at the radial gate was highly aerated.

4. Recommendations for Hydraulic Model Tests

The following recommendations are made to try to gain an improved understanding of the mechanism for the formation of a vortex in the shaft:

- Although the 1 in 50 scale hydraulic model is not sufficiently large to accurately model the formation of vortices, it is nevertheless recommended that this model is utilized to observe the flow patterns as follows:

- For the dam water level and intake level at the time of the trial and with the radial gate fully open check the flow patterns and air entrainment for small incremental closures of the emergency gate similar to those undertaken for the trial. If possible measure the air releases and the flow of water for the various emergency gate openings.
- If no vortex forms repeat the above but introduce mild circular perturbations to the water in the intake shaft either by stirring action or by temporarily blocking the flow through one of the intakes into the tower (try clockwise and counter clockwise rotation).
- Repeat with stronger perturbations until a vortex forms with the gate at about 66% open and then observe the air entrainment and release from the air shaft for incrementally reducing openings. If possible measure the flow of water and of air for the various emergency gate openings.
- Repeat for other intake gate selections and water levels in the dam.

- Compare the modelled air releases with those measured by James Metcalf on 12 June.
- Obtain from DWAF the actual flow measurements at the Crump weir downstream, and compare these with the hydraulic model results, if necessary adjusted by computer model routing to account for the times of incremental gate lowering and the plunge pool and channel storage effects upstream of the Crump weir.
- Obtain the records for the pressure cells outside the conduit to check whether these also indicate the reducing pressures in the conduit due to the entrainment of air.
- Prepare a report on the above.

5. Safety Recommendations

The following recommendations are made:

- Air Shaft: The rectagrids at the top of the air shaft were blown 3 m to 4 m into the air as indicated in Table 1 and fortunately only caused a minor injury to James Metcalf but could easily have killed him and the observer from the Cape Argus. Therefore as human lives would be endangered in the event that the emergency gate is purposefully or inadvertently operated in the future, it is strongly recommended that the rectagrid is removed and that the air shaft is extended upwards by at least 1.8 m by constructing a reinforced concrete chimney around the air shaft.

- Radial Gate House: The accounts of observers that the intermittent release and removal of large volumes of air could perhaps have damaged the radial gate house have already been taken into account and the contractor has been instructed to replace all windows with grids. It is also understood that there was a considerable amount of water spray in the gate house during the emergency gate closure and earlier during the commissioning tests there was also spray from the leaking gate seals.

As the electrical equipment for operating the radial gate will be exposed to the weather to a greater extent by the removal of the windows and possibly to spray, it is suggested that consideration be given to constructing a small weatherproof enclosure around the electrical equipment in the gate house.

Table C.1. Air Shaft Velocity Observations By James Metcalf on 12 June 2008

Time	Hand-held Schiltnecht Anemometer **Air Shaft (±1.5m x 1m) Air Velocity Reading: (32 second average** logged by electronic unit)	**Gate Degree Closed (Open)**	**Remarks** (NB: Anemometer held down on top of Mentis Grid Cover)
12 June 08	**m/s**		
13h00	Observer not present	0%	Air velocity & direction unknown (suspect ingestion of air – i.e.: "down shaft"
13h01	Ditto	5.5%	
13h02	Ditto	11.1%	
13h03	Ditto	16.7%	
13h04	Observer setting up instrument	22.2%	
13h05	3.5m/s	27.8% (72%)	Air Vel Direction unknown
13h06	8.75m/s	33.3% (67%)	Notebook in which air velocity readings were being recorded handed to second observer (Cape Argus Reporter) since up-velocity (out of shaft) causing notebook to be "blown away"
13h07	12.44m/s	38.9%	Up-shaft air flow

		(56%)	
13h08	14.2m/s	44.4%	Ditto
Time	Hand-held Schiltnecht Anemometer **Air Shaft (±1.5m x 1m) Air Velocity Reading: (32 second average** logged by electronic unit)	**Gate Degree Closed (open)**	**Remarks** (NB: Anemometer held down on top of Mentis Grid Cover)
13h09	19.8m/s	50% (50%)	Ditto
13h10	21.7m/s	55.5%	Increasing difficulty in holding anemometer down on shaft top grid cover due to high-velocity outflow (anemometer wooden case became air-borne at about this stage)
13h11	22.3m/s	61.1% (30%)	Air flows ”surging” constantly at (say) 10 cycles per minute and getting stronger all the time
13h12	26.0m/s	66.7% (32)	Observer finds it increasing difficult to hold down anemometer and to hold his arm horizontal whilst lying down on the shaft top cover, due to progressively rising air up-flow velocity
13h13	35 m/s	72.2% (28%)	Last reading before……..
13h14	Probably of the order of 45m/s (160km/hr)	77.8% (17%)	Mentis grid cover blown off top of shaft, lifted to a height of about 3 or 4 metres, tipping observer off the shaft top and against the upstream concrete wall, and then falling back to the ground, striking/injuring[1] the observers right foot (which was aligned along the toe of the wall
13h15	?	83.3%	Anemometer retrieved from the top of the shaft (loss prevented by being attached to the output cable to the electronic unit)
13h16	?	88.9%	No further readings
13h17	?	94.4%	
13h18	?	100%	

[1] “Ring toe” found to be crushed; writer is taken to a Franschhoek surgery wef ±2pm. Wound inspected by Dr Alex Heywood at about 3 pm, stitched up & dressed & appropriate medication given

Table C.2. Air Velocities and Flows Released from 1.8 m^2 Air Shaft

Time	Air Velocity		Air Flow
	m/s	km/hr	cu m/s
13h06	8.75	32	16
13h07	12.44	45	22
13h08	14.2	51	26
13h09	19.8	71	36
13h10	21.7	78	39
13h11	22.3	80	40
13h12	26	94	47
13h13	35	126	63
13h14	45	162	81

ANNEXURE D1: Photographs of Berg River Dam Model (as-built outlet)

Photograph 1: Layout of Berg River Dam Model

Photograph 2: Emergency gate, base of air shaft and outlet conduit

Photograph 3: Radial gate chamber and ski-jump at end of outlet conduit

Photograph 4: Outlet conduit

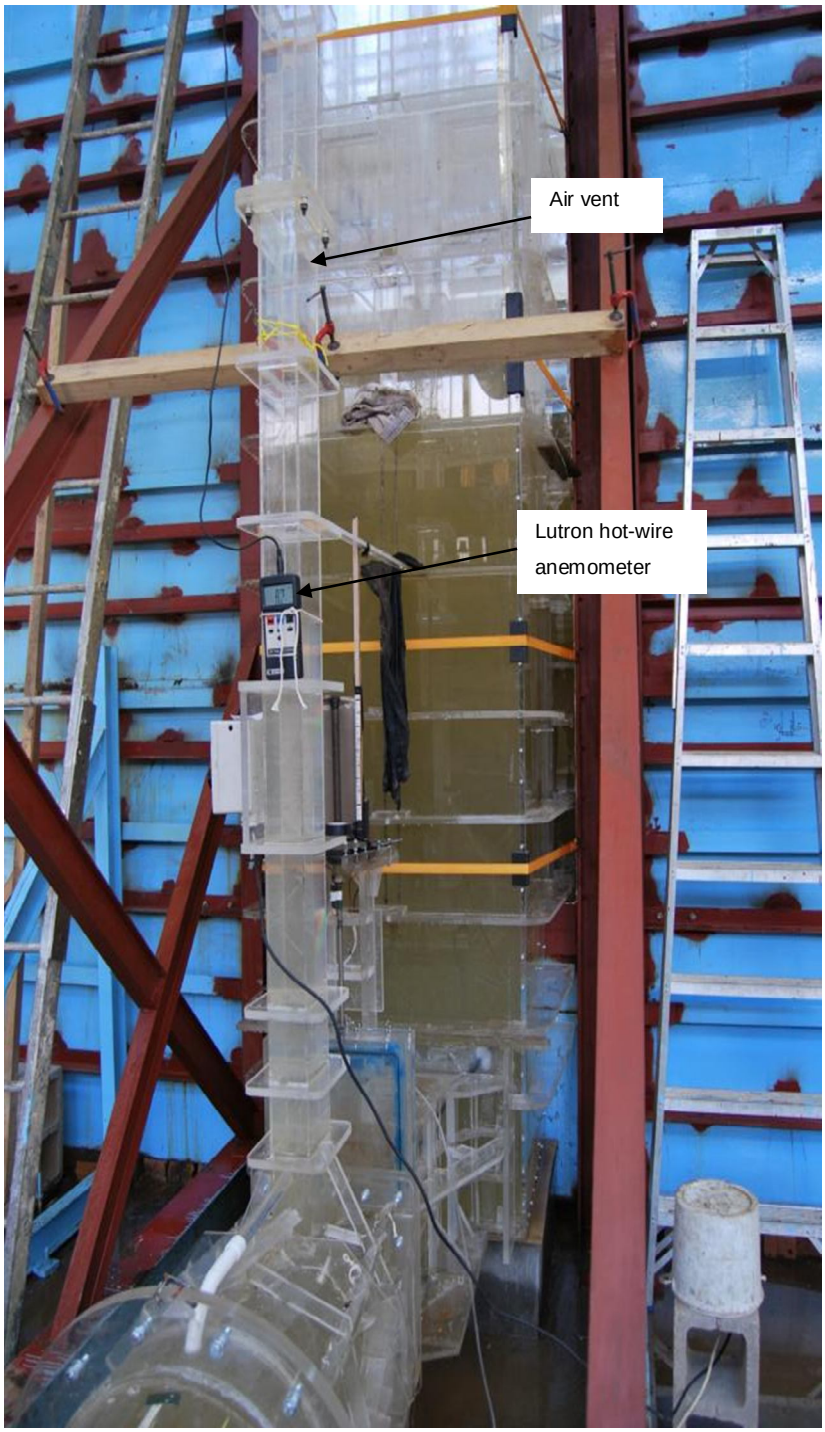

Photograph 5: Lutron hot-wire anemometer (wind velocity meter)

Photograph 6: Second bend

Photograph 7: Second bend

ANNEXURE D2: Photographs *of the Modified Berg River Dam Model*

Modification 1: The ski-jump was removed at the end of the conduit, with the second bend and radial gate chamber still intact (**Photograph 7**). The radial gate was not modelled.

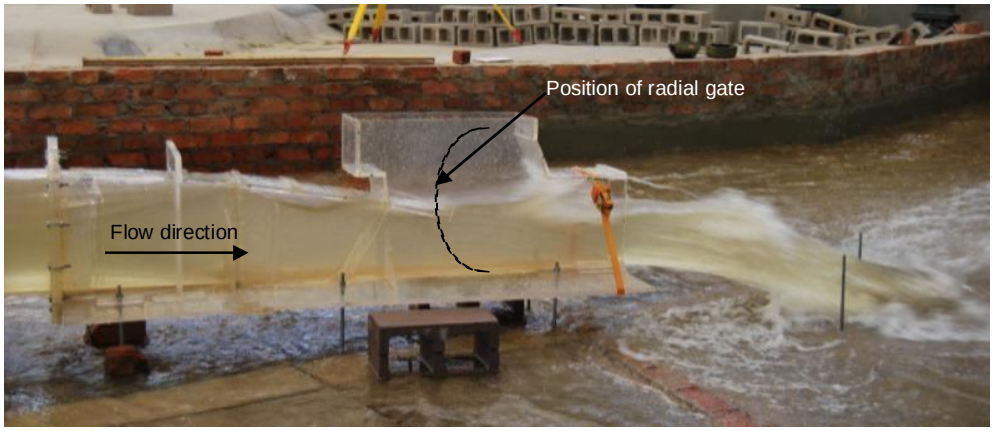

Photo 7: Modification 1 – ski-jump removed

Modification 2: The second bend (downstream) and ski-jump were removed, but the radial gate chamber was still connected to the end of the outlet conduit **(Photograph 8**).

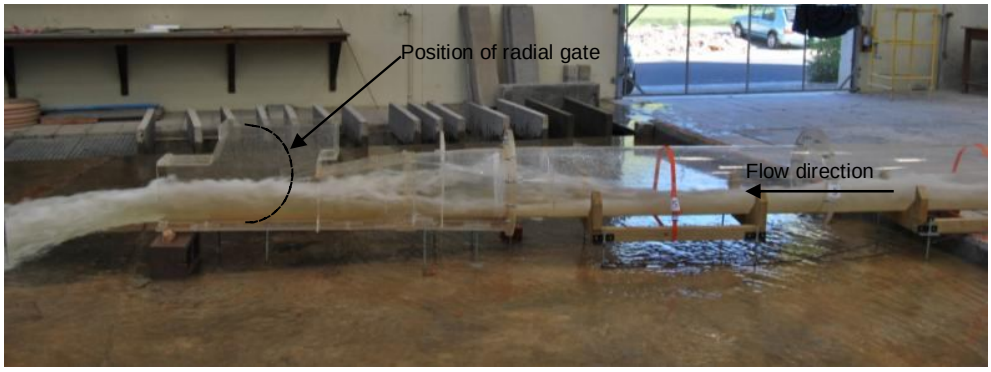

Photograph 8: Modification 2 – ski-jump and second bend removed

Modification 3: Only the second bend (downstream) was removed, but the radial gate chamber and the ski-jump were still intact with the outlet conduit (**Photograph 9**).

Photograph 9: Modification 3 – second bend removed

Modification 4: The radial gate chamber and ski-jump were removed, but with the second bend still intact (**Photograph 10**).

Photograph 10: Modification 4 – ski-jump and radial gate chamber removed

Modification 5: Extra air outlet pipe before tapered section (450 mm, 2.4 m long – prototype) (**Figure** 4.29 **11**). The radial gate was closed by 197 mm (prototype) to restrict the discharge to 204 m^3/s. Please note that the tapered section formed part of the model configuration.

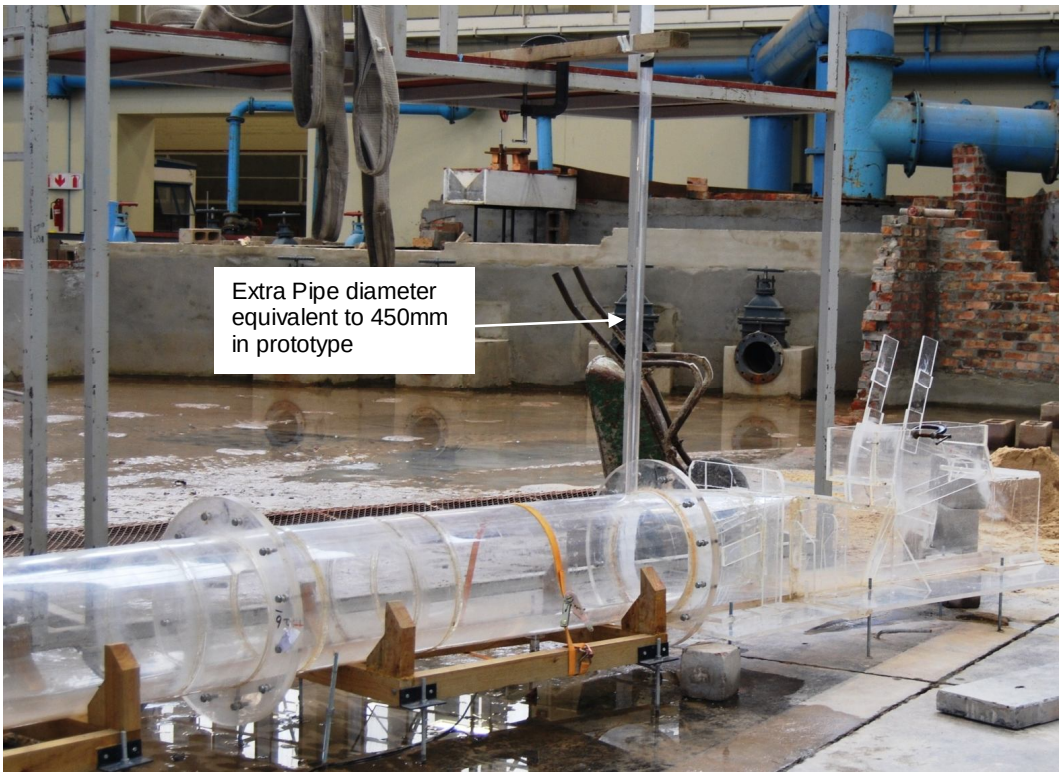

Photograph 11: Modification 5 – ski-jump and radial gate chamber removed

ANNEXURE D3: Photographs of the Berg River Dam (Prototype)

Photograph 12: Outlet conduit being built

Photograph 13: Commissioning test (2008)

Photograph 14: Commissioning test (2008) (close-up)

Photograph 15: Commissioning test (close-up)

Photograph 16: Inside radial gate chamber

Photograph 17: Top view of flood release during commissioning test (2008)

Photograph 18: Berg River Dam outlet structures during construction phase

Photograph 19: Inlet tower (wet and dry well) and bridge to inlet tower under construction

ANNEXURE E: Flow Pattern for Transient Gate Closure Simulations

The water flow conditions for all the water levels, gate closure rates and model configurations were similar, except for the six minute gate closure rate tests and for modification 4: ski-jump and radial gate chamber removed.

The flow conditions at each gate opening (10% intervals) are discussed below:

a) 100% and 90% gate opening:

All tests, except 6 min gate closure and modification 4

- No continuous air entrainment through air vent.
- Air shaft acts as a surge tower.
- Water oscillates in air vent with a period of 4 seconds (two seconds up and two seconds down) for the model (prototype oscillation period = 15 seconds (7.5 seconds up and 7.5 seconds down) (**Photograph 20**).
- Pressurised flow occurs in the outlet conduit, thus the conduit is flowing full downstream of the emergency gate (refer to **Photograph 21**).
- The air movement through the air vent was not sensitive to the closure rate, but was directly related to the water head.
- No vortices were observed in the water tower.

6 min gate closure rate

- Flow conditions are similar to those mentioned above for the rest of the tests.

Modification 4: Ski-jump and radial gate chamber removed

- Continuous air entrainment. Air vent did not act as a surge tower
- Free surface flow occurred downstream of emergency gate.
- No hydraulic jump formed downstream of the emergency gate.

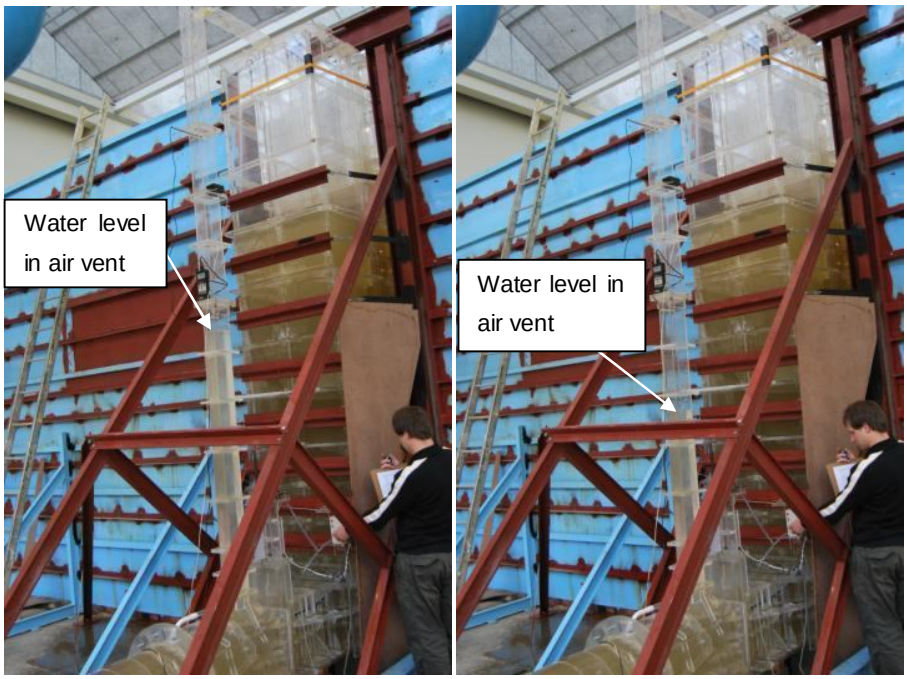

Photograph 20: Flow conditions at 100% gate opening (oscillation) – excl. modification 4

Photograph 21: Pressurised flow downstream of emergency gate – excl. modification 4

b) 80% gate opening:

All tests, except 6 min gate closure and modification 4

- No continuous air entrainment through air vent.
- Air vent still acts as a surge tower.
- Water in air vent oscillates irregularly.
- Pressurised flow still occurs downstream of the emergency gate, as shown in **Photograph 22**. Refer to **Photograph 23** for the flow conditions at the outlet for an 80% gate opening.
- The air movement through the air vent was not sensitive to the closure rate, but was directly related to the water head.
- No vortices were observed in the water tower.

6 min gate closure rate

- Flow conditions were similar as mentioned above for the rest of the tests.

Modification 4: Ski-jump and radial gate chamber removed

- Continuous air entrainment through air vent, air vent did not act as a surge tower
- Free surface flow occurred downstream of the emergency gate (**Photograph 24**).
- The outflow was not constricted by the conduit roof (**Photograph 25**)
- No hydraulic jump formed downstream of the emergency gate.

Photograph 22: Flow conditions at emergency gate for 80% gate opening – excl. Modification 4

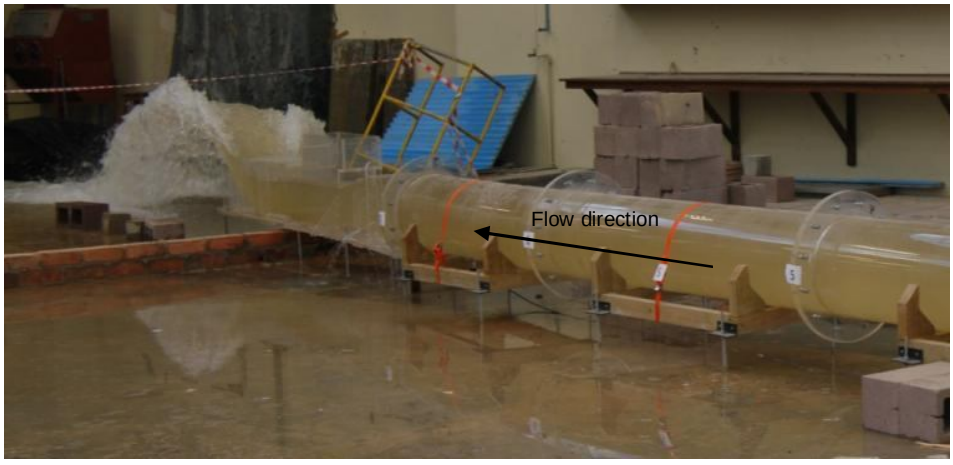

Photograph 23: Flow conditions at emergency gate for 80% gate opening –excl. modification 4

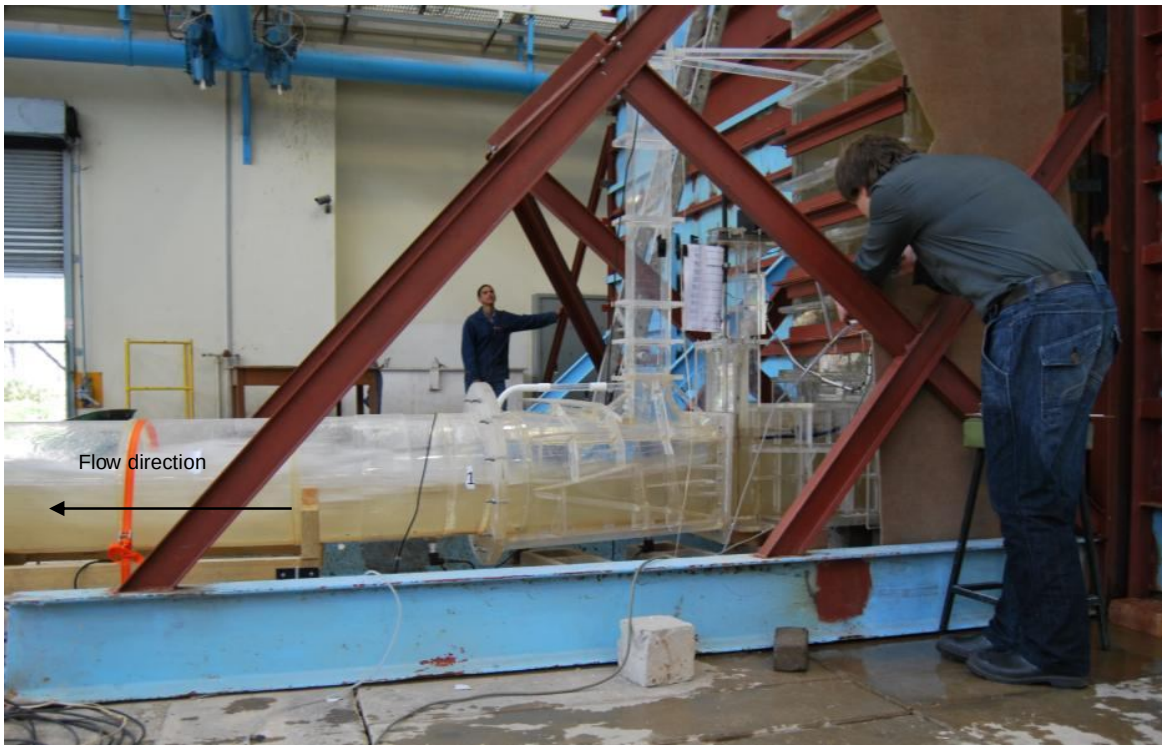

Photograph 24: Free surface flow at emergency gate at 80% gate opening for modification 4

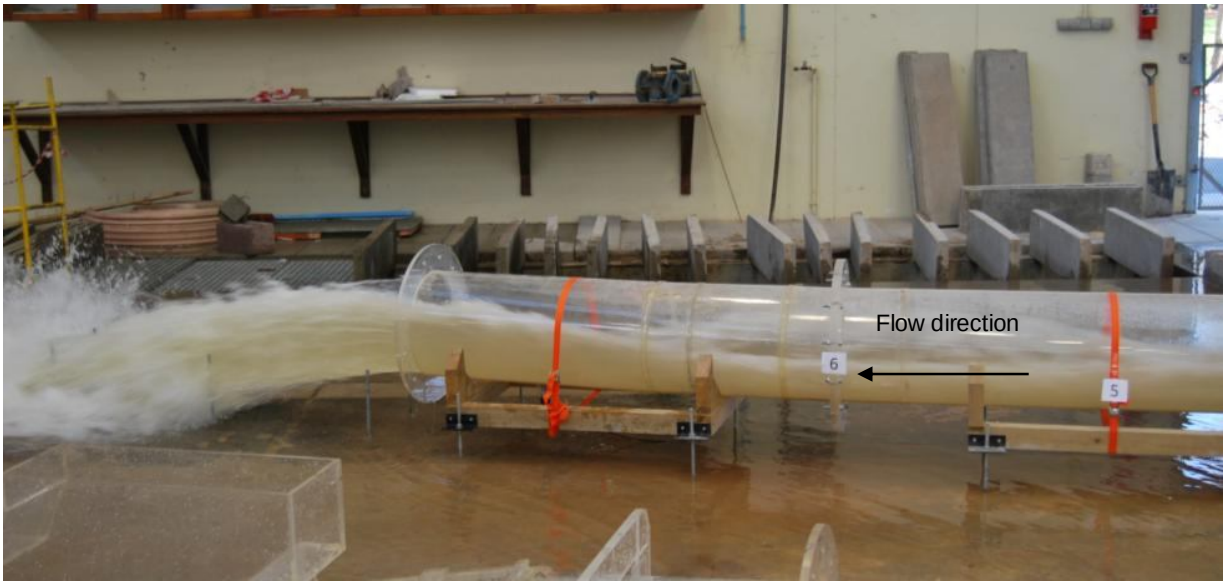

Photograph 25: Free surface flow downstream at 80% gate opening for modification 4

c) 70% gate opening:

All tests, except 6 min gate closure and modification 4

- Air entrainment into the air vent started when the gate was **70%** open (**Photograph 26**).
- An unstable hydraulic jump formed just downstream of the emergency gate for a 65% gate opening when the flow conditions change from pressurised to free surface flow (**Photograph 27**).
- The first bend (12°) in the conduit keeps the unstable hydraulic jump from moving freely downstream of the conduit.
- Pulsating flow occurred at the radial gate chamber, as the tapered section prohibited the flow to exit the conduit freely, as illustrated in **Photograph 28**.
- The air movement through the air vent was not sensitive to the closure rate, but was directly related to the water head.
- No vortices were observed in the water tower.

6 min gate closure rate

- Air entrainment started when the gate was **65%** open (**Photograph 26**).

Modification 4: Ski-jump and radial gate chamber removed

- Continuous air entrainment through air vent. The air vent did not act as a surge tower. Free surface flow occurred downstream of the emergency gate, as shown in **Photograph 29**.
- No hydraulic jump formed downstream of the emergency gate.
- Free surface flow occurred at the outlet of the conduit (**Photograph 29**).

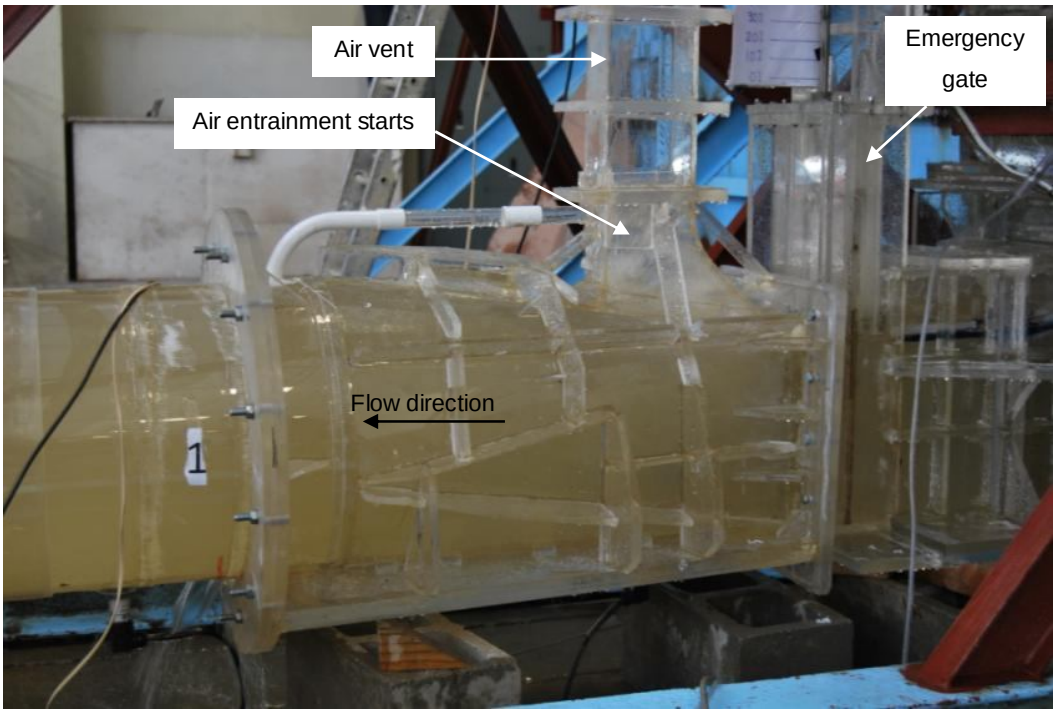

Photograph 26: Commencement of air entrainment– excl. modification 4

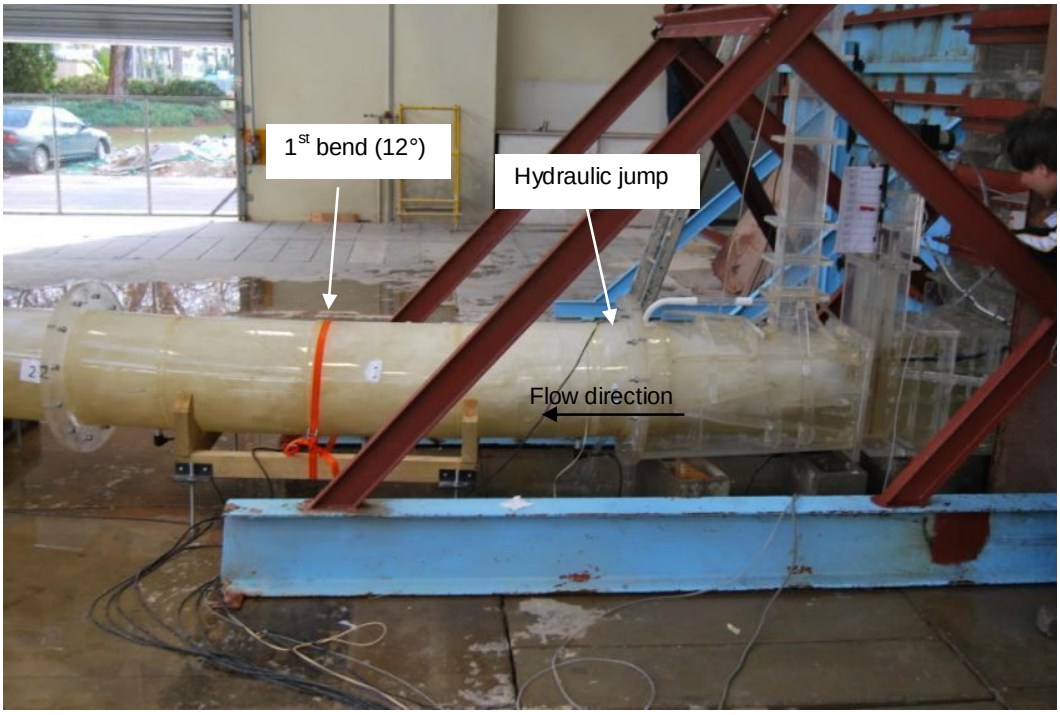

Photograph 27: Unstable hydraulic jump forms – excl. modification 4

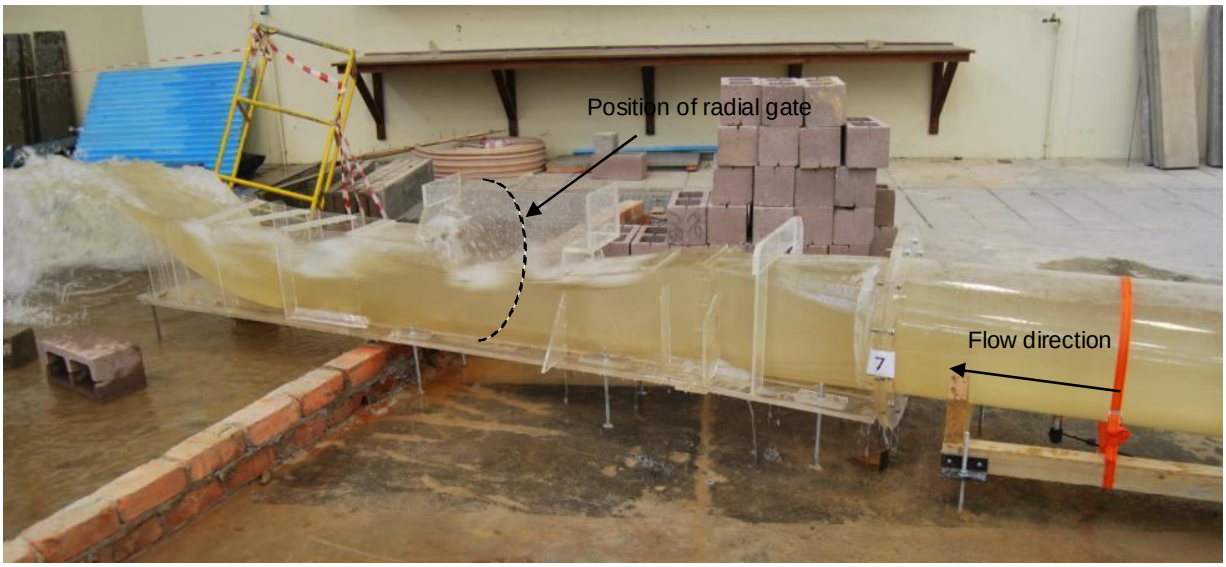

Photograph 28: Pulsating flow at radial gate chamber – excl. modification 4

Photograph 29 Free surface flow at emergency gate for 70% gate opening (modification 4)

Photograph 30: Free surface flow downstream for 70% gate opening (modification 4)

d) <u>60% gate opening:</u>

<u>All tests, except 6 min gate closure and modification 4</u>

- A well-defined hydraulic jump (unstable) formed just downstream of the emergency gate for a **60%** gate opening (**Photograph 31**).
- The jump is prohibited from moving downstream of the conduit due to the first bend (12°) in the conduit.
- The roof of the conduit sloped downwards to accommodate the radial gate chamber at the end of the conduit. This tapered section prohibited the free release of the air that had accumulated above the water in the outlet conduit. The air was thus released with a “pulsating” effect, as shown in **Photograph 32**.
- The air movement through the air vent was not sensitive to the closure rate, but was directly related to the water head.
- No vortices were observed in the water tower.

Photograph 31: Well-defined hydraulic jump d/s of emergency gate (all excl. Modification 4)

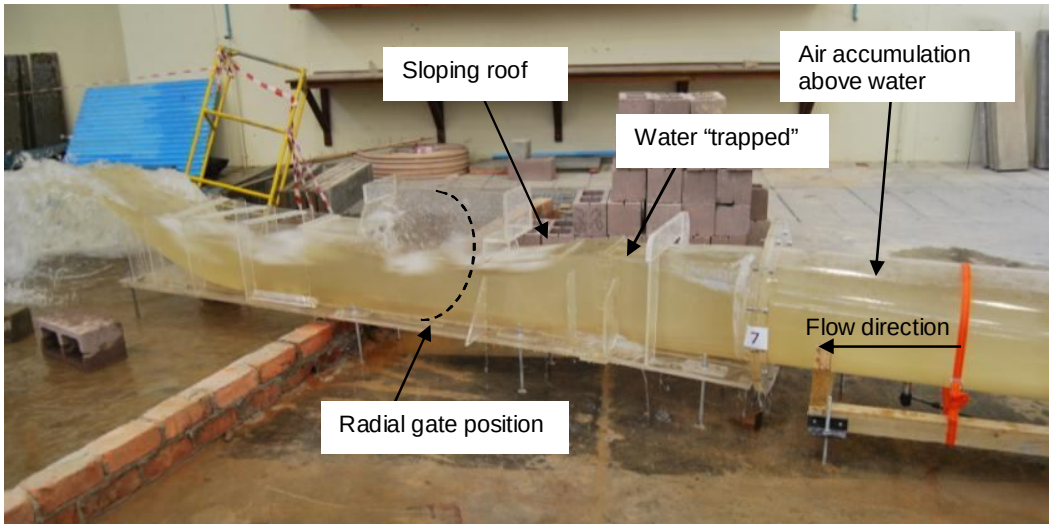

Photograph 32: Pulsating flow at outlet of conduit due to tapered section (all excl. modification 4)

6 min gate closure rate

- An unstable hydraulic jump formed just downstream of the emergency gate for a 60% gate opening when the flow conditions changes from pressurised to free surface flow (**Photograph 27**).
- The first bend in the conduit kept the unstable hydraulic jump from moving freely downstream of the conduit.
- The air velocity through the air vent was not sensitive to the closure rate, but was directly related to the water head.
- No vortices were observed in the water tower.

Modification 4: Ski-jump and radial gate chamber removed

- Free surface flow occurred downstream of the emergency gate and was released freely from the conduit as the tapered section of the radial gate chamber had been removed. No hydraulic jump was formed, as shown in **Photograph 33**.
- No pulsating flow occurred, as shown in **Photograph 34**.
- No vortices were observed in the water tower.

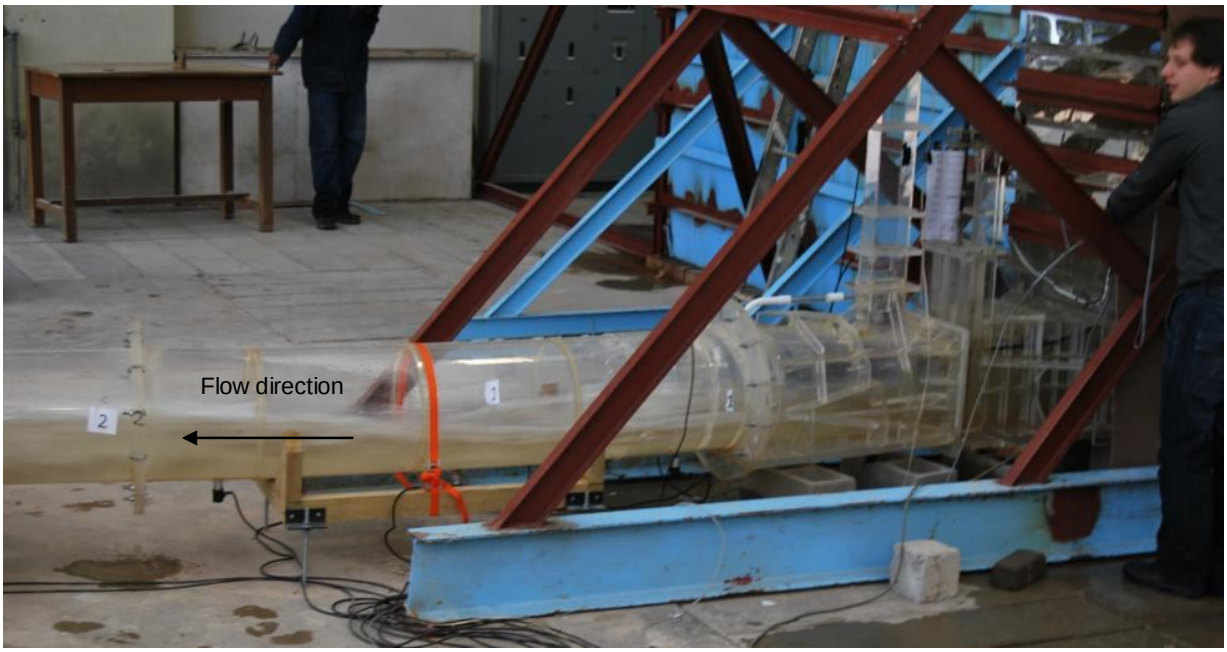

Photograph 33: Free surface flow at emergency gate for 60% gate opening for modification 4

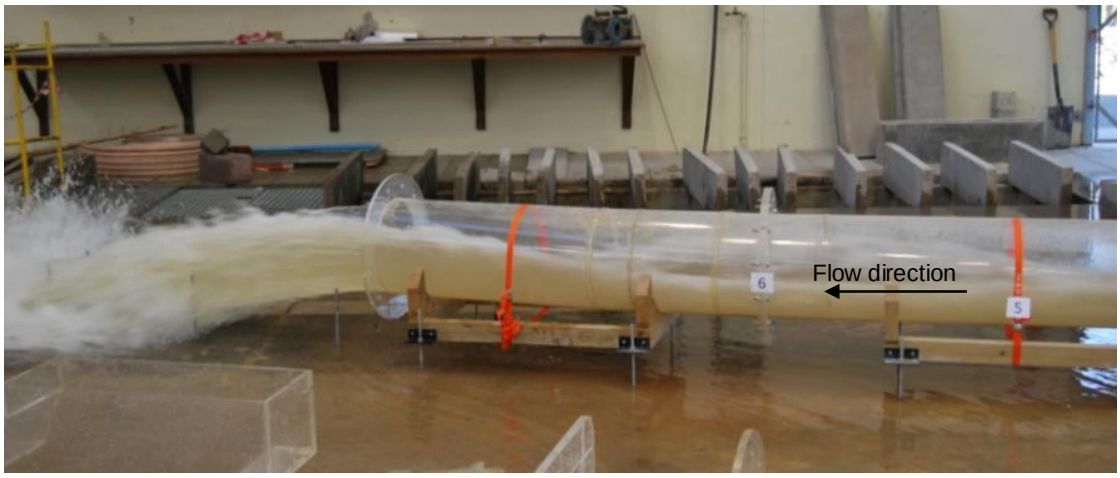

Photograph 34: Flow conditions at outlet for a 60% gate opening for modification 4

e) <u>50% gate opening:</u>

<u>All tests, except 6 min gate closure and modification 4</u>

- The unstable hydraulic jump was still positioned just downstream of the emergency gate at the first bend in the conduit (**Photograph 35**).
- The pulsating flow at the radial gate chamber increased (**Photograph 36**). The pulsating effect for the 30 minute gate closure rate was the most intense of the four different gate closure rates (six minutes, 12 minutes, 20 minutes and 30 minutes).
- The air movement through the air vent was not sensitive to the closure rate, but was directly related to the water head.
- No vortices were observed in the water tower.

Photograph 35: Flow conditions at emergency gate (all excl. modification 4)

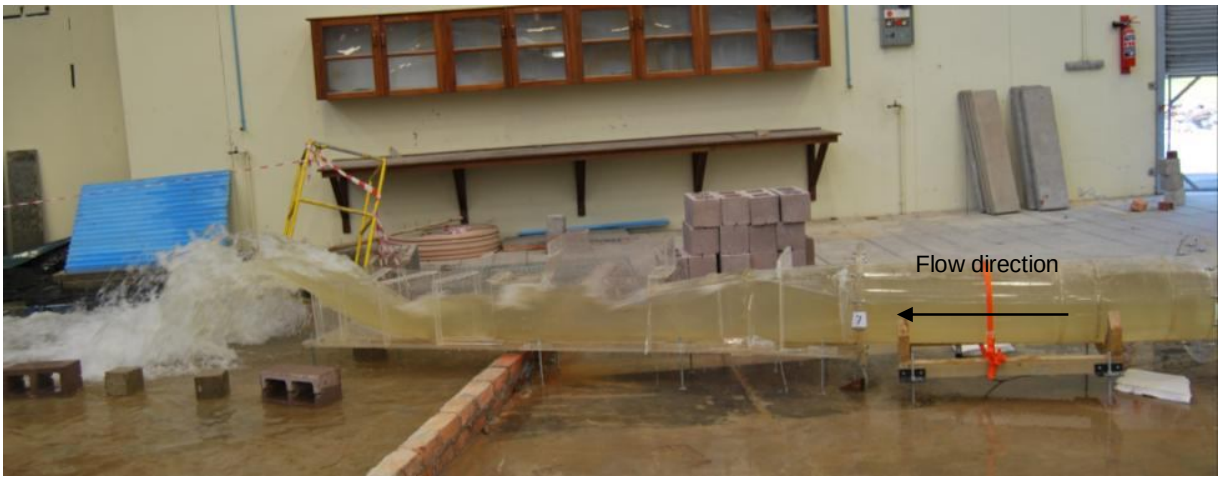

Photograph 36: Flow conditions at outlet (all excl. modification 4)

6 min gate closure rate

- A well-defined hydraulic jump (unstable) formed just downstream of the emergency gate for a **50%** gate opening (**Photograph 31**). The jump was prevented from moving downstream of the conduit due to the first bend in the conduit.

- This tapered section at the radial gate chamber prohibited the free release of air that had accumulated above the water along the conduit. The air was thus released with a “pulsating” effect, as shown in **Photograph 32**.
- The air movement through the air vent was not sensitive to the closure rate, but was directly related to the water head.
- No vortices were observed in the water tower.

Modification 4: Ski-jump and radial gate chamber removed

- Free surface flow occurred downstream of the emergency gate and was released freely from the conduit as the tapered section of the radial gate chamber had been removed (**Photograph 37**).
- No hydraulic jump formed, thus the air vent did not act as a surge tower.
- Free surface flow occurred at the outlet of the conduit, as shown in **Photograph 38**.
- No vortices were observed in the water tower.

Photograph 37: Free surface flow at emergency gate for a 50% gate opening for modification 4

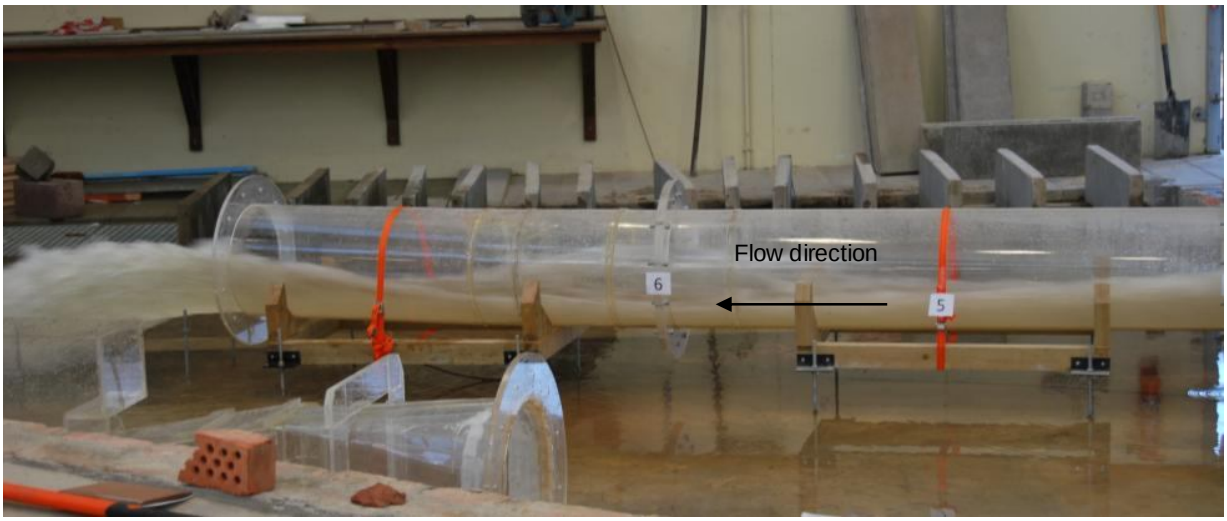

Photograph 38 Free surface flow at outlet for a 50% gate opening for modification 4

f) 40% gate opening:

All tests, except 6 min gate closure and modification 4

- The unstable hydraulic jump was pushed just downstream of the first bend in the conduit, as shown in **Photograph 39**.
- Free surface flow occurred downstream of the unstable hydraulic jump in the conduit, but the air was still “trapped” at the tapered section of the radial gate chamber (**Photograph 40**).
- The pulsating flow at the radial gate chamber continued, because the water sealed off the outlet, hindering the air from being released freely from the conduit.
- The air movement through the air vent was not sensitive to the closure rate, but was directly related to the water head.
- No vortices were observed in the water tower.

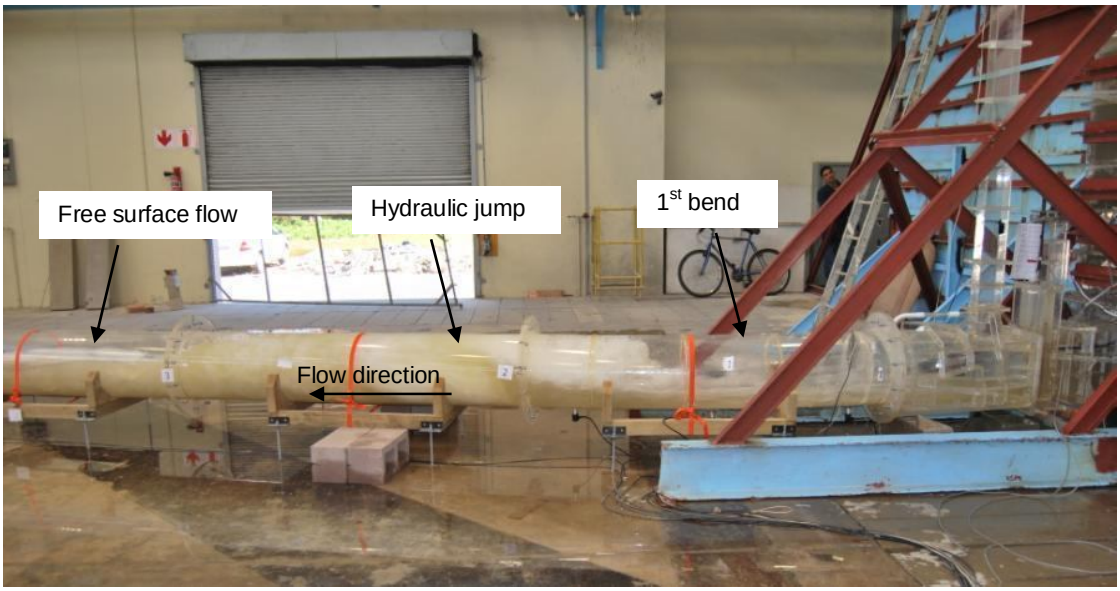

Photograph 39: Hydraulic jump pushed past 1st bend

Photograph 40: Water sealing of outlet of conduit at tapered section of radial gate chamber

<u>6 min gate closure rate</u>

- The unstable hydraulic jump was kept in position just downstream of the emergency gate at the first bend in the conduit (**Photograph 35**).

- The pulsating flow at the radial gate chamber increased, but was not as intense as when compared to the other three gate closure rates (12 minutes, 20 minutes and 30 minutes) (**Photograph 36**).
- The air movement through the air vent was not sensitive to the closure rate, but was directly related to the water head.
- No vortices were observed in the water tower.

Modification 4: Ski-jump and radial gate chamber removed

- Free surface flow occurred downstream of the emergency gate (**Photograph 41**). Thus, air and water were released freely from the conduit as the tapered section of the radial gate chamber was removed (**Photograph 42**).
- No vortices were observed in the water tower.

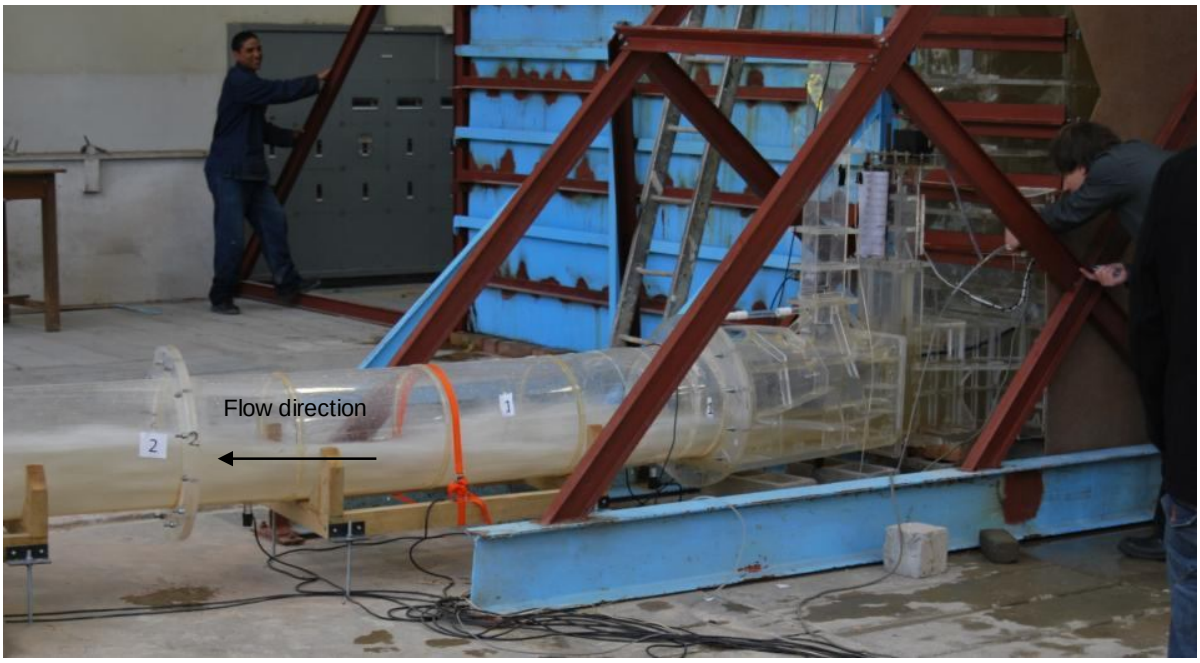

Photograph 41: Free surface flow at emergency gate for a 40% gate opening for modification 4

Photograph 42: Free surface flow at outlet for a 40% gate opening for modification 4

g) <u>30% gate opening:</u>

<u>All tests, except 6 min gate closure and modification 4</u>

- For gate openings between 37% and 32%, the unstable hydraulic jump was no longer in contact with the roof of the conduit because the water discharge decreased as the gate closed. The unstable hydraulic jump moved downstream in the conduit with a high velocity. The reason for this was that the wetted perimeter was less than when the conduit was flowing full, resulting in less friction. The tapered section caused a blockage of the air passage above the free surface water, therefore preventing normal circulation of air from the tunnel outlet, as illustrated in **Photograph 43**below. It must be noted that the largest volumes of air released from the air vent occurred when the unstable hydraulic jump moved downstream and became “trapped” at the radial gate chamber.
- Spray flow occurred just downstream of the emergency gate, as shown in **Photograph 44**.
- The air movement through the air vent was not sensitive to the closure rate, but was directly related to the water head.
- No vortices were observed in the water tower.

Photograph 43: Hydraulic jump "trapped" by tapered section of radial gate chamber

Photograph 44: Spray flow occurred at small gate openings

<u>6 min gate closure rate</u>

- The unstable hydraulic jump was pushed just past the first bend in the conduit, as shown **Photograph 39**.

- Free surface flow occurred downstream of the unstable hydraulic jump in the conduit, but the air was still “trapped” at the tapered section of the radial gate chamber (**Photograph 40**).
- The pulsating flow at the radial gate chamber continued because the water sealed off the outlet, hindering the air from being released freely from the conduit.
- The air movement through the air vent was not sensitive to the closure rate, but was directly related to the water head.

Modification 4: Ski-jump and radial gate chamber removed

- Free surface flow occurred downstream of the emergency gate (**Photograph 45**), as the radial gate chamber and ski-jump were removed, therefore allowing the water to leave the conduit unrestricted (**Photograph 46**).
- No vortices were observed in the water tower.

Photograph 45: Free surface flow at emergency gate for a 30% gate opening for modification 4

Photograph 46: Free surface flow at outlet for a 30% gate opening for modification 4

h) 20% gate opening:

All tests, except 6 min gate closure and modification 4

- The unstable hydraulic jump was pushed out of the conduit for gate openings of 25% to 20%. Thereafter, free surface flow occurred along the outlet conduit and the air and water were able to leave the conduit unhindered, as shown in **Photograph 47**. The water flow in the conduit was very little (about 84 m^3/s – prototype value) because the discharge decreased as the gate opening decreased.
- No vortices were observed in the water tower.

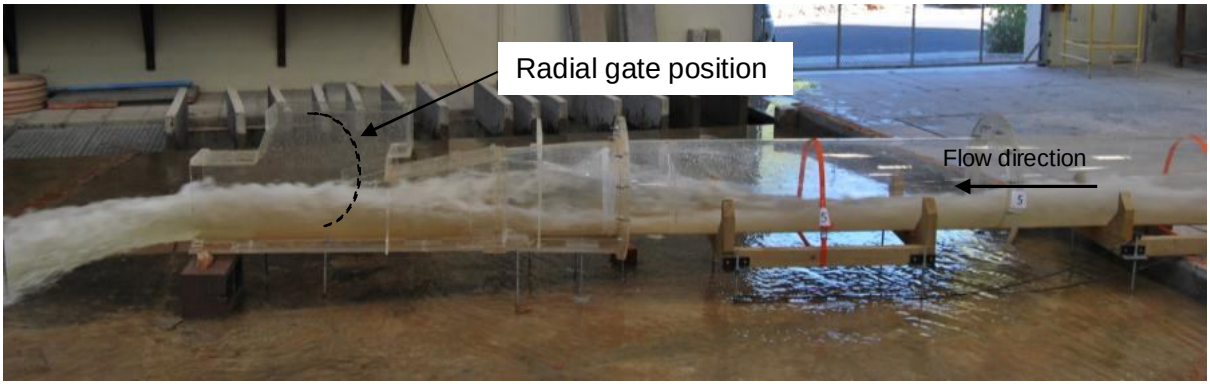

Photograph 47: Hydraulic jump pushed out of conduit – all excl. modification 4

6 min gate closure rate

- For gate openings of between **23%** and **20%**, the unstable hydraulic jump moved downstream in the conduit, but it was "trapped" by the tapered section of the radial gate chamber, as illustrated in **Photograph 43**. The largest volumes of air released from the air vent occurred when the unstable hydraulic jump moved downstream and got "trapped" at the radial gate chamber.
- The unstable hydraulic jump was not pushed out of the conduit before the test ended.
- Spray flow occurred just downstream of the emergency gate (**Photograph 44**).
- No vortices were observed in the water tower.

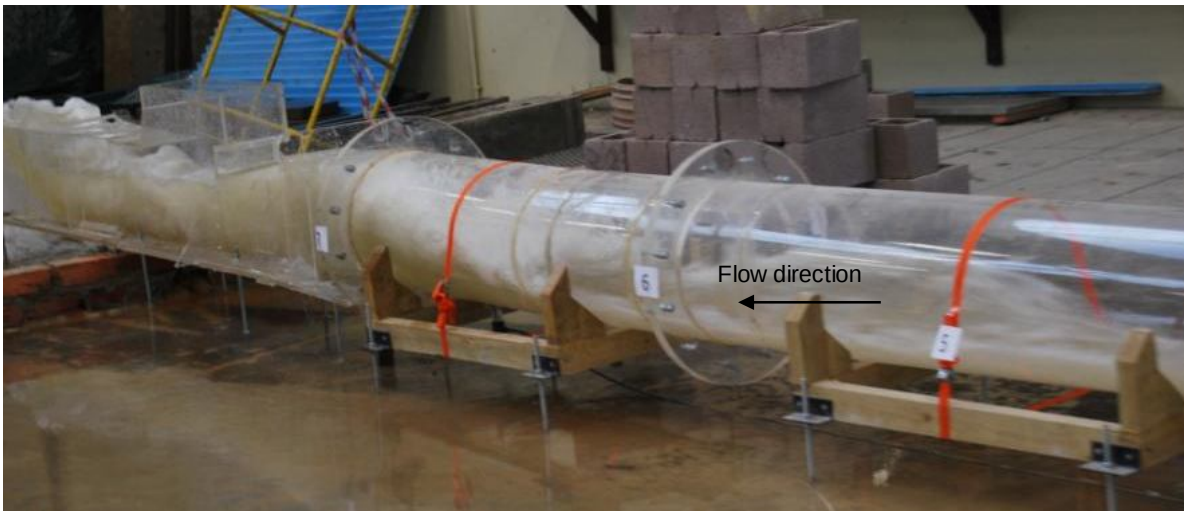

Photograph 48: Flow condition for 6 min gate closure rate and a 20% gate opening – all excl. modification 4

Modification 4: Ski-jump and radial gate chamber removed

- Free surface flow occurred downstream of the emergency gate, as the radial gate chamber and ski-jump were removed, therefore allowing the water to leave the conduit unrestricted (**Photograph 49** and **50**).
- No vortices were observed in the water tower.

Photograph 49: Free surface flow upstream for 20% gate opening for modification 4

Photograph 50: Fee surface flow at outlet for 20% gate opening for modification 4

ANNEXURE F: Radial Gate Partially Closed

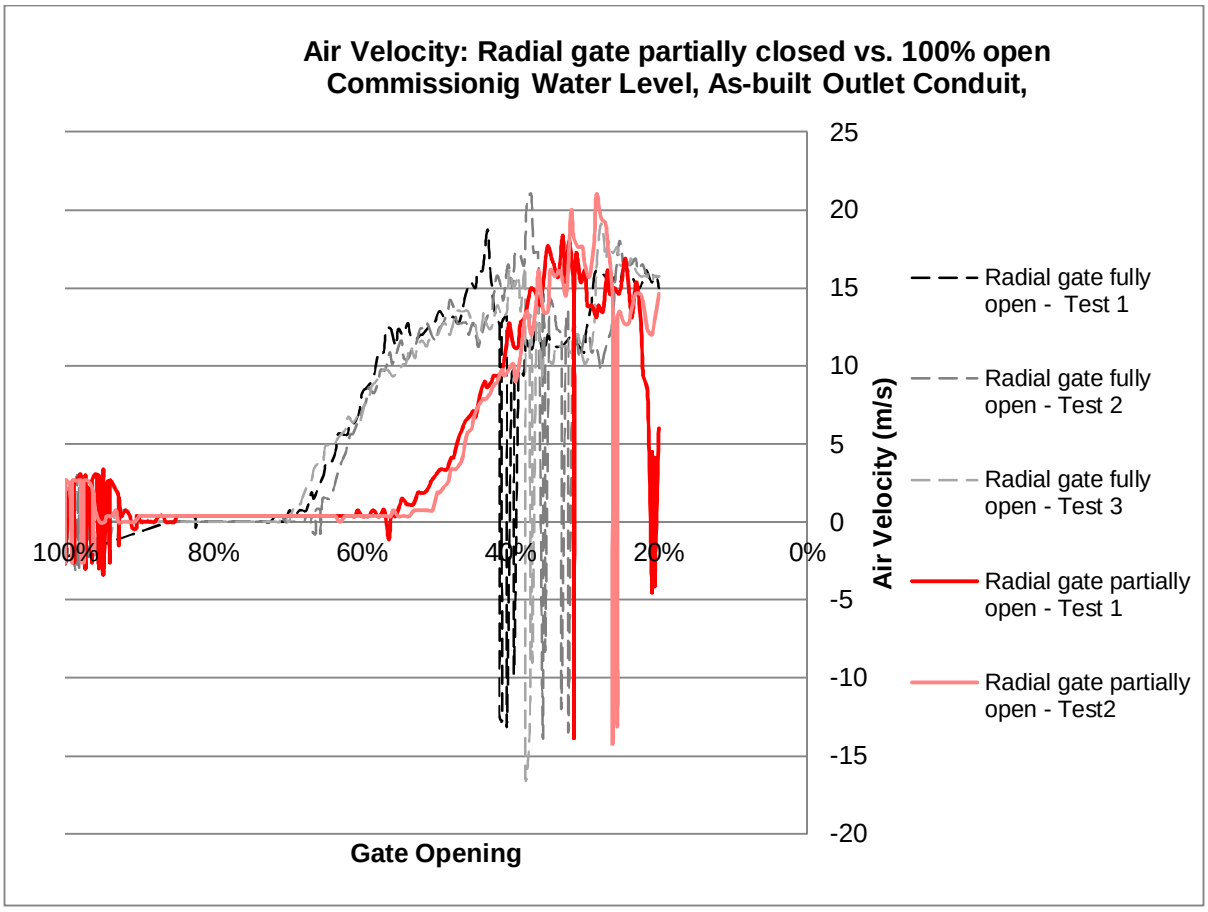

Graph F1: Air Velocity – radial gate partially closed vs. 100% open

The following is evident from **Graph F1**:

- The air blowback for the tests where the radial gate is partially closed is of the same magnitude as for the tests when the radial gate was fully open.
- The air blowback for the tests when the radial gate was partially closed occurred later in gate closure, but more repeated tests would are required to confirm this.

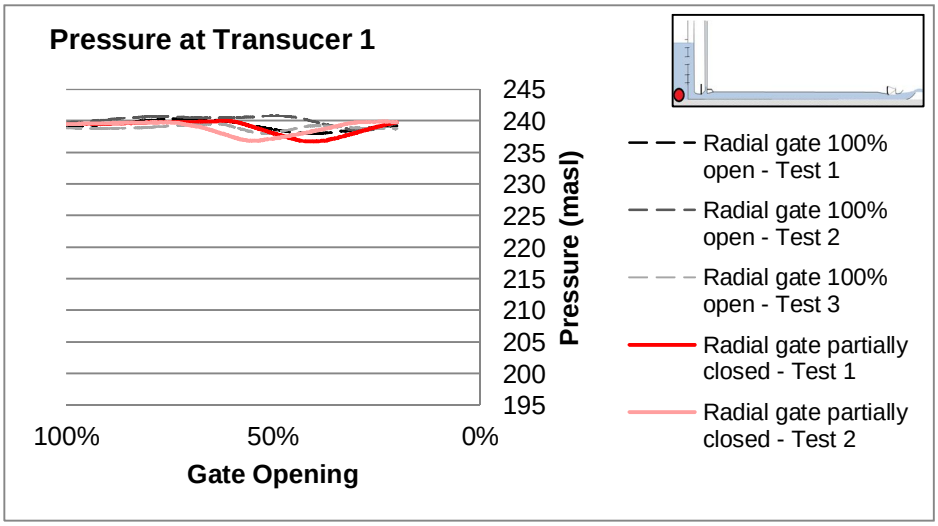

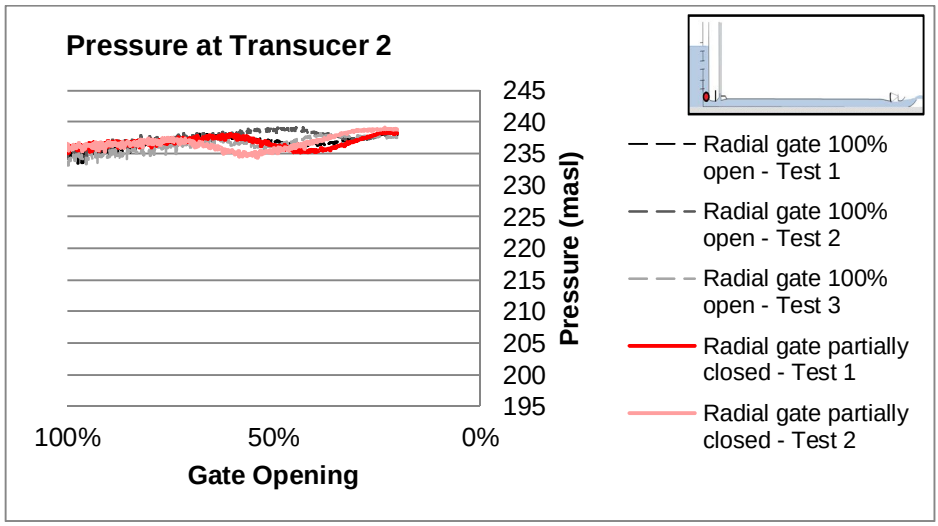

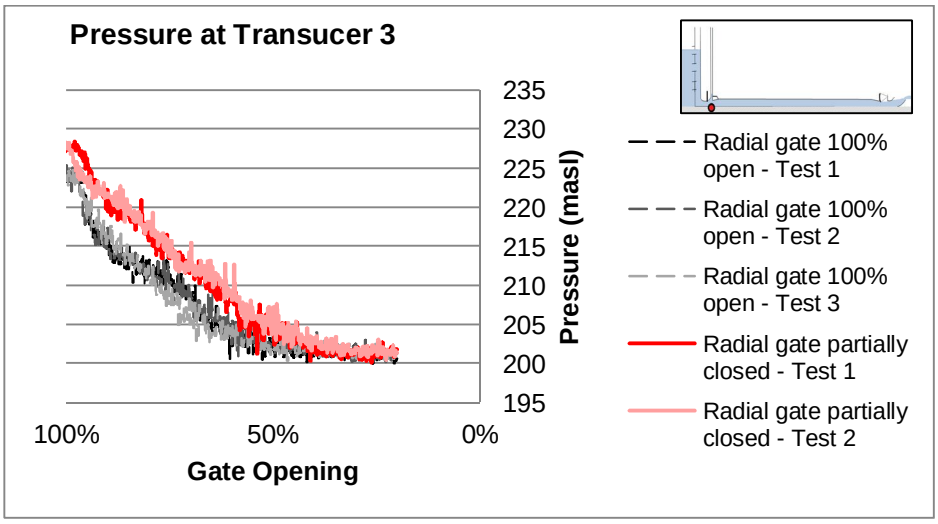

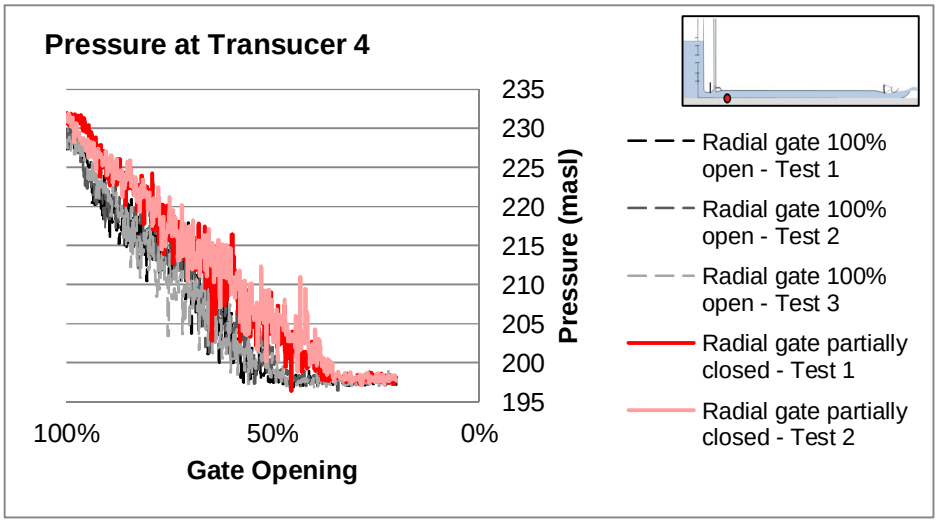

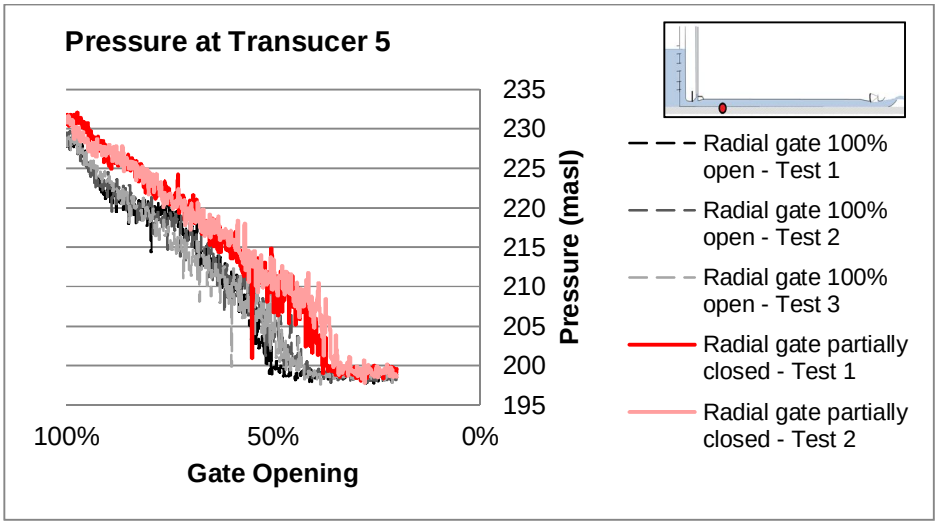

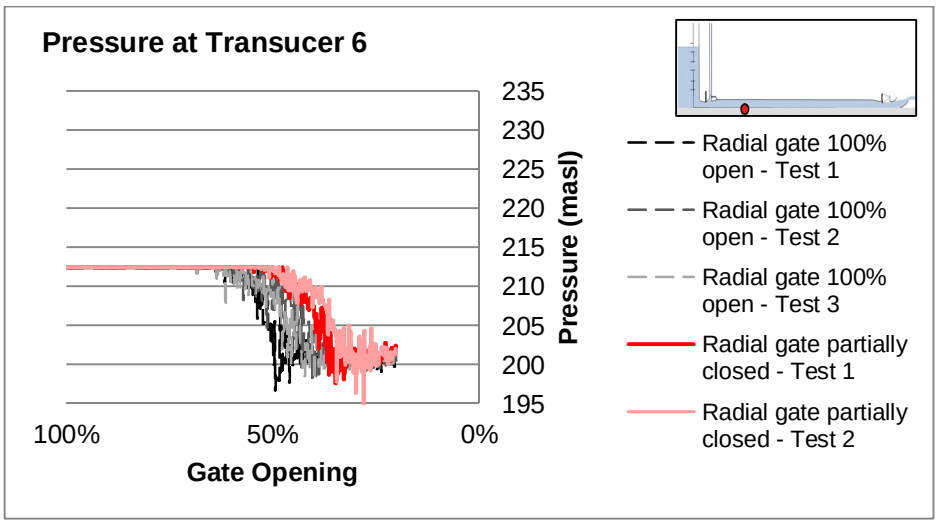

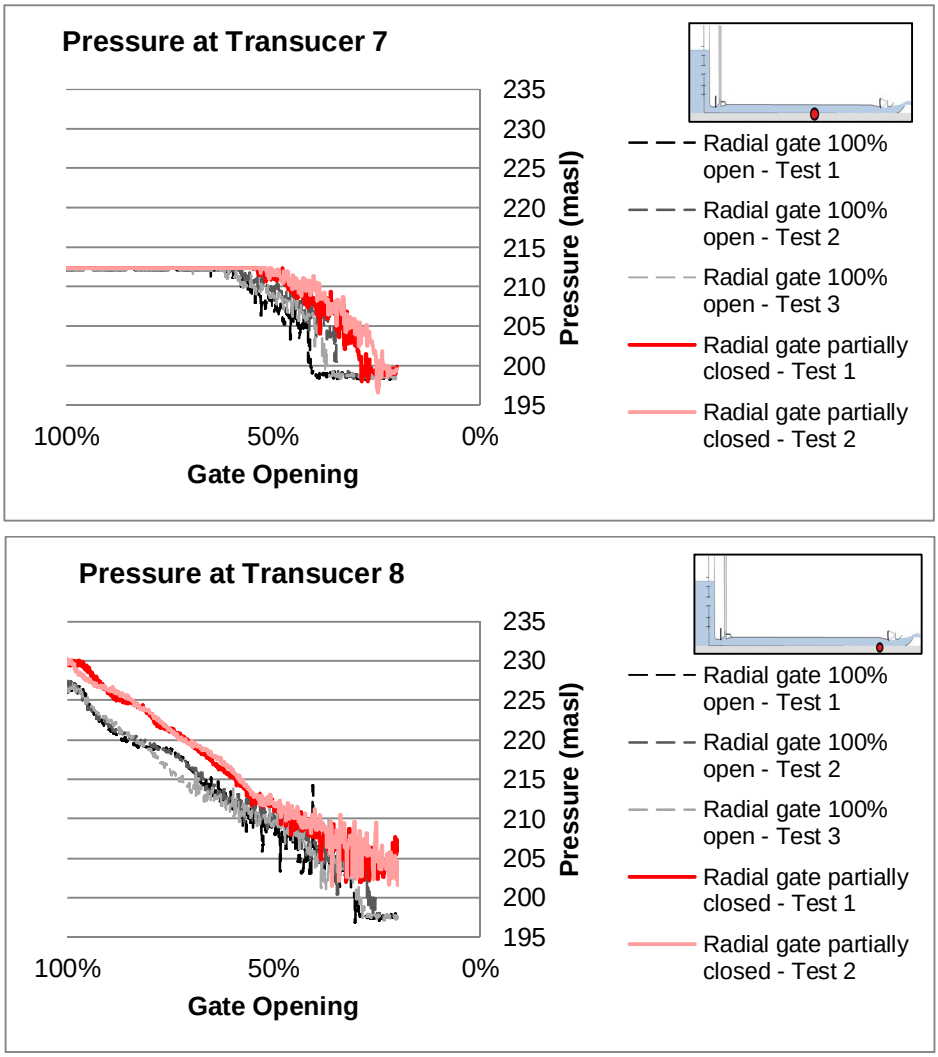

Graph F2: Pressure – radial gate partially closed vs. 100% open

The following is evident from **Graph F2**:

- The pressures recorded for the tests with the radial gate partially closed were slightly higher in magnitude as for the tests when the radial gate was fully open.
- Similar trends were observed in the pressure for the tests with the radial gate partially closed and for the test with the radial gate fully open.

ANNEXURE G: Vortex Entrainment Results

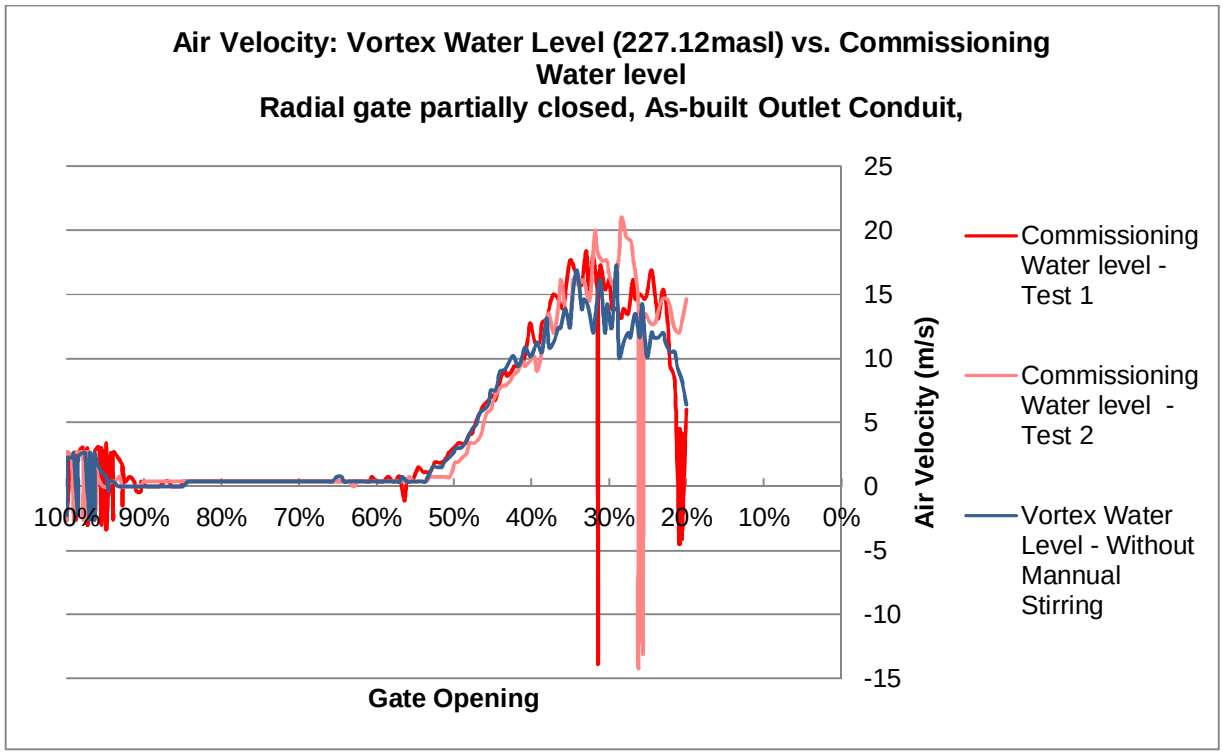

Graph G1: Pressure – radial gate partially closed vs. 100% open

The following is evident from **Graph G2**:

- No air blowback phenomenon occurred at the vortex water level (227.12 masl).
- The air velocities for the vortex water level was of similar magnitude to those recorded for the tests performed at commissioning water level (250 masl) (radial gate partially closed for both sets of tests).

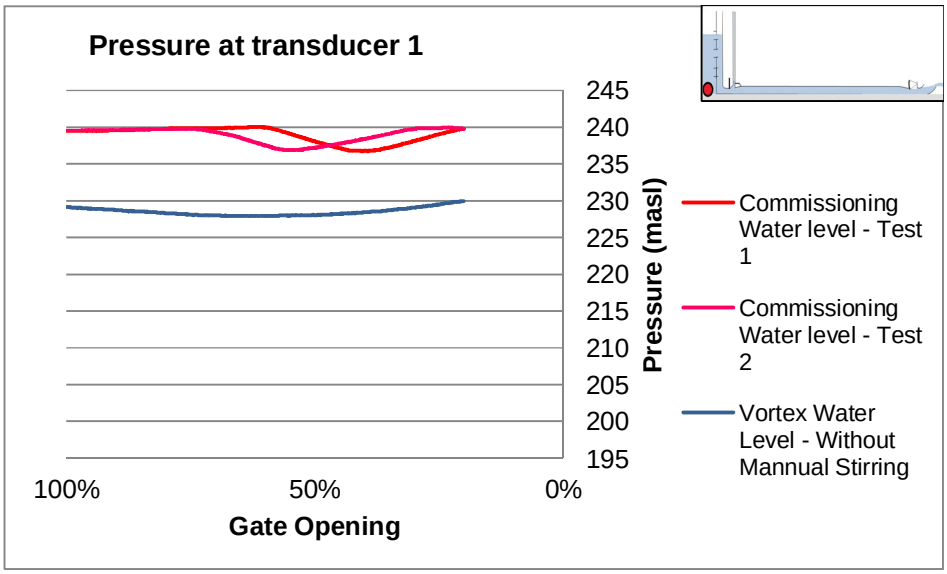

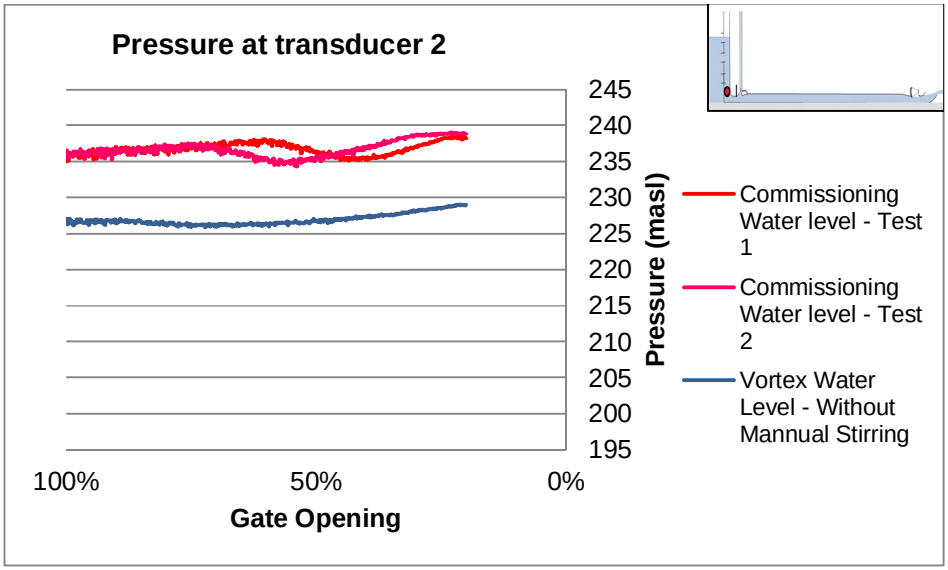

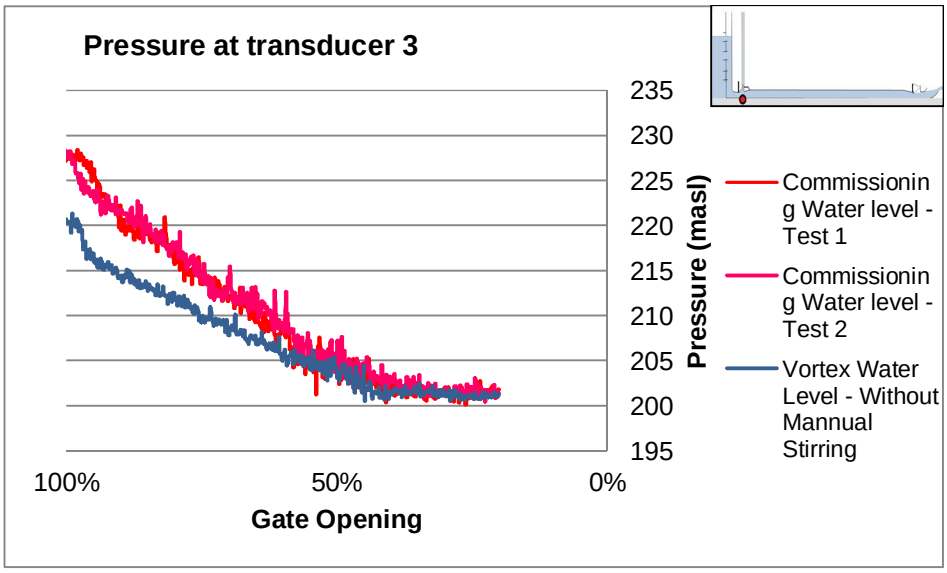

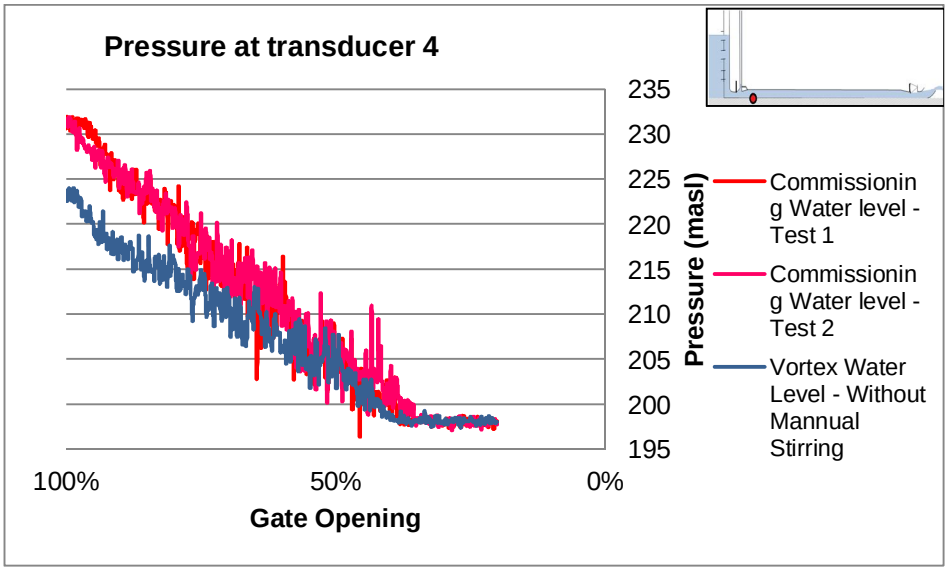

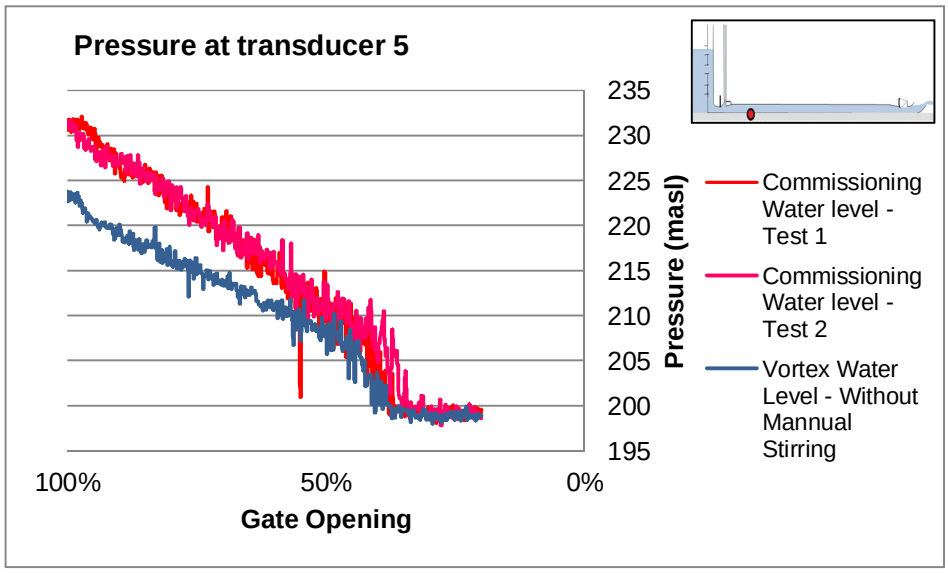

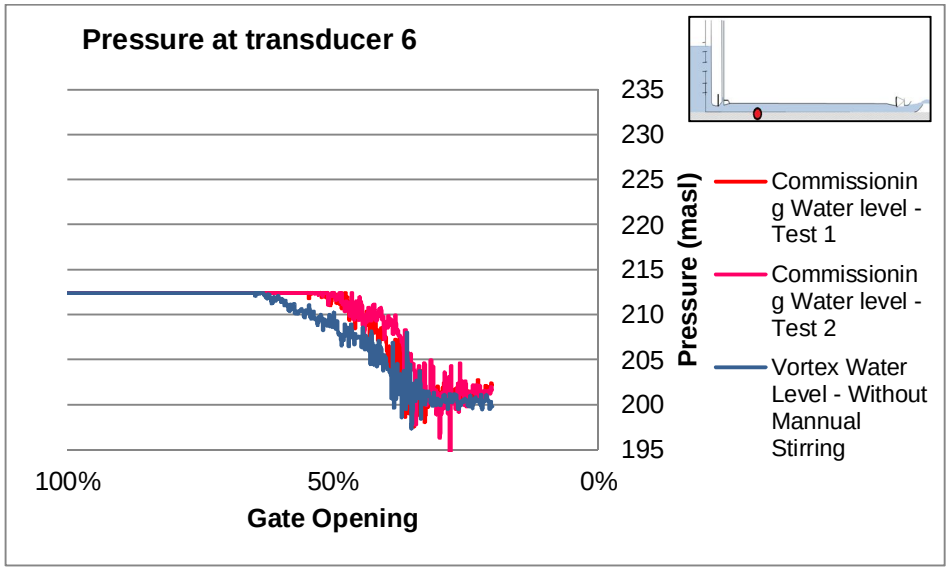

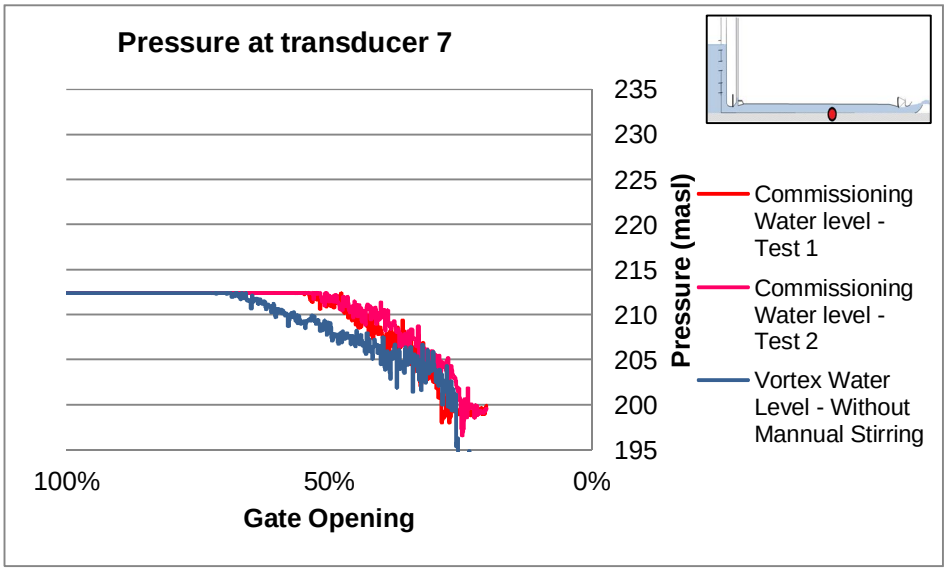

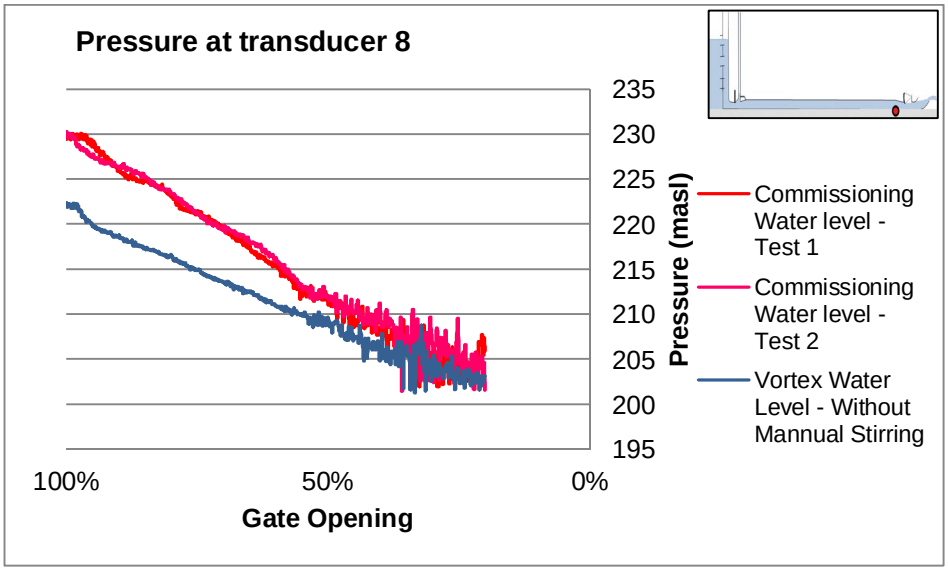

ANNEXURE H: Transient Gate Closures: As-built Outlet Conduit

ANNEXURE H1: Full Supply Level

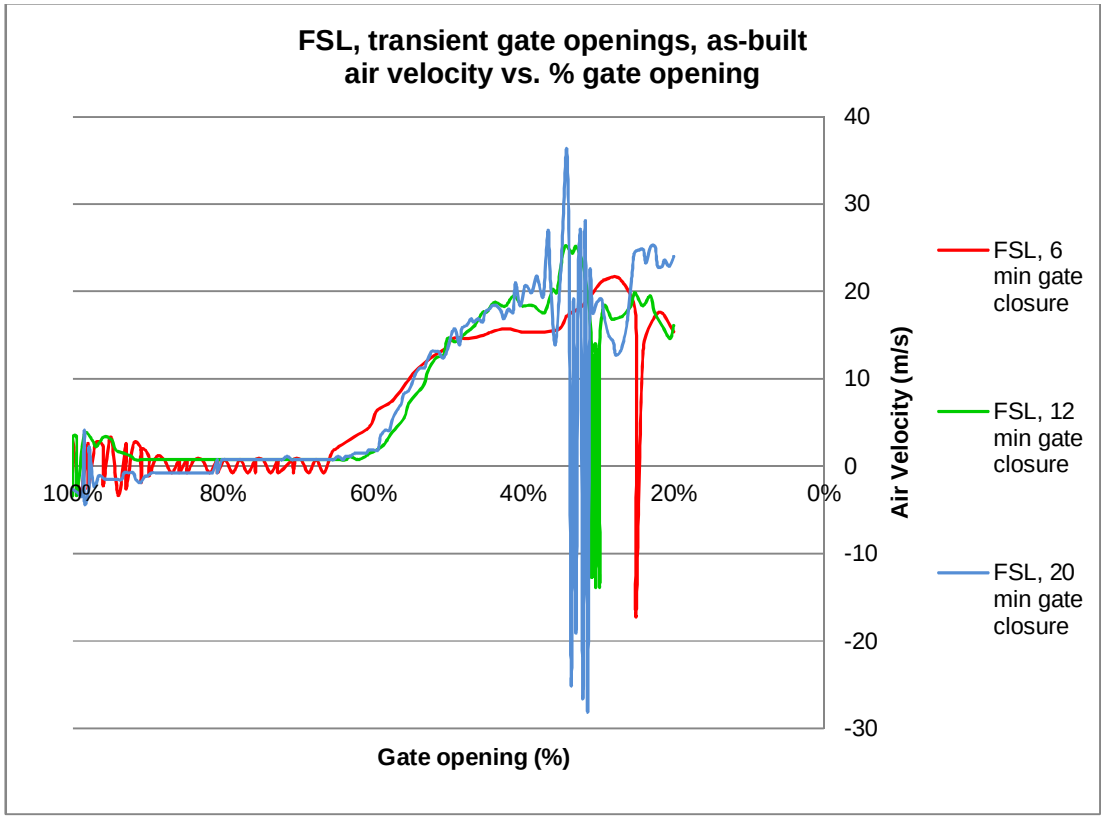

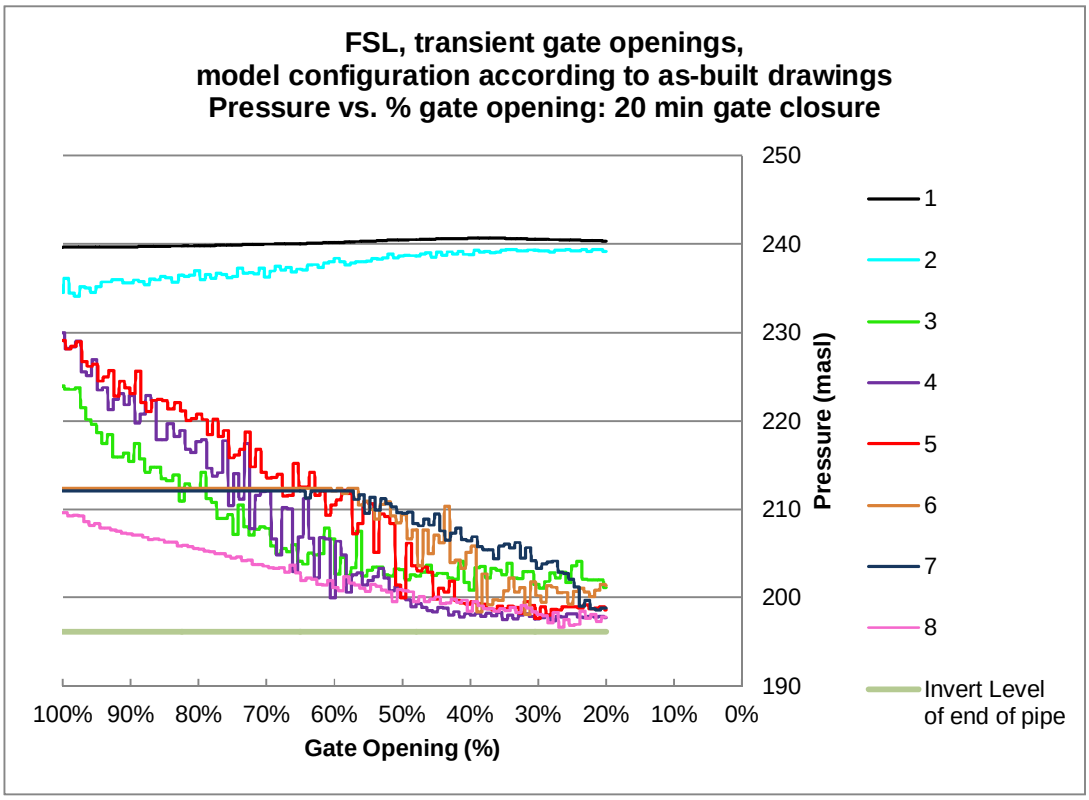

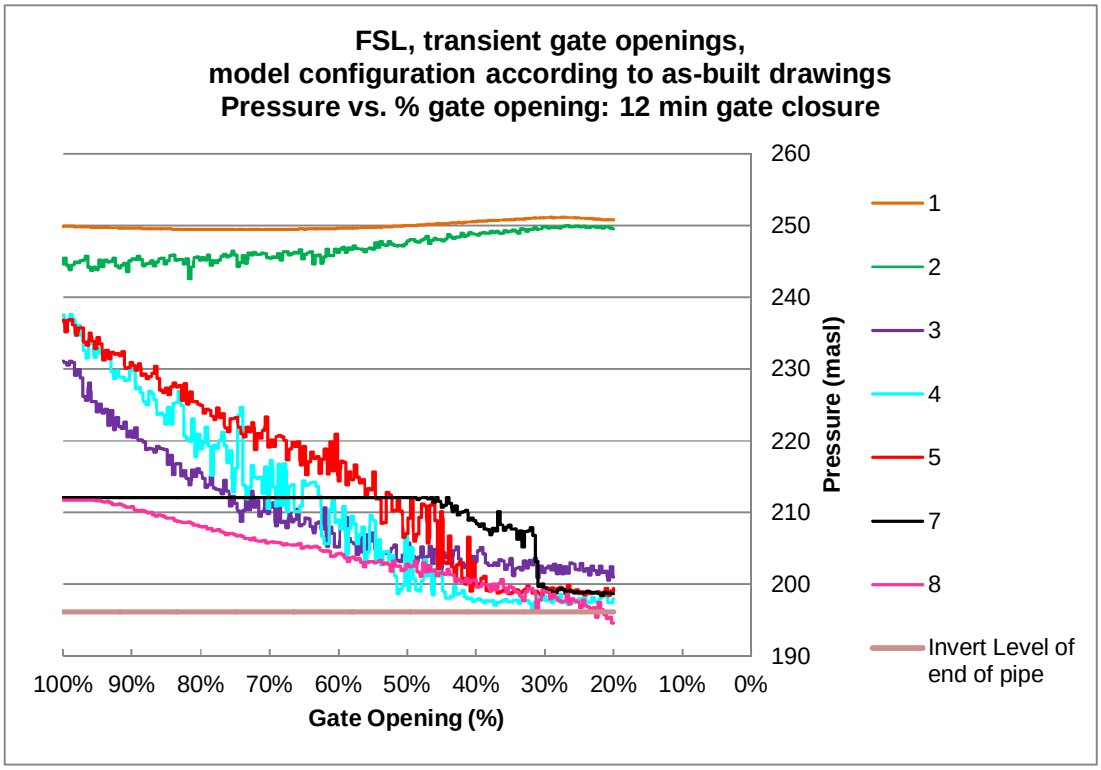

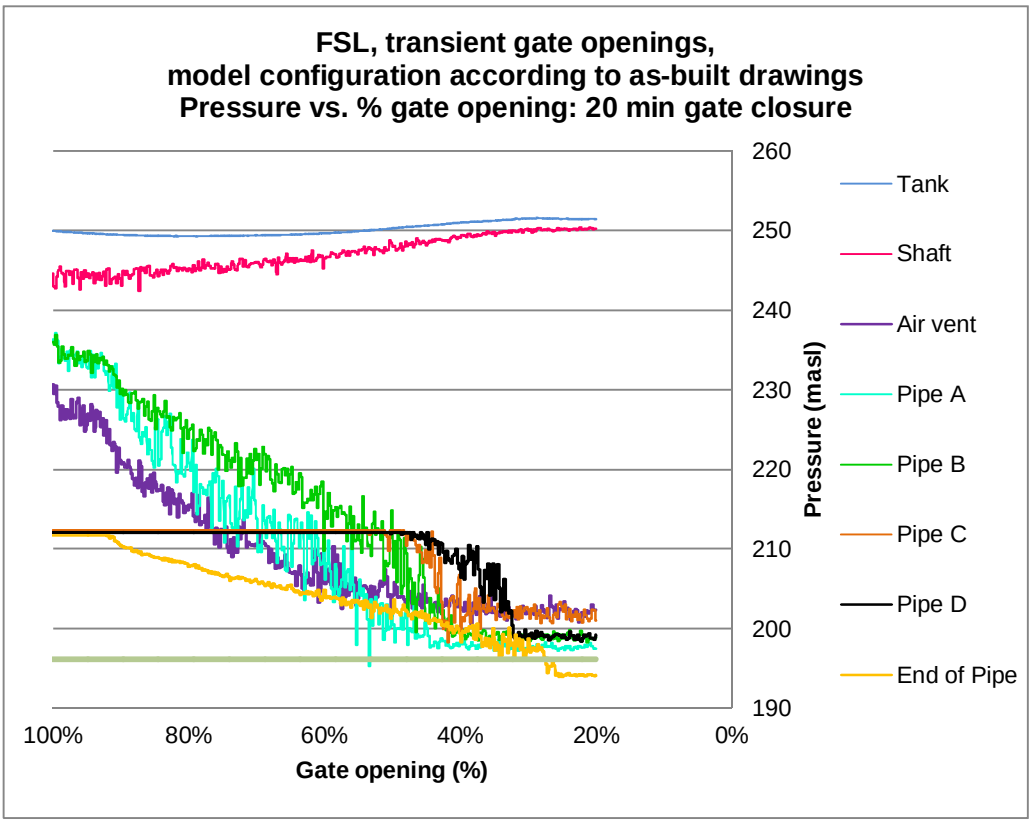

ANNEXURE H2: Commissioning Water Level

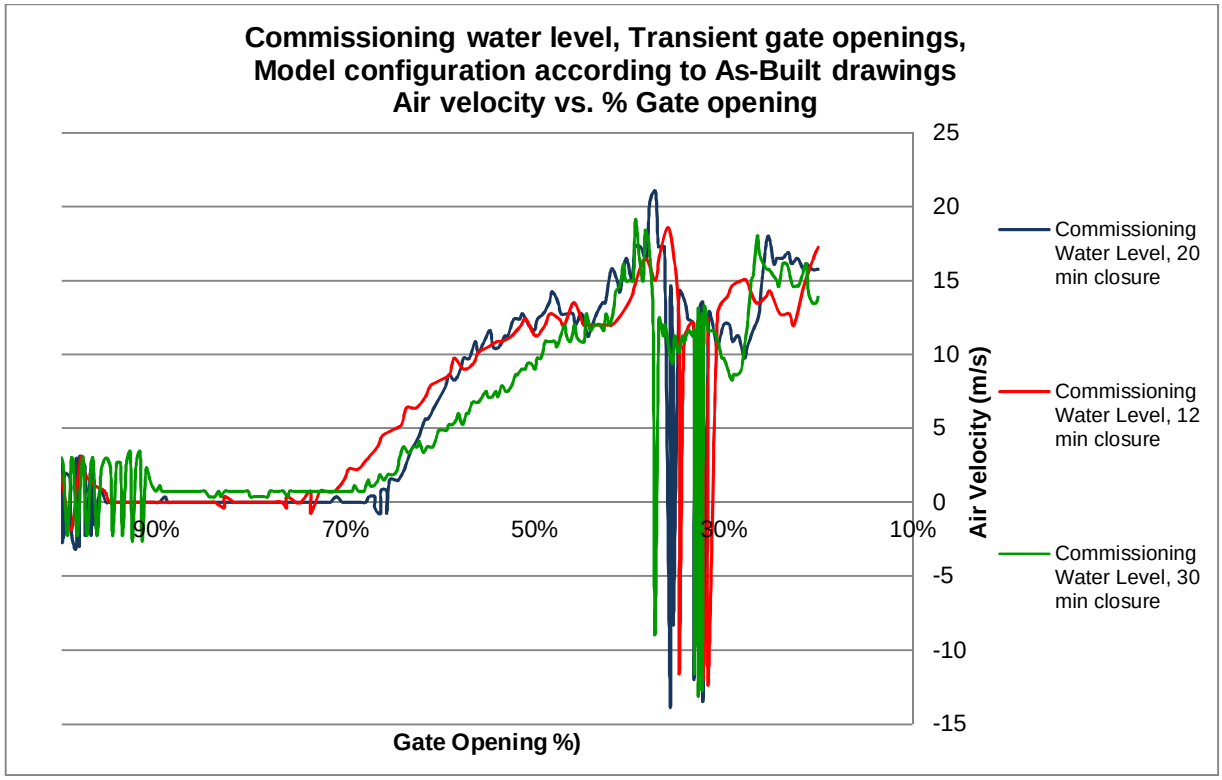

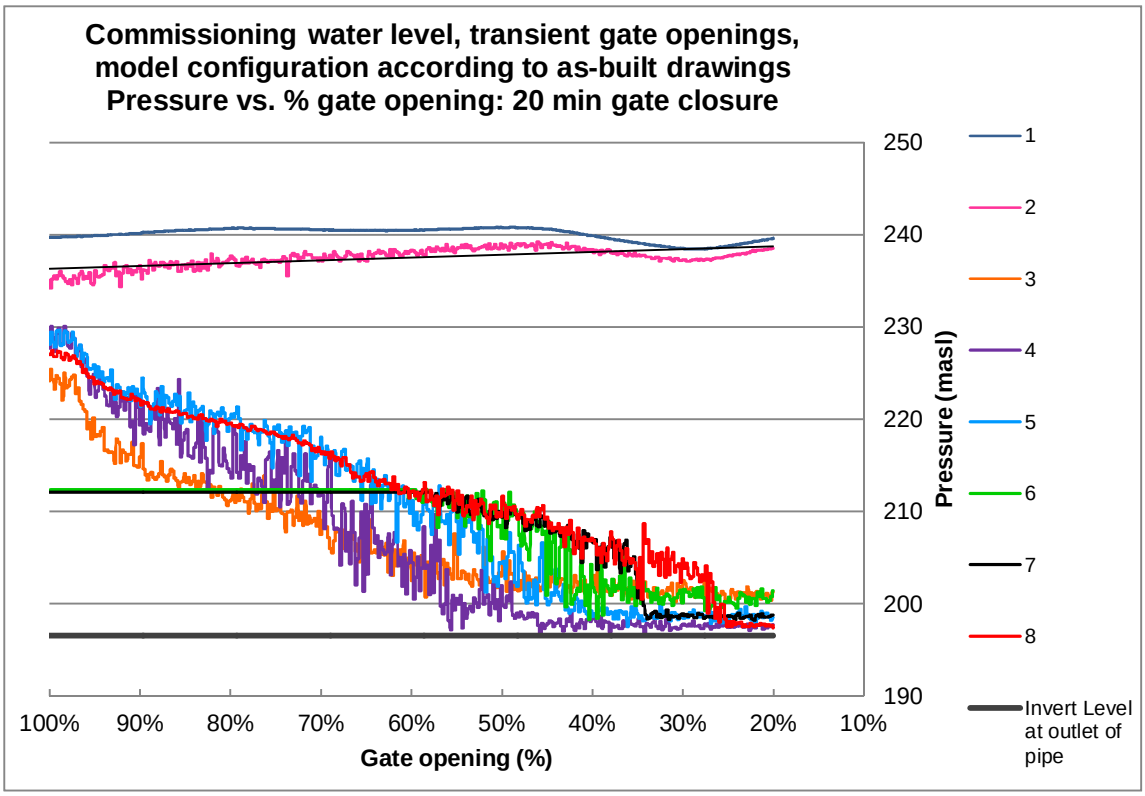

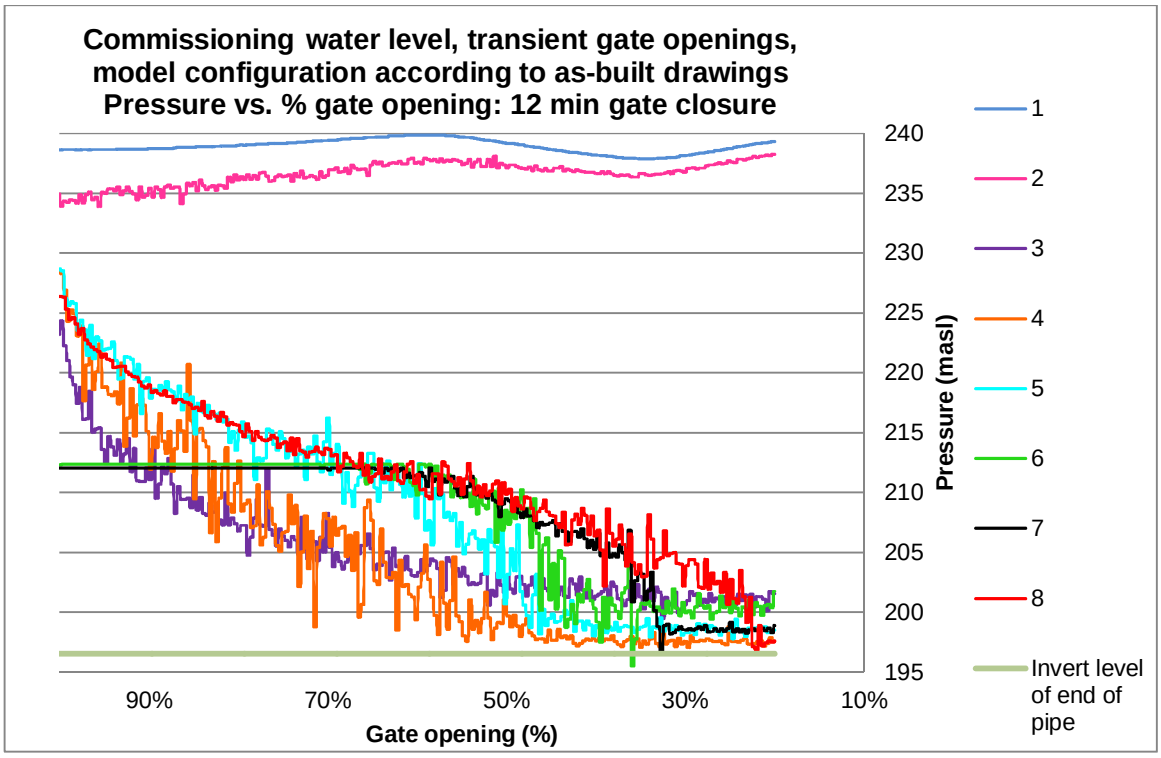

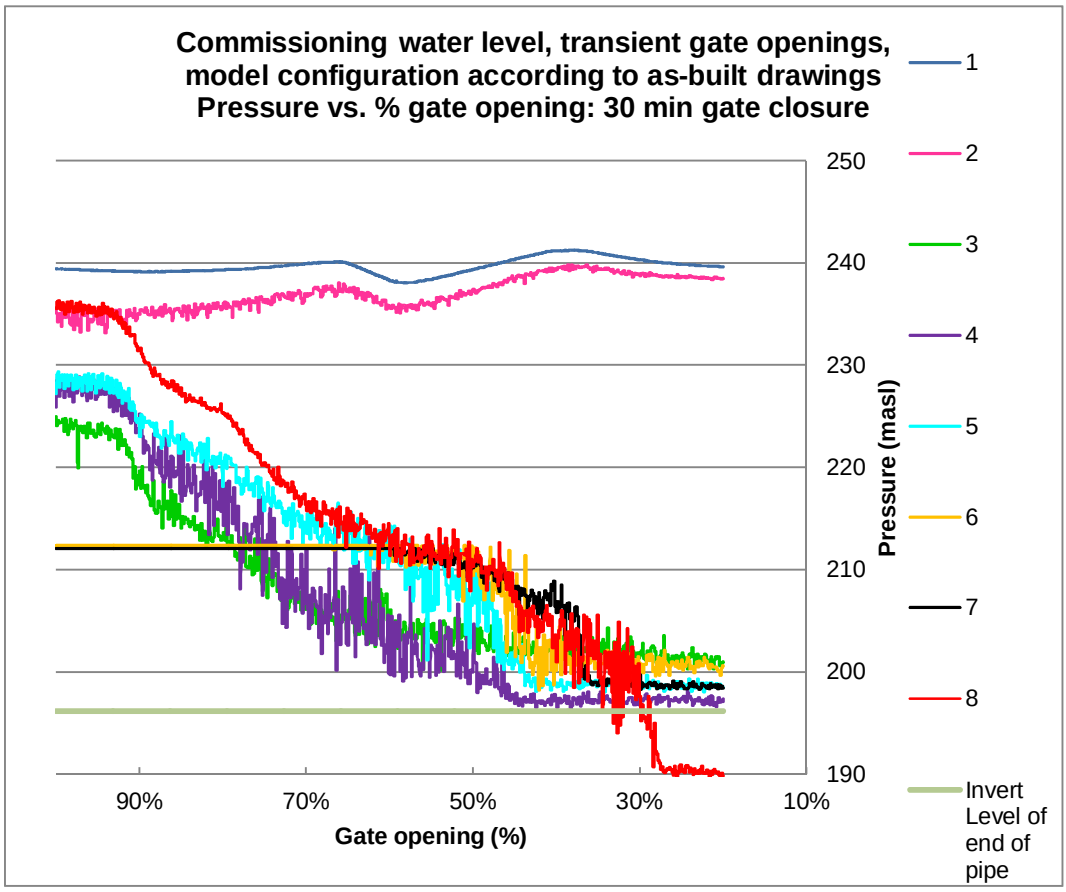

ANNEXURE H3: Lower Water Level

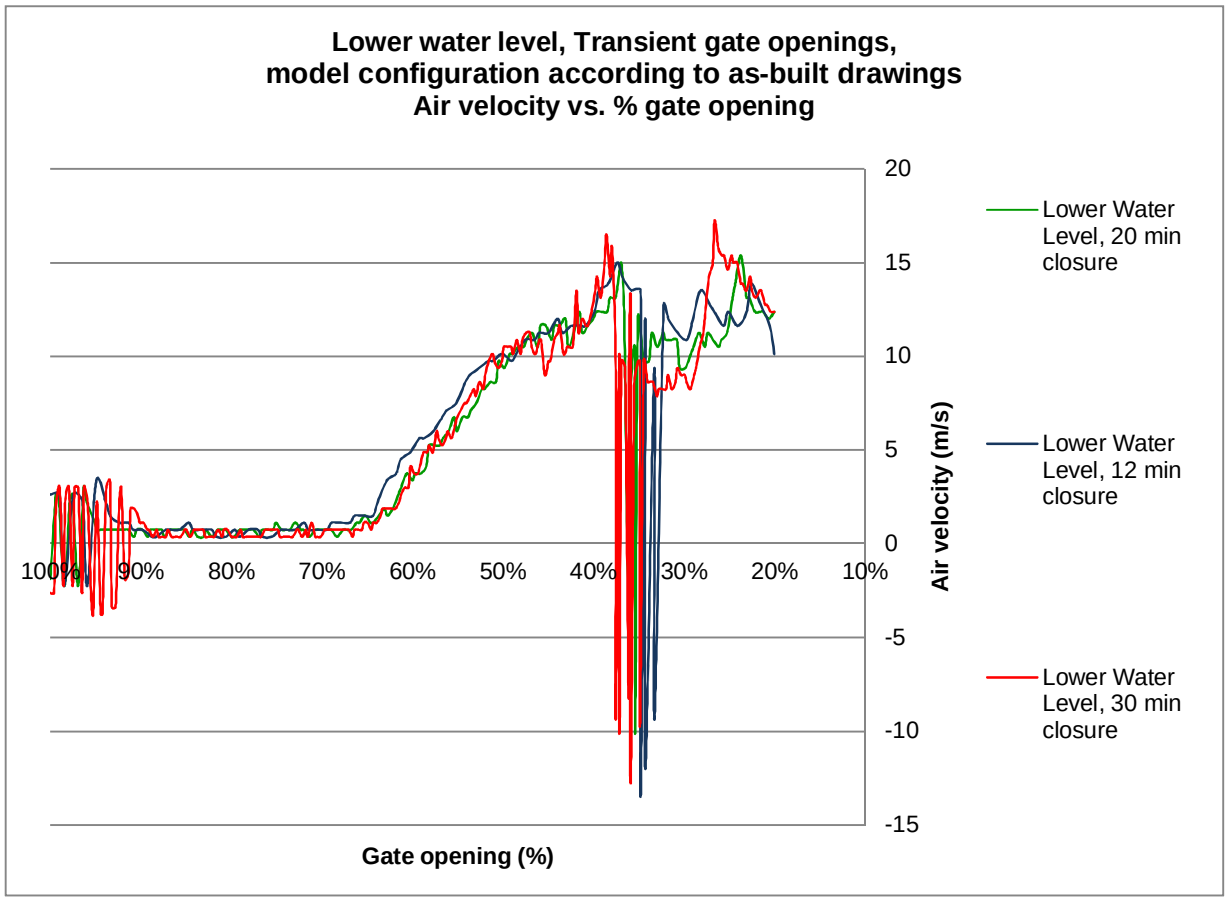

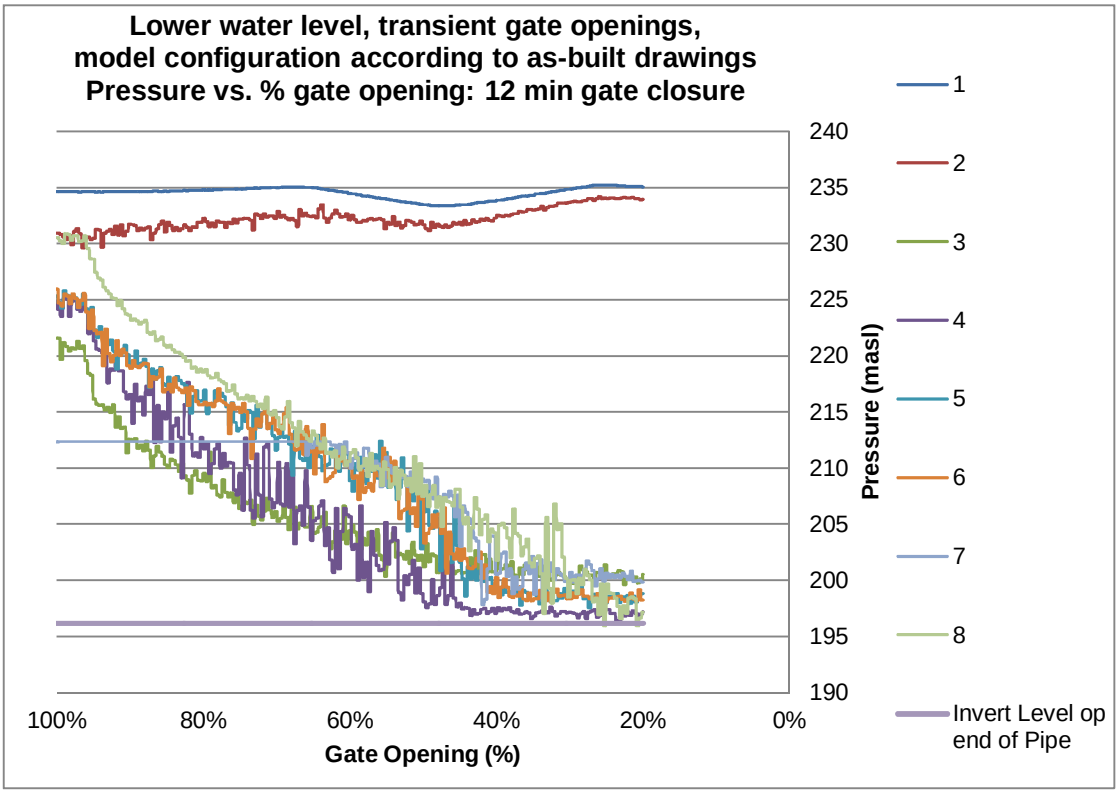

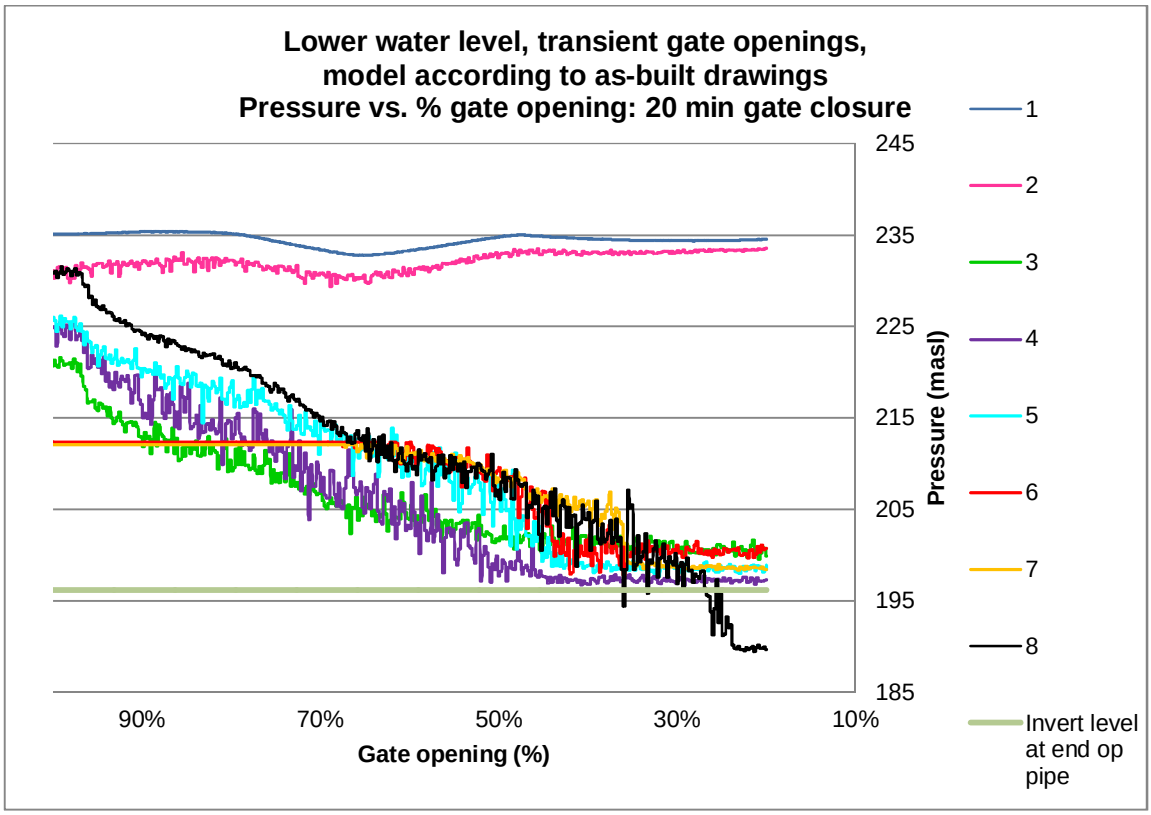

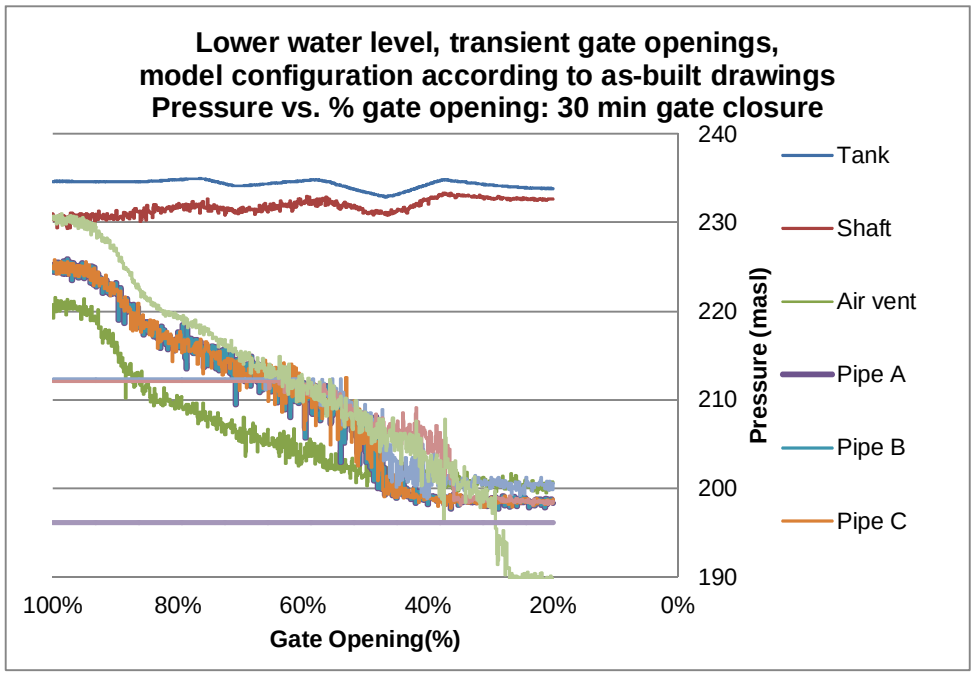

ANNEXURE I: Transient Gate Closures: Modified Outlet Conduit

ANNEXURE I1: Air Velocity – Closing Gate Simulations; Commissioning Water Level; Modification 1

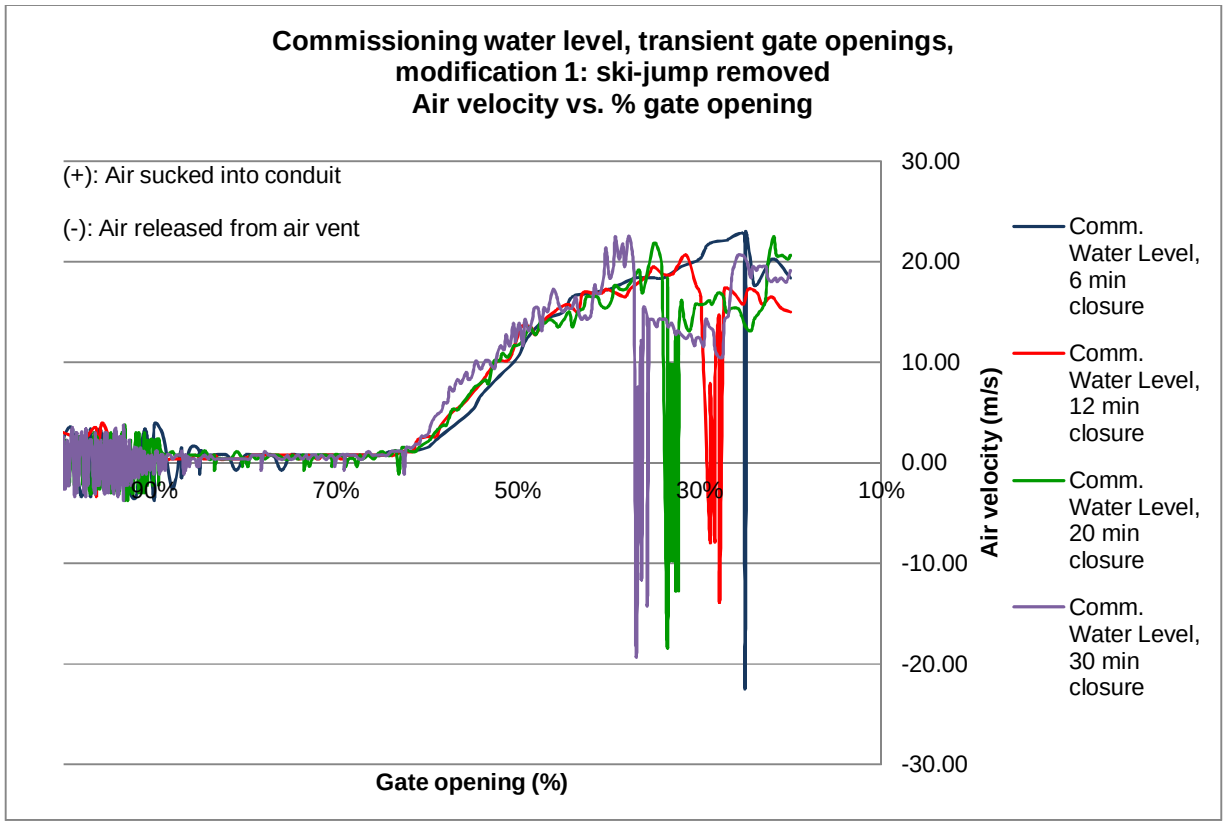

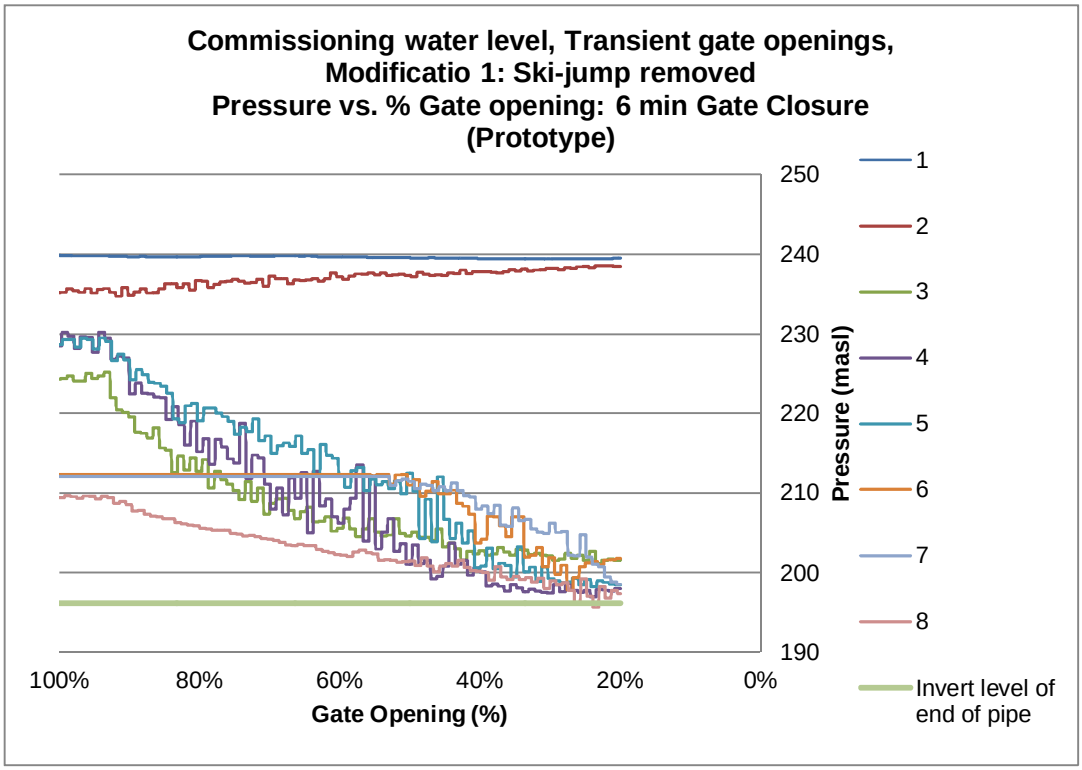

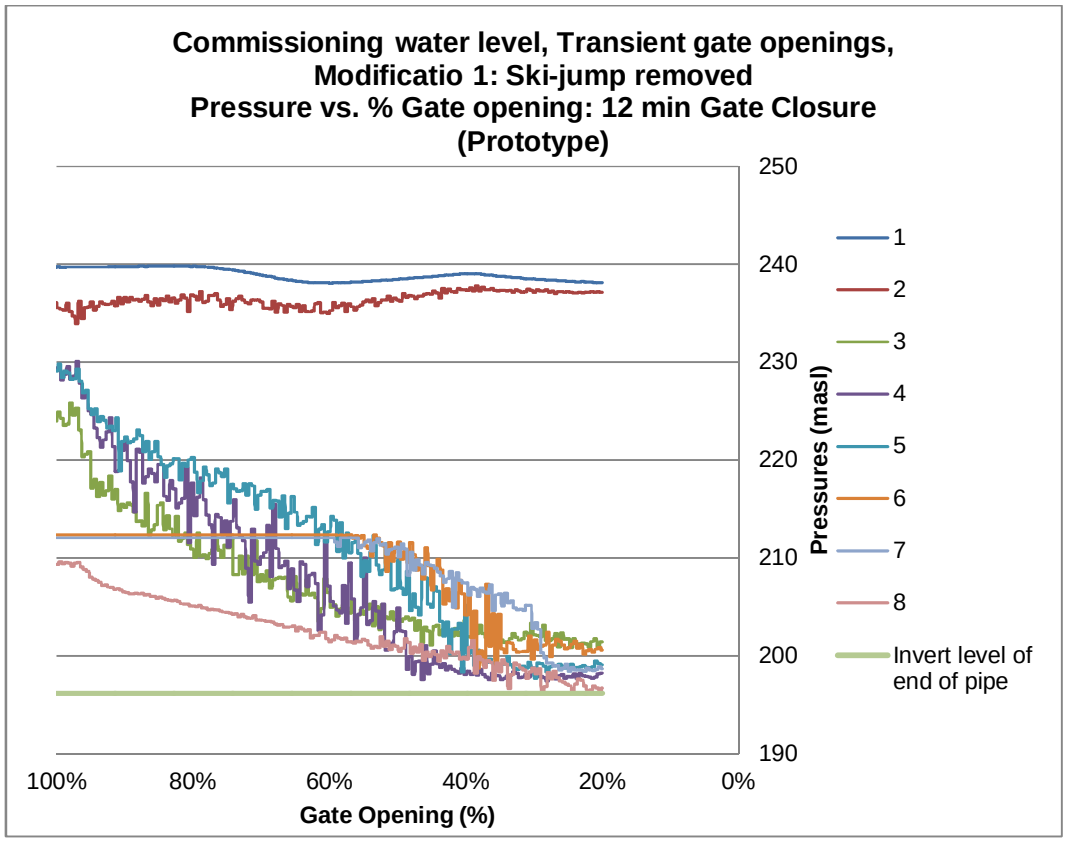

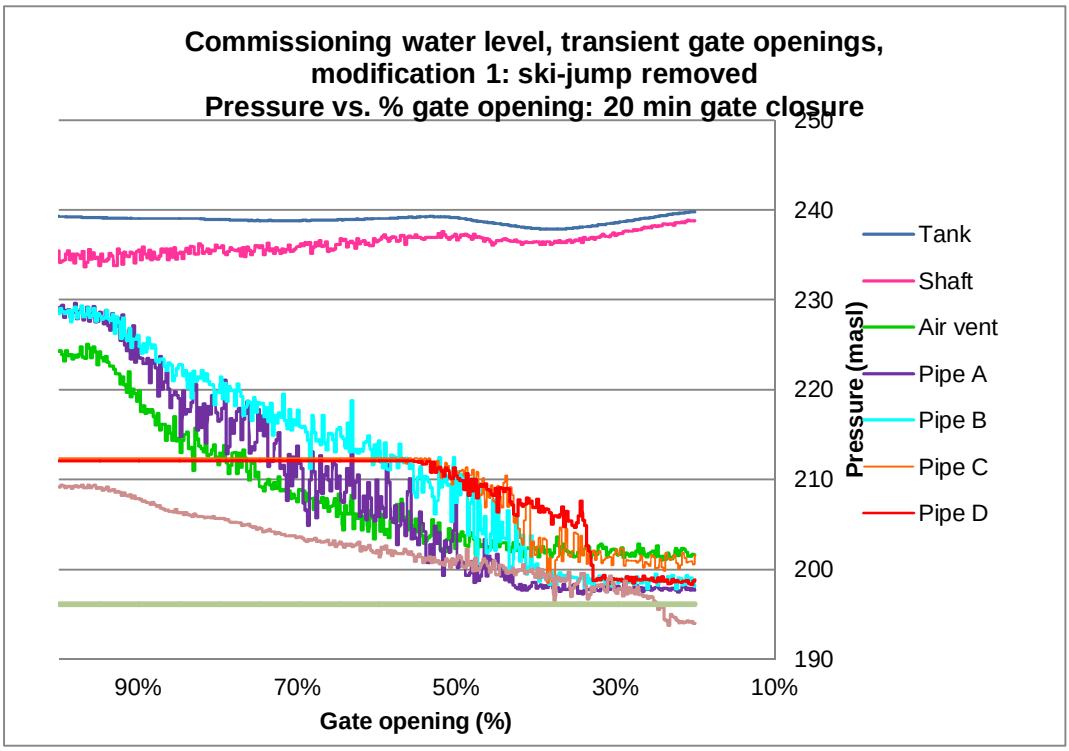

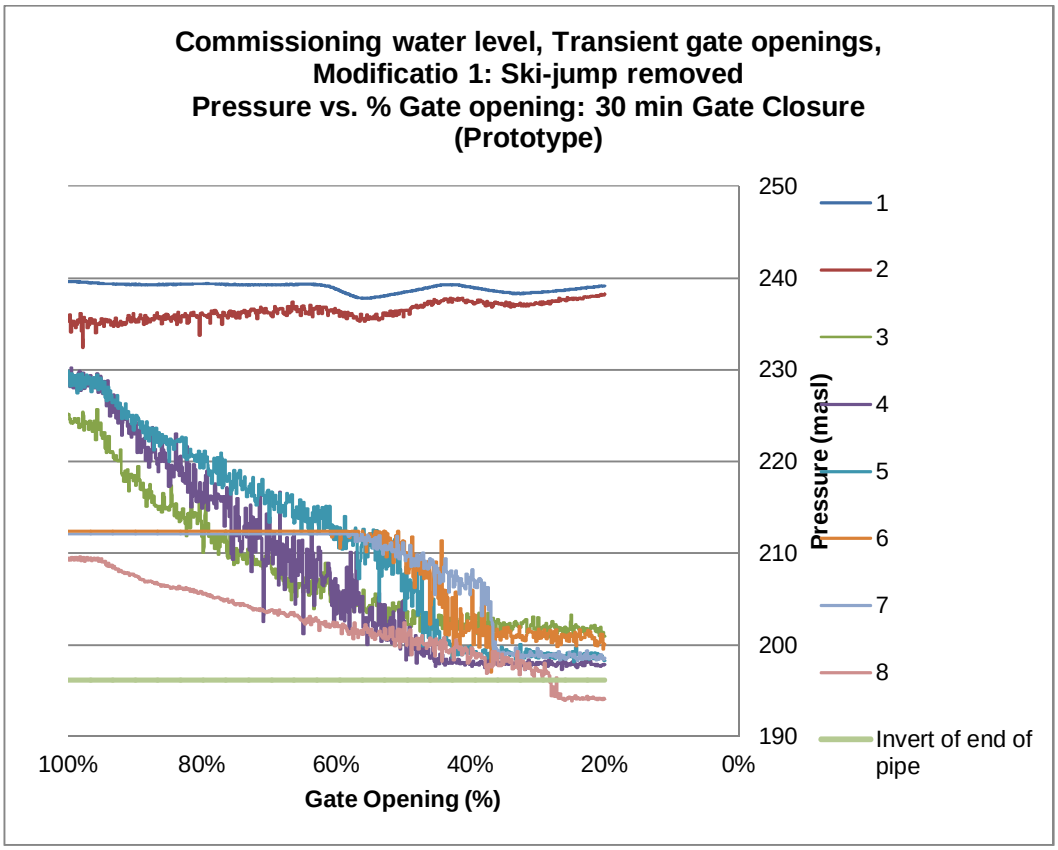

ANNEXURE I2: Air Velocity – Closing Gate Simulations; Commissioning Water Level; Modification 2

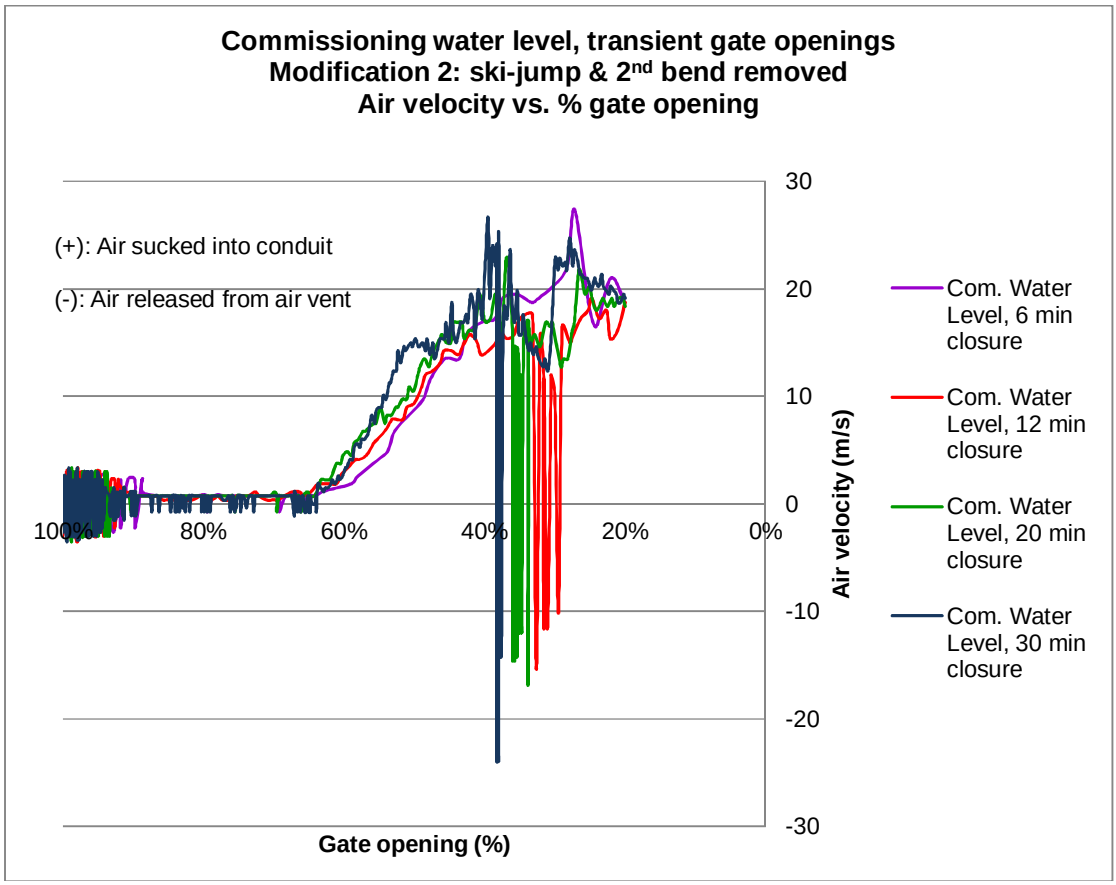

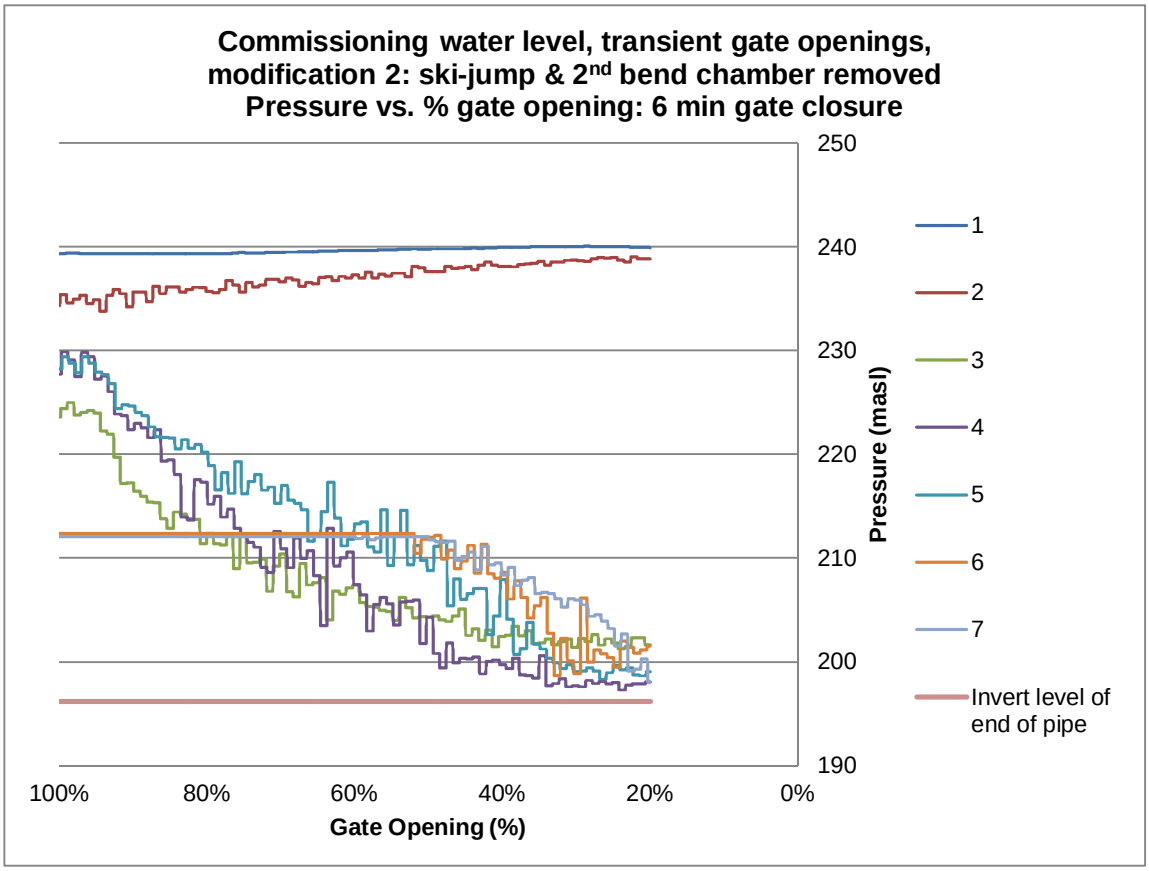

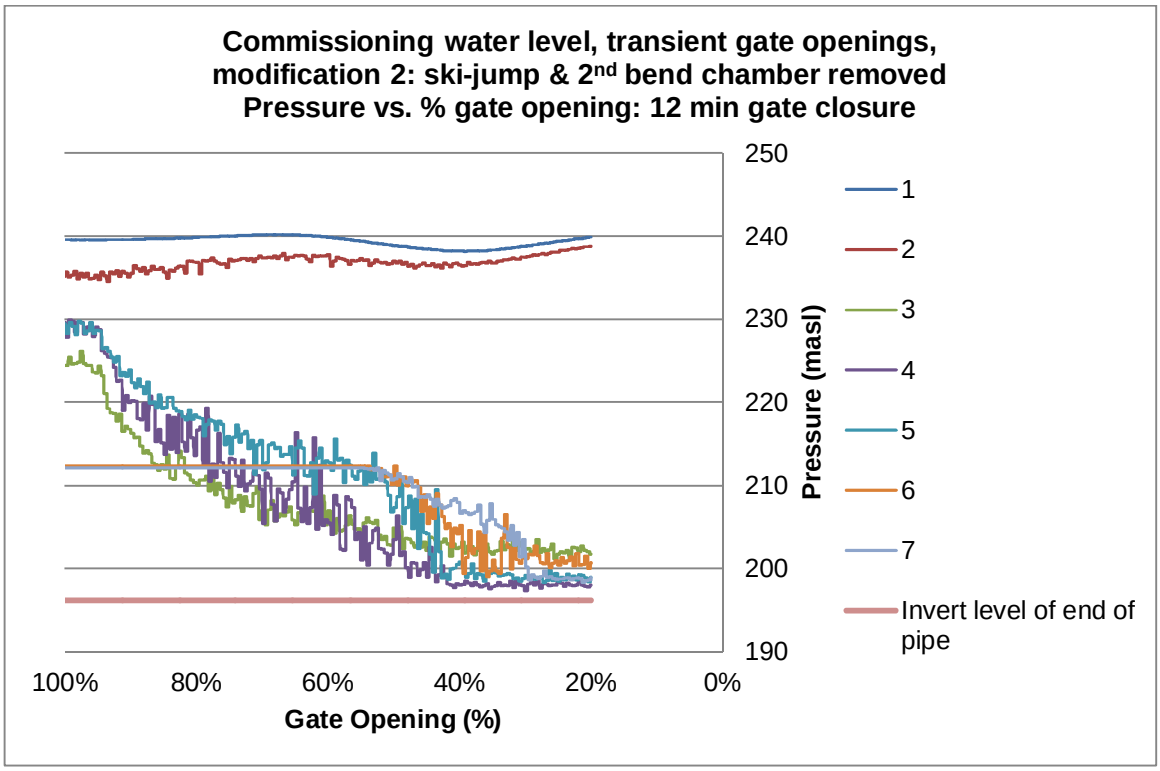

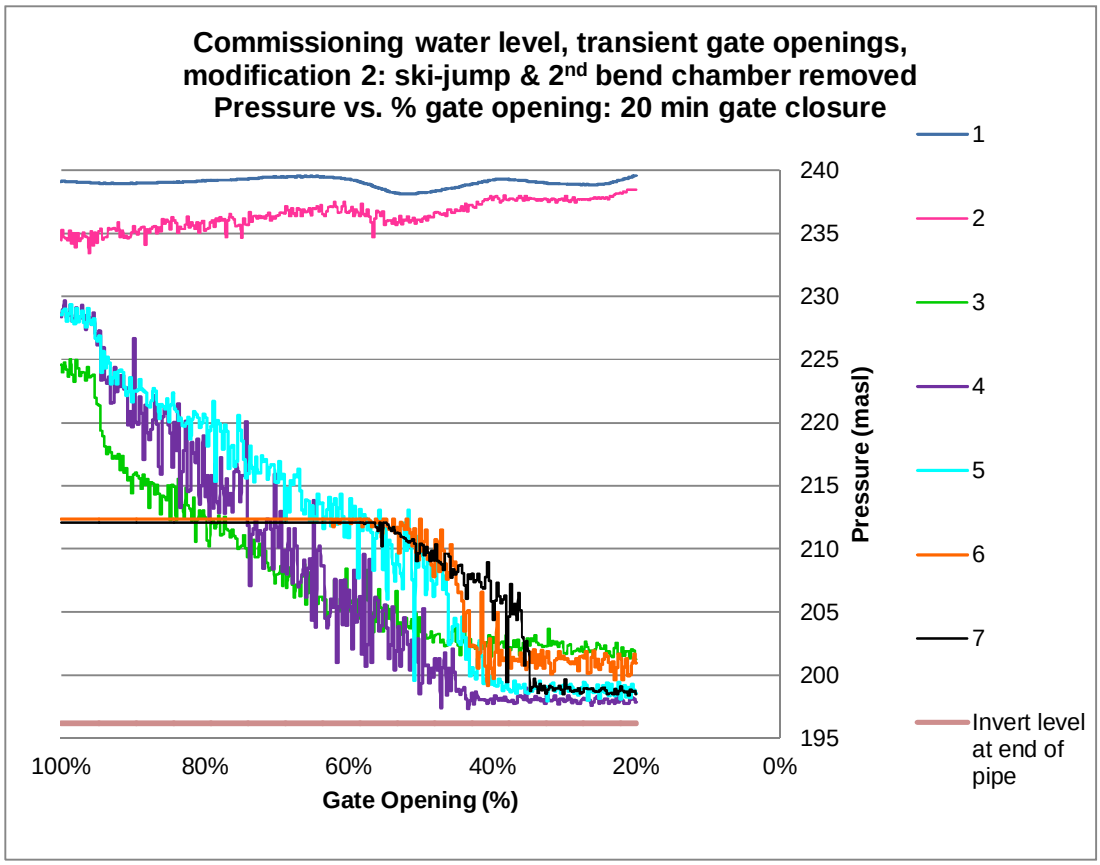

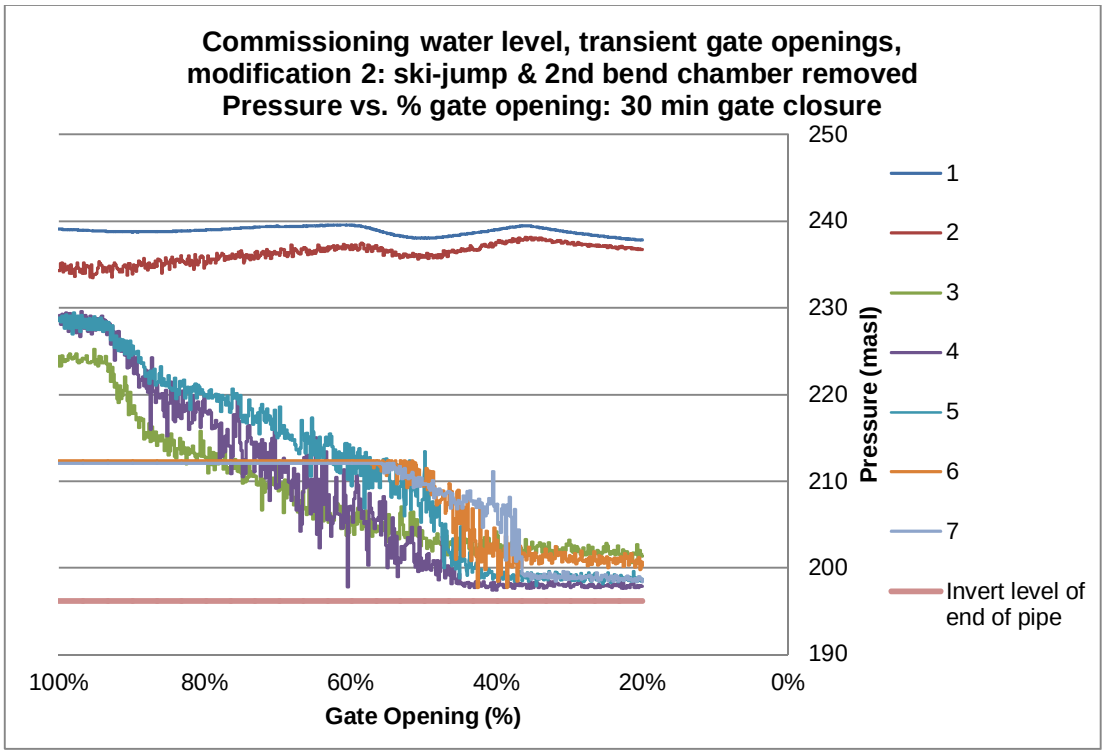

ANNEXURE I3: Air Velocity – Closing Gate Simulations; Commissioning Water Level; Modification 3

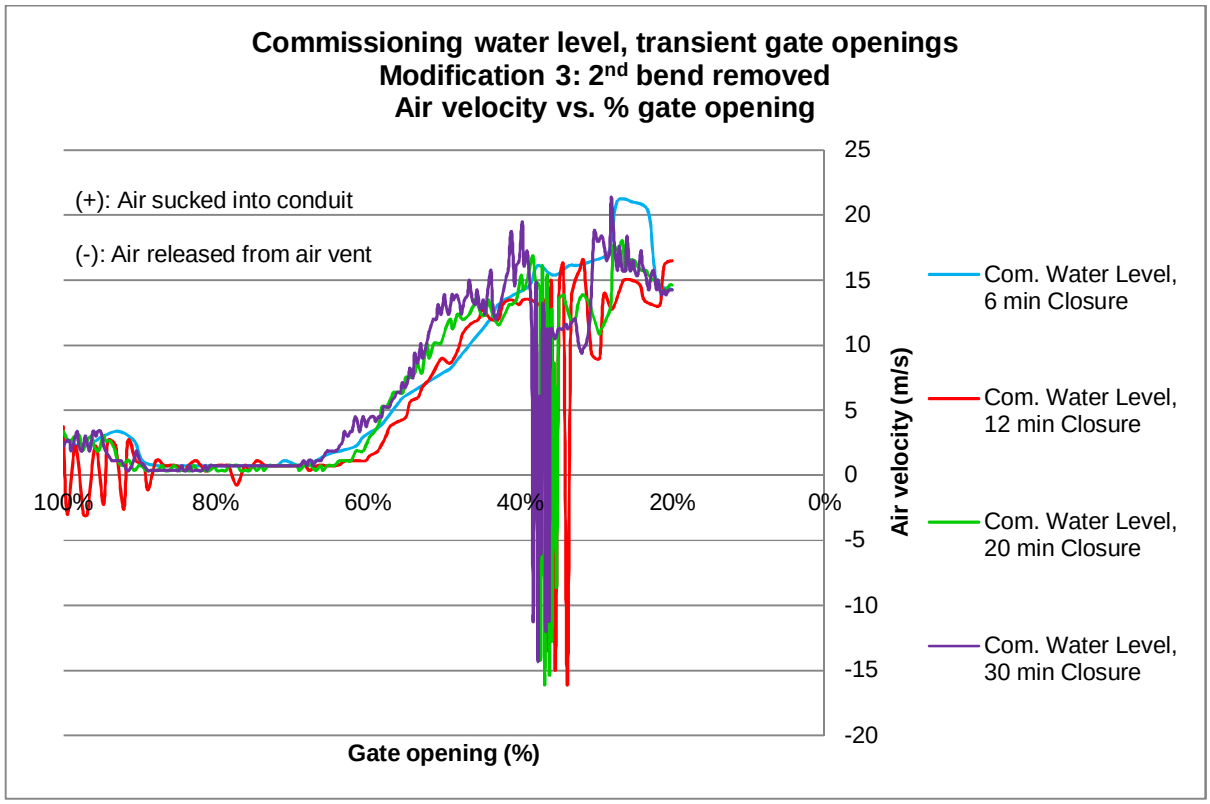

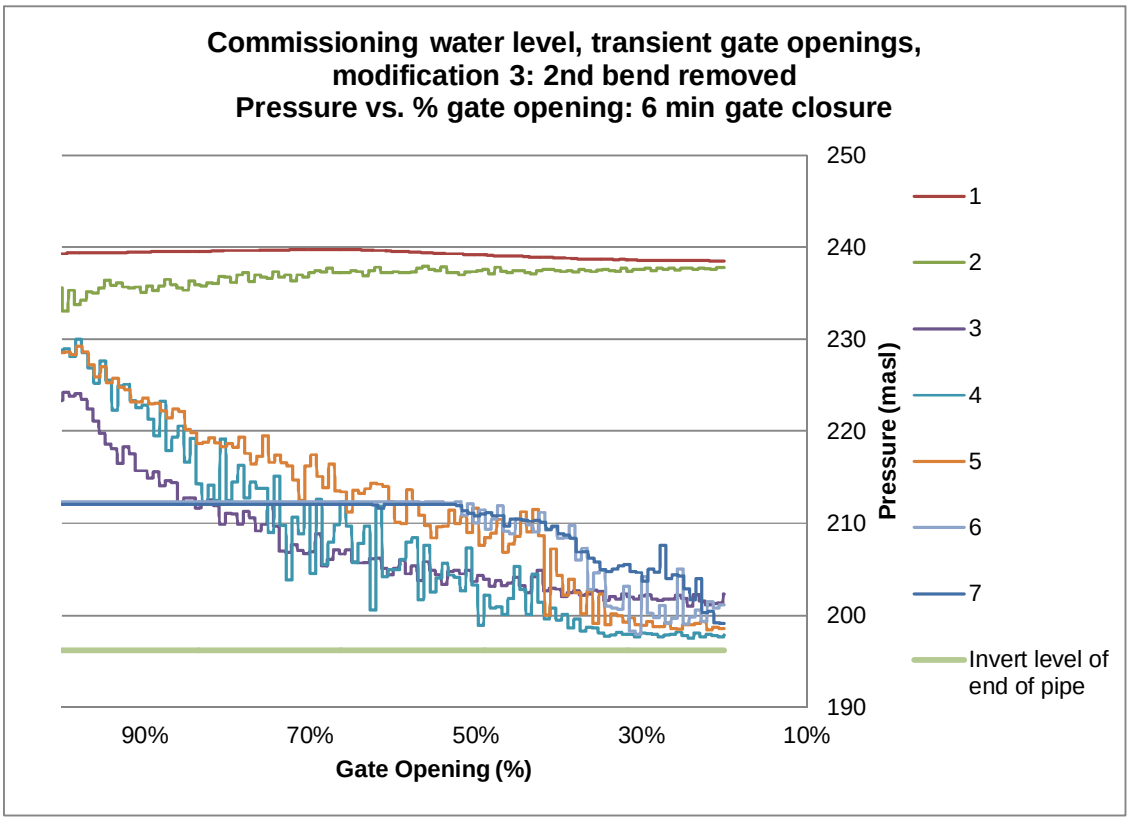

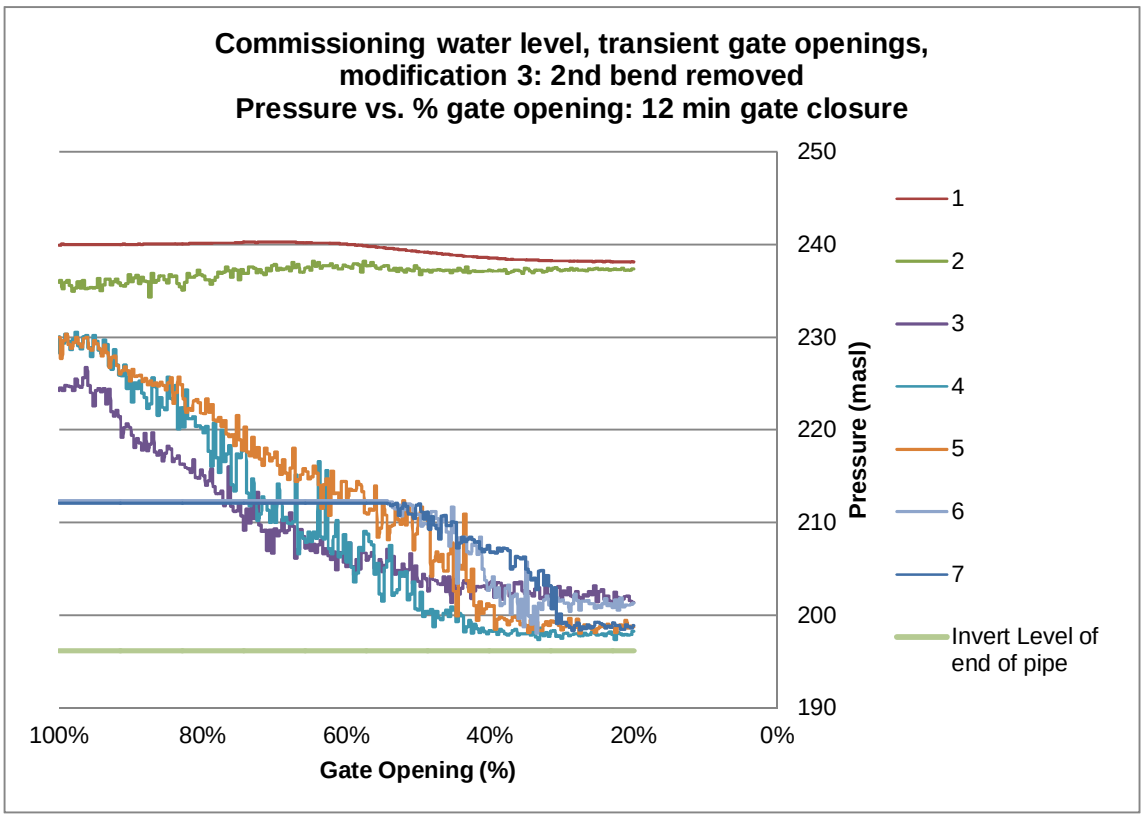

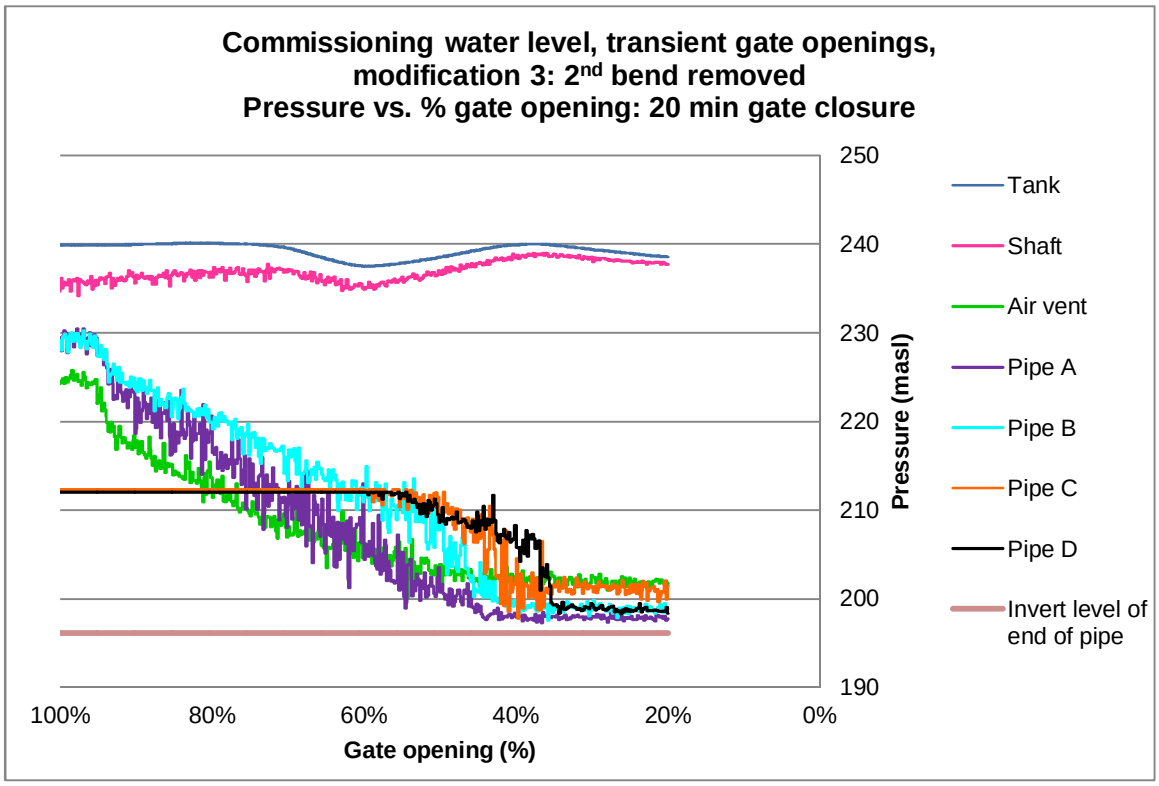

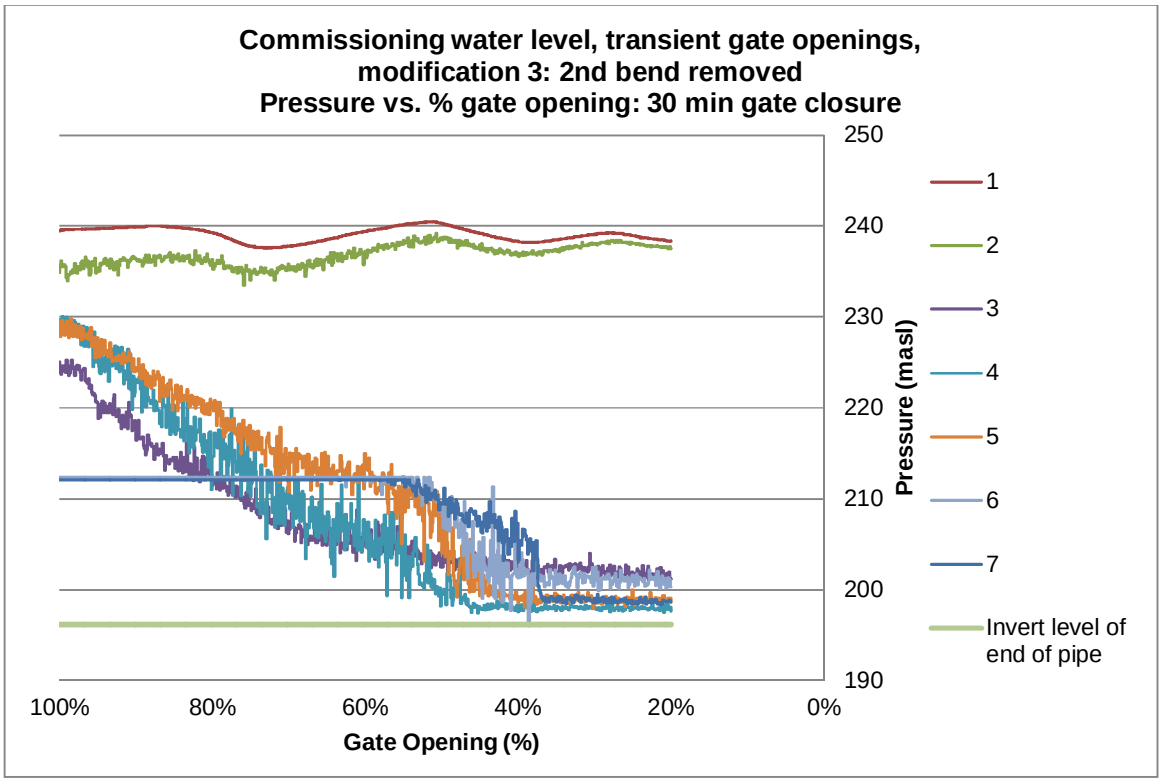

ANNEXURE I4: Air Velocity – Closing Gate Simulations; Commissioning Water Level; Modification 4

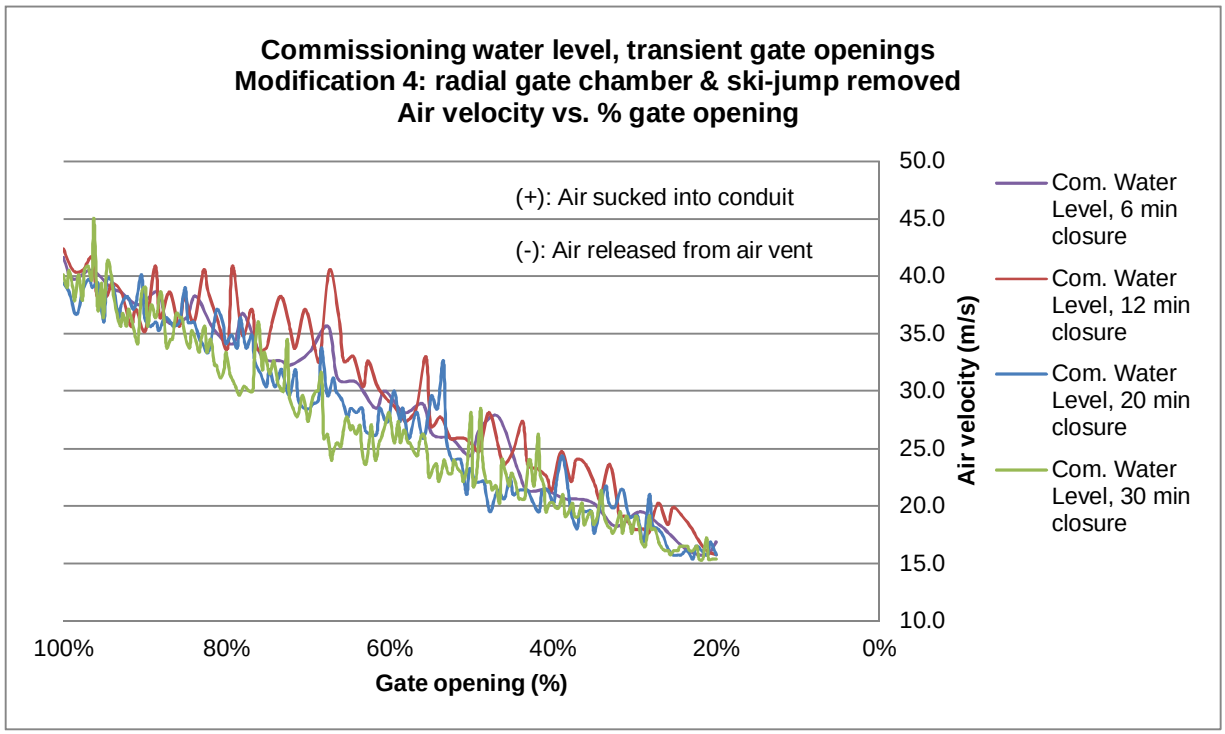

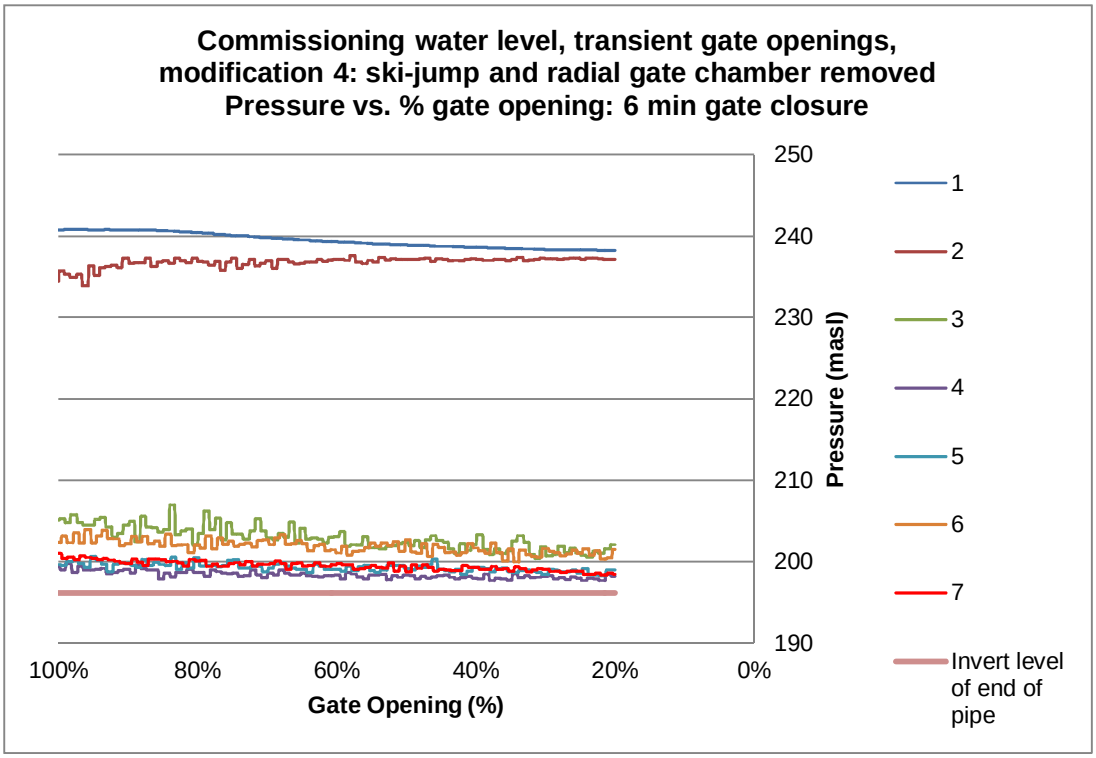

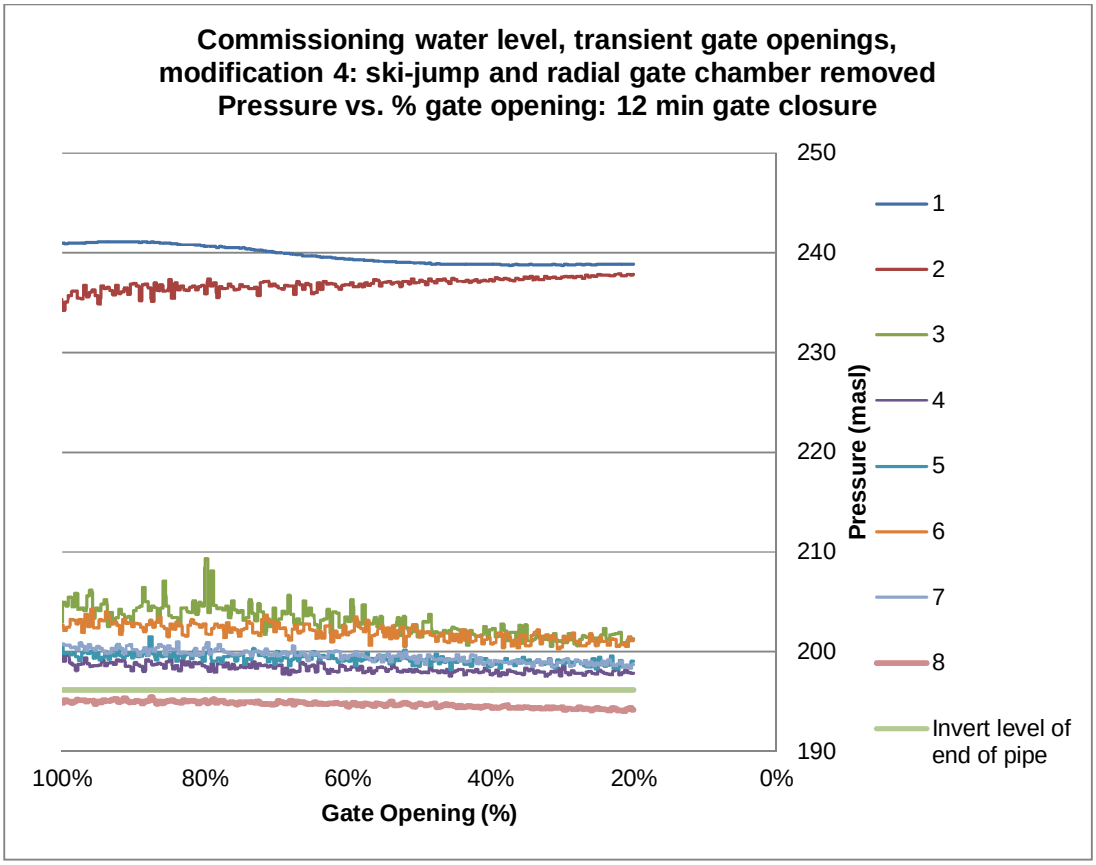

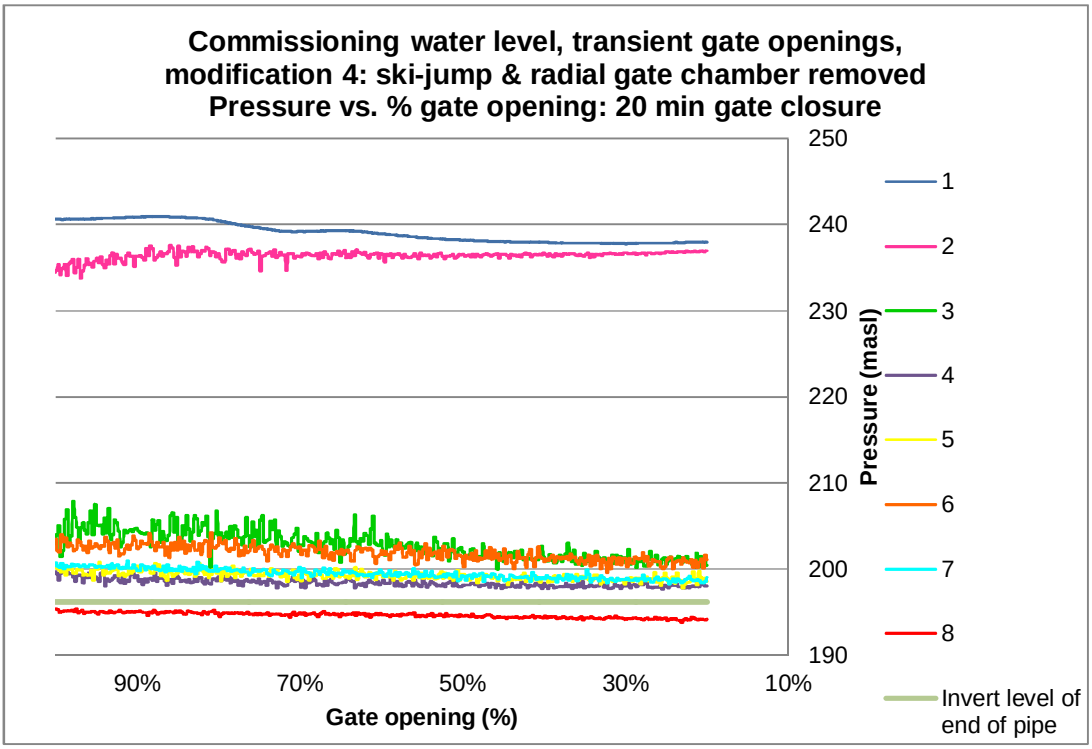

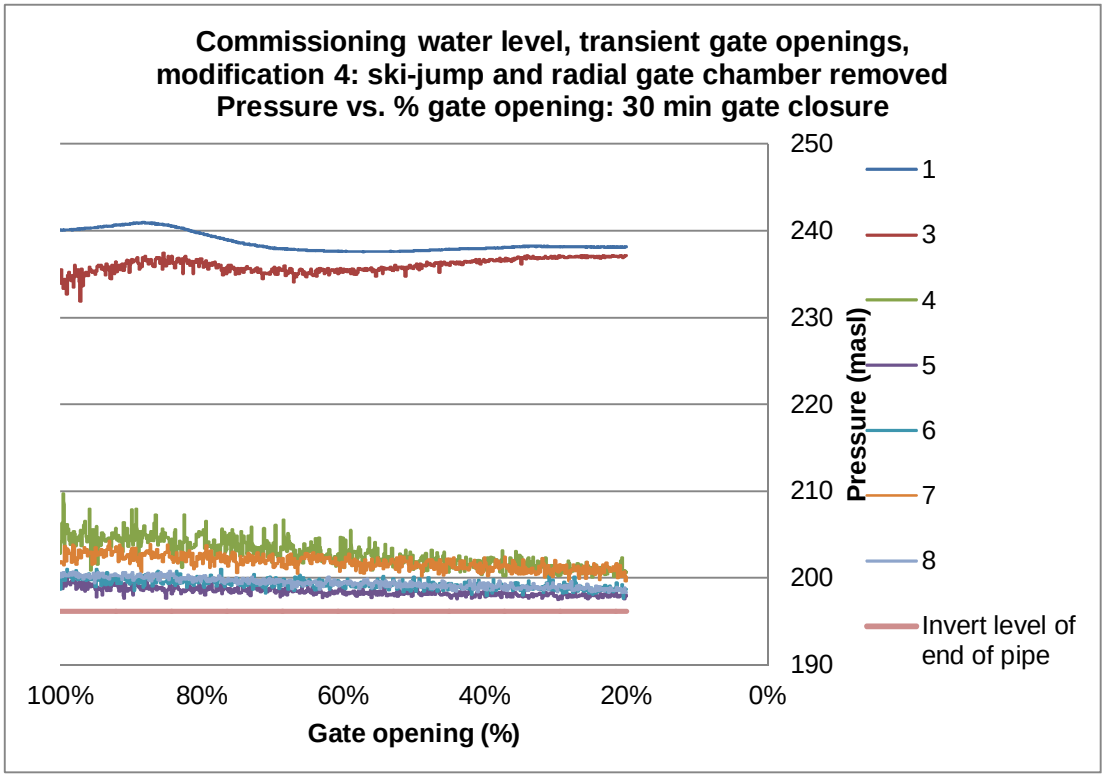

ANNEXURE I5: Air Velocity – Closing Gate Simulations; Commissioning Water Level; Modification 5

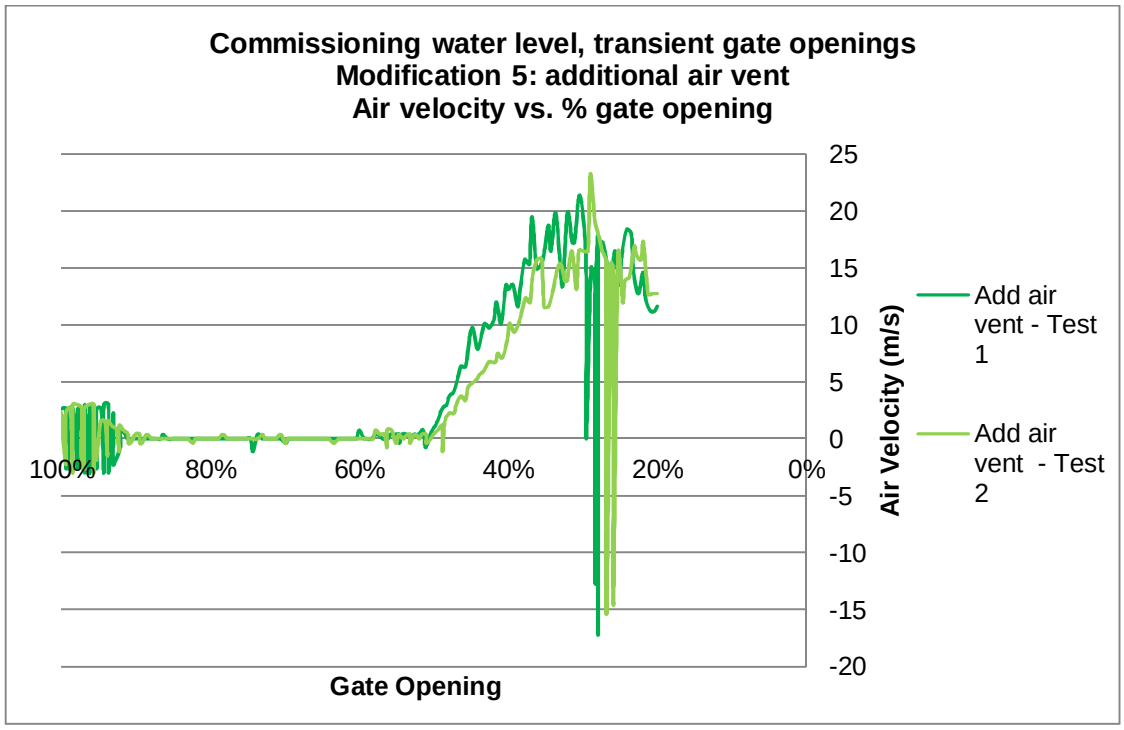

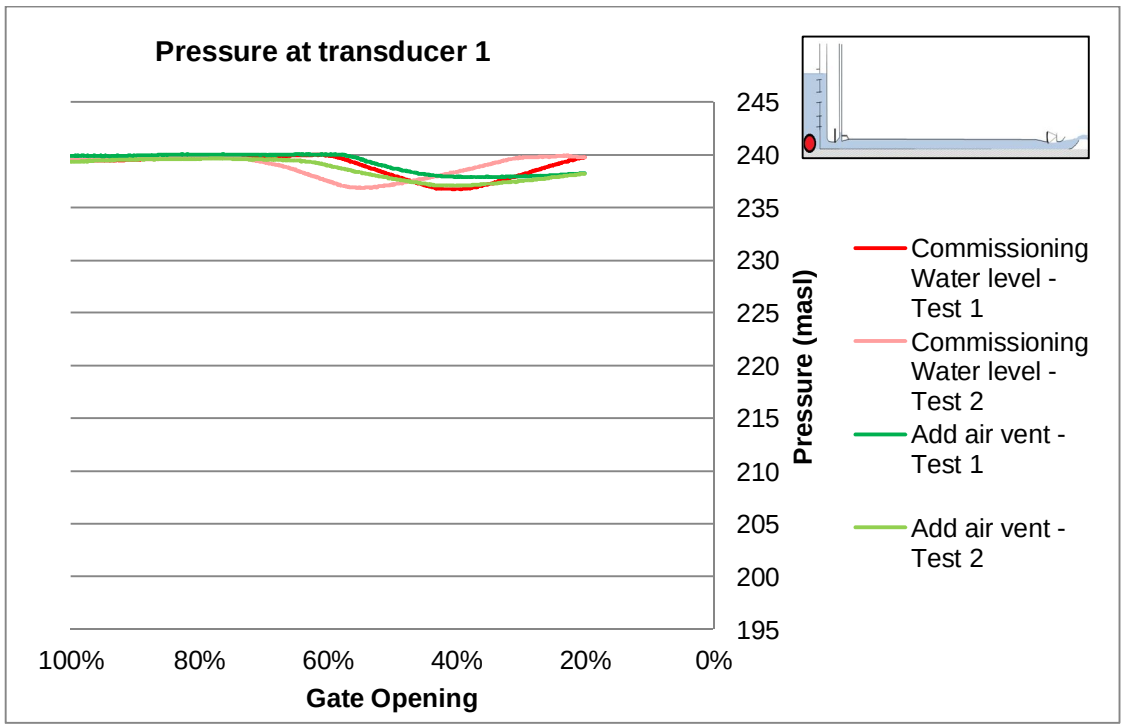

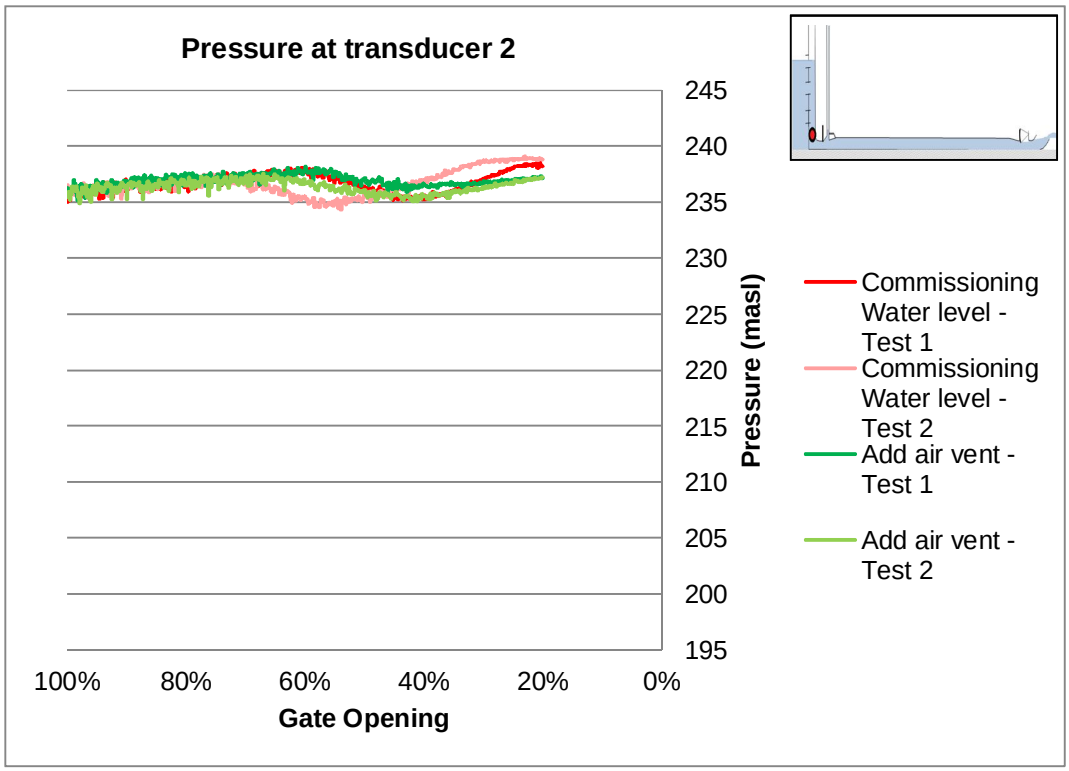

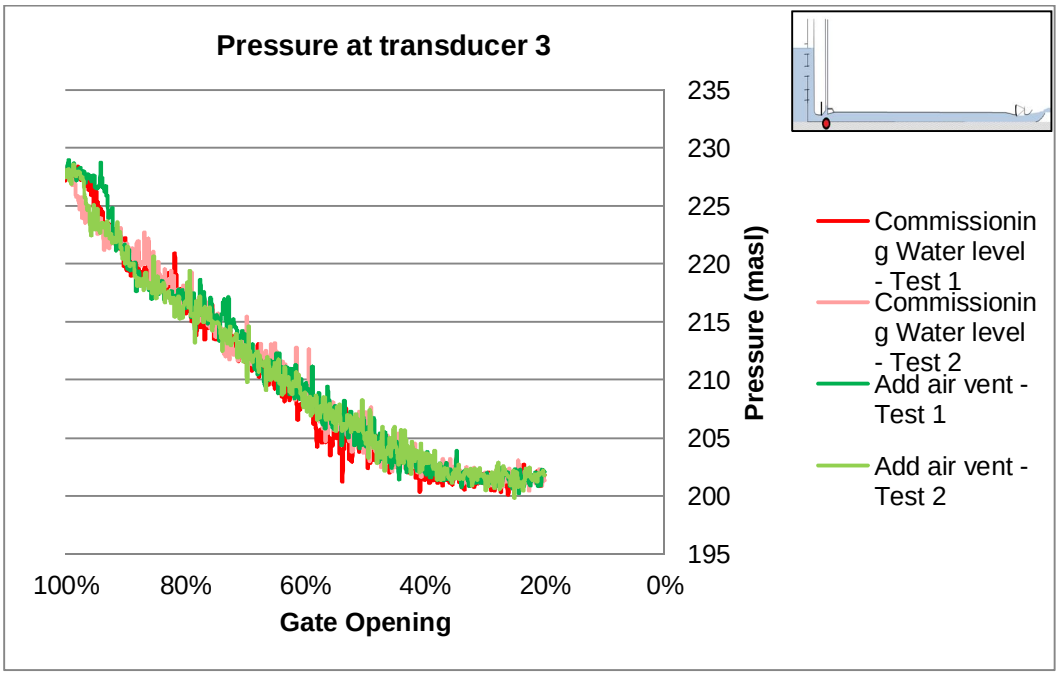

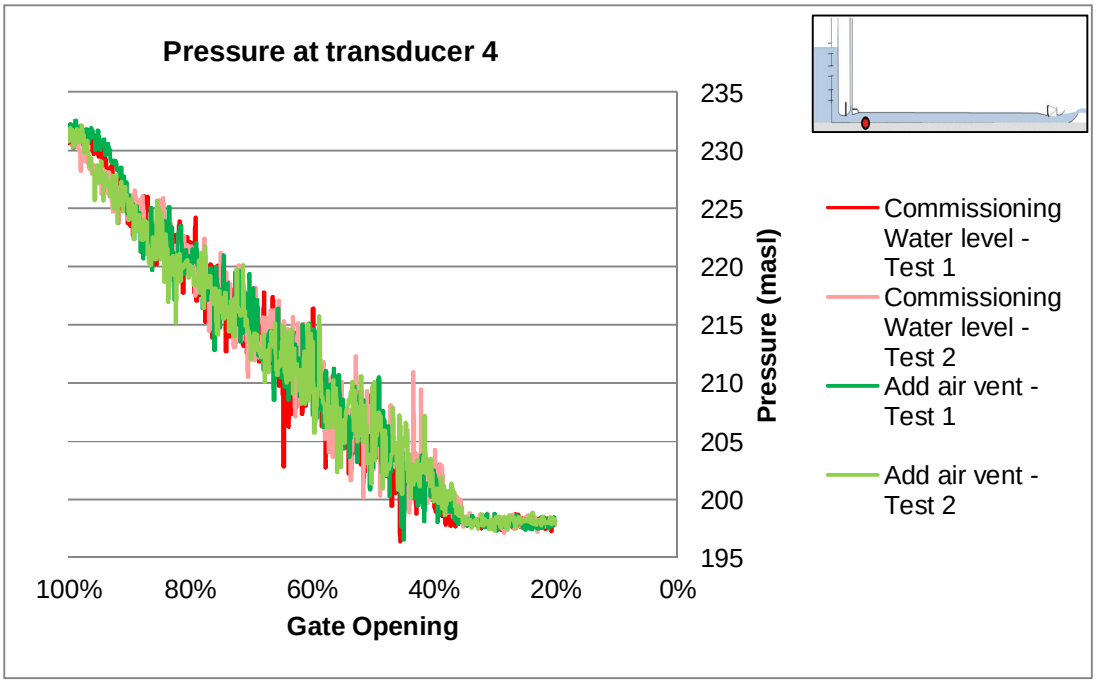

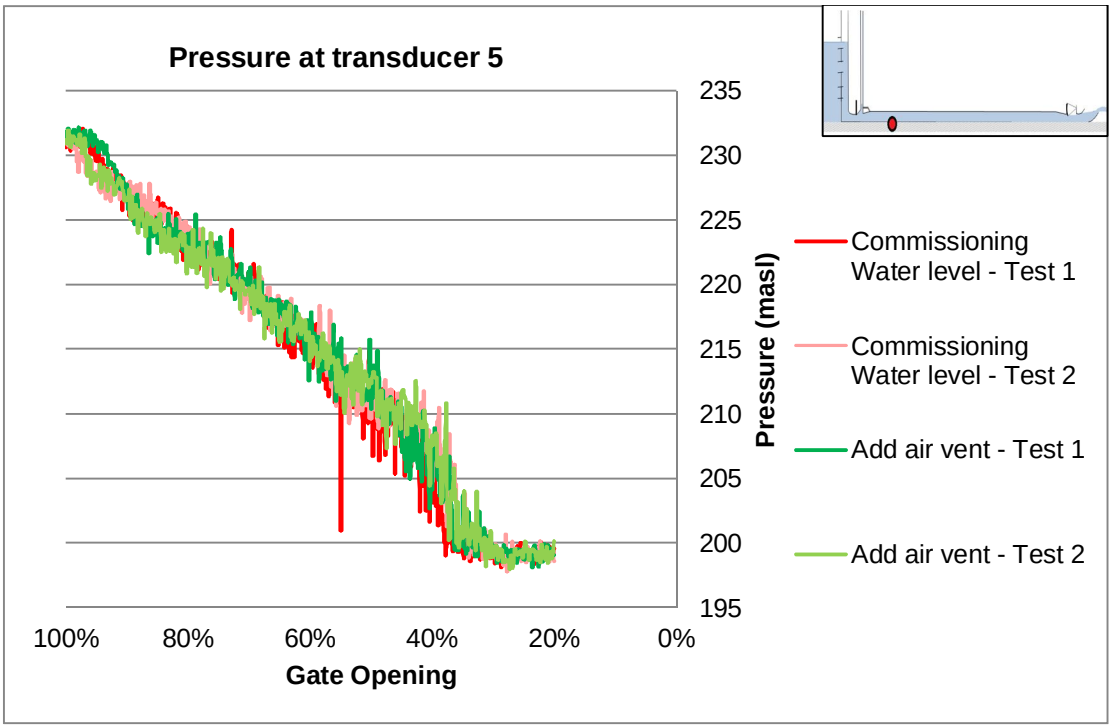

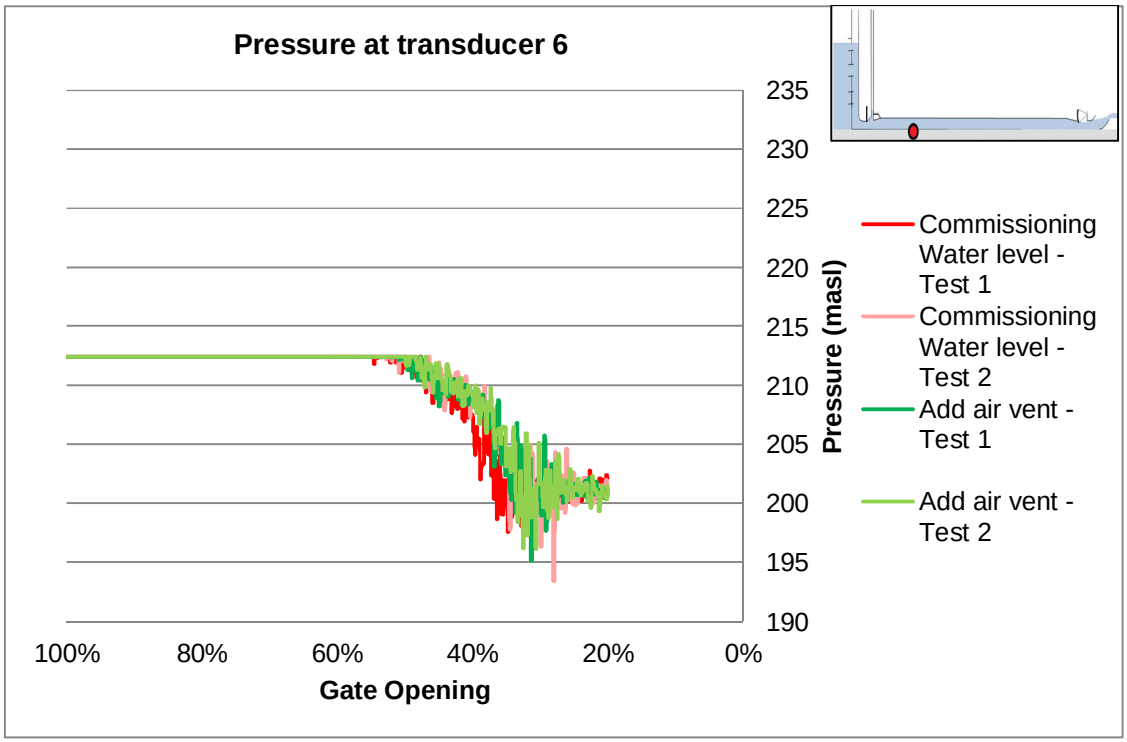

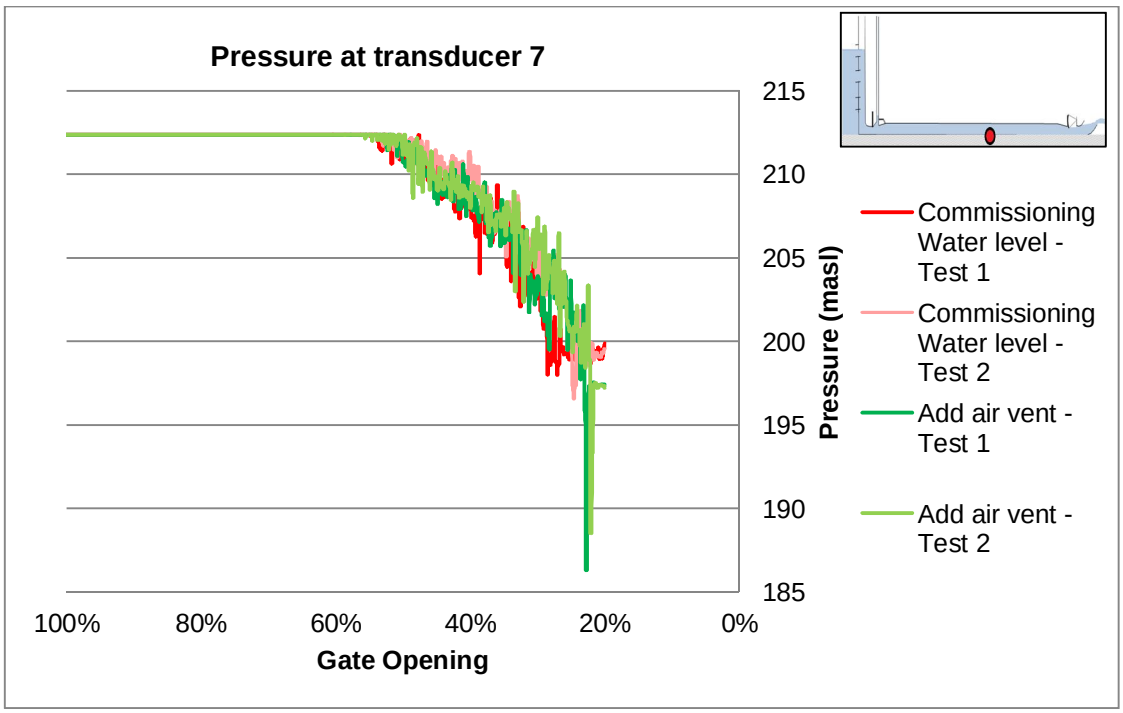

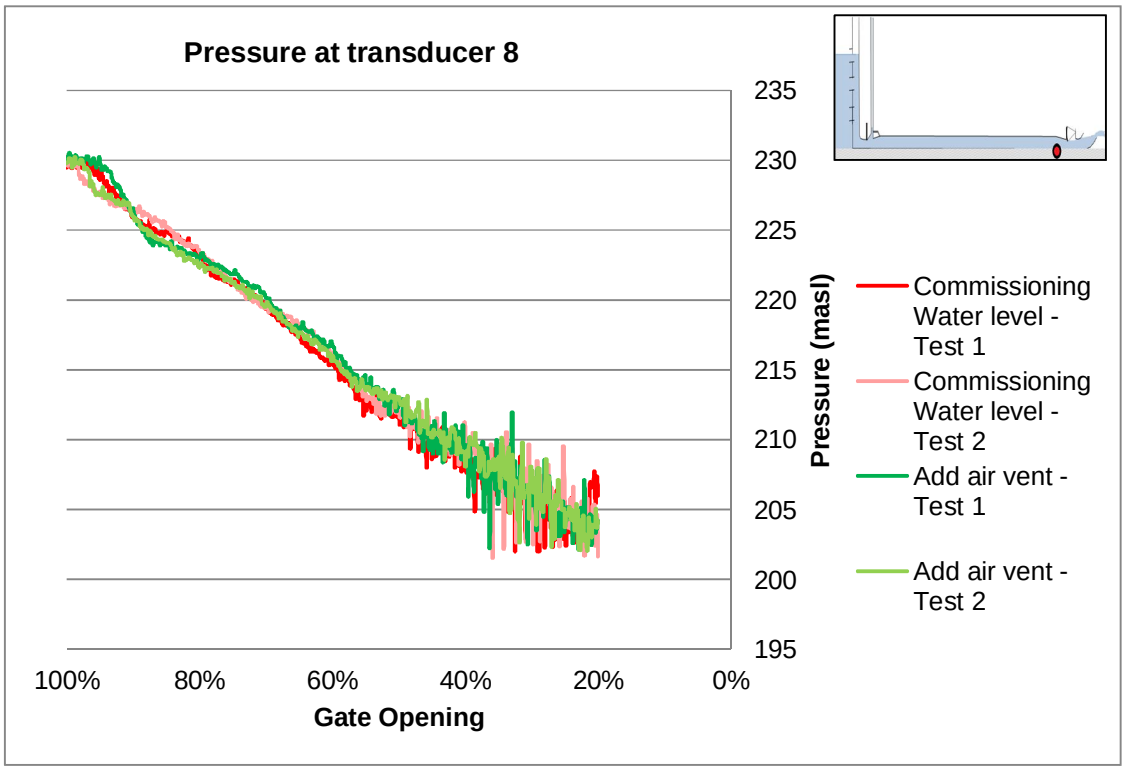

ANNEXURE J: Discussion of Results of Modification 1, 2 and 3.

1. Modification 1 – Only Ski-jump Removed

The configuration of the model was modified by removing the ski-jump at the end of the conduit, but the second bend and radial gate chamber were still intact (**Figure 4.26**). The air flow and direction in the air vent (**Graph J1 (a)**) and the instantaneous pressure (**Graph J1 (b)**) along the outlet conduit were measured for the tests conducted on the model with its configuration according to the modification 1.

The different emergency gate closure rates that were under evaluation were six minutes, 12 minutes, 20 minutes and 30 minutes. As mentioned previously, the initial gate closure rates of 12 minutes and 20 minutes were selected on the basis of the design manual for operating the emergency closing gate and the commissioning test of 2008 respectively. The six minute and 30 minute gate closure rates were selected as the experimental work progressed.

1.1. Discussion: Air Velocity and direction (Commissioning Water Level, modification 1)

For gate openings between 100% and 65%, the air vent acted as a surge tower and the water oscillated in the air vent. Air was released from (negative airflow) and sucked into (positive airflow) the air vent according to the oscillating water in the vent, which can be seen in **Graph J1 (a)**.

The measured air velocity through the air vent for the simulations run on the model with the ski-jump removed (modification 1), as shown in **Graph J1 (a)**, is higher than for the simulations run on the model with its configuration according to the *as-built* drawings for the same gate closure rates with the commissioning water level under evaluation.

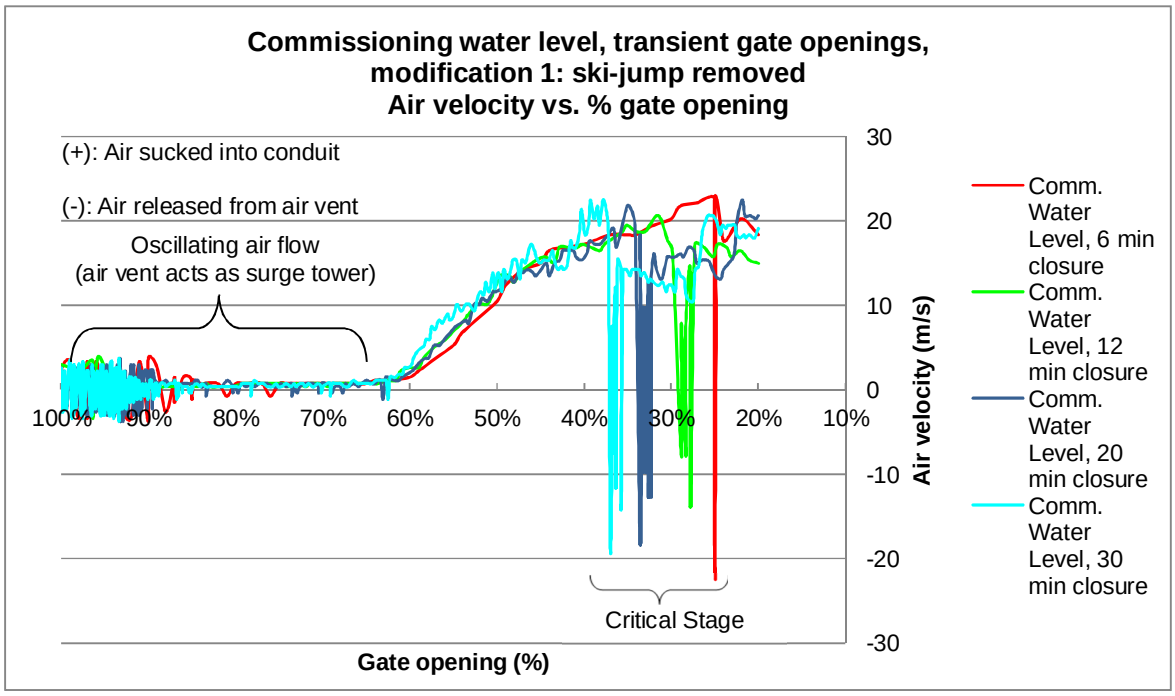

(a)

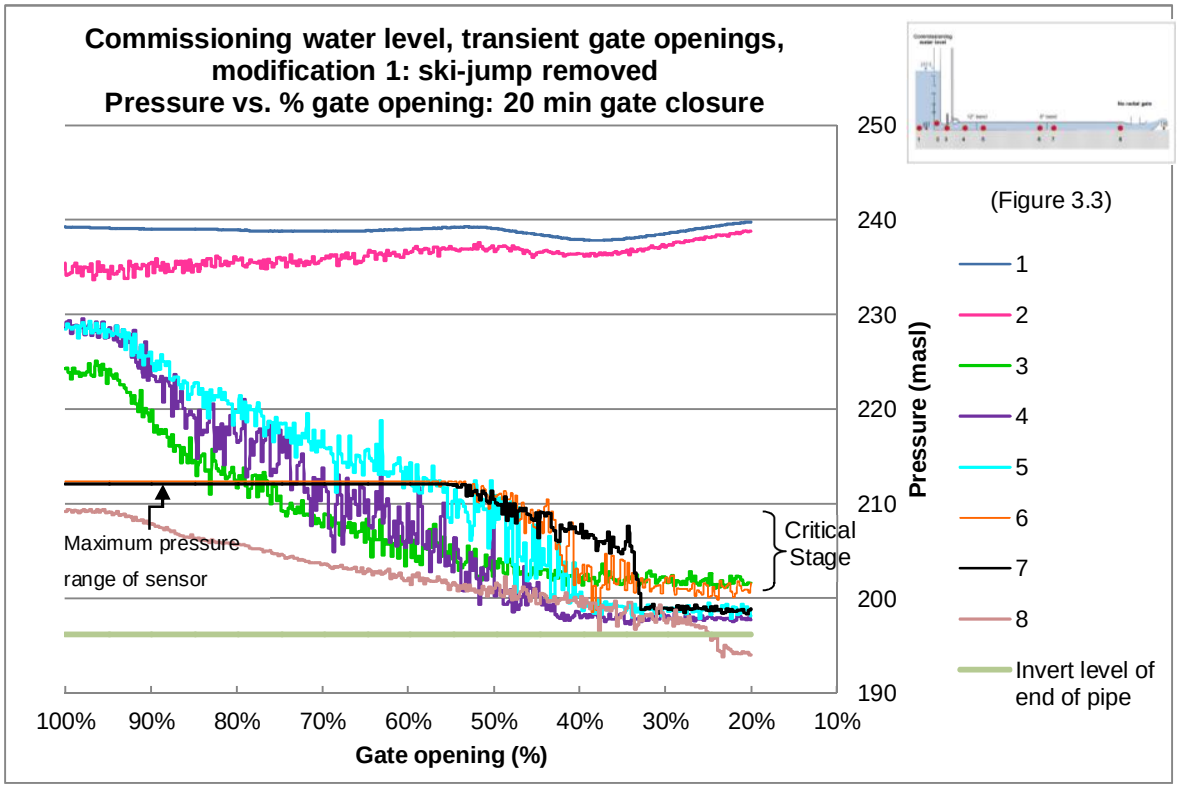

(b)

Graph J1: (a) Air velocity and (b) Instantaneous Pressures for different gate closure rates (Commissioning Water Level, transient gate closure, modification 1)

It can be seen from **Graph J1 (a)** that the release of air from the air vent occurred at larger gate openings when the gate closing rate was longer, as the transient conditions were variable. The reason for this is that the formations of the unstable hydraulic jump had not developed fully from the emergency gate to the radial gate chamber for faster gate closure rates. This phenomenon corresponds with the results obtained for the simulations run on the model with its configuration according to the as-built drawings subjected to the FSL, commissioning water level and the lower water level.

It can also be observed from **Graph J1 (a)** that, during the critical stage, gate opening of approximately 37% to 25%, the air release fluctuated from being sucked in through the air vent to being released. The direction of the air flow was changing rapidly (nine times per second). It appears that the duration of these fluctuation periods was shorter for the shorter gate closure periods. The explanation is that the formation of the unstable hydraulic jump has not yet exited the outlet pipe (reached the radial gate at the ski-jump), as discussed above.

The maximum air velocity out of the air vent and the maximum air velocity sucked into the conduit for the different gate opening rates, as illustrated in **Graph J1 (a)**, are summarised in **Table J1**.

From **Table J1** it can be seen that the phenomenon where air is released from the air vent still occurred for the various gate closure rates and for gate openings of between 37% and 25%. Thus, the release of air through the air vent was not sensitive to the rate of closure, which is similar to the conclusion for the simulations on the model with its configuration according to the as-built drawings.

Table J1: Maximum/Minimum Air entrained into Air Vent (Commissioning Water Level, Transient gate, Modification 1)

Gate closure rate (prototype values)	Gate opening (%)	Maximum air velocity released from air vent (m/s) (prototype values)	Gate opening (%)	Maximum air velocity sucked into conduit (m/s) (prototype values)
6 min	25%	-22.5	26%	22.50
12 min	28%	-13.9	31%	20.63
20 min	34%	-18.4	22%	22.50
30 min	37%	-18.4	39%	22.50

Refer to ***Annexure I1*** for the air velocity graphs of the various gate opening periods for modification 1 (ski-jump removed) subjected to the commissioning water level.

1.2. Discussion: Pressure (Commissioning Water Level, modification 1)

Graph J1 (b) shows the pressure measured along the outlet conduit. It can be seen that the pressures in the water tank (reservoir – pressure transducer number 1) and water shaft (wet well – pressure transducer 2) were relatively constant for the duration of the simulation. This means that the water level in the tank was kept relatively constant at the water level under evaluation for the duration of the test.

Negative pressures were experienced just upstream of the radial gate chamber (pressure transducer number 8) for gate openings of 25% and smaller.

A sudden decrease in pressure occurred in the outlet conduit section upstream of the radial gate chamber (pressure transducer number 7) for gate openings 37% to 35% for the 20 minute gate closure rate.

Refer to ***Annexure I1*** for the pressure vs. gate opening graphs of the various gate opening periods subjected to the commissioning water level for modification 1: ski-jump removed.

1.3. Conclusion (Commissioning Water Level, modification 1)

It was observed that the air release fluctuated from being sucked in through the air vent to being released, and that a steep drop in pressure occurred at pressure transducer number 7 (section upstream of the radial gate chamber) for the same gate openings (critical stage).

The movement of air through the air vent was not sensitive to the gate closure rate for the range of tests carried out, since air was still being released from the air vent and the steep drop in pressure occurred, irrespective of the specific gate closure rate under evaluation.

It can be concluded that the ski-jump was not the cause for air reverse flow, as air was still being released from the air vent for all the tests done on the model with its configuration according to modification 1 (ski-jump removed).

These results obtained correspond to the results obtained for the tests done on the *as-built* conduit, as discussed in **Section 4.3.3.2**.

2. Modification 2 – Ski-jump and Second Bend Removed (8°)

The model configuration was modified by removing the ski-jump and the second bend at the end of the conduit, but the radial gate chamber was left intact (**Figure 4.27). Graph J2 (a)** shows the air velocity and direction measured in the air vent for various gate closure rates. **Graph J2 (b)** shows the pressures measured along the outlet conduit for a 20 minute gate closure rate. The commissioning water level was under evaluation.

2.1. Discussion: Air Velocity and direction (Commissioning Water Level, modification 2)

For gate openings between 100% and 65%, the air vent acted as a surge tower and the water oscillated in the air vent. Air was released from (negative airflow) and sucked into (positive airflow) the air vent according to the oscillating water in the vent, which can be seen in **Graph J2 (a)**.

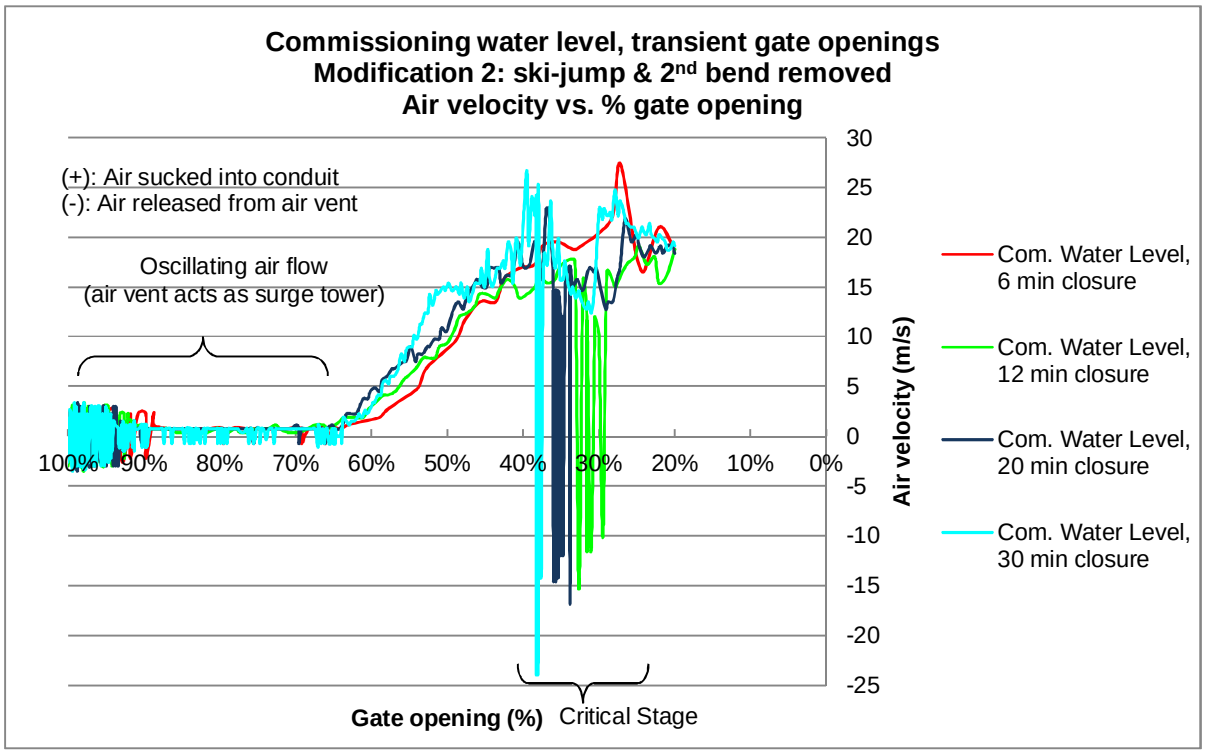

(a)

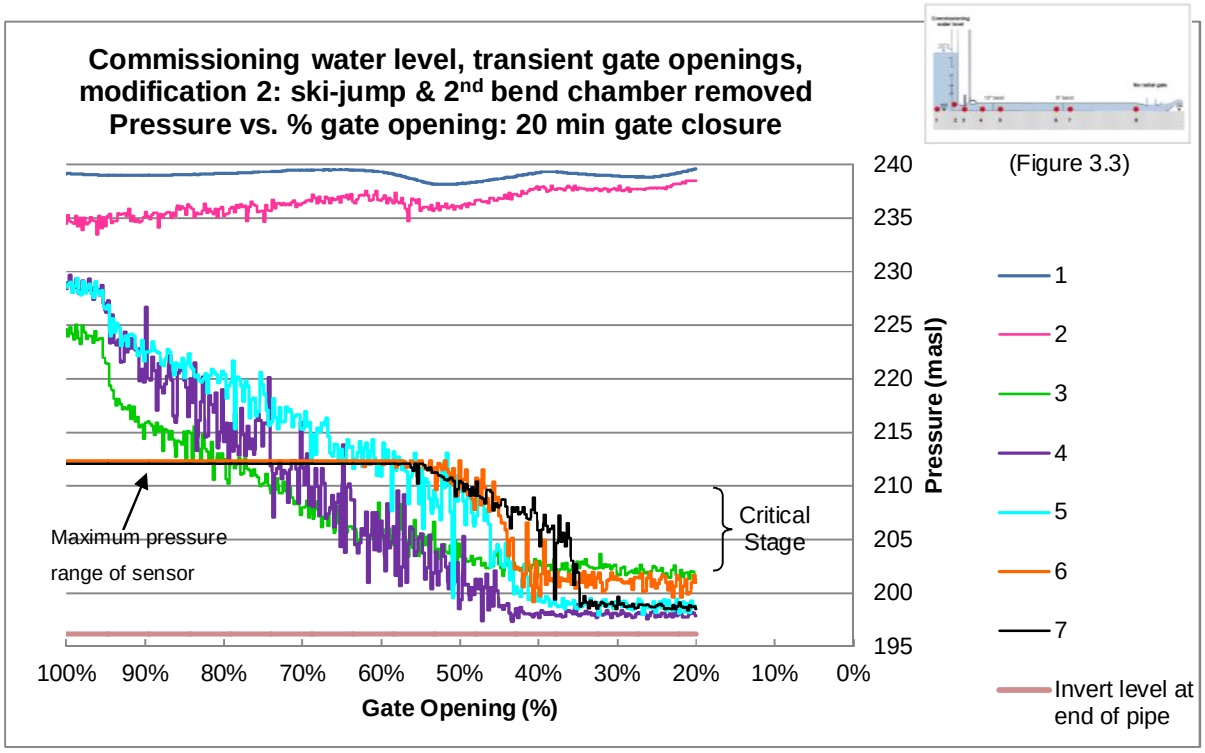

(b)

Graph J2: (a) Air velocity and (b) Instantaneous Pressures for different gate closure rates (Commissioning Water Level, transient gate closure, modification 2)

Graph J2 (a) illustrates that air is released from the air vent for larger gate openings for slower gate closure rates, which corresponds to the result of the simulations run on the model with its configuration according to the as-built drawings and to modification 1 (ski-jump removed). The reason for this is that the transient conditions are variable. It can be concluded that air is released from the air vent for simulations run on the model with the ski-jump and second bend removed (modification 2), irrespective of the gate closure rate. However, the gate closure rate determines at which gate opening the air would be released.

It was also observed from **Graph J2 (a)** that, during the critical stage, gate opening of approximately 37% to 29%, the air release fluctuated from being sucked in through the air vent to being released. The air flow direction was changing rapidly (seven times per second). It appears that the duration of these fluctuation periods was shorter for the shorter gate closure periods. The explanation for this is that the formation of the unstable hydraulic jump has not yet exited the outlet pipe (reached the radial gate at the ski-jump), as discussed above. Thus the transient conditions are variable, which is the reason for the release of air at smaller gate openings for faster gate closure rates.

The maximum air velocity released from the air vent and the maximum measured air velocity into the conduit for the different gate opening rates, as illustrated in **Graph J2 (a)**, are summarised in **Table J2**. The velocity of air released from and sucked into the conduit for the simulations run on the model without the ski-jump and second bend (modification 2) are very similar to the velocities measured on the model with only the ski-jump removed (modification 1). Thus, removing only the ski-jump or both the ski-jump and the second bend did not influence the release of air through the air vent.

The measured air velocity through the air vent for the simulations run on the model with the ski-jump and second bend removed (modification 2), as shown in **Table J2** above, is higher than for the simulations run on the model with its configuration according to the as-built drawings for the same gate closure rates with the commissioning water level under evaluation.

Table J2: Maximum/Minimum Air entrained into Air Vent (Commissioning Water Level, Transient gate, Modification 2)

Gate closure rate (prototype values)	Gate opening (%)	Maximum air velocity released from air vent (m/s) (prototype values)	Gate opening (%)	Maximum air velocity sucked into conduit (m/s) (prototype values)
6 min	93%	-2.6	27%	27.4
12 min	33%	-15.4	25%	19.1
20 min	34%	-16.9	37%	22.9
30 min	37%	-10.9	38%	23.3

Table J2 shows that the movement of air through the air vent was not sensitive to the gate closure rate, because air was still released, irrespective of the specific gate closure rate under evaluation.

These results (except for the six minute gate closure rate) correspond to the results obtained for the simulations run on the model with its configuration according to the as-built drawings and modification 1 (ski-jump removed).

Refer to ***Annexure I2*** for the air velocity graphs of the various gate opening periods for modification 2 (ski-jump and 2nd bend removed) for the commissioning water level.

2.2. Discussion: Pressure (Commissioning Water Level, modification 2)

From **Graph J2 (b)**, it can be seen that the pressures in the water tank (reservoir – pressure transducer number 1) and water shaft (wet well – pressure transducer number 2) were relatively constant for the duration of the simulation. This means that the water level in the tank was kept relatively constant at the water level under evaluation for the duration of the test.

It was observed that a sudden drop in pressure occurred upstream of the radial gate chamber (pressure transducer number 7) for gate openings 37% to 35% for the 20 minute gate closure rate.

No negative pressures were recorded.

Refer to ***Annexure I2*** for the pressure vs. gate opening graphs of the various gate opening periods subjected to the commissioning water level for modification 2: ski-jump and second bend removed.

2.3. Conclusion (Commissioning Water Level, modification 2)

The sudden decrease in pressure upstream from the radial gate chamber occurred at the same time as when air blow-back occurred in the air vent. The same conclusion was made for the tests done on the as-built outlet conduit and for modification 1.

The movement of air through the air vent was not sensitive to the gate closure rate for the range of tests carried out, since air was still released from the air vent and the steep drop in pressure occurred, irrespective of the specific gate closure rate under evaluation. Therefore, the combination of the second bend (8°) and the ski-jump was not the cause for air reverse flow.

3. Modification 3 – Second Bend Removed (8°)

The model configuration was modified by removing only the second bend (8°) at the end of the conduit, with the radial gate chamber and ski-jump still intact (**Figure 4.28).** The air velocity and direction measured in the air vent for the various gate closure rates subjected to the commissioning water level are shown in **Graph J3 (a)**. **Graph J3 (b)** shows the pressures measured along the outlet conduit for a 20 minute gate closure rate.

3.1. Discussion: Air Velocity and direction (Commissioning Water Level, modification 3)

For gate openings between 100% and 65%, the air vent acted as a surge tower and the water oscillated in the air vent. Air was released from (negative airflow) and sucked into (positive airflow) the air vent according to the oscillating water in the vent, which can be seen in **Graph J3 (a)**.

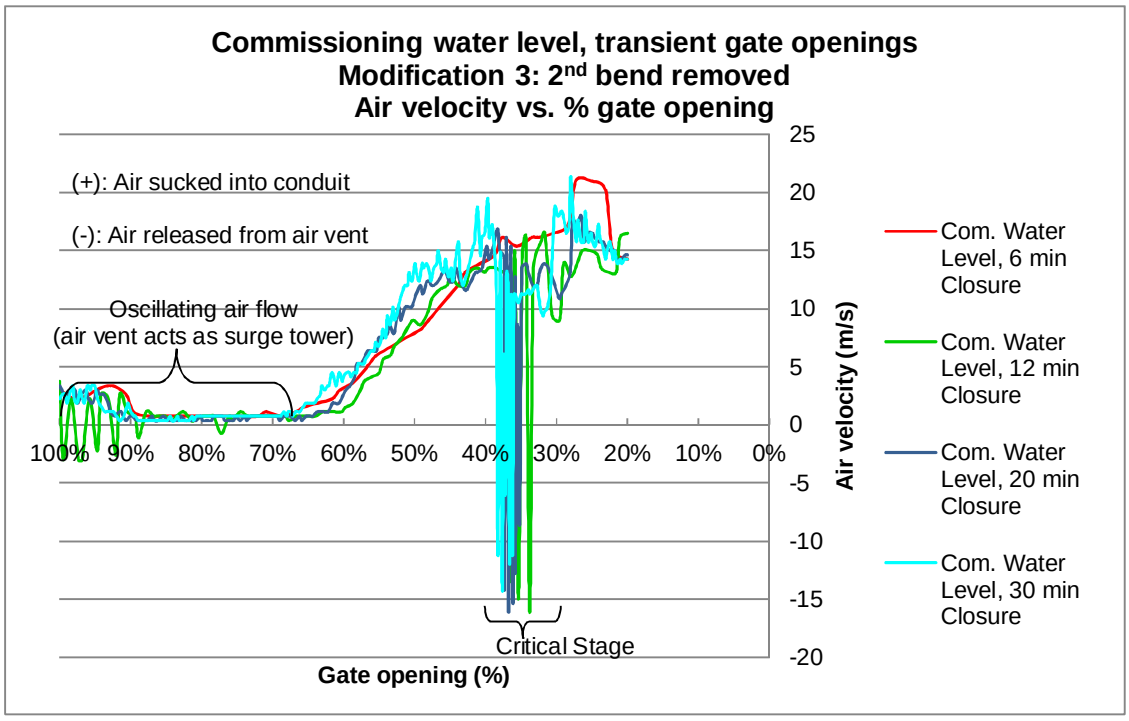

(a)

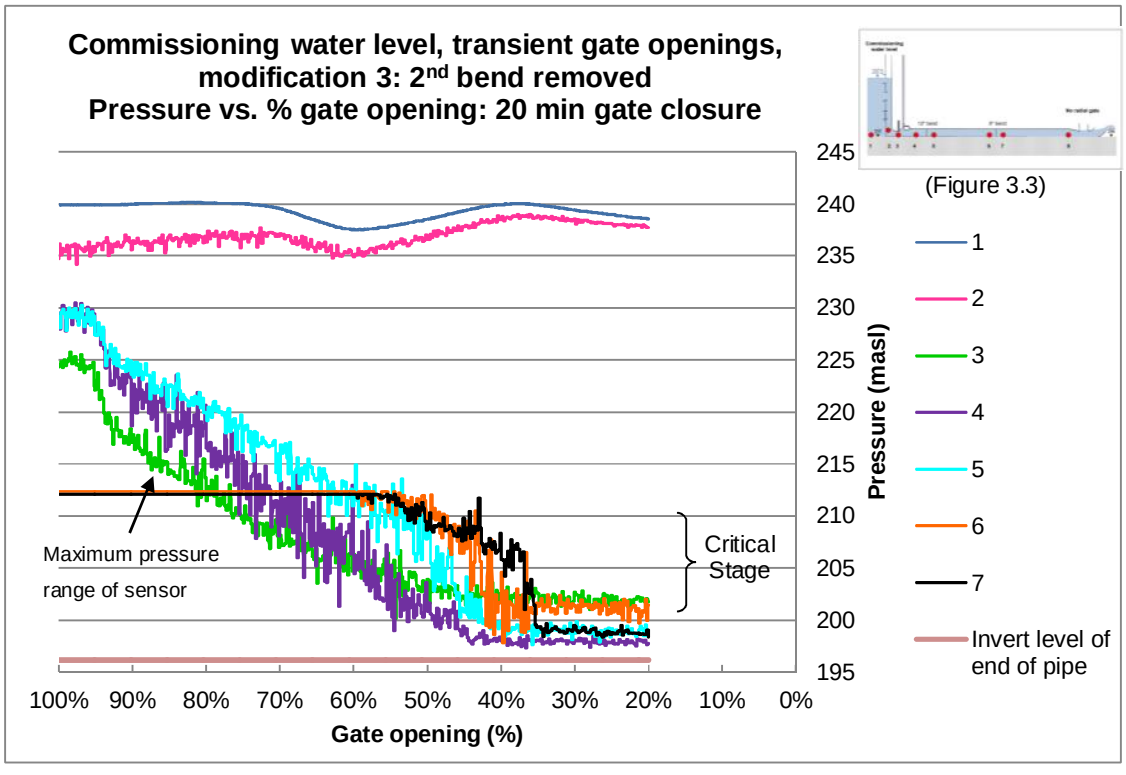

(b)

Graph J3: (a) Air velocity and (b) Instantaneous Pressures for different gate closure rates (Commissioning Water Level, transient gate closure, modification 3)

It was also observed from **Graph J3 (a)** that, during the critical stage, gate opening of approximately 38% to 24%, the air release fluctuated from being sucked in through the air vent to being released. The air flow direction was changing rapidly (seven times per second). It appears that the duration of these fluctuation periods was shorter for the shorter gate closure periods. The explanation is that the formation of the unstable hydraulic jump has not yet exited the outlet pipe (reached the radial gate at the ski-jump), as discussed above. Thus the transient conditions are variable, which is the reason for the release of air at smaller gate openings for faster gate closure rates.

The maximum air velocity released through the air vent and the maximum air velocity sucked into the conduit, as illustrated in **Graph J3 (a)** with the model configuration according to modification 3 (2nd bend removed), are summarised in **Table J3**.

Table J3: Maximum/Minimum Air entrained into Air Vent (Commissioning Water Level, Transient gate, Modification 3)

Gate closure rate (prototype values)	Gate opening (%)	Maximum air velocity released from air vent (m/s) (prototype values)	Gate opening (%)	Maximum air velocity sucked into conduit (m/s) (prototype values)
6 min	27%	-14.3	26%	21.0
12 min	34%	-16.1	20%	16.5
20 min	37%	-16.1	27%	18.0
30 min	38%	-14.3	28%	21.4

The velocity of air released from and sucked into the conduit for the simulations run on the model without the second bend (modification 3) are lower than the velocities measured on the model with only the ski-jump removed (modification 1) and when the ski-jump and second bend were removed (modification 2). However, the release of air through the air vent still occurred for gate openings between 38% and 25%. Thus, removing only the second bend (8°) in the conduit did not have an impact on the phenomenon of air that is released from the air vent.

It can also be seen from **Table J3** that the air released occurred at larger gate openings for slower gate closure rates, which corresponds to the results obtained from the simulations run on the model with its configuration according to the as-built drawings, modification 1 (ski-jump removed) and modification 2 (ski-jump and second bend removed).

Table J3 shows that the movement of air through the air vent is not sensitive to the gate closure rate, because air was still released, irrespective of the specific gate closure rate under evaluation.

These results correspond to the results obtained for the simulations run on the model with its configuration according to the as-built drawings, modification 1 (ski-jump removed) and modification 2 (ski-jump and second bend removed).

Refer to ***Annexure I3*** for the air velocity graphs of the various gate opening periods for modification 3 (only second bend removed) for the commissioning water level.

3.2. Discussion: Pressure (Commissioning Water Level, modification 3)

From **Graph J3 (b)** it can be seen that the pressures in the water tank (reservoir) and water shaft (wet well) were relatively constant for the duration of the simulation. This means that the water level in the tank was kept relatively constant at the water level under evaluation for the duration of the test.

No negative pressures were recorded.

A sudden decrease in the pressure in the outlet conduit upstream of the radial gate chamber (pressure transducer number 7) for gate openings 37% to 35% occurred (**Graph J3 (b)**), which corresponds to the gate openings when reverse air flow occurred for the 20 minute gate closure rate.

Refer to ***Annexure I3*** for the pressure vs. gate opening graphs of the various gate opening periods subjected to the commissioning water level for modification 3: second bend removed.

3.3. Conclusion (Commissioning Water Level, modification 3)

The sudden decrease in pressure upstream from the radial gate chamber occurred at the same time as when air blow-back occurred in the air vent. The same conclusion was made for the tests done on the as-built outlet conduit and for modification 1 and 2.

The movement of air through the air vent was not sensitive to the gate closure rate for the range of tests carried out, since air was still released from the air vent and the steep drop in pressure occurred, irrespective of the specific gate closure rate under evaluation. Therefore, the second bend (8°) was not the cause for air reverse flow.

ANNEXURE K: Stage Discharge Curve

Department of Water Affairs HYRATAB V159 Output 26/10/2011

Site G1H077 Bergriver Dam W-Component

Rating Table 1.01 28/05/2008 to Present Interpolation = Log CTF = 0.0000

Converting 101 Corrected Surface Water Level in Metres
Into 103 Uncorrected Surface Discharge in Cubic Metres/Second

G.H.	0	0.01	0.02	0.03	0.04	0.05	0.06	0.07	0.08	0.09
0.00	0.0	0.0155	0.0497	0.0951	0.149	0.211	0.280	0.355	0.435	0.521
0.10	0.611	0.707	0.806	0.910	1.02	1.13	1.25	1.37	1.49	1.62
0.20	1.75	1.88	2.02	2.16	2.30	2.44	2.59	2.74	2.90	3.06
0.30	3.22	3.43	3.69	4.00	4.33	4.69	5.08	5.48	5.91	6.35
0.40	6.81	7.29	7.79	8.30	8.82	9.36	9.92	10.5	11.1	11.7
0.50	12.3	12.9	13.5	14.2	14.9	15.5	16.2	16.9	17.6	18.3
0.60	19.1	19.8	20.6	21.3	22.1	22.9	23.7	24.5	25.3	26.1
0.70	27.0	27.8	28.7	29.6	30.4	31.3	32.2	33.1	34.1	35.0
0.80	35.9	36.9	37.8	38.8	39.8	40.8	41.8	42.8	43.8	44.8
0.90	45.8	46.9	47.9	49.0	50.1	51.1	52.2	53.3	54.4	55.5
1.00	56.7	57.8	58.9	60.1	61.2	62.4	63.6	64.8	66.0	67.2
1.10	68.4	69.6	70.8	72.1	73.3	74.6	75.8	77.1	78.4	79.6
1.20	80.9	82.2	83.6	84.9	86.2	87.5	88.9	90.2	91.6	93.0
1.30	94.3	95.7	97.1	98.5	99.9	101	103	104	106	107
1.40	109	110	111	113	114	116	117	119	120	122
1.50	124	125	127	128	130	131	133	135	136	138
1.60	139	141	143	144	146	148	149	151	153	154
1.70	156	158	159	161	163	164	166	168	170	171
1.80	173	175	177	179	180	182	184	186	188	190
1.90	192	194	194A	194A	194A	194A	194A	194A	194A	194A
2.00	194A	194A	194A	194A	194A	194A	194A	194A	194A	194A
2.10	194A	194A	194A	194A	194A	194A	194A	194A	194A	194A
2.20	194A	194A	194A	194A	194A	194A	194A	194A	194A	194A
2.30	194A	194A	194A	194A	195A	195A	195A	195A	195A	195A
2.40	195A	195A	195A	195A	195A	195A	195A	195A	195A	195A
2.50	195A	195A	195A	195A	195A	195A	195A	195A	195A	195A
2.60	195A	195A	195A	195A	195A	195A	195A	195A	195A	195A
2.70	195A	195A	195A	195A	195A	195A	195A	195A	195A	195A
2.80	195A	195A	195A	195A	195A	195A	195A	195A	195A	195A
2.90	195A	196A	196A							

---------- Notes ----------
All rated data has been coded as reliable
except where the following tags are used...
A ... Above Rating

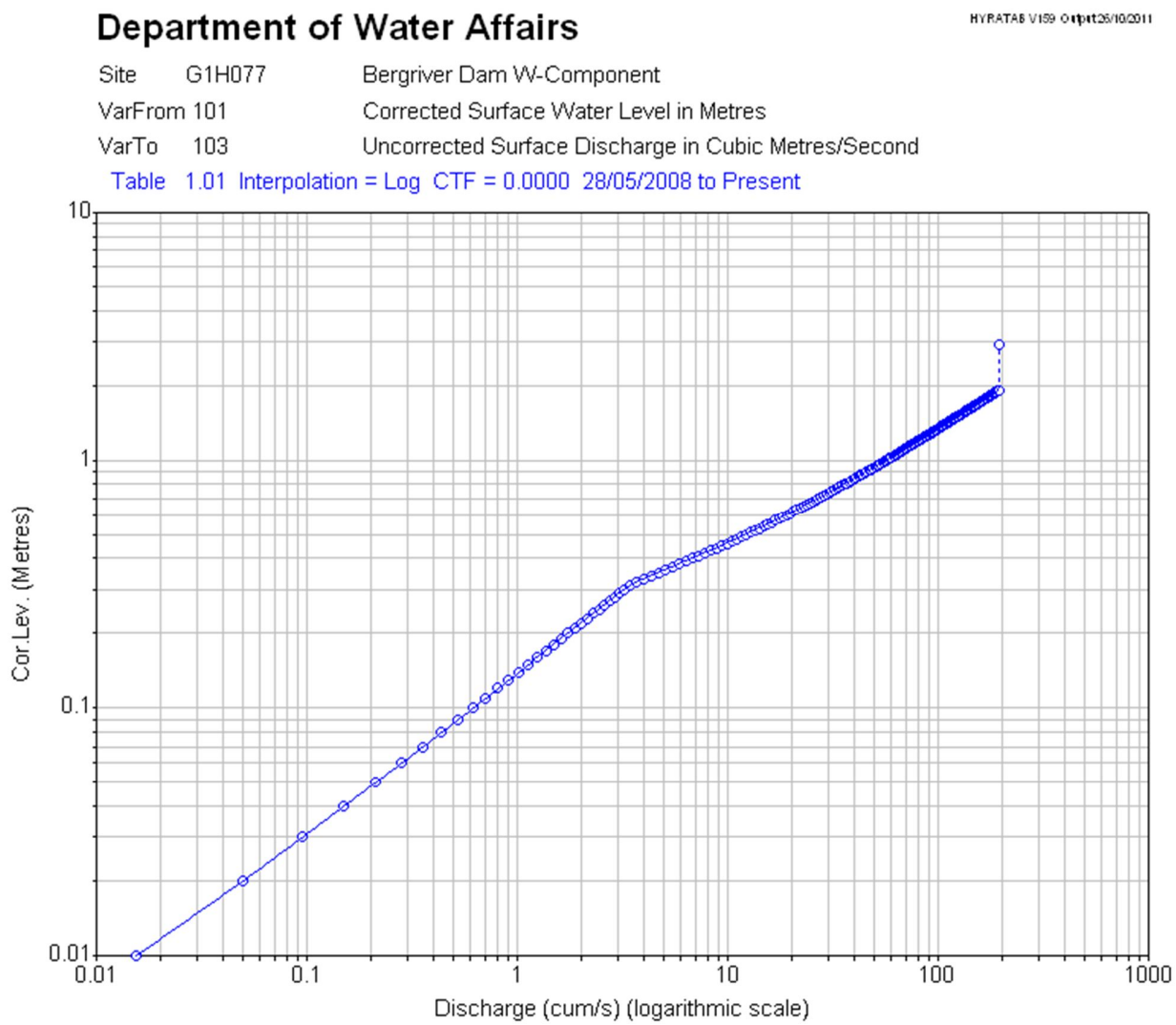
Department of Water Affairs
HYRATAB V159 Output:26/10/2011
Site G1H077 Bergriver Dam W-Component
VarFrom 101 Corrected Surface Water Level in Metres
VarTo 103 Uncorrected Surface Discharge in Cubic Metres/Second
Table 1.01 Interpolation = Log CTF = 0.0000 28/05/2008 to Present
Cor.Lev. (Metres)
10
1
0.1
0.01
0.01
0.1
1
10
100
1000
Discharge (cum/s) (logarithmic scale)